

AN INVESTIGATION OF THE HISTORICAL AND PROJECTED OCCURRENCE OF THE SOUTH AFRICAN MID-SUMMER DROUGHT AND ITS IMPLICATIONS FOR THE AGRO-WATER BUDGET

Report

to the Water Research Commission

edited by

Michael G. Mengistu^{1,2}, Cobus Olivier¹,

Abiodun M. Adeola^{1,3} and Hannes Rautenbach³

¹South African Weather Service, Pretoria

²School of Agricultural, Earth and Environmental Sciences, University of KwaZulu-
Natal

³School of Health Systems and Public Health, Faculty of Health Sciences, University
of Pretoria

Report No. 2830/1/22

ISBN 978-0-6392-0421-5

June 2022



Obtainable from:

Water Research Commission

Private Bag X03

Gezina, 0031

South Africa

orders@wrc.org.za or download from www.wrc.org.za

DISCLAIMER

This report has been reviewed by the Water Research Commission (WRC) and approved for publication. Approval does not signify that the contents necessarily reflect the views and policies of the WRC, nor does mention of trade names or commercial products constitute endorsement or recommendation for use.

EXECUTIVE SUMMARY

MOTIVATION

South Africa is an arid country and is frequently subjected to devastating droughts. For this reason, a considerable amount of climatic research has focused on the occurrence, intensity, impact and prediction of drought on both an annual and a seasonal basis. However, short-term droughts (dry spells) are arguably as important, if not more so, to the agricultural sector than seasonal shortfalls in rainfall. It is often not the occurrence of a dry spell, but its intensity, and when this dry period occurs, that is of vital significance. Various crops, such as maize, are vulnerable to dry spells during specific phenological stages. Water stress is one of the major limiting factors in dryland (rain-fed) maize production. Its effects include stunted growth, delayed maturity and low crop productivity. Water stress during the initial growth stage of maize is influenced by surface soil moisture. During this period, less water is required for survival. However, the plant requires more water in the late vegetative growth stage. The flowering stage has been found to be the stage in which maize is most sensitive to water stress, leading to reductions in crop growth, biomass production and – finally – crop yield. Therefore, planting dates should be chosen in such a way that sensitive plant growth stages coincide with favourable climatic conditions, and not with mid-summer dry spells (Du Plessis, 2003). Generally, in most dryland maize-growing areas, yield reduction occurs because seasonal rainfall distribution is erratic (Du Toit et al., 2002). Moreover, sporadic mid-summer dry spells could aggravate this problem, since water availability is the most pressing and significant factor limiting the production of dryland maize in South Africa.

The mid-summer period is particularly important, since a lack of rain for even a few days during this period may reduce maize yields. It has been observed that, in the summer rainfall region of South Africa, there is a hiatus in rainfall during mid-summer, when the baroclinic (mid-latitude cyclonic) regime in early summer switches to a dominantly barotropic (tropical) system, which is characteristic in late summer. The factors that control this switch in rainfall regimes need to be understood so that timely predictions can be made for the occurrence of short-term mid-summer dry spells. With the exception of a study by Grobler in 1993, little research has been devoted to these short-term droughts in South Africa, although a similar phenomenon, called the mid-season break, has been recognised in Zimbabwe. The aim of this project was therefore to conduct an in-depth study of the mid-summer dry spells in the major maize-growing areas in the summer rainfall region of South Africa.

PROJECT OBJECTIVES

This project is designed to build on the study of Grobler (1993) on mid-summer droughts in the summer rainfall region of South Africa. The aims of this project were as follows:

- Create a “quality checked” database of daily observed rainfall in the summer rainfall region of South Africa
- Perform a detailed temporal analysis of daily summer rainfall at different locations to identify singularities that are related to the South African mid-summer dry spells
- Perform synoptic diagnoses to identify the synoptic weather system and sea surface temperature drivers of the South African mid-summer dry spells
- Determine whether mid-summer dry-spell anomalies are captured in historical climate model simulations
- Generate climate change projections of possible future changes in the time of occurrence, frequency and intensity of the South African mid-summer dry spells
- Use a crop model to estimate the impact of the South African mid-summer dry spells on the agro-water budget and maize yields
- Produce and implement a recommended planting date early warning system for application in the agricultural sector

DATA AND METHODOLOGY

Daily district rainfall data from the South African Weather Service (SAWS)'s data bank was used to investigate mid-summer dry spells (Kruger and Nxumalo, 2017). Rainfall was measured at either individual rainfall stations or automatic weather stations (AWSs). Mid-summer dry spells occur approximately between mid-December and mid-January. The summer period is defined as the six-month period extending from October to March. From the summer rainfall region, only 16 districts with homogeneous rainfall and seasonality for the major maize-growing areas were used in this report.

From the daily district rainfall, pentad summations (totals for periods of five days) were calculated following the methodology used in Grobler (1993). Pentads were calculated using Julian days, for example, Pentad 1 refers to 1–5 January, and Pentad 73 refers to 27–31 December. The extra leap year day, 29 February, was added to Pentad 10. Eight pentads between 12 December (the start of Pentad 70) and 20 January (the end of Pentad 4) were selected for a detailed analysis of mid-summer rainfall for the major maize-growing areas of South Africa. Dry- and wet-spell analysis has been carried out using the Markov chain probability model for the threshold value of 3 mm rainfall depth per day (15 mm per pentad). A pentad with less than 15 mm rainfall was considered a dry pentad, and a pentad with 15 mm or more rainfall was considered a wet pentad. The Markov chain probability model calculates the initial probabilities of getting a dry or a wet spell for a given pentad. The calculation of conditional probabilities provides information on the dry spell, followed by a dry or wet spell, and vice versa.

A global reanalysis dataset from the European Centre for Medium-range Weather Forecasts (ECMWF), known as the Fifth Generation ECMWF Atmospheric Reanalyses of the Global Climate (ERA5) model, was used for climate circulation data (ERA5, 2019). ERA5 provides hourly estimates of many atmospheric, land and oceanic climate variables. For the analysis of the lower and mid-troposphere, two fields were obtained from the Copernicus Climate Data Store (CDS). These fields are daily 850 hPa and 500 hPa geopotential heights, measured at 00:00 coordinated universal time (UTC). Self-organising maps (SOMs) were used for the synoptic classification using the ERA5 global reanalysis dataset, and Ward's clustering technique was applied to objectively group the SOM circulation patterns into groups with similar characteristics. Climate drivers, such as the El Niño Southern Oscillation (ENSO) were also investigated to identify the synoptic weather system drivers of the South African mid-summer dry spells.

For the climate change predictions of rainfall, eight individual global circulation models (GCMs) that participated in the Fifth Phase of Coupled Model Inter-comparison Project (CMIP5) were dynamically downscaled to a finer spatial resolution ($0.44^\circ \times 0.44^\circ$) using the Rossby Centre Regional Atmospheric Model (RCA4). Daily rainfall data from these eight individual GCMs, downscaled using the RCA4 model (Coordinated Regional Climate Downscaling Experiment (CORDEX)) for the reference period (1951–2005), was used for the dry-spell analysis. The downscaled simulations from the CMIP5 GCM were evaluated against the SAWS's district observations. Model-simulated daily precipitation flux was first converted to mm using a scalar multiple of 86 400. The values nearest to the latitude and longitude of the district observations were then extracted for easy comparison with the district rainfall. Different metrics were used to assess how well the CORDEX model simulated dry spells for South Africa's summer rainfall region.

A simple water balance model was used to assess the impact of mid-summer dry spells on the agricultural water budget. The AquaCrop model was used to investigate the impact of dry spells on maize yield in the primary maize-growing regions of South Africa. A simple climatic water budget analysis was done following the methodology of Thornthwaite (1948) and Thornthwaite and Mather (1955), which uses precipitation (P) and potential or reference evapotranspiration (ET_0) to estimate moisture surplus or deficit. The Food and Agriculture Organisation (FAO)'s AquaCrop simulation model was used to estimate maize yield and investigate the impact of mid-summer dry spells on maize yield. The FAO's AquaCrop model is a water-driven simulation model (generic crop water productivity model) (Raes et al., 2018; Steduto et al., 2009).

Daily SAWS district rainfall data was used to calculate onset and cessation for each season for the respective observed and simulated (historical and future) scenarios. Onset was calculated as days since 1 September (earliest potential start of the summer season) and cessation as days since 1 February (earliest expected cessation dates) of the following year. This data was then fitted to a normal distribution curve, from which the cumulative probabilities were calculated at various confidence levels. The onset of rains was defined as the last day in which rainfall of 25 mm or above had been accumulated over the previous 10 days, and at least 20 mm accumulated in the subsequent 20 days (Tadross et al., 2009). The additional 20 mm of cumulative rainfall over the next 20 days ensured that there was enough moisture for germination and the early development stage. The cessation of the rainy season was defined as three consecutive dekads (10-day periods) with less than 20 mm rainfall each, occurring after 1 February (Tadross et al., 2009).

RESULTS AND DISCUSSION

Spatial and temporal analysis of the mid-summer dry spells for the summer rainfall region of South Africa

Dry spell frequency analyses were used to investigate the impacts of sub-seasonal rainfall variability on crop yield since seasonal rainfall totals alone do not explain the relationship between rainfall and crop yields. This study investigated the spatial and temporal occurrences of the mid-summer dry spells based on magnitude, length and time of occurrence in the major maize-growing areas of the summer rainfall region of South Africa. Three thresholds of 5 mm, 10 mm and 15 mm total rainfall for a pentad were used to analyse dry spells. Dry-spell analysis showed that dry pentads occurred during mid-summer with differing intensity, duration and frequency across the summer rainfall region. The annual frequency of dry pentads for the mid-summer period ranged between 0 and 4 pentads for the 5 mm threshold, and between 1 and 7 pentads for the 10 mm and 15 mm thresholds. The non-parametric Mann-Kendall trend analysis of the dry pentads indicates that there is no significant trend in the frequency of dry spells at a 95% confidence level. The initial and conditional probabilities of getting dry spells using the Markov chain probability model also showed that there is a 32 to 80% probability that a single pentad will be dry using the 15 mm threshold. There is a 5 to 48% probability of experiencing two consecutive dry pentads and a 1 to 29% probability of having three consecutive dry pentads. The duration and intensity of dry spells, as well as the Markov chain probabilities, showed a decrease in dry spells from west to east of the maize-growing areas of the summer rainfall region of South Africa.

Synoptic analysis of the mid-summer dry spells for the summer rainfall region of South Africa

An approach to better understand intra-seasonal rainfall characteristics is to investigate the intra-seasonal variability of daily weather circulation systems. The most common approach to synoptic climatology is to partition the atmospheric state into broad categories, and to relate these synoptic categories to some dependent variable. SOMs offer an alternative technique to synoptic climatology for visualising the complex distribution of synoptic states and for weather pattern identification. In this study, the synoptic weather systems associated with mid-summer dry spells over South Africa were investigated using SOMs and Ward's clustering technique. Climate drivers, such as ENSO, were also investigated to identify the synoptic weather system drivers of the South African mid-summer dry spells. Ward's clustering results indicate two primary weather patterns that dominate the mid-summer season, namely the strong subtropical ridge influence, and the troughs and easterly weather. The climate driver results show that ENSO has a strong influence on the mid-summer weather patterns.

Evaluation of CORDEX in simulating historical dry spells over the major maize-producing regions of South Africa

This study examined dry spells using total pentad rainfall output from historical climate model simulations using the CORDEX RCA4 model over the major maize-producing regions of South Africa. Historical observations were compared with model simulations of dry spells for the mid-summer period from 1951–2005. Generally, results indicated an underestimation of dry spells, compared to the climatologically observed values from the CORDEX models for the mid-summer period. There are, however, some regions within the study area that compare well to the observed scenario, indicating specific small-scale inadequacies to be further investigated. Investigations of upper-air tropical circulation diagnostics and the position of the Intertropical Convergence Zone (ITCZ) also clearly show that the RCA4 simulations differ from the observed scenario, indicating that large-scale upper-air circulations are not captured in the model simulations.

The impact of mid-summer dry spells on the agro-water budget and maize yield potential in the major maize-growing regions of South Africa

Water stress is one of the major limiting factors in dryland maize production in South Africa. The maize-growing season experiences different rainfall characteristics, such as dry spells, which affect the phenology and crop yields. The mid-summer period is particularly important for agriculture since a lack of rain during this period negatively affects crop yields. This study investigated the impact of South African mid-summer dry spells on the annual water budget and on maize yield. A simple water balance model was used to assess the impact of mid-summer dry spells on the agricultural water budget. The AquaCrop model was used to investigate the impact of dry spells on maize yield in the primary maize-growing regions of South Africa. The climatic water budget results showed moisture deficits for all pentads during mid-summer, with median deficits ranging from 5 to 25 mm per pentad. The highest deficit was experienced in Pentad 73 (27–31 December) and Pentad 1 (1–5 January). The warm and dry western maize-growing region has the highest total deficits (> 130 mm) during mid-summer, when compared to the cool and temperate eastern maize-growing regions. The impact of mid-summer dry spells on maize yield was also assessed using the AquaCrop model for three years with a high, medium and low frequency of dry spells. The results indicated that the impact of mid-summer dry spells on maize yield is evident, showing higher yields for the 2004/05 growing season, with a low frequency of dry spells. The 2000/01 growing season, which had a high frequency of mid-summer dry spells, produced the lowest yield. The impact of mid-summer dry spells on maize yield is more pronounced in the warm and dry western maize-growing region, showing the lowest yield when compared to the cool and temperate eastern maize-growing regions.

Guidelines and an early warning system

Planting during the recommended optimum period for an area will assist farmers to gain higher yields using favourable climatic conditions. Dry spells during the flowering stage of maize can cause yield losses. The flowering stage may vary between different cultivars of maize and the growing environment. For example, the flowering stage occurs about 65 days after emergence in medium-growing maize hybrids. Different varieties of maize are planted in the study area, and the flowering stages vary from region to region, depending on the maize cultivar used. The optimum planting dates based on the onset of rainfall, and the duration and occurrence of mid-summer dry spells, are presented in this report. The information can be used to create general guidelines and an early warning system for optimum maize planting dates for the major maize-growing regions. The occurrence and duration of mid-summer dry spells might also assist in identifying high-risk dates and avoiding water stress during the maize flowering period for the different growing regions and locations.

CONCLUSIONS

Rainfall is one of the most important factors limiting dryland crop production in South Africa. The mid-summer period is of particular significance, since a lack of rain for a few days during this period may affect crop yield considerably. In this study, dry-spell frequency analyses are used to investigate the effects of sub-seasonal rainfall variability on crop yields, since variability in seasonal rainfall totals alone do not show the relationship between rainfall and crop yields. However, little research has been dedicated to short-term drought studies in South Africa.

In this study, a dry spell was defined as a pentad with a rainfall total that is less than a predefined threshold. Three thresholds of 5 mm, 10 mm and 15 mm total rainfall for a pentad were used to analyse dry spells. In this study, the spatial and temporal occurrences of the mid-summer dry spells based on magnitude, length and time of occurrence were investigated in the summer rainfall region of South Africa. The dry-spell analysis showed that dry pentads occur during mid-summer at different intensities, duration and frequency across the maize-growing areas of the summer rainfall region. The non-parametric Mann-Kendall trend analyses for the dry pentads during mid-summer for 16 selected homogeneous rainfall districts indicate that there was no significant trend in the frequency of dry spells at the 95% significance level. Furthermore, the Markov chain probability analysis showed a decrease in the probability of dry spells from west to east in the study area. An analysis of the duration and intensity of dry spells also showed a decrease from west to east in the study area.

Ward's clustering results show that two main weather patterns dominate the mid-summer season: those associated with influences from the strong subtropical ridge and those associated with troughs and easterly weather phenomena. However, the variation within these dominant patterns seems to be the cause of a higher occurrence of dry and wet spells with the subtropical ridge patterns relating to differences in dry and wet spells over the north-east of South Africa, and the troughs and easterly weather relating to differences over the central and southern parts of South Africa. The climate driver results show that ENSO has a strong influence on the mid-summer weather patterns. Other climate drivers such as the Southern Annular Mode (SAM) and the South-West Indian Ocean show no significant influences.

This study also examined dry spells using total pentad rainfall output from historical climate model simulations using the CORDEX RCA4 model over the major maize-producing regions of South Africa. Historical observations were compared with model simulations of dry spells for the mid-summer period from 1951 to 2005. Generally, an underestimation of dry spells was detected between the modelled and observed climatological dry spell occurrences for the mid-summer period. Some regions within the study area, however, seem to capture the climatological occurrence of dry spells well, which suggests possible small-scale inadequacies in the models. This is an avenue for further investigation. The models' dry spell simulations were severely hampered by the general wet bias of the CORDEX simulations. Investigations of the upper-air tropical circulation diagnostics and the position of the ITCZ also clearly show that the RCA4 simulations are different from the observed scenarios, indicating that large-scale upper-air circulations are not captured in the model simulations.

The climatic water budget results showed that moisture deficits occurred for all the districts and pentads during mid-summer, with median deficits ranging from 5 to 25 mm per pentad. The highest deficit was experienced in Pentad 73 and Pentad 1. The impact of mid-summer dry spells on maize yield was also assessed using the AquaCrop model for three years with a high, medium and low frequency of dry spells. The results indicate that the impact of mid-summer dry spells on maize yield is evident, showing higher yields for the 2004/05 maize-growing season, with a low frequency of dry spells. The 2000/01 maize-growing season, with its high frequency of mid-summer dry spells, produced the lowest yield. The impact of mid-summer dry spells on maize yield is more pronounced in the dry and warm western maize-growing region, which shows the lowest yield compared to the cool and temperate eastern maize-growing regions.

RECOMMENDATIONS

The results of the dry-spell analyses indicated that mid-summer dry spells occurred at different intensities, duration and frequency across the maize-growing areas of South Africa's summer rainfall region. The maize-growing season experiences different rainfall characteristics, such as dry spells, which affect phenology and crop yield.

Results from this study could be used to adjust planting dates to ensure that the water-sensitive growth stages of maize do not coincide with the mid-summer dry-spell periods. In addition, soil and water conservation techniques, such as in-field rainwater harvesting, are viable options to alleviate water stress during this period in rainfed maize production. The research presented in this study contributes significantly to research on short-term drought (dry spells) in South Africa and addresses some of the research gaps in dry-spell analysis studies, which are of utmost importance for rainfed crop production. The findings from this study will assist farmers and decision makers to adjust the planting dates of summer crops to ensure favourable growing conditions during the water stress-sensitive growth stages. Information on the climatic water budget could also be used as a guide to plan supplementary irrigation during the mid-summer dry period. Databases created based on rainfall and dry-spell analyses from this study will assist future dry-spell and drought investigations and studies.

The optimum planting dates for some areas in the warm western maize-growing region are already shifting towards late December and January. Future research should focus on the analysis and characteristics of dry spells in the warm western maize-growing region and their impacts on crop yield.

CAPACITY BUILDING AND TECHNOLOGY TRANSFER

The building of research capacity was achieved by registering students at the University of KwaZulu-Natal and the University of Pretoria (Appendix A).

DATA STORAGE

All processed data has been stored on servers at the South African Weather Service:

Contact: Michael Mengistu

Email: michael.mengistu@weathersa.co.za

Enquiries: Tel: 012 367 6237

ACKNOWLEDGEMENTS

The research in this report emanated from a non-solicited project funded by the Water Research Commission (WRC) in KSA 1 and 2 (Water Resource and Ecosystems), Thrust 4 (Environmental Change and Adaptation), Programme 2 (Climate Change and Variability). The research team is sincerely grateful to the WRC for funding and managing the project. The project was managed by Dr Brilliant Petja. The research team also wishes to sincerely thank the following members of the project's reference group for their contributions and guidance:

- Dr Brilliant Petja Water Research Commission (Chairman)
- Prof Babatunde Abiodun University of Cape Town
- Dr Olivier Crespo University of Cape Town
- Dr Alistair Clulow University of KwaZulu-Natal
- Dr Mokhele Moeletsi Agricultural Research Council
- Prof Sue Walker Agricultural Research Council
- Prof Roland Schulze University of KwaZulu-Natal
- Ms Lynette Herbst Aurecon
- Prof Kingsley Ayisi University of Limpopo
- Dr Hector Chikoore North-West University

While sections of this report are author-specific, contributing authors included the following:

M.G. Mengistu^{1,2}, C. Olivier¹, A.M. Adeola^{1,4}, S. Daniel^{1,2}, K. Mathole^{1,3}, J.O. Botai^{1,2,3}, S. Landman¹, C. Engelbrecht^{1,3}, T. Makgoale¹, T. Masithela¹, H. Rautenbach⁵, J. Olivier⁶

¹ South African Weather Service, Private Bag X097, Centurion, South Africa

² School of Agricultural, Earth and Environmental Sciences, University of KwaZulu-Natal, South Africa

³ Department of Geography, Geoinformatics and Meteorology, University of Pretoria, South Africa

⁴ UP Institute for Sustainable Malaria Control, School for Health Systems and Public Health, University of Pretoria, South Africa

⁵ School of Health Systems and Public Health, Faculty of Health Sciences, University of Pretoria

⁶ Department of Environmental Sciences, University of South Africa, South Africa

TABLE OF CONTENTS

EXECUTIVE SUMMARY	i
ACKNOWLEDGEMENTS	vii
LIST OF FIGURES.....	xi
LIST OF TABLES.....	xvii
LIST OF ABBREVIATIONS.....	xix
CHAPTER 1: INTRODUCTION	1
1.1 BACKGROUND AND RATIONALE	1
1.1.1 Research aim and objectives	1
1.1.2 Structure of the report	2
CHAPTER 2: Database creation.....	3
2.1 SOUTH AFRICAN SUMMER RAINFALL REVIEW	3
2.2 DAILY RAINFALL DATA AND RAINFALL STATIONS	4
2.3 DATA FOR THE STUDY AREA.....	6
CHAPTER 3: SPATIAL AND TEMPORAL ANALYSIS OF THE MID-SUMMER DRY SPELLS FOR THE SUMMER RAINFALL REGION OF SOUTH AFRICA.....	8
3.1 ABSTRACT	8
3.2 INTRODUCTION.....	9
3.3 DATA AND METHODOLOGY.....	10
3.4 RESULTS AND DISCUSSION.....	12
3.4.1 Time series analysis of mid-summer rainfall.....	12
3.4.2 Spatial analysis of mid-summer rainfall	20
3.4.3 Impacts of dry spells on maize production.....	23
3.5 SUMMARY AND CONCLUSIONS.....	24
CHAPTER 4: SYNOPTIC ANALYSIS OF THE MID-SUMMER DRY SPELLS FOR THE SUMMER RAINFALL REGION OF SOUTH AFRICA.....	26
4.1 ABSTRACT	26
4.2 INTRODUCTION.....	27
4.3 DATA AND METHODOLOGY.....	28
4.3.1 Data sources	28
4.3.2 Methodology.....	29
4.4 RESULTS AND DISCUSSION.....	30
4.4.1 Circulation pattern classification	30
4.4.2 Relative frequency of dry spells	35
4.4.3 Influence of climate drivers	37
4.5 SUMMARY AND CONCLUSION	39

CHAPTER 5: EVALUATION OF CORDEX MODELS IN SIMULATING HISTORICAL DRY SPELLS OVER MAJOR MAIZE-PRODUCING REGIONS OF SOUTH AFRICA	40
5.1 ABSTRACT	40
5.2 INTRODUCTION.....	41
5.3 DATA AND METHODOLOGY.....	42
5.3.1 Data sources	42
5.3.1.1 The European Centre for Medium-range Weather Forecasts reanalysis	42
5.3.2 Methodology.....	44
5.4 RESULTS AND DISCUSSIONS	44
5.4.1 CORDEX model evaluation.....	44
5.4.2 Upper-air tropical circulations diagnostics and ITCZ position	47
5.5 CONCLUSIONS	52
CHAPTER 6: CLIMATE CHANGE PROJECTIONS OF THE MID-SUMMER DRY SPELLS OVER THE MAIZE-PRODUCING REGION OF SOUTH AFRICA.....	53
6.1 ABSTRACT	53
6.2 INTRODUCTION.....	54
6.3 DATA AND METHODS	55
6.3.1 Study area.....	55
6.3.2 Data and time periods	56
6.4 RESULTS AND DISCUSSIONS	57
6.4.1 Model evaluation	57
6.4.2 Dry spell projections	63
6.5 CONCLUSIONS.....	81
CHAPTER 7: THE IMPACT OF MID-SUMMER DRY SPELLS ON THE AGRO-WATER BUDGET AND MAIZE YIELD POTENTIAL IN THE MAJOR MAIZE-GROWING REGIONS OF SOUTH AFRICA	83
7.1 ABSTRACT	83
7.2 INTRODUCTION.....	84
7.3 DATA AND METHODOLOGY.....	85
7.3.1 Climatic water budget.....	85
7.3.2 Maize yield estimation.....	86
7.4 RESULTS AND DISCUSSION.....	88
7.4.1 Climatic water budget.....	88
7.4.2 Maize yield estimation using AquaCrop.....	92
7.5 SUMMARY AND CONCLUSIONS.....	96
CHAPTER 8: GUIDELINES AND EARLY WARNING SYSTEM	97
8.1 BACKGROUND.....	97
8.2 DATA AND METHODOLOGY.....	98
8.3 GUIDELINES AND EARLY WARNING SYSTEM.....	100

8.3.1 Observed and projected rainfall onset	100
8.3.2 Observed and projected rainfall cessation.....	106
8.3.3 Optimum planting dates and occurrence of mid-summer dry spells.....	111
CHAPTER 9: CONCLUSIONS AND RECOMMENDATIONS	112
9.1 CONCLUSIONS.....	112
9.2 RECOMMENDATIONS.....	113
CHAPTER 10: REFERENCES	114
APPENDIX A: Capacity Building.....	124
APPENDIX B: Onset of Summer Rainfall	126
APPENDIX C: Cessation of Summer Rainfall.....	130

LIST OF FIGURES

Figure 2.1: Maps indicating South African average rainfall totals over the period October to March. Rainfall for the entire country is given in the left map, while only areas that receive average rainfall totals of > 300 mm over the period October to March are depicted in the right map.	3
Figure 2.2: A map indicating the location of the 71 rainfall stations obtained with daily rainfall totals for the period January 1980 to December 2017. The stations are numbered according to rainfall district reference. The stations to the right of the red line receive average rainfall totals of < 300 mm over the period October to March (40 stations in total).	6
Figure 2.3: (A) A map indicating the areas in South Africa that receive at least 60% of its annual rainfall during October to March. (B) Rainfall distribution for District 62 during the mid-summer period.	7
Figure 3.1: October to March rainfall totals compared with the annual rainfall totals (1979 to 2018) using the Climate Prediction Centre (CPC)'s unified gauge-based analysis of global daily precipitation.....	11
Figure 3.2: (A) Rainfall districts for South Africa with provincial borders (SAWB, 1972), showing the 16 selected districts with red polygons. (B) A map showing maize-growing areas (AgWeb, 2015).	11
Figure 3.3: Rainfall seasonality for four different maize-growing regions of South Africa. The black line is the median; the box covers the first and third quantile (25 th and 75 th percentiles); the whiskers are 1.5 times the interquartile range; and the dots are outliers outside this range.	13
Figure 3.4: Pentad rainfall distributions for the 16 district rainfall regions contained within the revised study area. The black line is the median; the box covers the first and third quantile (25 th and 75 th percentiles); whiskers are 1.5 times the interquartile range; and the dots are outliers outside this range.	14
Figure 3.5: Pentad anomaly frequency below average thresholds of 5 mm, 10 mm and 15 mm for eight pentads in December and January, covering the four different maize-growing regions of South Africa	15
Figure 3.6: The number of pentads below average thresholds of 5 mm, 10 mm and 15 mm for the eight pentads in December and January (1985–2015) covering South Africa's four different maize-growing regions.....	16
Figure 3.7: The mean episode of dry spells during mid-December and mid-January using a threshold value of 15 mm for the period 1985–2015	21
Figure 3.8: The standard deviation of the episode of dry spells during mid-December and mid-January using a threshold value of 15 mm for the period 1985–2015.....	21
Figure 3.9: The mean maximum duration of dry pentads during mid-December and mid-January using a threshold value of 15 mm for the period 1985–2015	22
Figure 3.10: The standard deviation of the maximum duration of dry pentads during mid-December and mid-January using a threshold value of 15 mm for the period 1985–2015.....	23

Figure 4.1: District rainfall regions in South Africa (a), and the rainfall occurrence during the four main seasons, Dec-Jan-Feb (DJF) (b), Mar-Apr-May (MAM) (c), Jun-Jul-Aug (JJA) (d) and Sep-Oct-Nov (SON) (e). The size of the black dots is scaled to the relative rainfall received in each season. 29

Figure 4.2: A 7 x 5 matrix output from the SOM indicating the normalised circulation patterns for the period 1979–2018 (850 hPa shaded and 500 hPa contour). The percentage of occurrence per node is also indicated. 31

Figure 4.3: The number of occurrences (y-axis) per month (x-axis), indicating the annual cycle per node 32

Figure 4.4: The average ERA5 geopotential heights (850 hPa shaded and 500 hPa contour) per node 33

Figure 4.5: The eight clusters from the 35 SOM nodes identified by Ward’s clustering indicated in red boxes surrounding the matching nodes 33

Figure 4.6: The 850 hPa circulation patterns per node for the mid-summer period (12 December to 20 January). The number of days of the possible 1 400 days per node is indicated above each node. Clustered patterns A to H indicate clusters identified by Ward’s clustering system (Figure 4.5). 34

Figure 4.7: Relative frequencies of dry (< 15 mm, left) and wet (> 30 mm, right) spells during mid-summer pentads for Region 74 (as an example). Node frequencies ordered according to their total relative occurrence (bold black line). 35

Figure 4.8: Relative frequency difference of dry (< 15 mm) and wet (> 30 mm) spells during mid-summer pentads for nodes 34 (left) and 35 (right). Coloured dot size is scaled first by mid-summer rainfall totals, and then by the magnitude of the difference between the dry and the wet spells. 36

Figure 4.9: Relative frequency difference of dry (< 15 mm) and wet (> 30 mm) spells during mid-summer pentads for nodes 27 (left) and 28 (right). Coloured dot size is scaled first by mid-summer rainfall totals, and then by the magnitude of the difference between the dry and the wet spells. 36

Figure 4.11: Relative frequency difference of dry (< 15 mm) and wet (> 30 mm) spells during mid-summer pentads for nodes 13 (left) and 14 (right). Coloured dot size is scaled first by mid-summer rainfall totals, and then by the magnitude of the difference between the dry and the wet spells. 37

Figure 4.12: Node correlations with ENSO Niño 3.4 SSTs. The numbers in the cells indicate the nodes. They have a similar structure to previous node figures, with * indicating the significance level (* = 90%; ** = 95%; *** = 99%). Shading indicates the correlation values. 38

Figure 4.13: Node correlations with the SAM Index. The numbers in the cells indicate the nodes. They have a similar structure to previous node figures, with * indicating the significance level (* = 90%; ** = 95%; *** = 99%). Shading indicates the correlation values. 38

Figure 4.14: Node correlations with SWIO. The numbers in the cells indicate the nodes. They have a similar structure to previous node figures, with * indicating the significance level (* = 90%; ** = 95%; *** = 99%). Shading indicates the correlation values. 39

Figure 5.1: District rainfall regions in South Africa (SAWB, 1972), showing the study area with 16 selected districts marked with red polygons 43

Figure 5.2: Probability density functions for the eight CORDEX models (red) and observed (black) dry spell occurrences during mid-summer for districts 60, 61, 62 and 72. There are a maximum of eight pentads in the mid-summer period. 45

Figure 5.3: Probability density functions for the eight CORDEX models (red) and observed (black) dry spell occurrences during mid-summer for districts 63, 73, 74 and 75 46

Figure 5.4: Probability density functions for the eight CORDEX models (red) and observed (black) dry spell occurrences during mid-summer for districts 83, 84, 85 and 91 46

Figure 5.5: Probability density functions for the eight CORDEX models (red) and observed (black) dry spell occurrences during mid-summer for districts 86, 87, 92 and 93 47

Figure 5.6: Early summer months' climatology of the velocity potential in ERA5 and the three models of CORDEX-Africa. Climatology-based period: 1979–2005. Contour intervals are $0.5 \times 10^7 \text{ m}^2\text{s}^{-1}$ 48

Figure 5.7: The late winter to spring months' climatology of the velocity potential in ERA5 and the three CORDEX-Africa models. Climatology-based period: 1979–2005. Contour intervals are $0.5 \times 10^7 \text{ m}^2\text{s}^{-1}$ 49

Figure 5.8: Zonal mean velocity potential field for the corresponding VP CORDEX region as shown in Figure 5.1. Red stars serve as the estimate for the location of the ITCZ. Latitudes have been limited from 30° N to 30° S for defining the region of the tropics. 50

Figure 5.9: ITCZ location standardised index for different months (i.e. October to March) 51

Figure 5.10: Correlation between the November ITCZ position and November–December rainfall for all 94 districts. Districts where correlation is significant at the 95% level of confidence are indicated with red stars. 51

Figure 6.1: Map of South Africa showing (A) October to March rainfall totals compared with annual rainfall totals (1979 to 2019) using a CPC unified gauge-based analysis of global daily precipitation, and (B) the maize-growing areas (Maize Belt) of South Africa 55

Figure 6.2: Comparison between the observed number of consecutive dry days for October to March from ERA5 (the first column) and the associated multi-model mean consecutive dry days simulated by the RCA4 RCM (the middle column) for the period 1979–2005. The mean bias between the observed scenario and the simulated number of consecutive dry days is indicated by the maps in the third column. A dry spell is computed for more than five consecutive days with rainfall less than 1 mm (first row), 2 mm (second row) and 3 mm (third row). 58

Figure 6.3: Comparison between the observed number of consecutive dry days for December to January from ERA5 (the first column) and associated multi-model mean consecutive dry days simulated by the RCA4 RCM (the middle column) for the period 1979–2005. The mean bias between the observed scenario and the simulated number of CDDs is indicated by the maps in the third column. A dry spell is computed for more than five consecutive days with rainfall less than 1 mm (first row), 2 mm (second row) and 3 mm (third row). 59

Figure 6.4: ERA 5 comparison between the observed pentads' total rainfall and multi-model mean simulated totals for pentads 68, 69 and 70 in terms of total precipitation (mm) for the period 1979–2005 60

Figure 6.5: ERA 5 comparison between the observed pentads' total rainfall and multi-model mean simulated totals for pentads 71, 72 and 73 in terms of total precipitation (mm) for the period 1979–2005 61

Figure 6.6: ERA 5 comparison between the observed pentads' total rainfall and multi-model mean simulated totals for pentads 1, 2 and 3 in terms of total precipitation (mm) for the period 1979–2005 62

Figure 6.7: ERA 5 comparison between the observed pentads' total rainfall and multi-model mean simulated totals for pentads 4, 5 and 6 in terms of total precipitation (mm) for the period 1979–2005 63

Figure 6.8: Projected number of consecutive dry days for summer (October to March) over the summer rainfall areas of South Africa using a precipitation threshold of 1 mm for the periods 2036–2065 (top left) and 2066–2095 (top right) under the conditions of RCP4.5, and 2036–2065 (bottom left) and 2066–2095 (bottom right) under the conditions of RCP8.5. A dry spell is defined as more than five consecutive days with less than 1 mm of rainfall. 64

Figure 6.9: Projected number of consecutive dry days for summer (October to March) over the summer rainfall areas of South Africa using a precipitation threshold of 2 mm for the periods 2036–2065 (top left) and 2066–2095 (top right) under the conditions of RCP4.5, and 2036–2065 (bottom left) and 2066–2095 (bottom right) under the conditions of RCP8.5. A dry spell is defined as more than five consecutive days with less than 2 mm of rainfall. 65

Figure 6.10: Projected number of consecutive dry days for summer (October to March) over the summer rainfall areas of South Africa using a precipitation threshold of 3 mm for the periods 2036–2065 (top left) and 2066–2095 (top right) under the conditions of RCP4.5, and 2036–2065 (bottom left) and 2066–2095 (bottom right) under the conditions of RCP8.5. A dry spell is defined as more than five consecutive days with less than 3 mm of rainfall. 66

Figure 5.11: Projected number of consecutive dry days for mid-summer (December to January) over the summer rainfall areas of South Africa using a precipitation threshold of 1 mm for the periods 2036–2065 (top left) and 2066–2095 (top right) under the conditions of RCP4.5, and 2036–2065 (bottom left) and 2066–2095 (bottom right) under the conditions of RCP8.5. A dry spell is defined as more than five consecutive days with less than 1 mm of rainfall. 67

Figure 6.12: Projected number of consecutive dry days for mid-summer (December to January) over the summer rainfall areas of South Africa using a precipitation threshold of 2 mm for the periods 2036–2065 (top left) and 2066–2095 (top right) under the conditions of RCP4.5, and 2036–2065 (bottom left) and 2066–2095 (bottom right) the under conditions of RCP8.5. A dry spell is defined as more than five consecutive days with less than 2 mm of rainfall. 68

Figure 6.13: Projected number of consecutive dry days for mid-summer (December to January) over the summer rainfall areas of South Africa using a precipitation threshold of 3 mm for the periods 2036–2065 (top left) and 2066–2095 (top right) under the conditions of RCP4.5, and 2036–2065 (bottom left) and 2066–2095 (bottom right) under the conditions of RCP 8.5. A dry spell is defined as more than five consecutive days with less than 3 mm of rainfall 69

Figure 6.14: Projected total precipitation (mm) for Pentad 1 (1–5 January for the periods 2036–2065 (top left) and 2066–2095 (top right) under the conditions of RCP4.5, and 2036–2065 (bottom left) and 2066-2095 (bottom right) under the conditions of RCP8.5 70

Figure 6.15: Projected total precipitation (mm) for Pentad 2 (6–10 January) for the periods 2036–2065 (top left) and 2066–2095 (top right) under the conditions of RCP4.5, and 2036–2065 (bottom left) and 2066–2095 (bottom right) under the conditions of RCP8.5 71

Figure 6.16: Projected total precipitation (mm) for Pentad 3 (11–15 January) for the periods 2036–2065 (top left) and 2066–2095 (top right) under the conditions of RCP4.5, and 2036–2065 (bottom left) and 2066–2095 (bottom right) under the conditions of RCP8.5 72

Figure 6.17: Projected total precipitation (mm) for Pentad 4 (16– 20 January) for the periods 2036–2065 (top left) and 2066–2095 (top right) under the conditions of RCP4.5, and 2036–2065 (bottom left) and 2066–2095 (bottom right) under the conditions of RCP8.5 73

Figure 6.18: Projected total precipitation (mm) for Pentad 5 (21–25 January) for the periods 2036–2065 (top left) and 2066–2095 (top right) under the conditions of RCP4.5, and 2036–2065 (bottom left) and 2066–2095 (bottom right) under the conditions of RCP8.5 74

Figure 6.19: Projected total precipitation (mm) for Pentad 6 (26–30 January) for the periods 2036–2065 (top left) and 2066–2095 (top right) under the conditions of RCP4.5, and 2036–2065 (bottom left) and 2066–2095 (bottom right) under the conditions of RCP8.5 75

Figure 6.20: Projected total precipitation (mm) for Pentad 68 (2–6 December) for the periods 2036–2065 (top left) and 2066–2095 (top right) under the conditions of RCP4.5, and 2036–2065 (bottom left) and 2066–2095 (bottom right) under the conditions of RCP8.5 76

Figure 6.21: Projected total precipitation (mm) for Pentad 69 (7–11 December) for the periods 2036–2065 (top left) and 2066–2095 (top right) under the conditions of RCP4.5, and 2036–2065 (bottom left) and 2066–2095 (bottom right) under the conditions of RCP8.5 77

Figure 6.22: Projected total precipitation (mm) for Pentad 70 (12–16 December) for the periods 2036–2065 (top left) and 2066–2095 (top right) under the conditions of RCP4.5, and 2036–2065 (bottom left) and 2066–2095 (bottom right) under the conditions of RCP8.5 78

Figure 6.23: Projected total precipitation (mm) for Pentad 71 (17–21 December) for the periods 2036–2065 (top left) and 2066–2095 (top right) under the conditions of RCP4.5, and 2036–2065 (bottom left) and 2066–2095 (bottom right) under the conditions of RCP8.5 79

Figure 6.24: Projected total precipitation (mm) for Pentad 72 (22–26 December) for the periods 2036–2065 (top left) and 2066–2095 (top right) under the conditions of RCP4.5, and 2036–2065 (bottom left) and 2066–2095 (bottom right) under the conditions of RCP8.5 80

Figure 6.25: Projected total precipitation (mm) for Pentad 73 (27 –31 December) for the periods 2036–2065 (top left) and 2066–2095 (top right) under the conditions of RCP4.5, and 2036–2065 (bottom left) and 2066–2095 (bottom right) under the conditions of RCP8.5 81

Figure 7.1: (A) Rainfall districts for South Africa with provincial borders (SAWB, 1972), showing the 16 selected districts with red polygons. (B) A map showing the major maize-growing regions with optimum planting dates (Source: Grain SA and Agbiz Research)..... 85

Figure 7.2: Mean climatic total pentad rainfall distribution (A) and evapotranspiration (ET_0) distribution (B) for District 62 within the cool eastern maize-growing region of South Africa..... 88

Figure 7.3: Mean climatic total pentad rainfall distribution (A) and evapotranspiration (ET_o) distribution (B) for District 74 within the temperate eastern maize-growing region of South Africa 89

Figure 7.4: Mean climatic total pentad rainfall distribution (A) and evapotranspiration (ET_o) distribution (B) for District 84 within the warm and dry western maize-growing region of South Africa 89

Figure 7.5: Mid-summer climatic water budget ($P - ET_o$) distribution for District 62 within the cool eastern maize-growing region of South Africa. The black line is the median, the box covers the first and third quantiles (25th and 75th percentiles), the whiskers are 1.5 times the interquartile range and the dots are outliers outside this range. 90

Figure 7.6: Mid-summer climatic water budget ($P - ET_o$) distribution for District 74 within the temperate eastern maize-growing region of South Africa. The black line is the median, the box covers the first and third quantiles (25th and 75th percentiles), the whiskers are 1.5 times the interquartile range and the dots are outliers outside this range. 90

Figure 7.7: Mid-summer climatic water budget ($P - ET_o$) distribution for District 84 within the warm, dry western maize-growing region of South Africa. The black line is the median, the box covers the first and third quantiles (25th and 75th percentiles), the whiskers are 1.5 times the interquartile range and the dots are outliers outside this range. 91

Figure 7.8: Pentad anomaly frequency below average thresholds of 5 mm, 10 mm and 15 mm for the eight mid-summer pentads in December and January for District 62 in the cool eastern maize-growing region of South Africa 92

Figure 7.9: Pentad anomaly frequency below average thresholds of 5 mm, 10 mm and 15 mm for the eight mid-summer pentads in December and January for District 74 in the temperate eastern maize-growing region of South Africa 93

Figure 7.10: Pentad anomaly frequency below average thresholds of 5 mm, 10 mm and 15 mm for the eight mid-summer pentads in December and January for District 84 in the warm, dry western maize-growing region of South Africa 93

Figure 7.11: AquaCrop maize crop growth simulation for District 62 showing rainfall, canopy cover and transpiration, and root zone water depletion for the 2000/01 maize- growing season 94

Figure 8.1: Maize growth stages (PANNAR, 2016) 98

Figure 8.2: Rainfall districts for South Africa with provincial borders (SAWB, 1972), showing the 16 selected districts with red polygons 99

Figure 8.3: A map showing South Africa’s maize-growing areas (AgWeb, 2015) 99

Figure 8.4: The cumulative probability of rainfall onset for regions 62 and 86 using the daily SAWS rainfall district data and climate change projections 101

Figure 8.5: The cumulative probability of rainfall cessation for regions 62 and 86 using the daily SAWS rainfall district data and climate change projections 106

LIST OF TABLES

Table 2.1: The station numbers and names, as well as positions (latitude and longitude: see Figure 2.2) of the 71 rainfall stations for which daily rainfall data was obtained. The associated rainfall district numbers are also indicated. The stations in green shaded boxes were defined as those that receive average rainfall totals of > 300 mm over the period October to March (40 stations in total).	4
Table 3.1: The non-parametric Mann-Kendall test of dry pentads using three thresholds for 16 homogeneous rainfall districts for the mid-summer period (1985 to 2015)	15
Table 3.2: Markov chain probability results for the 16 rainfall districts in the study area for the mid-summer period (1985–2015) using a threshold value of 3 mm rainfall per day (15 mm per pentad). (A) Probability for a single dry pentad – P_D . (B) Probability for a dry pentad given the previous pentad being dry – P_{DD} . (C) Probability of two consecutive pentads being dry, starting with the pentad – 2D. (D) Probability of three consecutive pentads being dry starting with the pentad – 3D.	17
Table 4.1: Seasonal circulation patterns based on Ward's clustering	32
Table 4.2: Percentage of days per node for the mid-summer period (12 December to 20 January) ...	34
Table 5.1: List of global circulation models used in the study.....	43
Table 6.1: Projections from eight global climate models used for downscaling to a finer spatial resolution (0.4° x 0.4°) using the RCA4 regional climate model.....	56
Table 7.1: The length of the district climate dataset used for the water budget and yield analysis.....	86
Table 7.2: The range of planting density and planting dates for the three major maize-growing areas of South Africa.....	87
Table 7.3: Summary of the climatic water budget ($P - ET_0$) for all the districts in the study area during mid-summer	91
Table 7.4: AquaCrop maize yield estimates ($t\ ha^{-1}$) using three recommended planting dates and three years of varying dry-spell frequencies for District 62 in the cool eastern maize-growing region of South Africa... ..	95
Table 7.5: AquaCrop maize yield estimates ($t\ ha^{-1}$) using three recommended planting dates and three years of varying dry-spell frequencies for District 74 in the temperate eastern maize-growing region of South Africa.....	95
Table 7.6: AquaCrop maize yield estimates ($t\ ha^{-1}$) using three recommended planting dates and three years of varying dry-spell frequencies for District 84 in the warm, dry western maize-growing region of South Africa.....	95
Table 8.1: Probability of rainfall onset for the study site using daily SAWS rainfall district data from 1979 to 2014. Probability indicates onset to occur on or before the listed dates.	102
Table 8.2: Probability of rainfall onset for the study site using daily CORDEX historical data from 1976 to 2005. Probability indicates onset to occur on or before the listed dates.	102
Table 8.3: Probability of rainfall onset for the study site using daily CORDEX data for RCP4.5 from 2006 to 2035. Probability indicates onset to occur on or before the listed dates.	103

Table 8.4: Probability of rainfall onset for the study site using daily CORDEX data for RCP4.5 from 2036 to 2065. Probability indicates onset to occur on or before the listed dates. 103

Table 8.5: Probability of rainfall onset for the study site using daily CORDEX data for RCP4.5 from 2066 to 2095. Probability indicates onset to occur on or before the listed dates. 104

Table 8.6: Probability of rainfall onset for the study site using daily CORDEX data for RCP8.5 from 2006 to 2035. Probability indicates onset to occur on or before the listed dates. 104

Table 8.7: Probability of rainfall onset for the study site using daily CORDEX data for RCP8.5 from 2036 to 2065. Probability indicates onset to occur on or before the listed dates. 105

Table 8.8: Probability of rainfall onset for the study site using daily CORDEX data for RCP8.5 from 2066 to 2095. Probability indicates onset to occur on or before the listed dates. 105

Table 8.9: Probability of rainfall cessation for the study site using daily SAWS rainfall district data from 1979 to 2014. Probability indicates cessation to occur on or before (after February) the listed dates. 107

Table 8.10: Probability of rainfall cessation for the study site using daily historical CORDEX data from 1976 to 2005. Probability indicates cessation to occur on or before (after February) the listed dates. 107

Table 8.11: Probability of rainfall cessation for the study site using daily CORDEX data from 2006 to 2035 for RCP4.5. Probability indicates cessation to occur on or before (after February) the listed dates. 108

Table 8.12: Probability of rainfall cessation for the study site using daily CORDEX data from 2036 to 2065 for RCP4.5. Probability indicates cessation to occur on or before (after February) the listed dates. 108

Table 8.13: Probability of rainfall cessation for the study site using daily CORDEX data from 2066 to 2095 for RCP4.5. Probability indicates cessation to occur on or before (after February) the listed dates. 109

Table 8.4: Probability of rainfall cessation for the study site using daily CORDEX data from 2006 to 2035 for RCP8.5. Probability indicates cessation to occur on or before (after February) the listed dates. 109

Table 8.15: Probability of rainfall cessation for the study site using daily CORDEX data from 2036 to 2065 for RCP8.5. Probability indicates cessation to occur on or before (after February) the listed dates. 110

Table 8.16: Probability of rainfall cessation for the study site using daily CORDEX data from 2066 to 2095 for RCP8.5. Probability indicates cessation to occur on or before (after February) the listed dates. 110

Table 8.17: Optimum planting dates based on the cumulative probability (> 80%) of onset and high-risk dates with consecutive dry pentads during mid-summer. High-risk mid-summer dates are based on the Markov chain dry-spell probability analysis..... 111

LIST OF ABBREVIATIONS

AOGCM	Atmosphere-Ocean Global Climate Model
AR5	Fifth Assessment Report
AWS	Automatic Weather Station
CC	Canopy Ground Cover
CDD	Consecutive Dry Days
CDS	Climate Data Store (Copernicus)
CGCM	Global Coupled Ocean-atmosphere General Circulation Model
CMIP5	Fifth Phase of Coupled Model Inter-comparison Project
CORDEX	Coordinated Regional Climate Downscaling Experiment
CPC	Climate Prediction Centre
DD	Duration of Dry Spells
DSSAT	Decision Support System for Agrotechnology Transfer
ECMWF	European Centre for Medium-range Weather Forecast
ENSO	El Niño Southern Oscillation
EP	Episode of Dry Spells
ERA5	Fifth generation ECMWF Atmospheric Reanalyses of the Global Climate
ET _o	Reference Evapotranspiration
FAO	Food and Agriculture Organisation
GCM	Global Circulation Model
GHG	Greenhouse Gas
GPCC	Global Precipitation Climatology Centre
HI	Harvest Index
IPCC	Intergovernmental Panel on Climate Change
ITCZ	Intertropical Convergence Zone
LAI	Leaf Area Index
NOAA	National Oceanic and Atmospheric Administration
NWP	Numerical Weather Prediction

P	Precipitation
PCA	Principal Component Analysis
PDF	Probability Density Function
RCA4	Rosby Centre Regional Atmospheric Model
RCM	Regional Climate Model
RCP	Representative Concentration Pathway
SAM	Southern Annular Mode
SAST	South African Standard Time
SAWS	South African Weather Service
SMA	Simple Multi-model Averaging
SOM	Self-organising Maps
SST	Sea Surface Temperature
STD	Standard Deviation
SWIO	South-West Indian Ocean
TTT	Tropical Temperate Trough
UTC	Coordinated Universal Time
VP	Velocity Potential
Y	Crop Yield

CHAPTER 1: INTRODUCTION

1.1 BACKGROUND AND RATIONALE

South Africa is a semi-arid country with mean annual rainfall totals of below 500 mm (Taljaard, 1996). Southern Africa's summer rainfall experiences significant variability, with frequent recurrent wet and dry spells and severe droughts (Richard et al., 2001). Drought is a natural phenomenon that occurs when there is a temporal imbalance of water availability due to a persistent lower-than-average precipitation over a certain period of time (Pereira et al., 2009). Several studies in the past have focused on the occurrence, intensity, impact and prediction of drought on an annual and a seasonal basis. However, short-term droughts (dry spells) are equally vital to the agricultural sector, as the timing of the occurrence and intensity of the dry period is often more important than seasonal shortfalls in rainfall. Usman and Reason (2004) highlighted that a season with above-average rainfall may not be better than a below-average season over an agricultural region if the rainfall during the season is not well distributed in space and time. In other words, crops are more likely to do well with evenly distributed rains than with intermittent heavy showers interrupted by prolonged dry periods (Usman and Reason, 2004). Various crops, such as maize, are vulnerable to drought during specific phenological stages (Tadross et al., 2009; Mupangwa et al., 2011). Water stress is one of the major limiting factors in dryland (rain-fed) agriculture. Its effects include stunted growth, delayed maturity and low crop productivity (Mzezewa et al., 2010). The flowering stage of maize has been found to be the most sensitive stage to water stress, for example, leading to reductions in crop growth, biomass production and finally yield (Du Plessis, 2003; Masupha et al., 2016). Planting dates should be selected accordingly to ensure that the flowering stage coincides with normally favourable climatic conditions, and not with mid-summer drought periods (Du Plessis, 2003).

Rainfall has been identified as the most pressing and significant factor limiting dryland crop production in South Africa. The mid-summer period is of particular importance since a lack of rain for even a few days during this period may decrease crop yield. It has been observed that, in the summer rainfall region of southern Africa, there is a break in rainfall during mid-summer when the baroclinic (mid-latitude cyclonic) regime in early summer switches to a dominantly barotropic (tropical) system, characteristic of late summer (Bhalotra, 1984). Apart from a study by Grobler (1993), very little research has been devoted to short-term drought in South Africa, although a similar phenomenon, called the mid-season break, has been recognised in Zimbabwe (Unganai and Mason, 2002).

In this study, a thorough analysis is conducted on the characteristics of mid-summer dry spells in South Africa. The research required high-quality rainfall data, which was obtained from the South African Weather Service's data network, which made the investigation of the frequency, intensity and duration of mid-summer dry spells in the summer rainfall areas of South Africa possible. The research included an investigation into the ability of climate models to capture these mid-summer dry spells, as well as a synoptic weather system analysis, in an effort to identify the atmospheric forcing that drives such droughts. The AquaCrop water productivity model was used to simulate the impact of mid-summer dry spells on maize yield. Lastly, guidelines and an early warning system were developed, which can be used for selecting optimum maize planting dates for the major maize-growing regions in South Africa.

1.1.1 Research aim and objectives

The overall aim of this project was to conduct an in-depth study of the mid-summer dry spells in the major maize-growing areas in the summer rainfall region of South Africa. The specific objectives of this project were to do the following:

- Create a "quality checked" database of daily observed rainfall in the summer rainfall region of South Africa
- Perform a detailed temporal analysis on daily summer rainfall at different locations to identify singularities that are related to the South African mid-summer dry spells
- Perform synoptic diagnoses in order to identify the synoptic weather system and sea surface temperature drivers of the South African mid-summer dry spells
- Determine whether mid-summer dry-spell anomalies are captured in historical climate model simulations
- Generate climate change projections of possible future changes in the time of occurrence, frequency and intensity of the South African mid-summer dry spells
- Use a crop model to estimate the impact of the South African mid-summer dry spells on the agro-water budget and maize yields
- Produce and implement a recommended planting date early warning system for application in the agricultural sector

1.1.2 Structure of the report

Over the duration of the project, eight deliverables were completed to address the aim and various project objectives. These deliverables were combined into this final report, consisting of five sections written in the format of a scientific paper. The remaining three sections address database creation, guidelines and an early warning system, and a report on a communication workshop that was held.

CHAPTER 2: DATABASE CREATION

2.1 SOUTH AFRICAN SUMMER RAINFALL REVIEW

The austral summer season, during which the mid-summer dry spells occur between approximately late December and early January, is defined as the six-month period that extends from October to March. In preparation for the research on mid-summer dry spells, the South African summer rainfall was reviewed to define the area that receives average rainfall totals of > 300 mm over the summer season. Only rainfall data across this area is considered in the research on mid-summer dry spells that follows.

For this purpose, long-term monthly rainfall averages, calculated across the reference period from 1981 to the near-present, were obtained from the Global Precipitation Climatology Centre (GPCC) (Schneider et al., 2016; Becker et al., 2013).

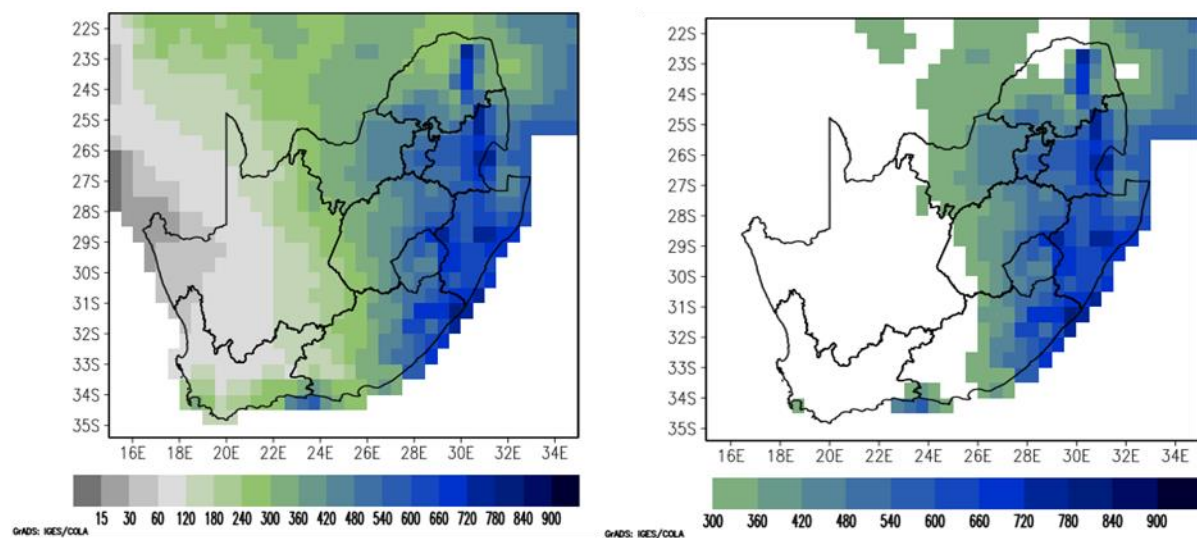


Figure 2.1: Maps indicating South African average rainfall totals over the period October to March. Rainfall for the entire country is given in the left map, while only areas that receive average rainfall totals of > 300 mm over the period October to March are depicted in the right map.

A map illustrating the South African average rainfall totals over the period October to March is depicted in Figure 2.1 (left). Total rainfall averages vary from as low as 15 mm in the far north-west, to higher than 840 mm in the mountainous areas in the eastern parts of the country. The higher summer rainfall is well captured across the eastern parts of the country (in blue), with some higher rainfall that is also experienced in the confined southern year-rainfall region (the southern border between the Western Cape and the Eastern Cape).

Areas that receive average rainfall totals of > 300 mm over the period October to March are depicted in Figure 2.1 (right) – defined as the study area. This area is confined to the eastern parts of South Africa, and includes most of Limpopo, most of the North West, most of the Free State, approximately half of the Eastern Cape, Gauteng, Mpumalanga and KwaZulu-Natal. The research will only consider this study area in analysing the influence of mid-summer dry spells on South Africa's agro-water budget and subsequent crop growth and yield.

2.2 DAILY RAINFALL DATA AND RAINFALL STATIONS

Since the mid-summer dry spells occur over a relatively short period (an average of one to two weeks), daily rainfall data was obtained from the SAWS's data bank. The rainfall was measured at either individual manual rainfall stations or automatic weather stations. As mentioned in Kruger and Nxumalo (2017), measurements at manual stations were done at 08:00 South Africa Standard Time (SAST) and represent the accumulated rainfall over the preceding 24 hours, while AWS data represents the total rainfall accumulated over the period between 08:00 SAST during the previous day up to 08:00 SAST on the current day. Only stations that were operational throughout the study period were selected, with at least 90% of daily values available. However, stations where zero rainfall was recorded over relatively long time periods, while surrounding stations recorded significant rainfall amounts, were flagged and removed.

The 71 stations for which data was obtained are listed in Table 2.1, where the rainfall district reference number, station number, station name and station position (latitude and longitude) are given. Although the stations cover the entire country, stations that received average rainfall totals of > 300 mm over the period October to March are shaded in green (40 stations in total). Data for the rest of South Africa will be kept aside for the possible interest of additional analysis in the area outside the study domain.

Table 2.1: The station numbers and names, as well as positions (latitude and longitude: see Figure 2.2) of the 71 rainfall stations for which daily rainfall data was obtained. The associated rainfall district numbers are also indicated. The stations in green shaded boxes were defined as those that receive average rainfall totals of > 300 mm over the period October to March (40 stations in total).

	District	Station number	Station name	Latitude	Longitude
1	1	0244405 5	Steinkopf	-29.27	17.74
2	2	0133202 2	Nieuwoudtville SAPD	-31.37	19.12
3	3	0062444 7	Piketberg-SAPD	-32.91	18.75
4	4	0022038 8	Vrugbaar	-33.63	19.04
5	5	0086007 4	Reenen	-32.11	19.51
6	6	0045184 2	Dwars in die Weg	-33.07	20.62
7	7	0003020 4	Cape Agulhas	-34.83	20.02
8	8	0027302 1	Calitzdorp – POL	-33.53	21.69
9	9	0048043 2	Prince Albert – TNK	-33.22	22.03
10	10	0029542 X	Roorivier	-33.55	22.82
11	11	0014063 4	Knysna – TNK	-34.05	23.05
12	12	0052590 5	Steytlerville – MAG	-33.33	24.34
13	13	0057048A9	Grahamstown – TNK	-33.32	26.49
14	16	0068010 3	Merweville – POL	-32.66	21.52
15	17	0049372 3	Rondawel	-33.20	22.66
16	19	0113673 X	Saaifontein	-31.72	21.88
17	20	0093074 X	Kamferskraal	-32.24	23.05
18	21	0073871 1	Kendrew Estates	-32.52	24.48
19	22	0076884 3	Albertvale – FRM	-32.74	26.01
20	25	0240891 0	Durban – Botanical Gardens	-29.85	31.01
21	26	0272121 2	Gingindhlovu	-29.03	31.57
22	27	0101192 X	Exwell Park	-32.21	27.10
23	28	0126082 4	Nkobongo	-31.87	28.04
24	30	0239482 0	Cedara	-29.54	30.27
25	31	0337795 0	Mahlabatini	-28.24	31.46
26	33	0596179 3	Skukuza	-24.99	31.59
27	38	0166238A6	Carnarvon – POL	-30.97	22.13

	District	Station number	Station name	Latitude	Longitude
28	39	0142805 X	Richmond C/K – TNK	-31.42	23.94
29	40	0096101 0	Roodebloem	-32.18	24.57
30	41	0120338 5	Tafelberg Hall	-31.56	25.19
31	42	0149204 3	Dordrecht Clarks Siding	-31.41	27.12
32	44	0334174 6	Moorside	-28.40	29.61
33	45	0372852 9	Hlobane	-27.70	30.98
34	46	0444203 6	Tafelkoppies	-26.88	30.62
35	47	0555567 2	Alkmaar	-25.45	30.82
36	49	0679164 3	Letaba District	-23.73	30.10
37	50	0722721 3	Hanglip	-23.02	29.92
38	52	0284008 4	Thornlea	-28.63	21.52
39	53	0253174 2	Marydale – POL	-29.41	22.11
40	54	0142153 5	Lekkervlei	-31.05	23.60
41	55	0145399 0	Grapevale	-31.15	25.23
42	56	0174600 4	Burgersdorp – POL	-31.00	26.33
43	57	0203657 9	Middelplaats	-30.45	26.87
44	60	0368831 1	Warden Skoolstraat	-27.85	28.96
45	61	0369505 9	Verkykerskop	-27.91	29.27
46	62	0443196 2	De Emigratie	-26.77	30.10
47	63	0517430 6	Machadodorp	-25.67	30.25
48	64	0678144 2	Kalkfontein	-23.90	29.58
49	68	0254589 8	Niekerkshoop – POL	-29.33	22.84
50	69	0227127 X	Hopetown	-29.62	24.08
51	70	0231279 9	Reddersburg – POL	-29.65	26.17
52	71	0232018 3	Cyferfontein	-29.80	26.52
53	72	0263280 X	Westminster Estate	-29.16	27.17
54	73	0402866 5	Driefontein	-27.44	28.00
55	74	0476040 3	Johannesburg – Zoological Gardens	-26.17	28.04
56	75	0477762 5	Witbank Strehla	-26.21	28.91
57	76	0590307 7	Nylsvley	-24.65	28.67
58	77	0675182 9	Villa Nora – POL	-23.53	28.13
59	79	0356285 4	Hopkins	-27.71	22.70
60	80	0359808 X	Boetsap	-27.97	24.45
61	81	0257845 5	Eureka	-29.08	24.48
62	82	0261722 8	Maselspoort Dam	-29.03	26.41
63	83	0329215 5	Ventersburg – MAG	-28.09	27.14
64	84	0434888 3	Ottosdal – POL	-26.81	26.00
65	85	0510308 6	Swartruggens – POL	-25.65	26.69
66	86	0588721 5	Rankins Pass – POL	-24.53	27.91
67	89	0468318 4	Vryburg Palmyra	-26.27	24.18
68	90	0432136 3	Vryburg Welgeleven	-26.76	24.58
69	92	0508649 3	Slurry	-25.81	25.85
70	93	0546314 1	Tuscany	-25.24	26.18
71	94	0423044 6	Rietfontein SAPS	-26.74	20.03

2.3 DATA FOR THE STUDY AREA

A map, depicting the distribution of the stations listed in Table 2.1, is given in Figure 2.2, where stations are numbered according to district rainfall reference. The red line separates the stations that receive average rainfall totals of > 300 mm over the period October to March on the right (defined as the study area) and the associated stations that receive < 300 mm of rain on the left. In an effort to further improve on the study area selection, a map is presented in Figure 2.3A, showing the percentage of total rainfall during the six summer months of October to March. The area where at least 60% of the annual rainfall occurs between October to March was further regarded as a priority area in the investigation of mid-summer dry spells. An example of rainfall distribution for District 62, indicating dry spells with rainfall less than 15 mm per pentad during the mid-summer period (pentads 70–73 and pentads 1–4) is shown in Figure 2.3B.

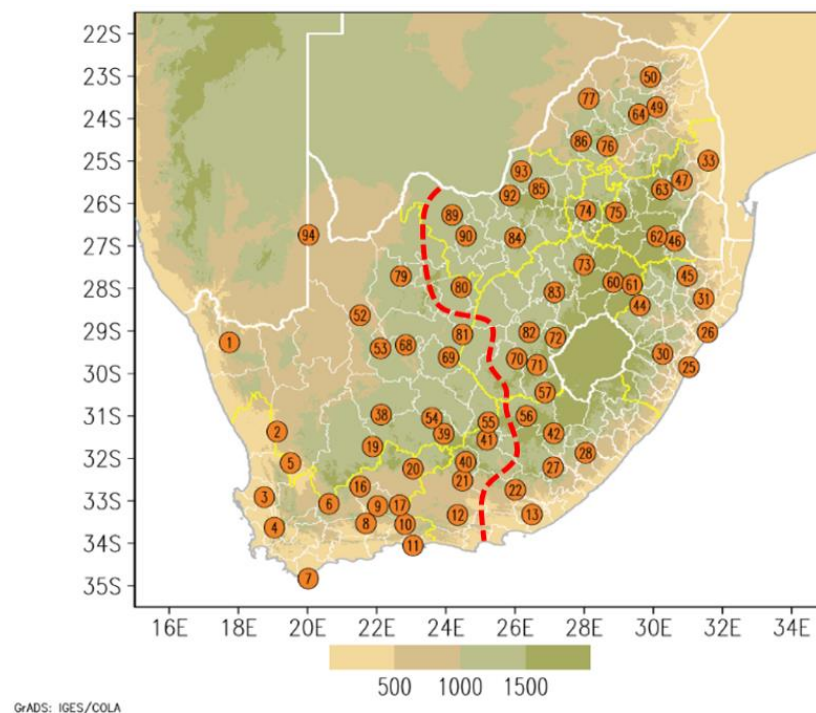


Figure 2.2: A map indicating the location of the 71 rainfall stations obtained with daily rainfall totals for the period January 1980 to December 2017. The stations are numbered according to rainfall district reference. The stations to the right of the red line receive average rainfall totals of < 300 mm over the period October to March (40 stations in total).

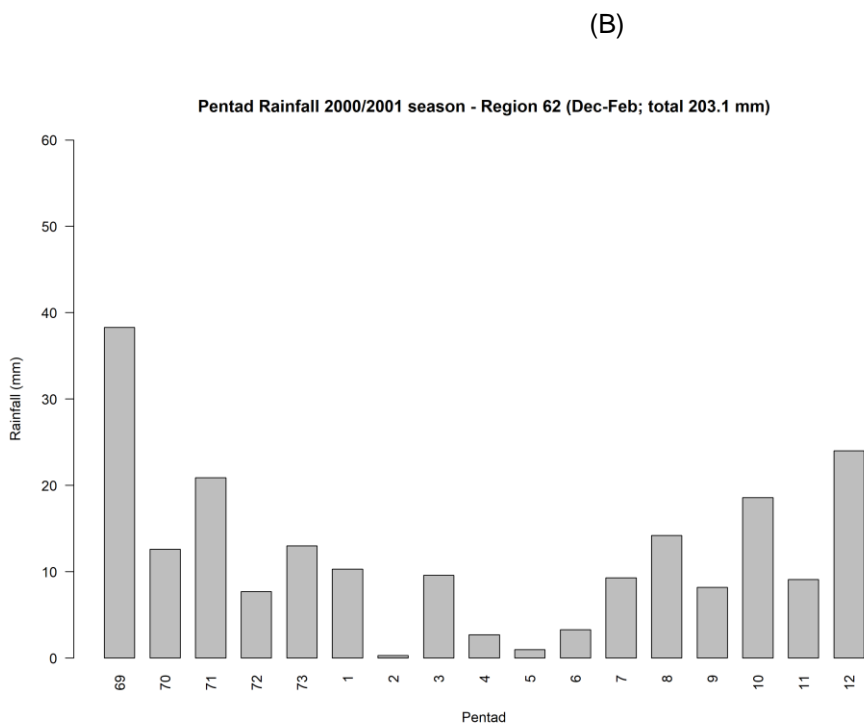
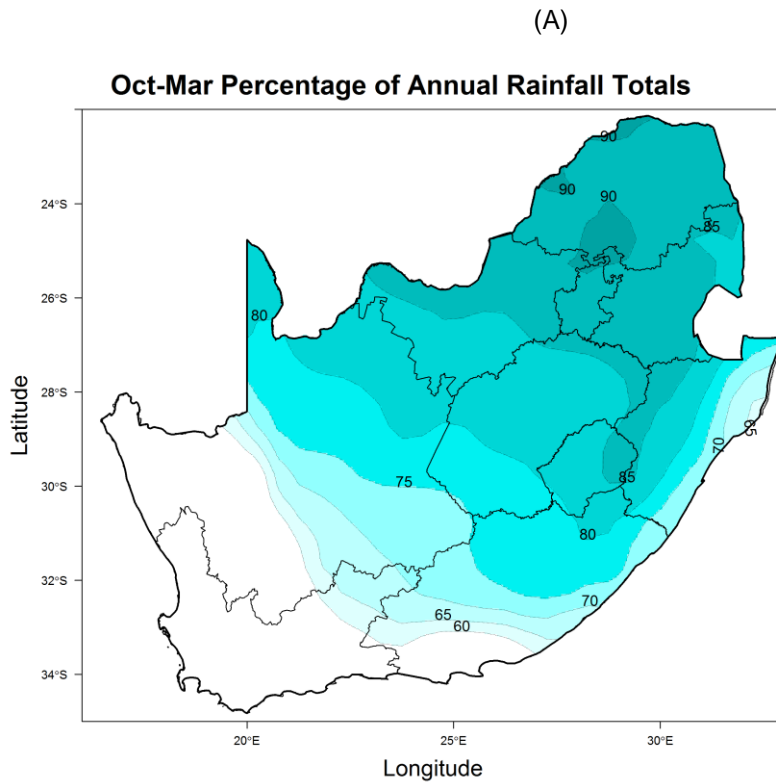


Figure 2.3: (A) A map indicating the areas in South Africa that receive at least 60% of its annual rainfall during October to March. (B) Rainfall distribution for District 62 during the mid-summer period.

CHAPTER 3: SPATIAL AND TEMPORAL ANALYSIS OF THE MID-SUMMER DRY SPELLS FOR THE SUMMER RAINFALL REGION OF SOUTH AFRICA

3.1 ABSTRACT

South Africa is frequently subjected to severe droughts and dry spells during the rainy season. Yet, rainfall is one of the most significant factors limiting dryland crop production in South Africa. The mid-summer period is particularly important for agriculture since a lack of rain during this period negatively affects crop yield. Dry-spell frequency analyses are used to investigate the impacts of sub-seasonal rainfall variability on crop yield since seasonal rainfall totals alone do not explain the relationship between rainfall and crop yield. In this study, the spatial and temporal occurrences of mid-summer dry spells are investigated, based on magnitude, length and time of occurrence in the major maize-growing areas of the summer rainfall region of South Africa. Three thresholds of 5 mm, 10 mm and 15 mm total rainfall for a pentad were used to analyse the dry spells. Dry-spell analysis showed that dry pentads occur during mid-summer with different intensities, duration and frequency across the summer rainfall region. The annual frequency of dry pentads for the mid-summer period ranged between 0 and 4 pentads for the 5 mm threshold, and 1 to 7 pentads for the 10 mm and 15 mm thresholds. The non-parametric Mann-Kendall trend analysis of the dry pentads indicates that there is no significant trend in the frequency of dry spells at a 95% confidence level. The initial and conditional probabilities of getting a dry spell using the Markov chain probability model showed that there is a 32 to 80% probability that a single pentad will be dry using the 15 mm threshold. There is a 5 to 48% probability of experiencing two consecutive dry pentads, and a 1 to 29% probability of having three consecutive dry pentads. The duration and intensity of dry spells, as well as the Markov chain probabilities, showed a decrease in the number of dry spells from west to east across the maize-growing areas in South Africa's summer rainfall region.

Keywords: Pentad rainfall; mid-summer; dry spells; Markov chain model; South Africa

3.2 INTRODUCTION

South Africa is a semi-arid country with a mean annual rainfall of below 500 mm (Taljaard, 1996). In most parts of South Africa, rainfall occurs during the austral summer months of October to March (Harrison, 1984; Hart et al., 2010). The most significant increase in rainfall over the summer rainfall region starts in September along the south-east and east coast, from where it spreads to the eastern interior during October, extending to the western interior from October to November (Taljaard, 1986). In December, a break in the rising rainfall occurs over parts of the summer rainfall region (Taljaard, 1986). Other distinct rainfall regions over South Africa are located along the southern coast of the country, where rainfall occurs all year round (Engelbrecht et al., 2014), as well as in the south-western region, which receives the majority of its rain during the austral winter months (Reason et al., 2002).

Southern Africa's summer rainfall experiences significant rainfall variability, with recurrent wet and dry spells and severe droughts (Richard et al., 2001). Drought is a natural phenomenon that occurs when there is a temporal imbalance of water availability due to a persistent lower-than-average precipitation over a certain period of time (Pereira et al., 2009). Several studies in the past have focused on the occurrence, intensity, impact and prediction of drought on an annual and seasonal basis. However, short-term drought (a dry spell) is equally vital to the agricultural sector, as the timing of the occurrence and intensity of the dry period is more important to plant growth than seasonal shortfalls in rainfall. Usman and Reason (2004) highlighted that a season with above-average rainfall may not be better than a below-average season over an agricultural region if the rainfall during the season is not well distributed in space and time. Crops are likely to grow better with evenly distributed rains than with intermittent heavy showers, interrupted by prolonged dry periods (Usman and Reason, 2004). Various crops, such as maize, are vulnerable to drought during specific phenological stages (Tadross et al., 2009; Mupangwa et al., 2011). Water stress is one of the major limiting factors in dryland (rain-fed) agriculture. Its effects include stunted growth, delayed maturity and low crop productivity (Mzezewa et al., 2010). The flowering stage of maize has been found to be the most sensitive to water stress, for example, leading to reductions in crop growth, biomass production and, finally, yield (Du Plessis, 2003; Masupha et al., 2016). Therefore, planting dates should be chosen to ensure that the flowering stage of maize coincides with normally favourable growing conditions, and not with mid-summer drought periods (Du Plessis, 2003).

Rainfall has been identified as the most pressing and significant factor limiting dryland (rain-fed) crop production in South Africa. The mid-summer period is particularly important since a lack of rain for even a few days during this period may decrease crop yield. Variability in seasonal rainfall totals alone may not explain the relationship between rainfall and crop yield, hence dry spell frequency analyses are used globally to investigate the implications of sub-seasonal rainfall variability on food security (Usman and Reason, 2004). Dry spells are defined as extended periods with no rainfall within a rainy season (Ngetich et al., 2014). Studies in semi-arid environments in sub-Saharan Africa have indicated that dry spells range between five and 15 days (Usman and Reason, 2004). It has been observed that, in the summer rainfall region of southern Africa, there is a break in rainfall during mid-summer when the baroclinic (mid-latitude cyclonic) regime in early summer switches to a dominantly barotropic (tropical) system, characteristic of late summer (Bhalotra, 1984). Apart from a study by Grobler (1993), little research has been devoted to short-term drought in South Africa, although a similar phenomenon, called the mid-season break, has been recognised in Zimbabwe (Unganai and Mason, 2002).

The rainfall time series is characterised by periods of wetness (wet spells) and dryness (dry spells). Therefore, a threshold for defining wet and dry days is required when analysing wet or dry rainfall spells, since the frequency distribution of the length of the spells is dependent on the selected threshold (Bärring et al., 2006). Different thresholds have been used internationally based on the aspect of the spells that needed to be considered.

Moon et al. (1994) and Martin-Vide and Gomez (1999) have used 0.1 mm per day; Frei et al. (2003), Douguedroit (1987), and Usman and Reason (2004) have used a threshold of 1.0 mm in daily precipitation; Perzyna (1994) used a threshold of 2.0 mm per day; and Ceballos et al. (2004) have used a threshold of 10 mm in daily rainfall for wet- and dry-spell analysis. In addition, Reddy (1990) used a threshold of 3 mm per day, which is the minimum rainfall depth threshold value for crops to satisfy their crop water requirement during a growing season.

In this study, a dry spell is defined as a period of five days (a pentad) during which rainfall totals are less than the predefined thresholds. In this study, three thresholds of 5 mm, 10 mm and 15 mm rainfall for a pentad were used to analyse dry spells. The study aims to perform a detailed spatial and temporal analysis of the occurrence of the mid-summer dry spells based on magnitude, and length and time of occurrence in South Africa's summer rainfall region.

3.3 DATA AND METHODOLOGY

Daily rainfall data from the South African Weather Service's data bank was used to investigate mid-summer dry spells. Rainfall was either measured at individual manual rainfall stations or automatic weather stations. As mentioned in Kruger and Nxumalo (2017), measurements at manual stations were done at 08:00 SAST, and represent the accumulated rainfall over the preceding 24 hours, while AWS data represents the total rainfall accumulated over the period between 08:00 SAST during the previous day to 08:00 SAST on the current day. Only stations that were operational throughout the study period were selected, with at least 90% of daily values available. In cases where zero rainfall was recorded for relatively long periods, while the surrounding stations recorded significant rainfall amounts, the data was flagged and removed (Kruger and Nxumalo, 2017).

Mid-summer dry spells occur between approximately late December and early January. The austral summer period is defined as the six-month period extending from October to March. A map illustrating the South African average rainfall totals, expressed as percentages, over the period October to March (1979–2018) is depicted in Figure 3.1. Climatological rainfall totals from October to March were calculated and related, as a percentage, to the annual rainfall totals (defined here as June to May to capture the full period from October to March). The study area receives 80% or more of its total annual rainfall in the period between October and March, as shown in Figure 3.1. Parts of the eastern coastal areas still receive significant rainfall during these months. However, they also receive rainfall during winter and spring, lowering the overall percentage for October to March (NCAR, 2018). From the summer rainfall region, which receives most of its rain between October and March (Figure 3.1), only 16 districts (Figure 3.2A) with homogeneous rainfall and seasonality (Kruger, 2011) from the maize-growing areas (Figure 3.2B) were used for further analysis. From the daily district rainfall (Kruger and Nxumalo, 2017), pentad summations were calculated, following the methodology used in Grobler (1993). Pentads were calculated using Julian days. For example, Pentad 1 refers to 1–5 January, while Pentad 73 refers to 27–31 December. The extra leap year day, 29 February, was added to Pentad 10. Eight pentads between 12 December (the start of Pentad 70) and 20 January (the end of Pentad 4) were selected for a detailed analysis of the mid-summer rainfall across the study area.

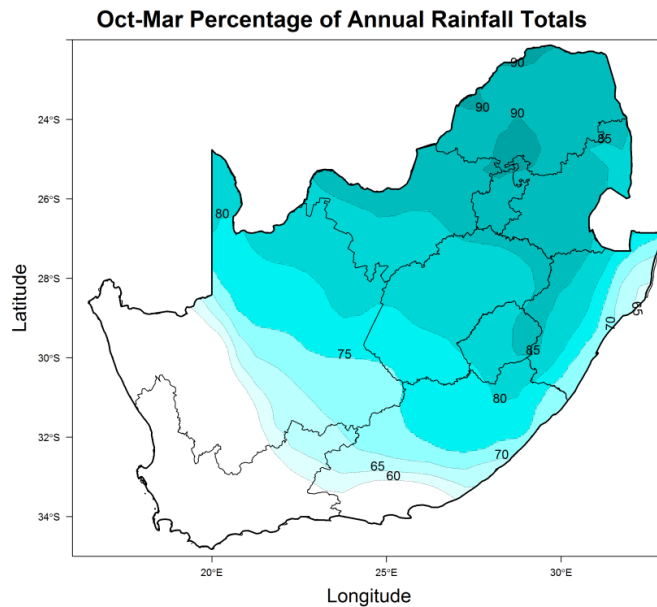


Figure 3.1: October to March rainfall totals compared with the annual rainfall totals (1979 to 2018) using the Climate Prediction Centre (CPC)'s unified gauge-based analysis of global daily precipitation

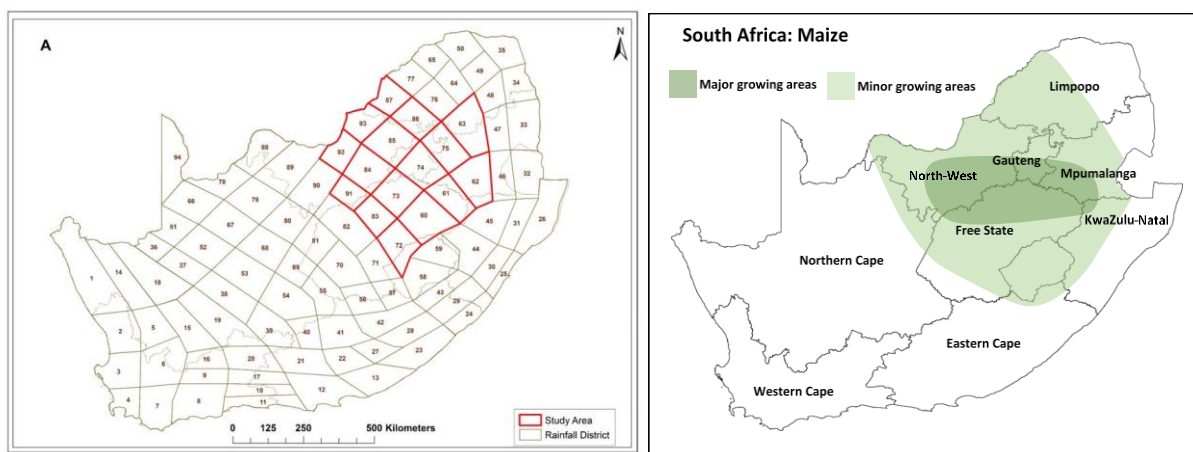


Figure 3.2: (A) Rainfall districts for South Africa with provincial borders (SAWB, 1972), showing the 16 selected districts with red polygons. (B) A map showing maize-growing areas (AgWeb, 2015).

A dry- and wet-spell analysis was carried out using the Markov chain probability model for the threshold value of 3 mm rainfall depth per day (15 mm per pentad). A pentad with less than 15 mm rainfall was considered a dry pentad, while a pentad with 15 mm or more rainfall was considered a wet pentad. The Markov chain probability model calculates the initial probabilities of getting a dry or wet spell for a given pentad. The calculation of conditional probabilities provides information on the dry spell, followed by a dry or wet spell, and vice versa. The calculation of initial and conditional probabilities is given below.

Initial probability:

$$P_D = F_D/N \tag{1}$$

$$P_W = F_W/N \tag{2}$$

Conditional probabilities:

$$P_{DD} = F_{DD}/F_D \quad (3)$$

$$P_{WW} = F_{WW}/F_W \quad (4)$$

$$P_{DW} = 1 - P_{WW} \quad (5)$$

Consecutive dry and wet pentad probabilities

$$2D = PDp1PDDp2 \quad (6)$$

$$2W = PWp1PWWp2 \quad (7)$$

$$3D = PDp1PDDp2 PDDp3 \quad (8)$$

$$3W = PWp1PWWp2 PWWp3 \quad (9)$$

where P_D is the probability of the pentad being dry; P_W is the probability of the pentad being wet; N is the number of years of data; F_D is the number of dry pentads; F_W is the number of wet pentads; P_{DD} is the probability of a dry pentad preceded by a dry pentad; P_{WW} is the probability of a wet pentad preceded by a wet pentad; P_{DW} is the probability of a dry pentad preceded by a wet pentad; F_{DD} is the number of dry pentads preceded by another dry pentad; F_{WW} is the number of wet pentads preceded by another wet pentad; $2D$ is the probability of two consecutive dry pentads starting with a particular pentad; $2W$ is the probability of two consecutive wet pentads starting with the pentad; $3D$ is the probability of three consecutive dry pentads starting with the pentad; $3W$ is the probability of three consecutive wet pentads starting with the pentad; P_{Dp1} is the probability of the pentad being dry (first pentad); P_{DDp2} is the probability of the second pentad being dry, given the preceding pentad being dry; P_{DDp3} is the probability of the third pentad being dry, given the preceding pentad being dry; P_{Wp1} is the probability of the pentad being wet (first pentad); P_{WWp2} is the probability of the second pentad being wet, given the preceding pentad being wet; and P_{WWp3} is the probability of the third pentad being wet, given the preceding pentad being wet.

3.4 RESULTS AND DISCUSSION

3.4.1 Time series analysis of mid-summer rainfall

Long-term mean monthly rainfall totals were plotted to investigate the seasonality and rainfall variability for all selected districts across the summer rainfall region. Results have indicated that the district rainfall plots exhibited austral summer rainfall seasonality with mean monthly rainfalls peaking in December. Examples of the plots are presented in Figure 3.3, showing rainfall seasonality for four districts covering different maize-growing regions of South Africa's summer rainfall areas.

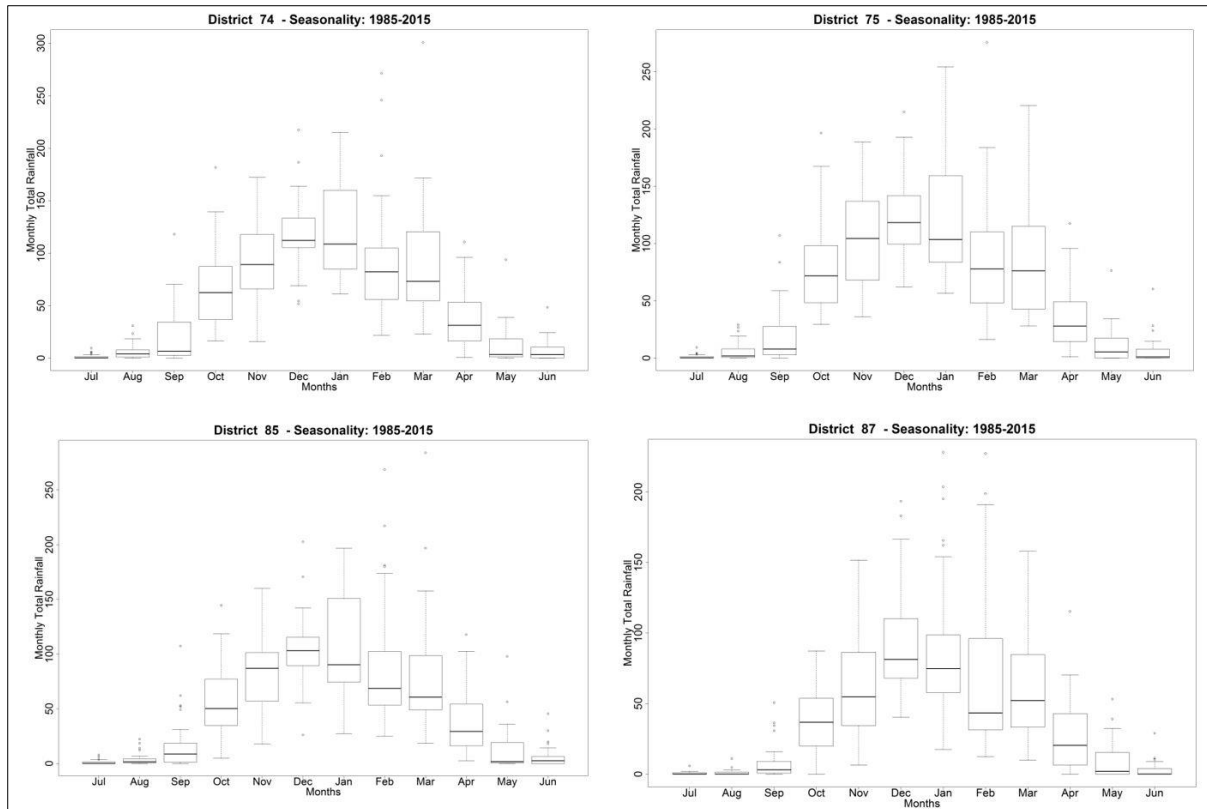


Figure 3.3: Rainfall seasonality for four different maize-growing regions of South Africa. The black line is the median; the box covers the first and third quantile (25th and 75th percentiles); the whiskers are 1.5 times the interquartile range; and the dots are outliers outside this range.

Most studies of mid-summer dry spells evaluate an existing climatological dry period within a typical summer season (Bhalotra, 1984; Karnauskas et al., 2013; Perdigón-Morales et al., 2018). During this relatively dry period, precipitation is reduced by up to 40%, and constitutes a clear signal of the bimodal nature of the summer precipitation (Perdigón-Morales et al., 2018). However, this does not seem to be the case for the summer rainfall region of central South Africa.

Pentad rainfall distributions for the 16 district rainfall regions contained within the study area are presented in Figure 3.4. Pentad rainfall distributions are clearly skewed towards the higher rainfall totals. This is a common feature with sub-monthly rainfall totals (e.g. days and weeks, or in this case, pentads). Rainfall totals for months and seasons tend to be less skewed compared to sub-monthly rainfall totals. This justifies the reason for defining dry periods with thresholds for the dry-spell analysis.

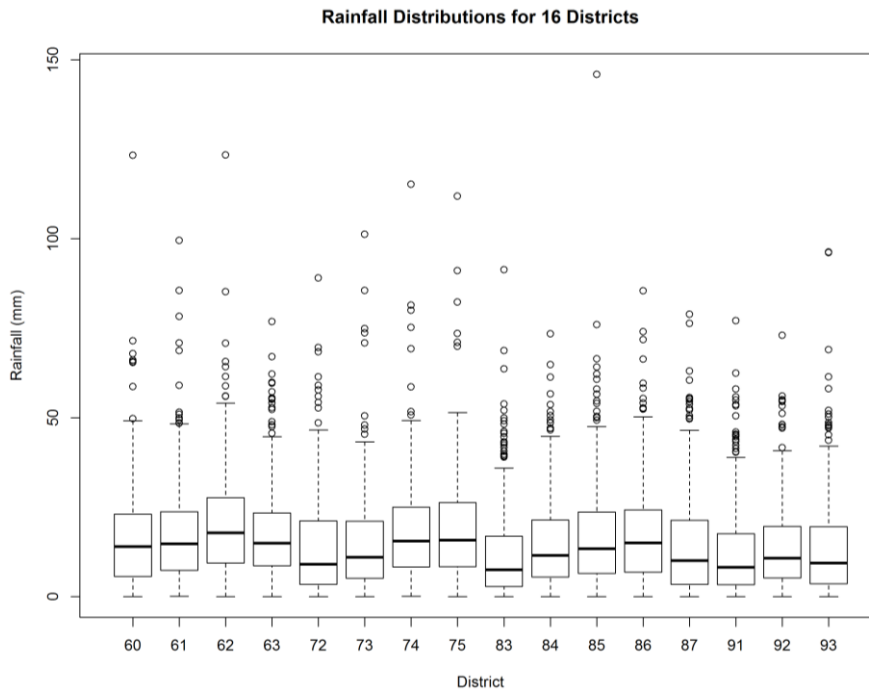


Figure 3.4: Pentad rainfall distributions for the 16 district rainfall regions contained within the revised study area. The black line is the median; the box covers the first and third quartile (25th and 75th percentiles); whiskers are 1.5 times the interquartile range; and the dots are outliers outside this range.

The total pentad rainfall for eight pentads in December and January was analysed to investigate the deviation from the climatological average of the number of dry pentads during the mid-summer period. Anomalies of dry pentad frequency are presented in Figure 3.5, using the three thresholds for the period 1985 to 2015. Negative values indicate fewer dry pentads, and positive values indicate more dry pentads during the mid-summer period. Anomalies of dry pentad frequency plots for the four districts covering the different maize-growing regions of the summer rainfall areas of South Africa are shown in Figure 3.5. The non-parametric Mann-Kendall trend test analysis was performed to investigate trends in the frequency of dry spells during the mid-summer period (Hipel and McLeod, 1994; Libiseller and Grimvall, 2002). The trend analysis results for the 16 districts are presented in Table 3.1 for the dry pentads during the mid-summer using the three thresholds. Results indicate that there is no significant trend in the frequency of dry spells at a 95% confidence level. However, District 61 showed a decrease in 15 mm pentad rainfall totals at a 92% confidence level. Districts 86 and 91 have also shown a decrease in 5 mm pentad rainfall totals at 92% and 93% confidence levels, respectively.

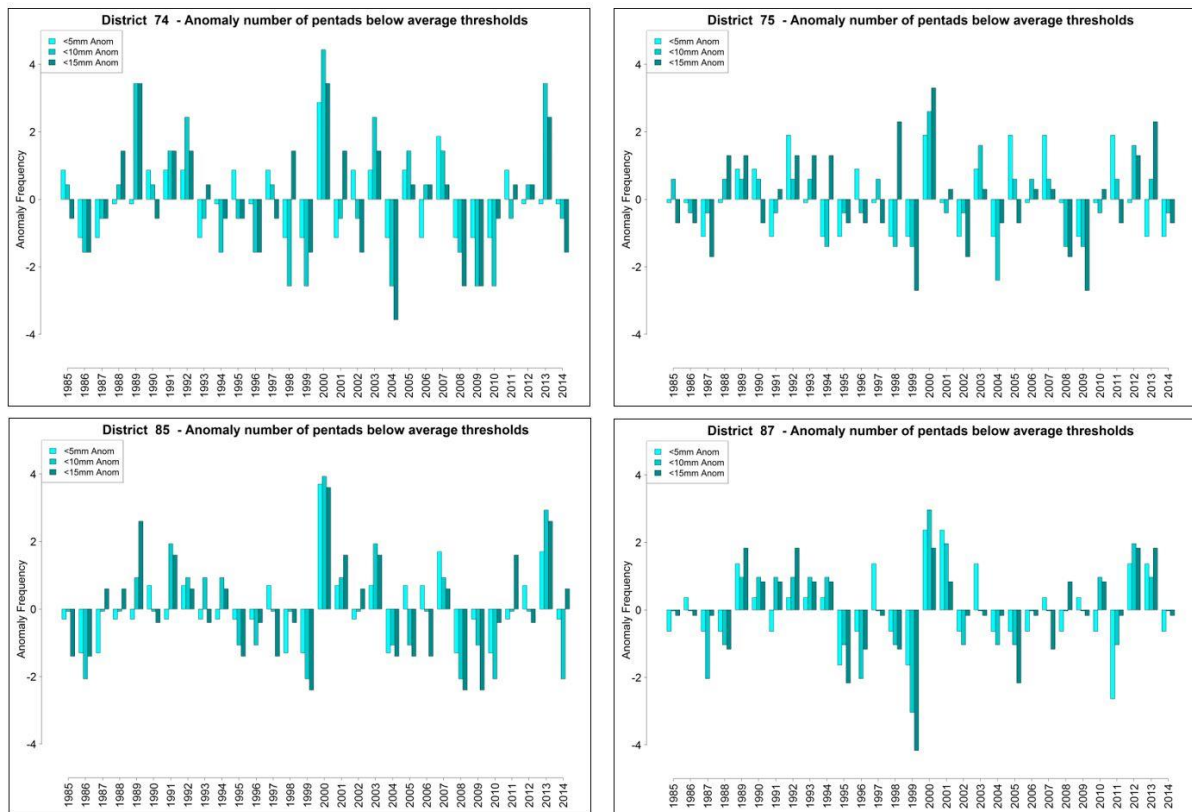


Figure 3.5: Pentad anomaly frequency below average thresholds of 5 mm, 10 mm and 15 mm for eight pentads in December and January, covering the four different maize-growing regions of South Africa

Box plots of annual frequencies of dry pentads during the mid-summer (December to January) using the three thresholds of 5 mm, 10 mm and 15 mm are presented in Figure 3.6. The bands inside the box plots show the medians and the ends of the whiskers (vertical lines), representing the minimum and maximum number of dry pentads. The number of dry pentads was higher for District 87 compared to districts 74, 75 and 85 (as shown in Figure 3.6), indicating more dry pentads for all three thresholds for the 30-year period.

Table 3.1: The non-parametric Mann-Kendall test of dry pentads using three thresholds for 16 homogeneous rainfall districts for the mid-summer period (1985 to 2015)

District	Thresholds					
	> 5 mm		> 10 mm		> 15 mm	
	Z-statistic	Attained significance level	Z-statistic	Attained significance level	Z-statistic	Attained significance level
60	-1.17	76%	-0.68	50%	-0.65	48%
61	-0.64	48%	-0.39	30%	-1.73	92%
62	0.06	5%	0.00	0%	0.91	63%
63	0.19	15%	-0.63	47%	-0.53	40%
72	-1.38	83%	-0.13	10%	-0.50	38%
73	0.00	0%	0.33	26%	0.35	28%
74	-0.25	19%	-0.56	43%	-0.64	48%

District	Thresholds					
	> 5 mm		> 10 mm		> 15 mm	
	Z-statistic	Attained significance level	Z-statistic	Attained significance level	Z-statistic	Attained significance level
75	-0.11	9%	-0.09	8%	- 0.15	12%
83	-1.24	79%	-1.31	81%	-0.75	55%
84	-0.02	1%	0.24	19%	-0.43	33%
85	1.21	77%	-0.86	61%	-0.13	10%
86	-1.76	92%	-1.43	85%	-0.57	43%
87	-0.02	2%	0.46	36%	0.24	19%
91	-1.81	93%	-0.62	47%	-0.50	38%
92	-0.17	13%	0.39	30%	0.53	40%
93	-1.18	76%	-0.45	35%	-0.67	50%

The Markov chain probability model was used for dry-spell analysis using a threshold value of 3 mm rainfall per day (15 mm per pentad), as presented in Table 3.2. A pentad with less than 15 mm rainfall was considered a dry pentad. The Markov chain probability model calculates the initial probabilities of getting a dry spell (P_D); the conditional probabilities of a dry spell followed by dry spell (P_{DD}); and two ($2D$) and three ($3D$) consecutive dry spells. Climatologically, districts 72, 83 and 93 have a higher likelihood of having consecutive dry spells than the other regions. Consecutive dry spells also seem more likely to occur during Pentad 73 and Pentad 1. These results are in agreement with the findings of Grobler (1993), which reported mid-summer dry spells for the study area that lasted on average seven to 14 days, occurring typically at the end of December and the beginning of January.

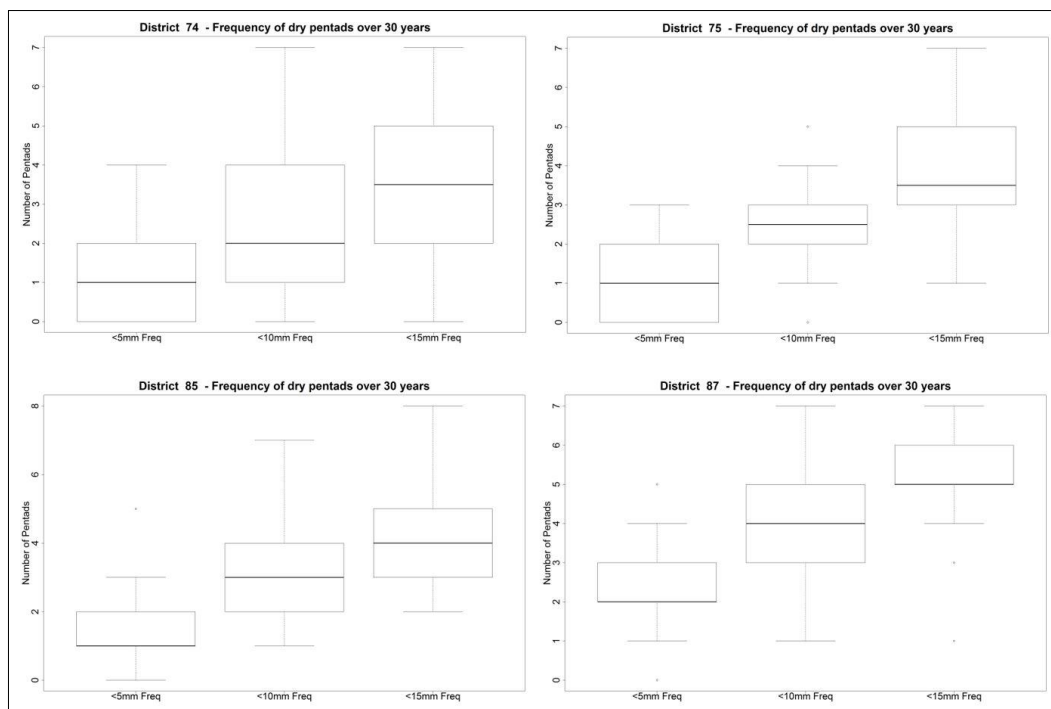


Figure 3.6: The number of pentads below average thresholds of 5 mm, 10 mm and 15 mm for the eight pentads in December and January (1985–2015) covering South Africa's four different maize-growing regions

Table 3.2: Markov chain probability results for the 16 rainfall districts in the study area for the mid-summer period (1985–2015) using a threshold value of 3 mm rainfall per day (15 mm per pentad). (A) Probability for a single dry pentad – P_D . (B) Probability for a dry pentad given the previous pentad being dry – P_{DD} . (C) Probability of two consecutive pentads being dry, starting with the pentad – 2D. (D) Probability of three consecutive pentads being dry starting with the pentad – 3D.

(A) P_D

District	Pentad							
	70	71	72	73	1	2	3	4
60	51.60	45.20	38.70	61.30	61.30	51.60	61.30	54.80
61	38.70	51.60	38.70	51.60	58.10	48.40	58.10	48.40
62	38.70	41.90	35.50	45.20	51.60	32.30	45.20	32.30
63	45.20	41.90	29.00	54.80	64.50	41.90	71.00	51.60
72	77.40	67.70	54.80	61.30	71.00	64.50	51.60	51.60
73	64.50	54.80	45.20	67.70	67.70	67.70	64.50	58.10
74	41.90	45.20	29.00	41.90	51.60	48.40	61.30	41.90
75	51.60	45.20	29.00	45.20	51.60	48.40	54.80	45.20
83	77.40	64.50	45.20	74.20	77.40	71.00	74.20	67.70
84	58.10	58.10	51.60	54.80	67.70	51.60	71.00	48.40
85	48.40	61.30	48.40	61.30	71.00	45.20	61.30	41.90
86	45.20	54.80	38.70	41.90	58.10	48.40	64.50	48.40
87	64.50	61.30	54.80	71.00	74.20	51.60	67.70	67.70
91	71.00	67.70	58.10	67.70	71.00	58.10	80.60	67.70
92	71.00	61.30	64.50	61.30	77.40	54.80	71.00	54.80
93	67.70	64.50	64.50	71.00	74.20	61.30	58.10	51.60

(B) P_{DD}

District	Pentad							
	70	71	72	73	1	2	3	4
60	29.00	22.60	25.80	25.80	33.30	35.50	29.00	35.50
61	22.58	19.35	25.81	25.81	26.67	25.81	25.81	25.81
62	9.70	16.10	12.90	19.40	20.00	19.40	12.90	12.90
63	12.90	19.40	12.90	16.10	36.70	16.10	32.30	32.30
72	41.90	54.80	41.90	29.00	50.00	51.60	29.00	29.00
73	29.00	32.30	29.00	25.80	46.70	58.10	38.70	38.70
74	16.10	19.40	19.40	9.70	20.00	32.30	29.00	19.40
75	12.90	22.60	16.10	9.70	20.00	35.50	25.80	16.10
83	41.90	48.40	25.80	35.50	63.30	61.30	48.40	48.40
84	22.60	35.50	25.80	25.80	40.00	48.40	41.90	35.50
85	19.40	22.60	35.50	25.80	46.70	41.90	32.30	25.80
86	16.10	22.60	22.60	16.10	20.00	35.50	32.30	29.00
87	22.60	41.90	32.30	41.90	56.70	41.90	38.70	41.90
91	54.80	51.60	35.50	41.90	53.30	51.60	45.20	54.80
92	41.90	45.20	41.90	41.90	50.00	51.60	35.50	29.00
93	35.50	38.70	41.90	45.20	56.70	58.10	32.30	25.80

(C) 2D

District	Pentad							
	70	71	72	73	1	2	3	4
60	11.70	11.70	10.00	20.40	21.70	15.00	21.70	14.20
61	7.49	13.32	9.99	13.76	14.98	12.49	14.98	10.93
62	6.24	5.41	6.87	9.03	9.99	4.16	5.83	4.16
63	8.70	5.40	4.70	20.10	10.40	13.50	22.90	15.00
72	42.50	28.40	15.90	30.60	36.60	18.70	15.00	15.00
73	20.80	15.90	11.70	31.60	39.30	26.20	25.00	13.10
74	8.10	8.70	2.80	8.40	16.60	14.00	11.90	4.10
75	11.70	7.30	2.80	9.00	18.30	12.50	8.80	8.70
83	37.50	16.60	16.00	47.00	47.50	34.30	35.90	30.60
84	20.60	15.00	13.30	21.90	32.80	21.60	25.20	12.50
85	10.90	21.70	12.50	28.60	29.80	14.60	15.80	8.10
86	10.20	12.40	6.20	8.40	20.60	15.60	18.70	6.20
87	27.10	19.80	23.00	40.20	31.10	20.00	28.40	37.10
91	36.60	24.00	24.30	36.10	36.60	26.20	44.20	24.00
92	32.00	25.70	27.10	30.60	40.00	19.50	20.60	14.20
93	26.20	27.10	29.10	40.20	43.10	19.80	15.00	21.60

(D) 3D

District	Pentad							
	70	71	72	73	1	2	3	4
60	3.01	3.01	3.33	7.25	6.31	5.32	5.61	3.20
61	1.93	3.44	2.66	3.55	3.87	3.22	3.38	3.17
62	0.81	1.05	1.37	1.75	1.29	0.54	0.75	0.81
63	1.13	0.87	1.72	3.24	3.36	4.36	6.65	2.42
72	17.80	8.20	8.00	15.80	10.60	5.40	4.40	3.90
73	6.00	4.10	5.40	18.40	15.20	10.20	5.60	3.40
74	1.57	0.85	0.56	2.71	4.83	2.72	1.15	0.92
75	1.88	0.70	0.56	3.20	4.73	2.01	1.71	1.41
83	9.70	5.90	10.10	28.80	23.00	16.60	16.20	11.80
84	5.30	3.90	5.30	10.60	13.70	7.70	6.50	3.60
85	3.88	5.61	5.83	11.99	9.60	3.76	3.06	2.09
86	2.30	2.00	1.25	2.98	6.65	4.53	2.42	1.81
87	8.70	8.30	13.00	16.90	12.00	8.40	15.60	20.40
91	13.00	10.08	12.99	18.65	16.54	14.38	15.69	9.30
92	13.40	10.80	13.50	15.80	14.20	5.60	5.30	3.70
93	11.00	12.20	16.50	23.40	13.90	5.10	6.30	9.80

3.4.2 Spatial analysis of mid-summer rainfall

The episode of dry spells (EP) is the number of consecutive dry spells (\geq two pentads) in one mid-summer period (mid-December and mid-January) averaged over a 30-year period with less than the threshold value of 15 mm per pentad. As shown in Figure 3.7, the mean EP values varied from 1.69 to 2.10 across the selected districts. Higher mean EP values were observed in districts 75, 86 and 91 in Mpumalanga, Limpopo and North West, respectively. Most dry spell episodes with higher EP values are concentrated in the north-central part of the study area. Similarly, the standard deviation (STD) of the EP values, shown in Figure 3.8, illustrates that the largest deviation from the mean EP value is in District 74. Although higher mean values of EP were noticed in the north-central part of the study area, deviations from the mean EP values are relatively small.

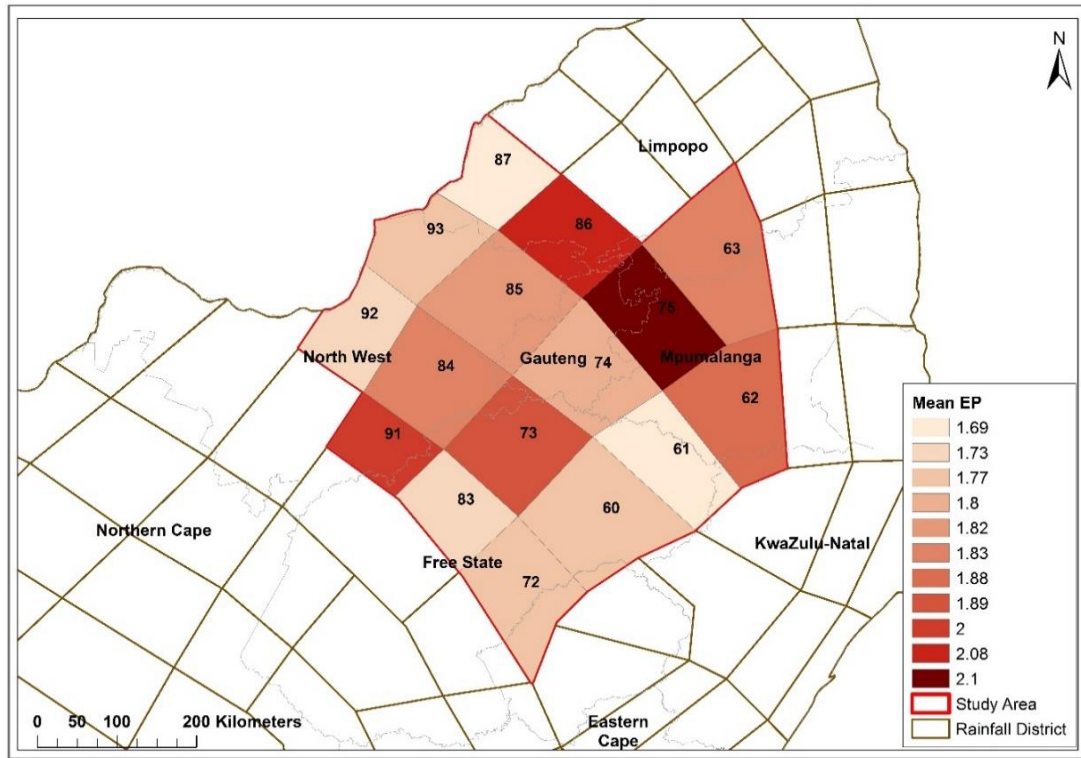


Figure 3.7: The mean episode of dry spells during mid-December and mid-January using a threshold value of 15 mm for the period 1985–2015

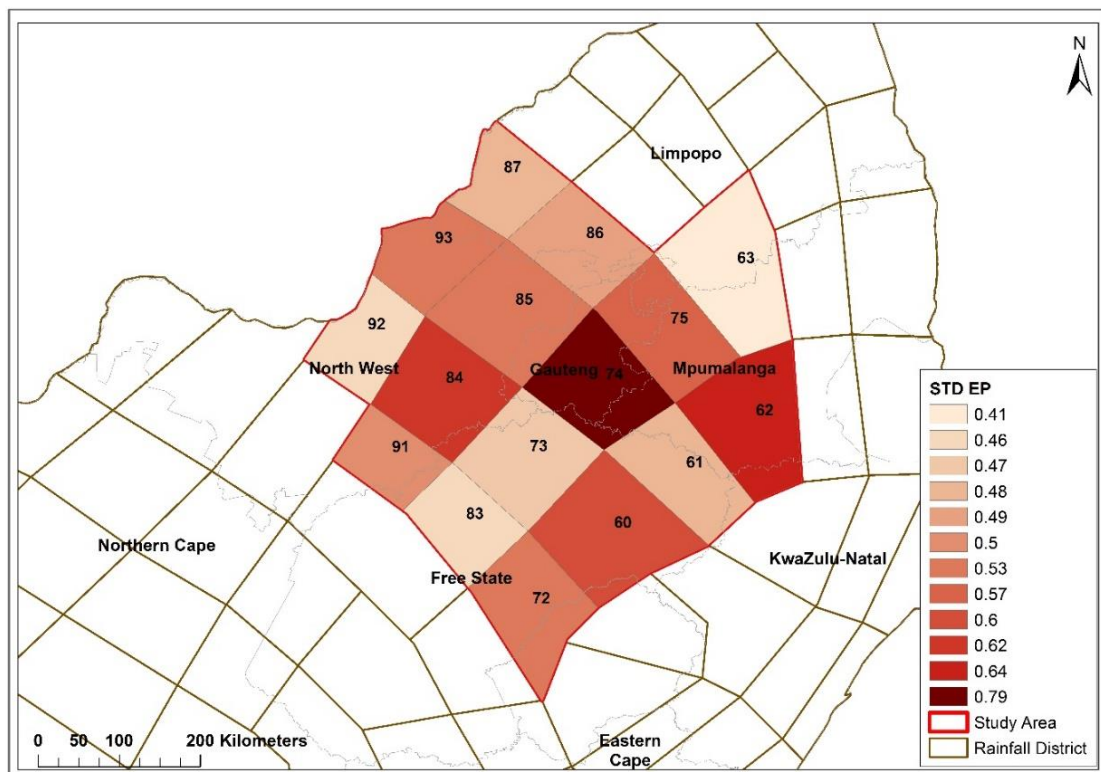


Figure 3.8: The standard deviation of the episode of dry spells during mid-December and mid-January using a threshold value of 15 mm for the period 1985–2015

The average maximum duration of dry spells (DD), which represents the maximum duration of consecutive dry spells using a threshold of 15 mm between mid-December and mid-January per year, is depicted in Figure 3.9. The associated deviations from the mean in each district (standard deviation of DD) is shown in Figure 3.10. There is a close range of mean DD values across the districts. However, there is a decline in the duration of dry spells from the west to the east of the study area. As shown in Figure 3.9, high mean DD values are noticeable in districts 83 and 92 in the Free State and North West. This indicates that dry pentads are more evident over these districts during the mid-summer period, compared to other districts. Larger deviations from the mean DD value were also observed for rainfall districts 83 and 92, compared to the other districts, as shown in Figure 3.10.

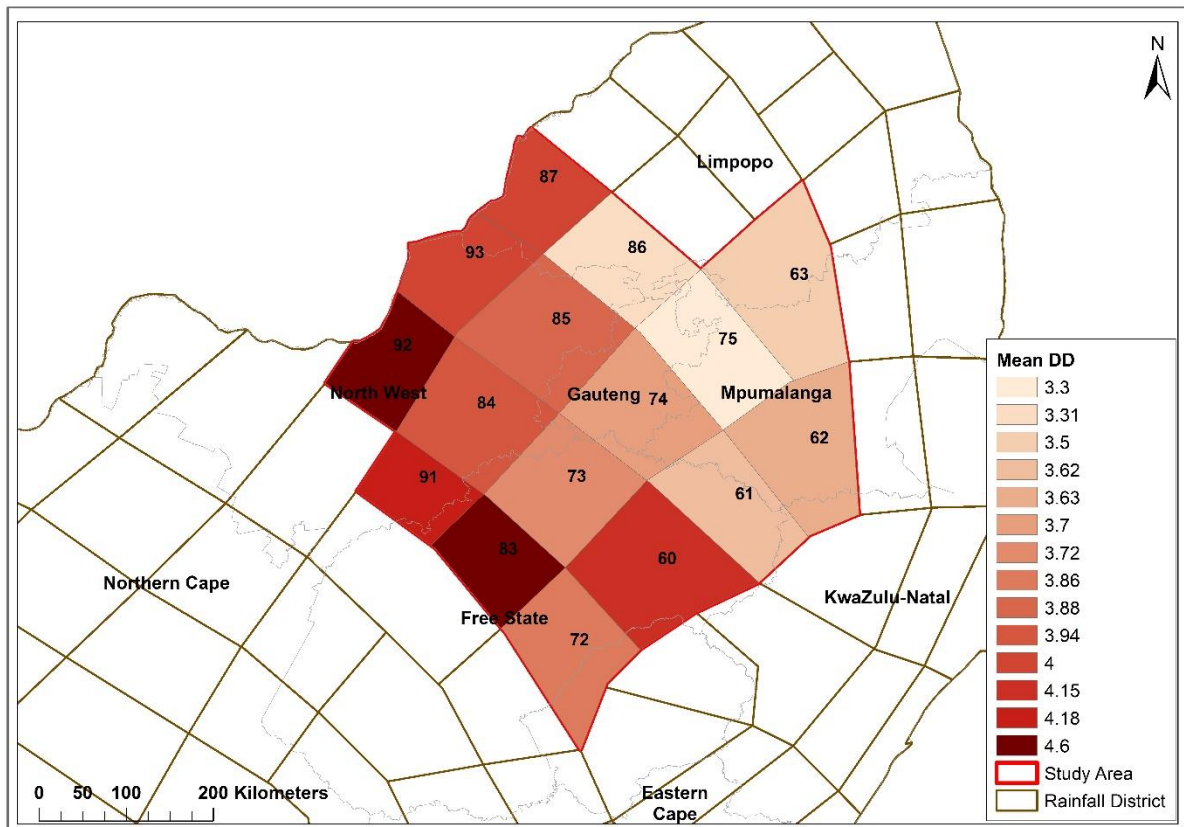


Figure 3.9: The mean maximum duration of dry pentads during mid-December and mid-January using a threshold value of 15 mm for the period 1985–2015

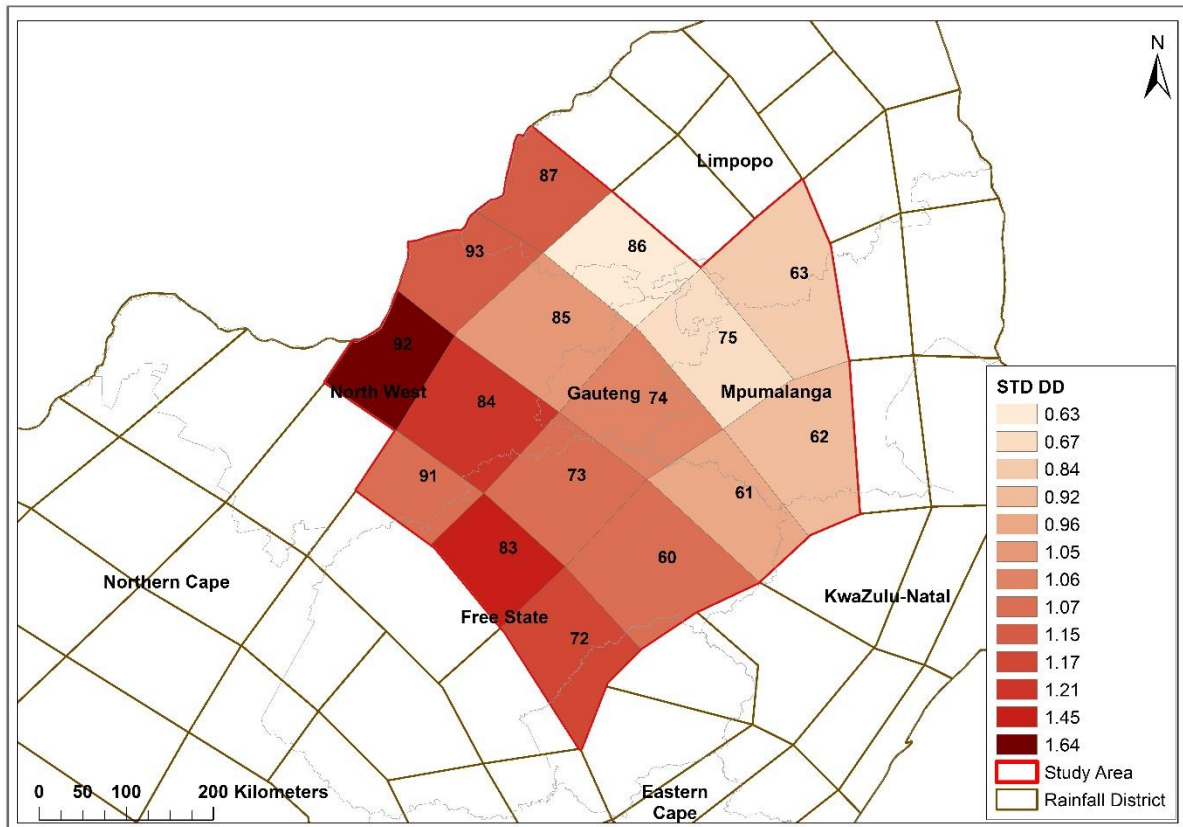


Figure 3.10: The standard deviation of the maximum duration of dry pentads during mid-December and mid-January using a threshold value of 15 mm for the period 1985–2015

3.4.3 Impacts of dry spells on maize production

Several studies on rainfall variability in southern Africa have reported both intra-seasonal and inter-annual variability in summer, which is the main cropping season of the region (Landman and Tennant, 2000; Usman and Reason, 2004; Tadross et al., 2005; Mupangwa et al., 2011; Cr  tat et al., 2011). This observed variability in rainfall and its impact on crop yield makes the southern African region prone to food insecurities. Although the relationships between the total rainfall and crop yield are clear, it is often the variability in seasonal rainfall characteristics, such as onset, cessation and dry spells, that are important and have adverse effects on agriculture (Tadross et al., 2009).

The maize-growing season experiences different rainfall characteristics, such as dry spells, which may impact on phenology and lead to reduced crop yield (Tadross et al., 2009; Moeletsi and Walker, 2012). Maize is mostly planted on drylands in most parts of southern Africa, which are sensitive to water stress (Zinyengere et al., 2014). The yield and quality of maize depend on the distribution of rainfall during the different phenological stages, in addition to other factors (Tadross et al., 2009, Mupangwa et al., 2011). Most studies have shown that maize plants are more sensitive to water stress during the silking and pollination stages, compared to the vegetative stage (Du Plessis, 2003; Masupha et al., 2016).

Several studies have been conducted on dry and wet spell analysis over southern Africa, with an emphasis on their impact on crop yield (e.g. Usman and Reason, 2004; Tadross et al., 2009; Mupangwa et al., 2011; Moeletsi and Walker, 2012; and Duffy and Masere, 2015). However, except for the study by Grobler (1993), little research has been devoted to mid-summer dry spells, which usually coincide with the water-sensitive growth stages of maize. In this study, a detailed spatial and temporal analysis of the mid-summer dry spells was performed for the maize-growing areas of the summer rainfall region in South Africa using three thresholds, 5 mm, 10 mm and 15 mm of total rainfall for a pentad.

As shown in the previous sections, the frequency (figure 3.5 and 3.6), magnitude (Figure 3.7) and duration (Figure 3.9) of mid-summer dry spells differ across the rainfall districts in the maize-growing areas of the summer rainfall region in South Africa. These results are in agreement with the findings of Grobler (1993), who reported an increase in length, intensity and probability of occurrence of dry spells from east to west across the study area.

The annual frequency of dry pentads for the mid-summer period ranged between 0 and 4 pentads for the 5 mm threshold, and 1 to 7 for the 10 mm and 15 mm thresholds, as presented in Figure 3.3. These results are comparable with the study of Usman and Reason (2004), who reported mean frequencies of dry spells for the study area ranging between 1 and 7 pentads using a threshold of 5 mm for the austral summer season (December to February). For meteorological and some hydrological applications, the 5 mm and 10 mm thresholds are useful and may suffice. However, for crop production, the 15 mm threshold pentad rainfall (3 mm per day) is more applicable. Reddy (1990) proposed the use of a 3 mm threshold per day (15 mm per pentad), which is the minimum rainfall depth threshold value for crops to satisfy their crop water requirement during a growing season. For regions with high evaporative demand, Stern et al. (2006) suggested using a higher threshold of 4.95 mm to define a wet day.

Markov chain probability results for the 16 rainfall districts considered in the study area for the mid-summer period (1985–2015) show that there is a 32 to 80% probability that a single pentad will be dry, using the 15 mm threshold (Table 3.2). There is also a 5 to 48% probability of experiencing two consecutive dry pentads, and for the same period, there is a 1 to 29% probability of having three consecutive dry pentads in the study area, as shown in Table 3.2. These results show the probabilities of mid-summer pentads with rainfall less than 15 mm for the different rainfall districts. During a dry pentad, crops might not be affected if enough soil moisture is available. However, districts that experience two and three consecutive dry pentads (e.g. 72, 83 and 93) are likely to be water-stressed. These dry spells, compounded with the high temperatures experienced during the study period, may harm the quality and yield of maize.

Information on dry spell characteristics, such as frequency, duration and intensity with respect to maize crop phenology, is very important for dryland maize production. Studies in parts of the study area in Limpopo by Mzezewa et al. (2010) and Tshililo (2017) have highlighted that dry spells are among the most important determinants of maize yield reduction, if coincided with the water stress-sensitive stages of the maize crop. Therefore, planting dates should be chosen to ensure that these stages coincide with normally favourable growing conditions, and not with mid-summer dry-spell periods (Du Plessis, 2003). *In-situ* rainwater harvesting is a viable option to alleviate water stress in dryland or rain-fed maize production. Moreover, information on the length of dry spells could be used to select drought-tolerant crop varieties and could also be used as a guide to plan supplementary irrigation during a mid-summer dry spell.

3.5 SUMMARY AND CONCLUSIONS

Rainfall is one of the most important factors limiting dryland crop production in South Africa. The mid-summer period is particularly significant, since a lack of rain for a few days during this period may affect crop yield negatively. Dry spell frequency analyses are used to investigate the effects of sub-seasonal rainfall variability on crop yield, since variability in seasonal rainfall totals alone do not necessarily show the relationship between rainfall and crop yield. However, little research has been dedicated to short-term drought studies in South Africa.

In this study, a dry spell was defined as a pentad with rainfall totals lower than a predefined threshold. Three thresholds, 5 mm, 10 mm and 15 mm of rainfall for a pentad, were used to analyse dry spells. This study investigated the spatial and temporal occurrences of the mid-summer dry spells based on magnitude, length and time of occurrence in the summer rainfall region of South Africa.

The existence of a climatological dry period within the main rainfall season was investigated using the monthly rainfall totals from October to March. The results show that, climatologically, mid-summer months do not experience lower rainfall than the early and late summer months. However, the dry-spell analysis showed that, during mid-summer, dry pentads occur with a different intensity, duration and frequency across the maize-growing areas of the summer rainfall region. The non-parametric Mann-Kendall trend analysis for the dry pentads during the mid-summer for 16 selected homogeneous rainfall districts indicates that there is no significant trend in the frequency of dry spells at a 95% significance level. The initial and conditional probabilities of getting a dry spell using the Markov chain probability model also showed that there is a 32 to 80% probability that a single pentad will be dry using the 15 mm threshold. There is a 5 to 48% probability of experiencing two consecutive dry pentads and a 1 to 29% probability of having three consecutive dry pentads. Consecutive dry spells mostly seem to occur during Pentad 73 (the end of December) and Pentad 1 (the beginning of January). Furthermore, the Markov chain probability analysis showed a decrease in the probability of dry spells from west to east of the study area. An analysis of the duration and intensity of dry spells also showed a decrease from west to east of the study area.

CHAPTER 4: SYNOPTIC ANALYSIS OF THE MID-SUMMER DRY SPELLS FOR THE SUMMER RAINFALL REGION OF SOUTH AFRICA

4.1 ABSTRACT

South Africa is a semi-arid country that is prone to the occurrence of droughts caused by significant temporal and spatial rainfall variability. The larger part of South Africa receives rainfall during the austral summer months. However, dry spells can occur over the summer rainfall region during this period. The occurrence of mid-summer dry spells is critical to crop production, since the timing of the breaks in rainfall relative to the crop growth stages can be more important than the total seasonal rainfall for crop production. An approach to better understand intra-seasonal rainfall characteristics is to investigate the intra-seasonal variability of daily synoptic-scale atmospheric circulation systems. The most common approach to synoptic climatology is to partition the atmospheric state into broad categories, and to relate these synoptic categories to some dependent variable. Self-organising maps offer a useful technique to classify synoptic circulation patterns, visualise the complex distribution of synoptic states and identify noticeable weather patterns. This study investigates the synoptic weather systems associated with mid-summer dry spells over South Africa. Self-organising maps were used for the synoptic classification using the ERA5 global reanalysis dataset. Ward's clustering technique was applied to objectively arrange the SOM circulation patterns into groups with similar characteristics. Climate drivers, such as ENSO, were also investigated to identify noticeable drivers of South African mid-summer dry spells in synoptic weather patterns. Ward's clustering results indicate two primary weather patterns that have a dominant effect on mid-summer rainfall patterns, namely the strong subtropical ridge, and the summer troughs and easterly weather. Results show that ENSO has a strong influence on the mid-summer weather patterns of the study area.

Keywords: Mid-summer; dry spells; synoptic climatology; climate drivers; self-organising maps

4.2 INTRODUCTION

South Africa is considered a semi-arid country with most of the country's annual rainfall totals below 500 mm (Taljaard, 1996). Across most of South Africa, rainfall occurs during the austral summer months (October to March). This rainfall results from large synoptic-scale rain-bearing systems like tropical temperate troughs (TTTs) and smaller convective-scale heat-induced thunderstorms (Harrison, 1984; Hart et al., 2010). The most significant increase in rainfall over the summer rainfall region follows a circular path that starts in September along the south-east and east coast, after which the increase in rainfall spreads to the eastern interior parts in October, extending to the western interior from October to November (Taljaard, 1986). In December, a break or hiatus occurs in the rising rainfall over large parts of the summer rainfall region (Taljaard, 1986). Dry spells occur during the summer season, with the mid-summer period being critical to agricultural crop production because it coincides with the moisture-sensitive growth stage of grain crops. The other distinct rainfall regions over South Africa occur along the southern coast of the country where rainfall occurs all year round (Engelbrecht et al., 2015), as well as in the south-western region, which receives the majority of its rain during the winter months due to passing mid-latitude cyclonic systems (Reason et al., 2002).

Southern Africa is a region prone to the occurrence of droughts and floods caused by significant temporal and spatial rainfall variability (e.g. Tyson, 1986; Jury and Levey, 1993; Lindesay, 1988; Mason and Joubert, 1997; Rouault and Richard, 2003; Malherbe et al., 2016). Summer rainfall variability has been linked to tropospheric circulation changes (Tyson, 1981; Miron and Tyson, 1984; Barclay et al., 1993), ENSO and regional sea surface temperature (SST) anomalies (Walker, 1990; Landman and Mason, 1999; Reason and Mulenga, 1999; Reason et al., 2000; Richard et al., 2000; Landman and Beraki, 2010). Of all the climate drivers, ENSO is the primary driver associated with summer rainfall variability, with El Niño events frequently associated with drier-than-normal conditions over southern Africa (e.g. Van Heerden et al., 1988) and a higher-than-normal occurrence of dry-spell frequencies over the summer rainfall regions (Usman and Reason, 2004).

Numerous studies have examined rainfall variability over the summer rainfall region of southern Africa (Harrison, 1984; Lindesay, 1988; Mason, 1995; Reason and Rouault, 2002) using monthly or seasonal anomalies. The dominant rainfall-producing weather system over southern Africa during the austral summer is composed of synoptic-scale TTTs (Tyson, 1986; Hart et al., 2012). The TTT system forms tropical-extratropical cloud bands and related atmospheric convection that extend along the northwest-southeast direction over both the land mass and the adjacent south-west Indian Ocean region (Harrison, 1984; Todd and Washington, 1999; Washington and Todd, 1999; Todd et al., 2004). The remaining summer rainfall amounts are produced by rain-bearing tropical convection mechanisms (Harrison, 1984; Jury et al., 1996), such as regional thermal low pressures (Tyson and Preston-Whyte, 2000; Reason et al., 2006). Although TTTs and rain-bearing tropical convection mechanisms are regarded as the primary summer synoptic rainfall-producing system over South Africa, their physical and dynamic characteristics are complex and not yet well understood (Crétat et al., 2012), even though their contribution to the summer rainfall has been quantified (e.g. Hart et al., 2012).

Temporal and spatial rainfall variability studies are paramount to many fields, such as agriculture and water resource management. For crop production, the distribution of rainfall can be more important than the total amount of rainfall received over the growing season. The timing of breaks in rainfall (dry spells) relative to the cropping calendar, rather than total seasonal rainfall, is fundamental to crop viability (Usman and Reason, 2004). Rainfall characteristics within a season can provide valuable information, which will result in a better understanding of rainfall variability (Tennant and Hewitson, 2002). To better understand the overall rainfall characteristics of a season, it is advisable to investigate the variability of daily weather circulation systems during the season. According to Hewitson and Crane (2002), the most common approach to synoptic climatology is to partition the atmospheric state into broad categories, and to relate these synoptic categories (or types) to some dependent variable.

Early approaches used classifications based on generalising the circulation into synoptic types (Yarnal et al., 2001). Self-organising maps (Kohonen, 2001) offer an approach to investigate synoptic climatology patterns. They are regarded as a suitable technique for visualising the complex distribution of synoptic states. Self-organising maps are also useful for weather pattern identification, where the daily transitions between weather patterns are important (Hewitson and Crane, 2002). SOMs have been used in several southern African region studies dealing with weather patterns (e.g. Hewitson and Crane, 2002; Tennant and Hewitson, 2002; Tozuka et al., 2014; Van Schalkwyk and Dyson, 2013; Engelbrecht et al., 2015).

In this study, SOMs were applied to explore the association between daily synoptic weather patterns and rainfall during the mid-summer period, which is occasionally associated with a decline in rainfall relative to the remainder of the summer season. The aim of this study is to perform a synoptic diagnosis to identify the synoptic weather system drivers of the South African mid-summer dry spells, which are known (e.g. Taljaard, 1986), but not yet well understood.

4.3 DATA AND METHODOLOGY

4.3.1 Data sources

4.3.1.1 European Centre for Medium-range Weather Forecasts re-analysis data

Synoptic circulation data was obtained from the global reanalysis dataset (ERA5, 2019) of the European Centre for Medium-range Weather Forecasts. ERA5 provides hourly estimates of a large variety of atmospheric, land and oceanic climate variables. The data covers the earth on a 30 km grid resolution and resolves the atmospheric flow and processes over 137 levels from the surface up to a height of 80 km. ERA5 includes information about uncertainties for all variables at reduced spatial and temporal resolutions (ECMWF, 2019). For the analysis of the lower and mid-troposphere, two fields were obtained from the Copernicus Climate Data Store. These fields are daily 850 hPa and 500 hPa geopotential heights, both measured at 00:00 UTC.

4.3.1.2 District rainfall

The South African Weather Service maintains an in-house rainfall dataset where the country is divided into 94 rainfall districts (SAWB, 1972) (Figure 4.1). The delineation of these districts was based on the annual changes of maximum rainfall, and the boundaries between the winter, whole-year and summer rainfall regions. A daily district rainfall total is calculated as the average of the daily values available in the district (Kruger and Nxumalo, 2017).

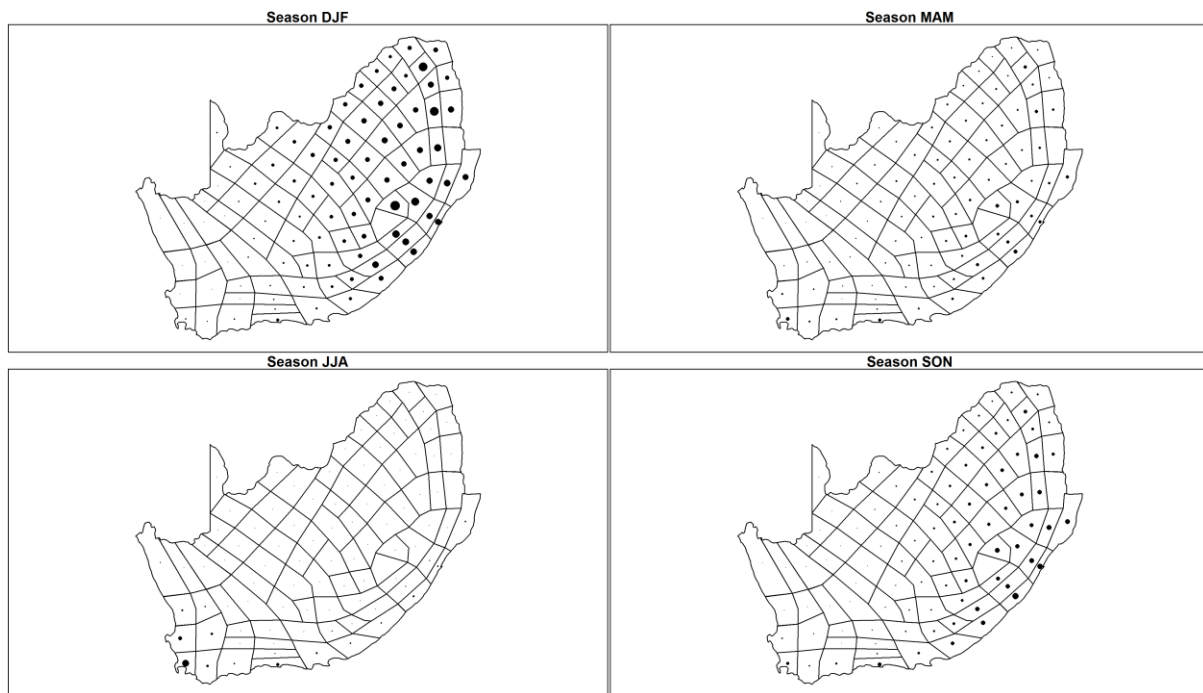


Figure 4.1: District rainfall regions in South Africa (a), and the rainfall occurrence during the four main seasons, Dec-Jan-Feb (DJF) (b), Mar-Apr-May (MAM) (c), Jun-Jul-Aug (JJA) (d) and Sep-Oct-Nov (SON) (e). The size of the black dots is scaled to the relative rainfall received in each season.

4.3.1.3 Climate drivers

At longer time scales (e.g. months to seasons), climate drivers have a distinct impact on the climate of southern Africa. Climate drivers to be investigated in this study are ENSO, the Southern Annular Mode and the South-West Indian Ocean (SWIO). Indices of these climate drivers were obtained from the State of the Ocean Climate website, administered by the National Oceanic and Atmospheric Administration (NOAA) (2019). The calculation methods used and information regarding the data can also be found at <https://stateoftheocean.osmc.noaa.gov/>.

It is well known that the climate drivers mentioned above have an influence on southern Africa's climate variability during the austral summer. Malherbe et al. (2016) investigated drought occurrences over South Africa linked to both ENSO and SAM. Reason and Mulenga (1999) highlighted studies of Walker (1990) and Mason (1995), where Walker (1990) suggested increased easterlies during warmer SWIO events, with a subsequent effect on TTTs. Mason (1995) suggested a significant influence of the TTTs through principal component analysis (PCA), coming from the SWIO region.

4.3.2 Methodology

4.3.2.1 Self-organising maps

A clustering system is used to group the daily atmospheric circulation into recognisable synoptic circulation patterns. The clustering of data tends to expose groups within a dataset, and each group will result in a distinct classification of the clustering variable (Tambouratzis and Tambouratzis, 2008). SOMs were used as a technique to cluster the forecasts (see Kohonen, 2001) since they have been used extensively in atmospheric sciences (e.g. Tennant and Hewitson, 2002; Engelbrecht et al., 2015; Lennard and Hegerl, 2015).

SOMs were used to conduct a synoptic classification for the period 1 January 1979 to 31 December 2018, based on daily 00Z 850 hPa and 500 hPa circulation patterns from the ERA5 reanalysis data. The native

ERA5 grid (0.25) was resampled to a $0.75^\circ \times 0.75^\circ$ horizontal grid. The SOM covered the domain of 10° to 40° S and 0° to 54° E to capture the influences of both the tropical and mid-latitude weather systems affecting southern Africa.

The dual dataset, after normalisation, was ingested into the SOM to create a 5×7 node matrix. SOMs with 35 nodes, derived from daily data for multiple calendar years, were considered for the southern African domain before capturing the main circulation patterns and their various configurations (e.g. Tennant and Hewitson, 2002; Engelbrecht et al., 2015). Each of the nodes in the matrix consists of a regular two-dimensional structure, based on the two variables clustered. The 850 hPa heights were chosen to develop the SOM together with the 500 hPa circulation patterns, as these atmospheric circulation levels influence rainfall over the region (e.g. Taljaard, 1996). The SOM subsequently calculated the accompanying 850 hPa circulation patterns with associated 500 hPa synoptic conditions. Ward's clustering technique was used to identify eight main circulation patterns from the 35 nodes, and is applied to objectively group the SOM circulation patterns into groups with similar characteristics (Wilks, 2011).

4.3.3.2 District rainfall analysis

From the daily district rainfall data, pentad summations were calculated following the methodology used in Grobler (1993). Pentads were calculated using Julian days. For example, Pentad 1 refers to 1–5 January and Pentad 73 refers to 27–31 December. The extra leap year day, 29 February, was added to Pentad 10. Eight pentads between 12 December (the start of Pentad 70) and 20 January (the end of Pentad 4) were selected for a detailed analysis of the mid-summer rainfall in the study area. A threshold of 3 mm per day (15 mm per pentad), which is the minimum rainfall needed for crops to satisfy their water requirement during a growing season, was used (Reddy, 1990), in combination with the accompanying atmospheric circulation as identified by the SOM analysis.

4.4 RESULTS AND DISCUSSION

4.4.1 Circulation pattern classification

The SOM performed on the 850 hPa and 500 hPa geopotential height fields is shown in Figure 4.2, with the seasonal cycle of occurrences for each of the nodes presented in Figure 4.3. Generally, the winter nodes are found in the left columns of the matrix, with the summer nodes in the right columns. A high degree of variability was observed within the typical winter circulation patterns (e.g. Node 1 versus Node 29) and the typical summer circulation patterns (e.g. Node 7 versus Node 35). However, take note that emphasis will be placed on investigating synoptic weather patterns during the South African mid-summer dry-spell period.

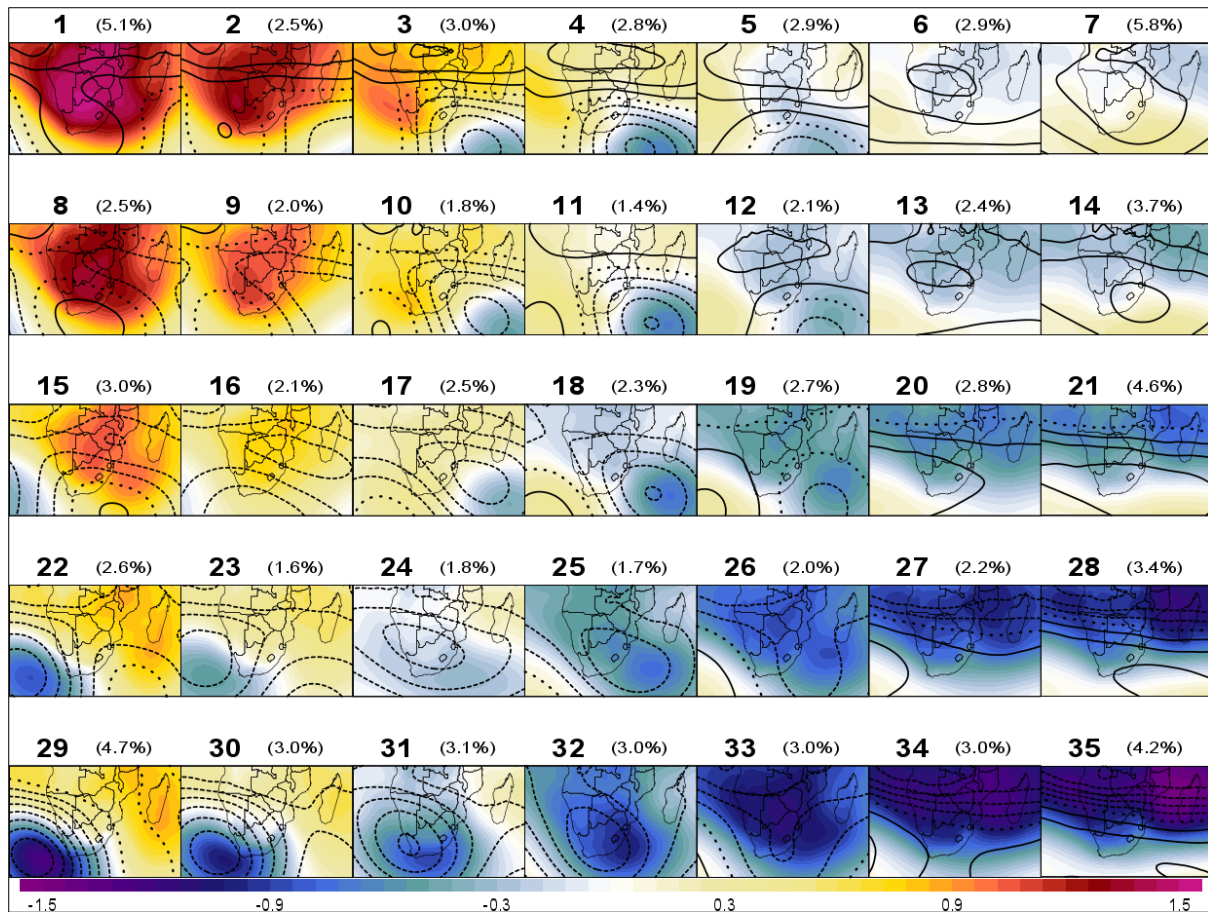


Figure 4.2: A 7 x 5 matrix output from the SOM indicating the normalised circulation patterns for the period 1979–2018 (850 hPa shaded and 500 hPa contour). The percentage of occurrence per node is also indicated.

Since the SOM was constructed using multi-variables (850 hPa and 500 hPa geopotential heights), the input data to the SOM analysis first needed to be normalised. Hence, for easier reference to weather systems, Figure 4.4 is a composite of the modelled geopotential heights used to construct the SOM. For ease of reference to the different weather systems affecting southern Africa, the 35 SOM nodes were also sorted into eight groups, with the SOM nodes in each group representing the various configurations of the particular weather system. This grouping of the SOM nodes into eight groups was achieved by applying Ward's clustering method (Figure 4.5). These eight groups constitute a range of weather systems and their different characteristics as found across the different seasons. A description of the eight circulation patterns (groups A to H), as well as the season to which they mostly relate, is given in Table 4.1.

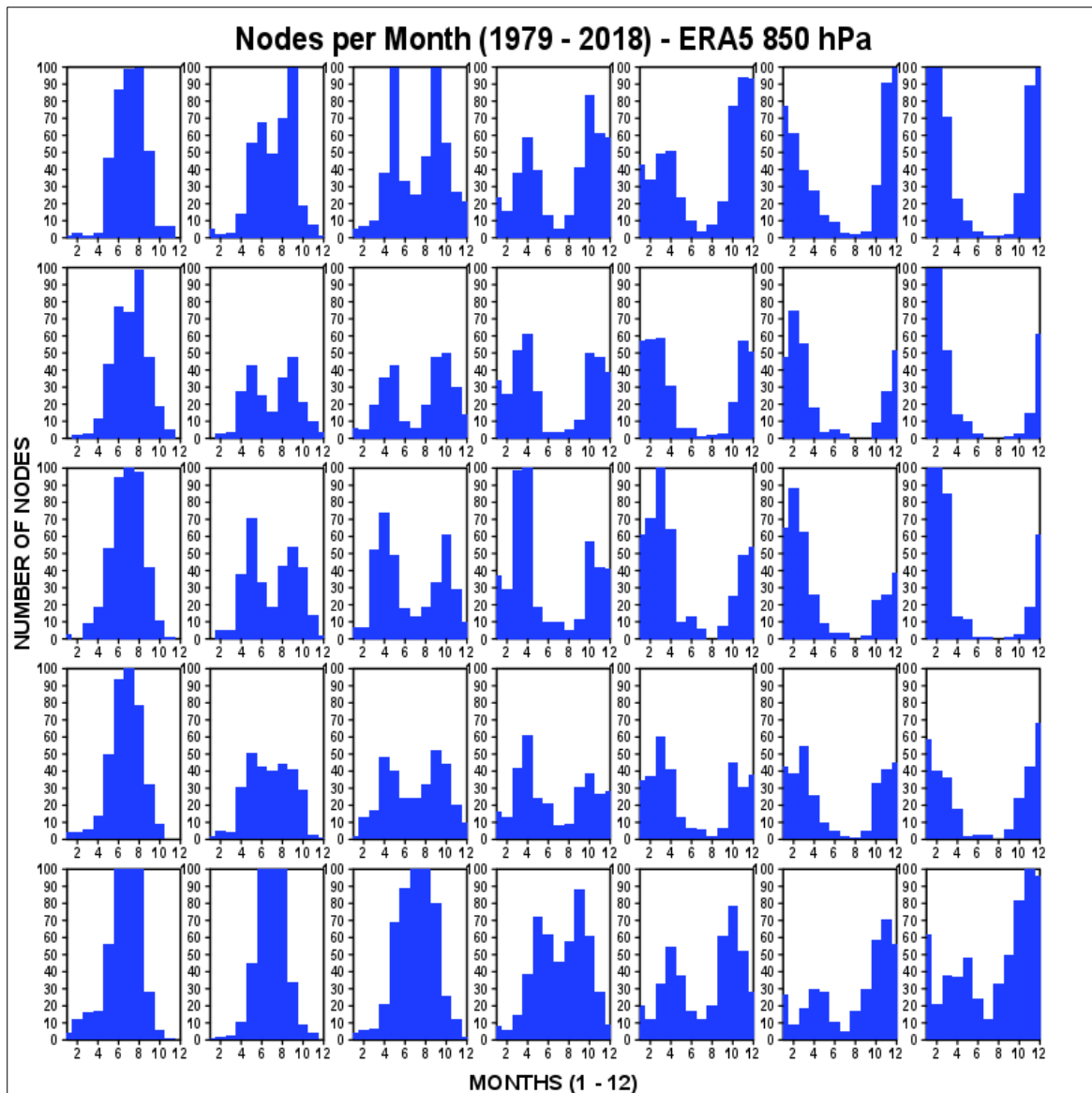


Figure 4.3: The number of occurrences (y-axis) per month (x-axis), indicating the annual cycle per node

Table 4.1: Seasonal circulation patterns based on Ward's clustering

Winter circulation patterns	Transition seasons	Summer circulation patterns
A: Anticyclonic circulation	D: Trough south-east of the subcontinent/ridging high	F: Ridging highs
B: Anticyclonic circulation, but less intense than that of Group A	E: Westerly wave activity	G: Westerly wave south of the country
C: Cold front passage		H: TTT / easterly weather

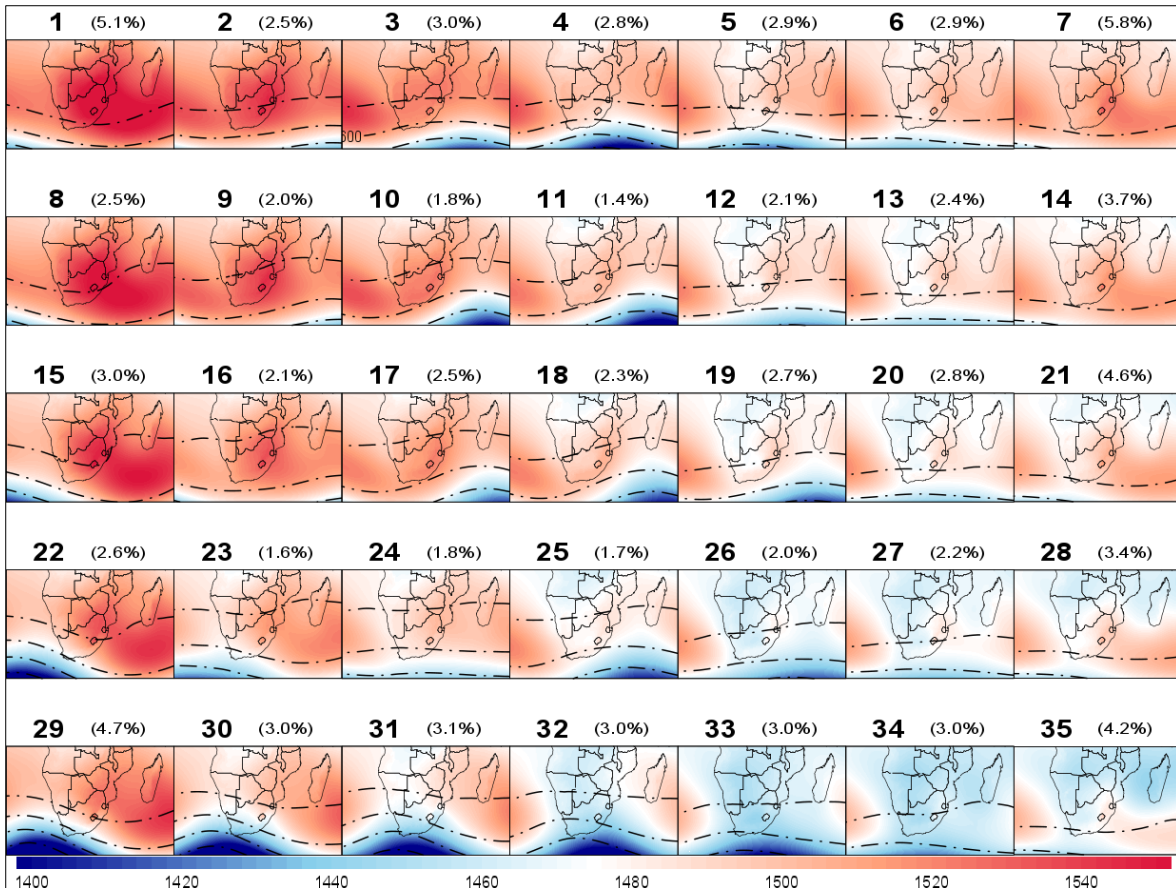


Figure 4.4: The average ERA5 geopotential heights (850 hPa shaded and 500 hPa contour) per node

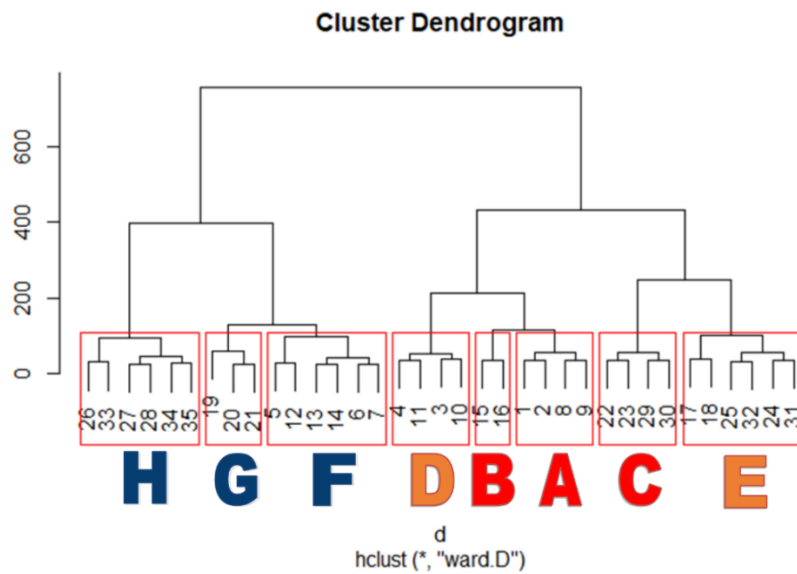


Figure 4.5: The eight clusters from the 35 SOM nodes identified by Ward's clustering indicated in red boxes surrounding the matching nodes

In Figure 4.6, all mid-summer days from 1979 to 2018 (1 400 days) are mapped to the SOM space in order to investigate the potential relationship between the occurrence of synoptic patterns and mid-summer rainfall characteristics. The groups, as identified by Ward's clustering, are also shown.

As indicated in Table 4.2, groups F, G and H contribute to more than 98% of the circulation during the defined mid-summer period. Of these groups, Group H occurs nearly half of the time (47.2%) during the defined mid-summer period. Also shown in Table 4.2, nodes 33, 34 and 35 occur 8%, 12% and 9.29% of the time, respectively. In circulation groups F and G, nodes 7, 13, 20 and 21 appear to have a noteworthy frequency of occurrences.

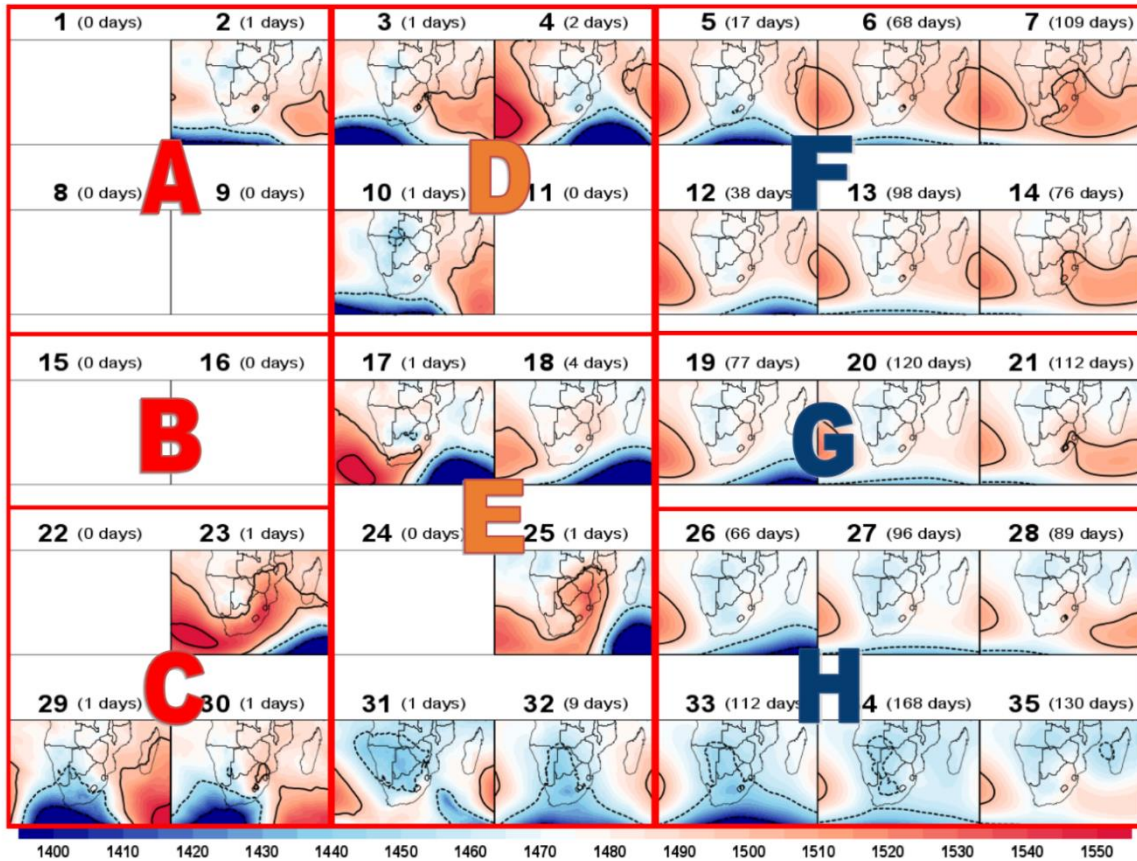


Figure 4.6: The 850 hPa circulation patterns per node for the mid-summer period (12 December to 20 January). The number of days of the possible 1 400 days per node is indicated above each node. Clustered patterns A to H indicate clusters identified by Ward’s clustering system (Figure 4.5).

Table 4.2: Percentage of days per node for the mid-summer period (12 December to 20 January)

1	2	3	4	5	6	7
0.00	0.07	0.07	0.14	1.21	4.86	7.79
8	9	10	11	12	13	14
0.00	0.00	0.07	0.00	2.71	7.00	5.43
15	16	17	18	19	20	21
0.00	0.00	0.07	0.29	5.50	8.57	8.00
22	23	24	25	26	27	28
0.00	0.07	0.00	0.07	4.71	6.86	6.36
29	30	31	32	33	34	35
0.07	0.07	0.07	0.64	8.00	12.00	9.29

4.4.2 Relative frequency of dry spells

Relative occurrence frequencies were calculated during overlapping occurrences in the SOM analyses, as well as the occurrence of pentad totals of below 15 mm and above 30 mm. For the purpose of this study, pentad totals of less than 15 mm are defined as dry spells, as more than 15 mm per pentad is required for crop growth during the mid-summer period. Wet spells are defined as pentads where more than 30 mm of rainfall occurred. The reason to consider both dry and wet spells is to simplify distinguishing SOM nodes from rain-bearing systems that provide good rainfall for crop growth against systems that are associated with the minimum rainfall requirement for crop growth during the mid-summer period. As an example of the calculation for the relative frequency difference maps, the relative frequencies of the 35 nodes for a district (within the maize-growing region) are presented in Figure 4.7. Node frequencies were sorted from high to low to accentuate their importance during mid-summer. Relative frequencies were calculated in three different instances: the relative frequency of the SOM nodes was calculated throughout all mid-summers over the entire 1979–2017 period; the data was split into two new time series, one which only had the nodes during dry spells and the other consisting of the nodes during wet spells; and the relative frequencies were recalculated for the two new series and the differences between the normal relative frequency. Results are presented in Figure 4.7.

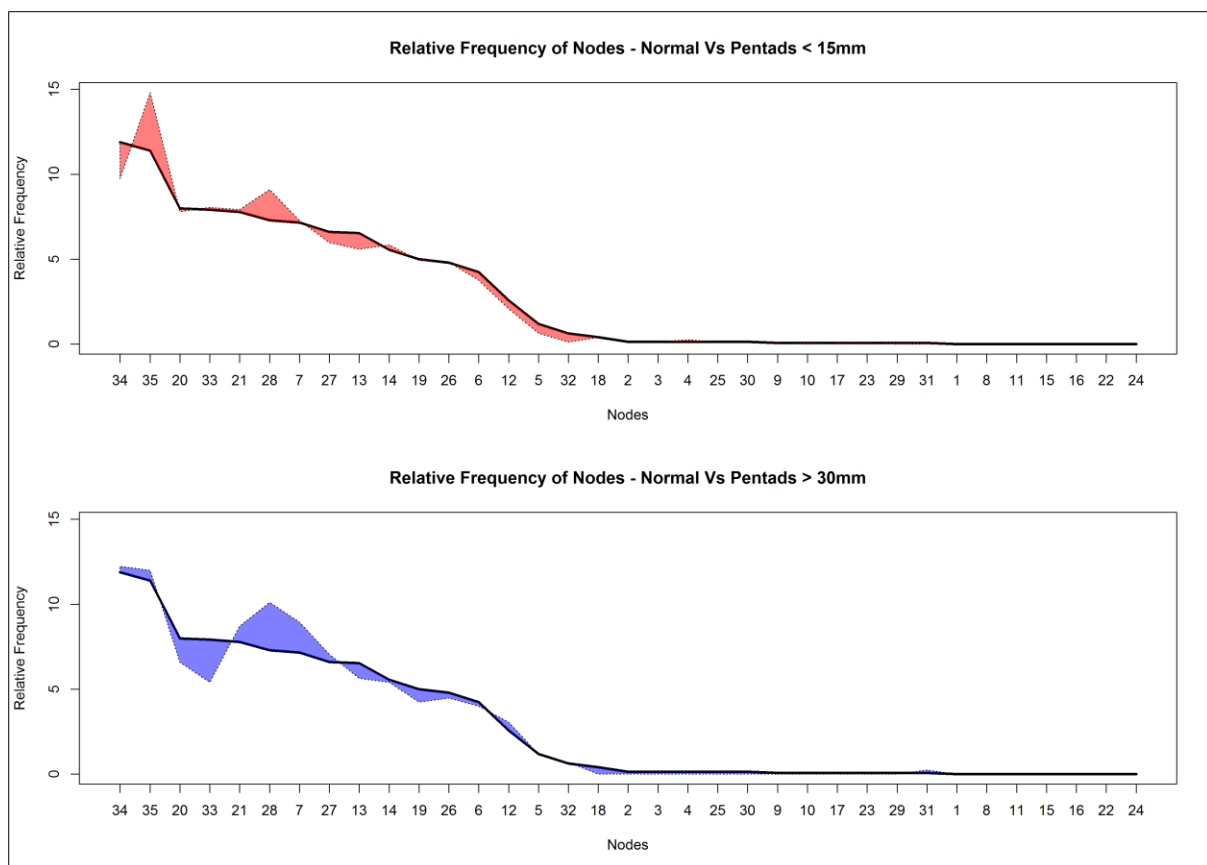


Figure 4.7: Relative frequencies of dry (< 15 mm, left) and wet (> 30 mm, right) spells during mid-summer pentads for Region 74 (as an example). Node frequencies ordered according to their total relative occurrence (bold black line).

The difference between the relative frequency of dry and wet spells for each of the 94 district rainfall regions was considered to map the possible influences of each of the 35 nodes on rainfall distribution during mid-summer, as shown in figures 4.8 to 4.11. Figure 4.8 illustrates the difference between nodes 34 and 35, both classified as TTTs and easterly weather, but with significantly different rainfall distribution during the mid-summer.

Node 34 is more associated with wetter pentads, whereas Node 35 is associated with dry pentads. Similarly, nodes 27 and 28 show the same effect (Figure 4.9), although these nodes occur relatively less frequently than nodes 34 and 35. Focusing on the ridging high group of nodes (F), similar differences were observed between the nodes in the second last and last columns (from Figure 4.3). Figures 4.10 and 4.11 show these differences between nodes 6 and 7, and 13 and 14, respectively.

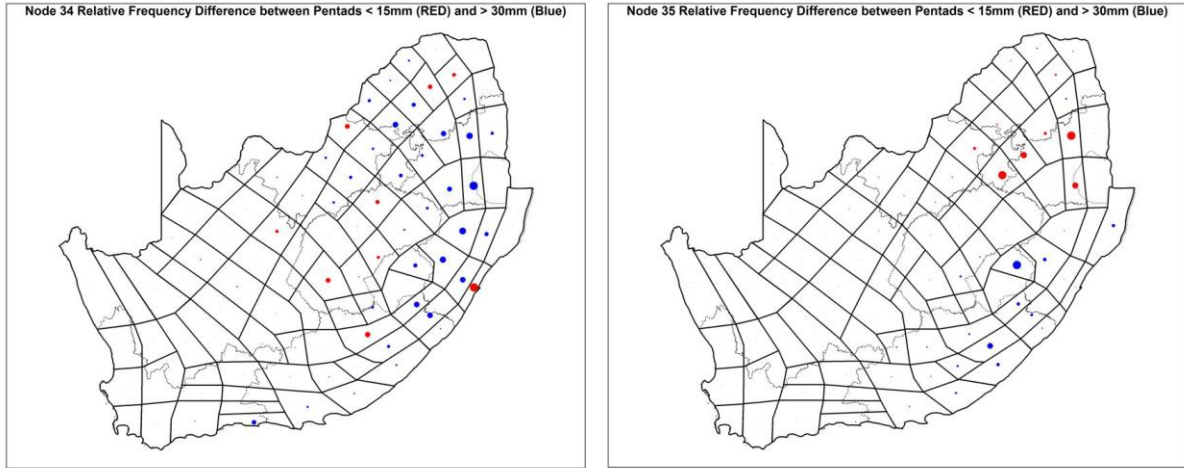


Figure 4.8: Relative frequency difference of dry (< 15 mm) and wet (> 30 mm) spells during mid-summer pentads for nodes 34 (left) and 35 (right). Coloured dot size is scaled first by mid-summer rainfall totals, and then by the magnitude of the difference between the dry and the wet spells.

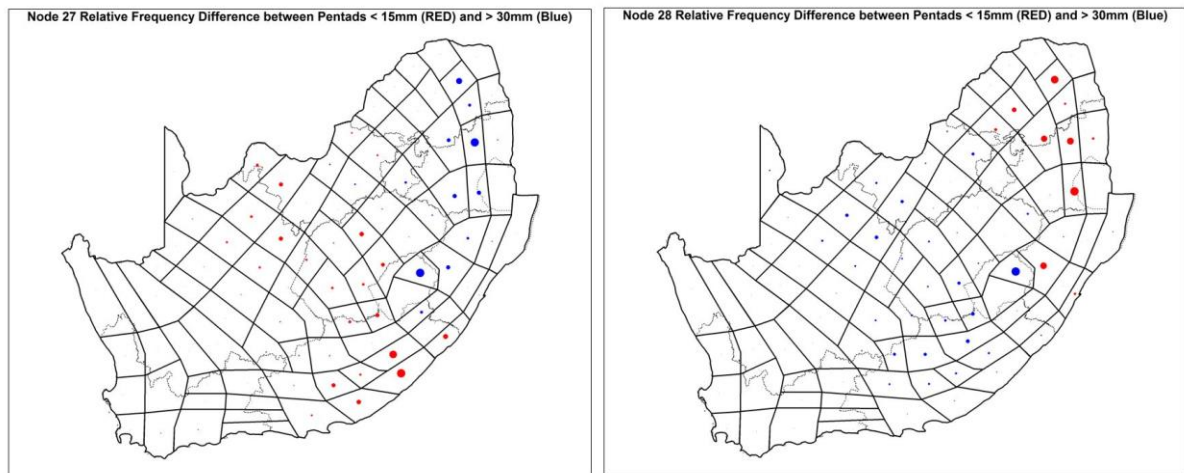


Figure 4.9: Relative frequency difference of dry (< 15 mm) and wet (> 30 mm) spells during mid-summer pentads for nodes 27 (left) and 28 (right). Coloured dot size is scaled first by mid-summer rainfall totals, and then by the magnitude of the difference between the dry and the wet spells.

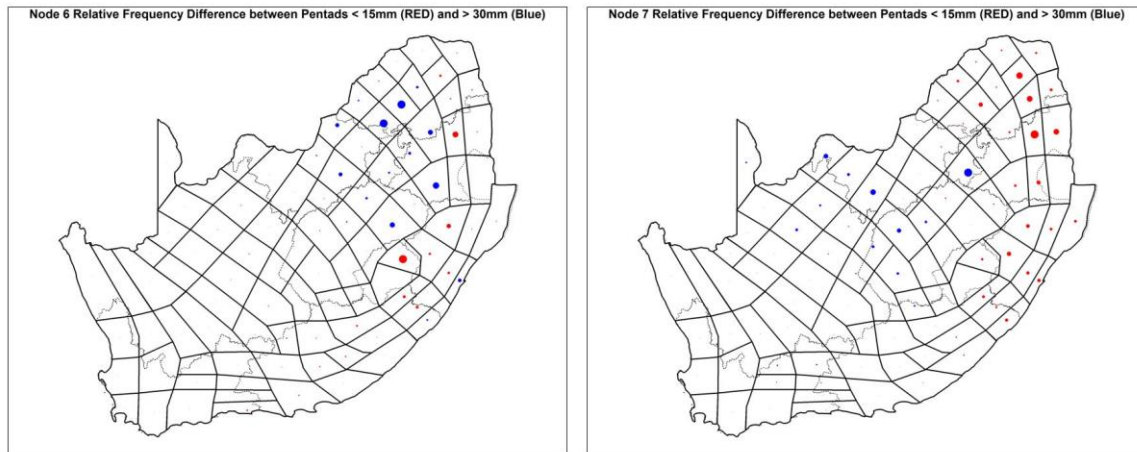


Figure 4.10: Relative frequency difference of dry (< 15 mm) and wet (> 30 mm) spells during mid-summer pentads for nodes 6 (left) and 7 (right). Coloured dot size is scaled first by mid-summer rainfall totals, and then by the magnitude of the difference between the dry and the wet spells.

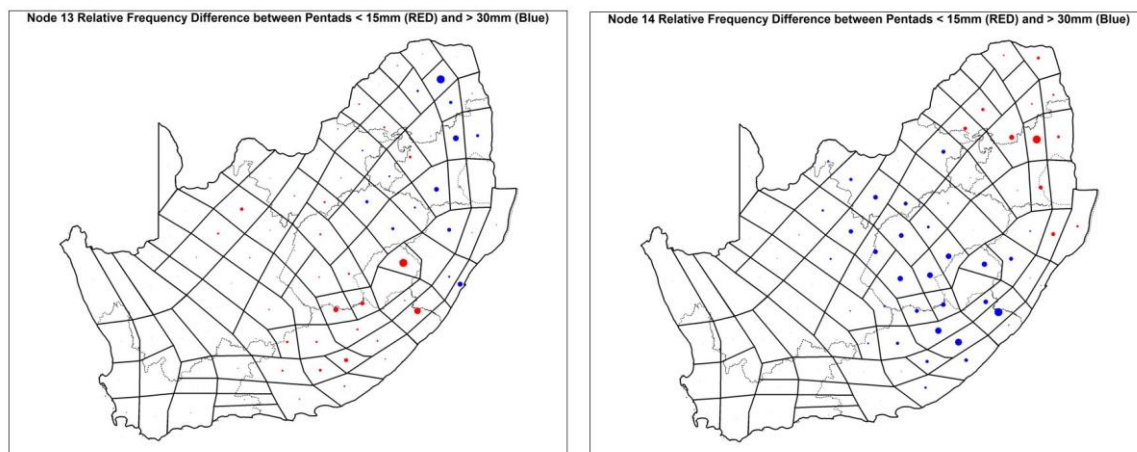


Figure 4.11: Relative frequency difference of dry (< 15 mm) and wet (> 30 mm) spells during mid-summer pentads for nodes 13 (left) and 14 (right). Coloured dot size is scaled first by mid-summer rainfall totals, and then by the magnitude of the difference between the dry and the wet spells.

Nodes 34 and 35 characterise the most pronounced difference in the occurrence of dry and wet spells. Even though nodes 34 and 35 are adjacent nodes within the SOM space, the subtle difference in the depth of the surface trough over the western interior (a deeper trough is evident in Node 34) and the ridge to the east of the country (Node 35) appears to have an influence on rainfall characteristics. The deeper surface trough over the western to central interior, displayed in Node 34, can aid in the higher frequency of > 30 mm rainfall events over the eastern interior, whereas the specific configuration of the ridge east of the country, as displayed in Node 35, can be associated with stable conditions over the north-eastern parts of the country, and hence a higher frequency of < 15 mm rainfall events. Node 33 is also an interesting node that is associated with a higher relative frequency of dry spells over the central interior of the country. This association can very likely be attributed to the westerly wind regime situated closer to the equator, and thus faster-moving troughs.

4.4.3 Influence of climate drivers

In an attempt to investigate whether the differences in rainfall intensities during pentads can be ascribed to larger-scale climate driver systems, each node's frequency during mid-summer was correlated with three specific climate drivers, ENSO, SAM and SWIO.

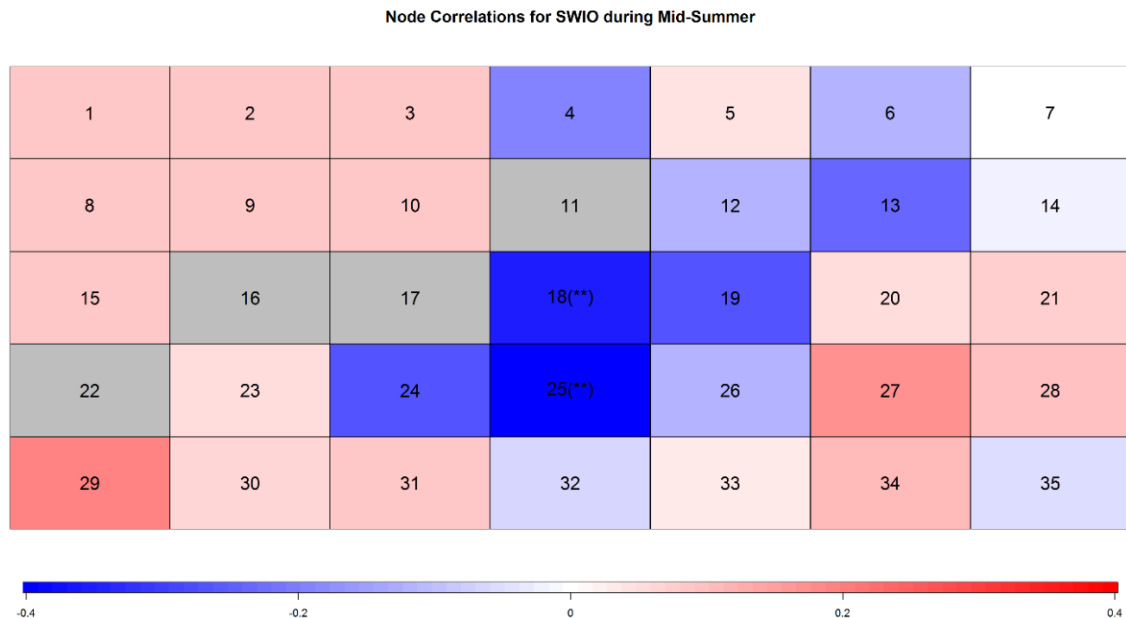


Figure 4.14: Node correlations with SWIO. The numbers in the cells indicate the nodes. They have a similar structure to previous node figures, with * indicating the significance level (* = 90%; ** = 95%; *** = 99%). Shading indicates the correlation values.

4.5 SUMMARY AND CONCLUSION

South Africa experiences significant temporal and spatial rainfall variability, which is responsible for frequent droughts and floods. Seasons with similar rainfall totals over southern Africa can have very different intra-seasonal rainfall characteristics, which poses climate-related challenges to rain-fed crop production in the region. Southern African summer rainfall variability has been associated with tropospheric circulation changes, ENSO and regional SST anomalies. During the mid-summer, a break in the rainfall (mid-summer dry spell) has been found to occur over the summer rainfall region of South Africa. This period is critical to agricultural crop production because it coincides with the moisture-sensitive growth stages of grain crops. An approach to better understand rainfall characteristics within a season is to investigate the variability of daily weather circulation systems. However, the physical and dynamic features of the rainfall-producing systems are very complex and not well understood.

In this study, SOMs were used to do a synoptic classification of the 850 hPa and 500 hPa geopotential heights. Ward's clustering was applied to objectively group the SOM circulation patterns into groups with similar characteristics for near-surface circulation. Relative frequency analysis of dry and wet spells using district rainfall data was used to link rainfall to the synoptic classification. Climate drivers that affect the southern African climate, such as ENSO, SAM and SWIO, were also investigated to identify possible synoptic weather system drivers of the South African mid-summer dry spells.

Ward's clustering results show that two main weather patterns dominate the mid-summer season: the influence of the strong subtropical ridge, and the troughs and easterly weather. However, the variation within these dominant patterns seems to be the cause of a higher occurrence of dry and wet spells, with the subtropical ridge patterns relating to differences in dry and wet spells over the north-east of South Africa, and the troughs and easterly weather relating to differences over the central and southern parts of South Africa. The climate driver results show that ENSO has a strong influence on the mid-summer weather patterns. However, this influence only distinguishes between the two main weather patterns during mid-summer, but not the variation within the weather patterns themselves. Other climate drivers, such as SAM and SWIO, show no significant influences.

CHAPTER 5: EVALUATION OF CORDEX MODELS IN SIMULATING HISTORICAL DRY SPELLS OVER MAJOR MAIZE-PRODUCING REGIONS OF SOUTH AFRICA

5.1 ABSTRACT¹

This study examined dry spells using total pentad rainfall output from historical climate model simulations obtained from CORDEX RCA4 over the major maize-producing regions of South Africa. Historical observations were compared with model simulations of dry spells for the mid-summer period from 1951 to 2005. Generally, RCA4 underestimates dry spells, compared to the climatologically observed values from the CORDEX models for the mid-summer period. There are, however, some regions within the study area that compare well with the observed scenarios, indicating specific small-scale inadequacies to be investigated further. Investigations of the upper-air tropical circulation diagnostics and the position of the ITCZ clearly show that the RCA4 simulations differ from the observed scenarios, indicating that large-scale upper-air circulations are not well captured in the model simulations.

Keywords: Dry spells; mid-summer; CORDEX; rainfall; upper air; ITCZ

¹ When making reference to this section, please cite as follows: Mengistu, M.G., Olivier, C., Mathole, K., Adeola, A. and Makgoale, T. 2021. Evaluation of CORDEX models in simulating historical dry spells over major maize-producing regions of South Africa. In: Mengistu et al. (Eds). 2021. An investigation of the historical and projected occurrence of the South African mid-summer drought and its implications for the agro-water budget. Water Research Commission, Pretoria, RSA, WRC Report K5/2830, Chapter 5.

5.2 INTRODUCTION

Climate change has significant effects on water resources, agriculture and other climate-sensitive sectors (Thomas et al., 2007). Extreme weather events, such as droughts, are widely projected to become more frequent, intense and severe as the global climate continues to warm up due to anthropogenic greenhouse gas emissions (Hegerl et al., 2004). Changes in extreme weather and climate events have significant impacts on agriculture, and are among the most serious challenges for food security and human wellbeing. Consequently, many studies have been conducted on analysing, or generating, possible near-to-long-term future projections of likely changes in climatic variables and indices (Giorgi and Bi, 2005).

Short- and long-term droughts are known to have a negative impact on agricultural production, food security and the economy (Loukas and Vasiliades, 2004). Short-term droughts (dry spells) are defined as periods of dry days with a precipitation deficit, resulting in water shortages and arid conditions. Information on the length of dry spells is important for deciding whether a particular crop or variety of crop is at risk, and to determine irrigation water demand (Mathugama and Peiris, 2011). Dry spells can be used as indicators of dry conditions, and are critical for crop production, as the timing of the occurrence of a drought relative to the cropping calendar is more important than the total seasonal rainfall (Usman and Reason, 2004). For example, the flowering stage of maize has been found to be the most sensitive to water stress, leading to reductions in crop growth, biomass production and, finally, crop yield (Du Plessis, 2003). In South Africa, rainfall is one of the most significant factors limiting dryland crop production. The mid-summer period is particularly important since a lack of rain for even a few days during this period may influence growth and eventually decrease crop yield. Dry-spell frequency analyses are used globally to investigate the implications of sub-seasonal rainfall variability on food security (Usman and Reason, 2004). Several studies in semi-arid environments in sub-Saharan Africa have indicated that dry spells range between 5 and 15 days (Usman and Reason, 2004). However, little research has been devoted to short-term droughts in South Africa. Furthermore, changes in rainfall amount and distribution caused by climate change can have a negative effect on crop yield and might not make marginal area crop production viable. Therefore, information on the future projection of dry spells is crucial for sustainable crop production and food security.

In recent decades, there is strong evidence of an increasing trend in the frequency, intensity and duration of extreme weather events, along with climate change (Wuebbles et al., 2014). Nowadays, advances in modelling the earth system allow for the use of global general circulation models to generate projections of extreme temperature and precipitation, and their associated indicators (Tebaldi et al., 2006). Global coupled ocean-atmosphere general circulation model (CGCM) simulations, forced with projected greenhouse gas and aerosol emissions, are the primary tools for studying the possible future changes in climate mean, variability and extremes (Kharin et al., 2007). Recently, numerous regional climate models (RCMs) were used to assess the impacts of climate change on hydrology and the environment (Frei et al., 2017; Chung et al., 2018; Varikoden et al., 2018).

For example, Alexander and Arblaster (2009) have used multiple GCMs to simulate observed trends in dry spells over Australia and to assess projected changes in climate extremes. They also highlighted the importance of validating climate simulations with respect to historical observations. The ability of a climate model to estimate the present climate and reproduce historical trends leads to higher confidence in projecting future climate (Reifen and Toumi, 2009; Wuebbles et al., 2014).

The climate in southern Africa is related to different oceanic and atmospheric patterns, such as the position of the ITCZ, which controls intra-annual rainfall variability. For upper-air diagnostics, an analysis of tropical circulations, with the most emphasis on the Hadley cell and the ITCZ, is important. Hadley circulation is considered to be one of the dominant large-scale circulation features over the tropics.

It is defined as the zonally symmetric meridional circulation with an ascending motion over the ITCZ, and the descending motion over the subtropical belt (Oort and Yienger, 1996; Trenberth et al., 2000; Tanaka et al., 2004). The rising in motion of the Hadley circulation is usually where potential velocity peaks are positive, especially in the tropics. It therefore coincides with the position of the ITCZ (Tanaka et al., 2004).

This study aims to investigate whether mid-summer dry spells are captured in historical climate model simulations over the summer rainfall region of South Africa. The study will also evaluate whether large-scale upper-air circulations are captured in the model simulations. However, in the methodology, careful consideration should be given to the analysis due to the existence of possible climate drift in the CORDEX simulations. Climate drift could possibly exist due to its existence in the driving models of the downscaled CORDEX models. These climate models exhibit spurious long-term changes that may distort the estimate of climate simulations (Gupta et al., 2013). Thus, instead of investigating time series analysis for verification, climatological statistics are evaluated for this study.

5.3 DATA AND METHODOLOGY

5.3.1 Data sources

5.3.1.1 The European Centre for Medium-range Weather Forecasts reanalysis

The European Centre for Medium-range Weather Forecasts recently released a global reanalysis dataset (ERA5), which was used in this study. ERA5 data provides hourly estimates of a large number of atmospheric, land and oceanic climate variables. The data covers the earth at a 30° x 30° grid resolution, and resolves the atmosphere using 137 horizontally orientated levels from the surface up to a height of 80 km. The ERA5 data includes information about uncertainties for all variables at reduced spatial and temporal resolutions (ECMWF, 2019). Zonal (U) and meridional (V) components of the wind from the ERA5 data at the 200 hPa pressure level, on a monthly time resolution, were used to compute velocity potential.

5.3.1.2 District rainfall

The South African Weather Service divides South Africa into 94 rainfall districts, which are presented in Figure 5.1. The delineation of these districts was mainly done according to the annual march of maximum rainfall, and the boundaries between the winter, whole-year and summer rainfall regions. A daily district rainfall total is calculated as the average of the daily values available in the district under consideration (Kruger and Nxumalo, 2017).

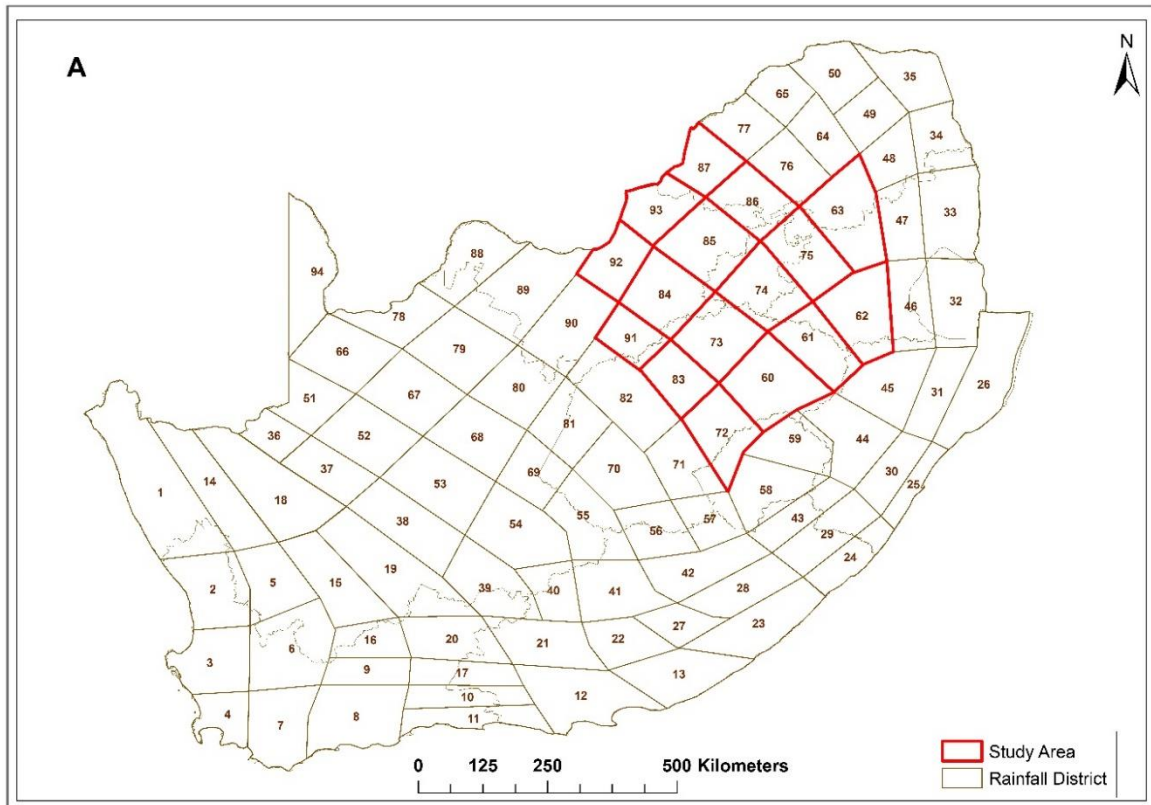


Figure 5.1: District rainfall regions in South Africa (SAWB, 1972), showing the study area with 16 selected districts marked with red polygons

5.3.1.3 Models

The regional climate models evaluated in this study form part of the regional climate models that participated in CORDEX-Africa. The CORDEX-Africa initiative aims to perform dynamic downscaling to produce high-resolution climate simulations over the African domain using forcing from atmosphere-ocean global climate models (AOGCMs). For this study, eight individual global circulation models that participated in CMIP5 (Table 5.1) were dynamically downscaled to a finer spatial resolution ($0.44^\circ \times 0.44^\circ$) using RCA4. The RCA4 model is a coupled ocean-atmosphere regional climate model based on the numerical weather prediction (NWP) model HARLAM (Undén et al., 2002). The RCA4's simulated projections formed part of the CORDEX initiative (Jones et al., 2011).

Table 5.1: List of global circulation models used in the study

Model name	Country	Resolution	Literature
CanESM2m	Canada	$2.8^\circ \times 2.8^\circ$	Arora et al. (2011)
CNRM-CM5	France	$1.4^\circ \times 1.4^\circ$	Voldoire et al. (2013)
CSIRO-Mk3	Australia	$1.9^\circ \times 1.9^\circ$	Rotstayn et al. (2013)
IPSL-CM5A-MR	France	$1.9^\circ \times 3.8^\circ$	Hourdin et al. (2013)
MIROC5	Japan	$1.4^\circ \times 1.4^\circ$	Watanabe et al. (2011)
MPI-ESM-LR	Germany	$1.9^\circ \times 1.9^\circ$	Ilyina et al. (2013)
NorESM1-M	Norway	$1.9^\circ \times 2.5^\circ$	Tjiputra et al. (2013)
GFDL-ESM2M	USA	$2.0^\circ \times 2.5^\circ$	Dunne et al. (2012)

5.3.2 Methodology

5.3.2.1 District rainfall analysis

From the daily district rainfall, pentad summations were calculated following the methodology used in Grobler (1993). Pentads were calculated using Julian days. For example, Pentad 1 refers to 1–5 January and Pentad 73 refers to 27–31 December. The extra leap year day, 29 February, was added to Pentad 10. Eight pentads between 12 December (the start of Pentad 70) and 20 January (the end of Pentad 4) were selected for a detailed analysis of the mid-summer rainfall in the study area. A threshold of 3 mm per day (15 mm per pentad), which is the minimum rainfall depth threshold for crops to satisfy their crop water requirement during a growing season, was used (Reddy, 1990) in the dry-spell analysis. The occurrence of dry spells (< 15 mm total rainfall in a pentad) was calculated and evaluated against the district rainfall dry spell occurrence using binary data (1 for a dry spell event and 0 for a non-event).

5.3.2.2 Model simulations

Daily rainfall data from eight individual global circulation models (Table 5.1), downscaled using RCA4 (CORDEX) for the reference period (1951–2005), was used for the dry-spell analysis. The downscaled simulations from the CMIP5 GCM were evaluated against the SAWS's district observations. Model-simulated daily precipitation flux was first converted to mm using a scalar multiple of 86 400. Values nearest to the latitude and longitude of district observations were then extracted for easy comparison with the district rainfall. Due to the fact that these climate simulations could be influenced by climate drift, a one-to-one comparison of daily, or pentad, rainfall totals is not recommended. Instead, the study focuses on the evaluation of the climatological occurrences of dry spells using probability density function (PDF) graphs. From the histograms of dry-spell occurrences in mid-summer (a number from 0–8, maximum eight pentads in mid-summer), all models and observation follow a normal distribution. Thus, it is possible to fit these results into a normal distribution graph for easier comparison. These PDF curves from the individual models can then be plotted against the observed dry-spell occurrence PDF graphs to compare whether the models underestimate or overestimate the dry spells.

5.3.2.3 Upper-air diagnostics

Variability of the intensity of tropical circulations can be measured using variables, such as velocity potential (VP). The VP is computed from zonal (U) and meridional (V) components of the wind, from ERA5 and CORDEX models, at 200 hPa, at monthly time intervals. The VP data is then zonally averaged, as it is assumed that information on the Hadley circulation is contained in the zonal mean field. The ERA5 data was obtained at a global scale, but for comparisons with the CORDEX models, data was re-gridded to the same domain as the models across the African region. Positive peaks in zonal mean fields of the VP represent the rising in motion, while negative peaks represent a sinking motion. For consistency, the tropics are defined as latitudes from 30° N to 30° S.

5.4 RESULTS AND DISCUSSIONS

5.4.1 CORDEX model evaluation

The evaluation of model simulation results are presented in figures 5.2 to 5.5, providing PDF graph comparisons with climatological observations. All 16 districts within the study area are presented. The graphs depict how closely the CORDEX models succeed in simulating the climatological occurrence of dry spells during the mid-summer period (eight pentads). The figures show the results from the eight models defined in Table 5.1, and whether these models generally over- or underestimate the occurrence of dry spells, depending on the location of the peak of the curve relative to the observation curve.

These PDF graphs indicate that the CORDEX models generally underestimate occurrences of dry spells over the study area. However, simulations for some of the regions, like regions 72, 85 and 87, are close to the observed occurrences of dry spells during mid-summer. Generally, some regions grossly underestimated the occurrence of dry spells, such as regions 61 and 63, which are in the wetter regions of the study area.

In summary, the CORDEX models did not perform well in simulating the climatological occurrence of dry spells across the whole study area, with the exception of a few regions. These results are consistent with other studies, indicating the general wet bias of CORDEX models over the South African region (Kalognomou et al., 2013).

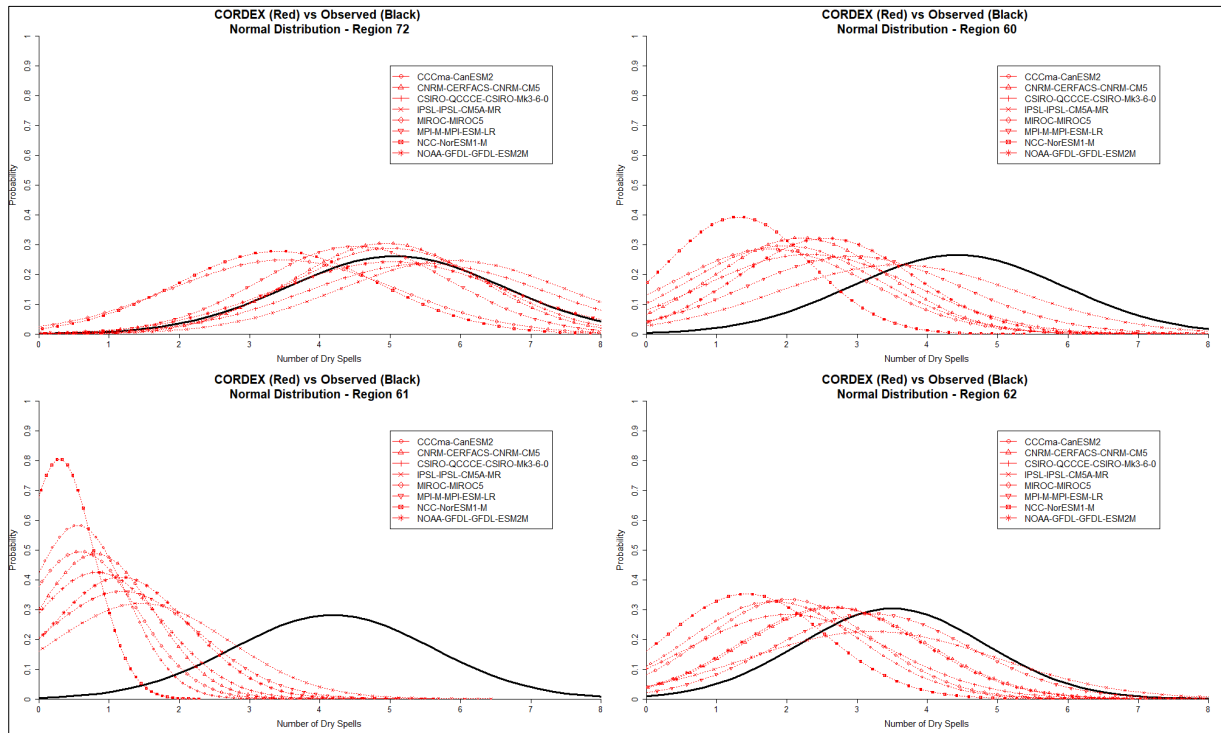


Figure 5.2: Probability density functions for the eight CORDEX models (red) and observed (black) dry spell occurrences during mid-summer for districts 60, 61, 62 and 72. There are a maximum of eight pentads in the mid-summer period.

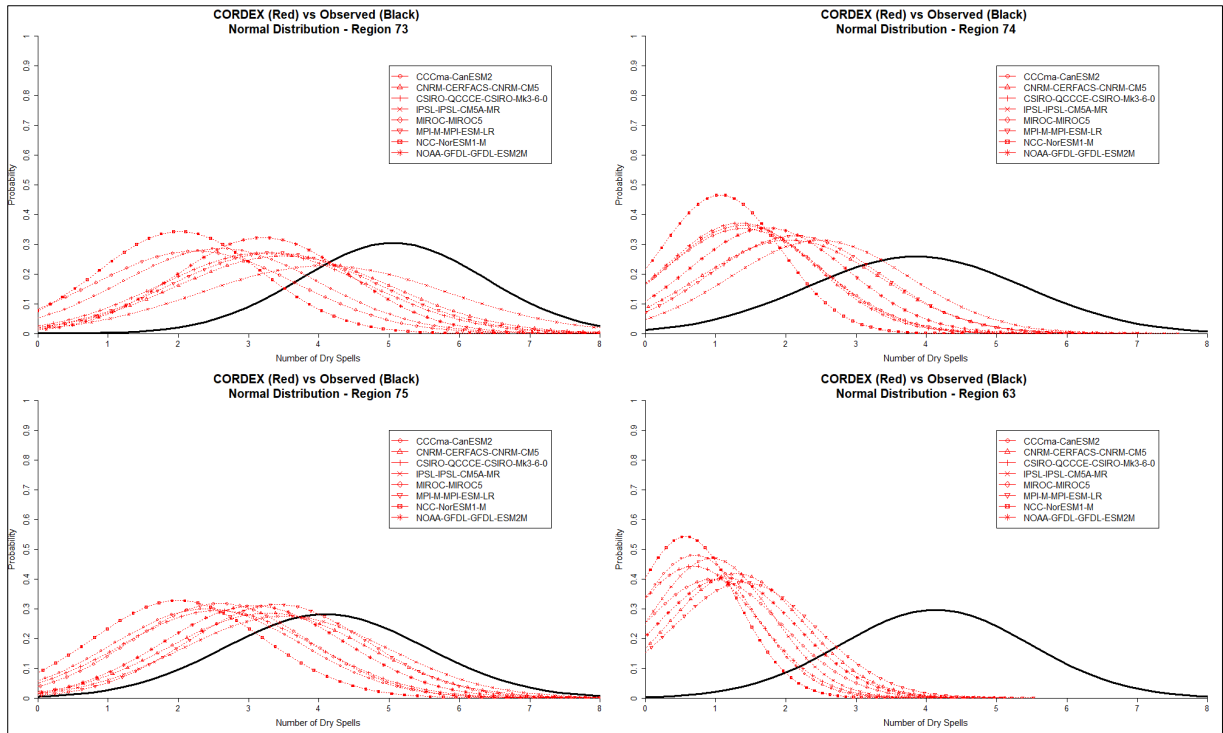


Figure 5.3: Probability density functions for the eight CORDEX models (red) and observed (black) dry spell occurrences during mid-summer for districts 63, 73, 74 and 75

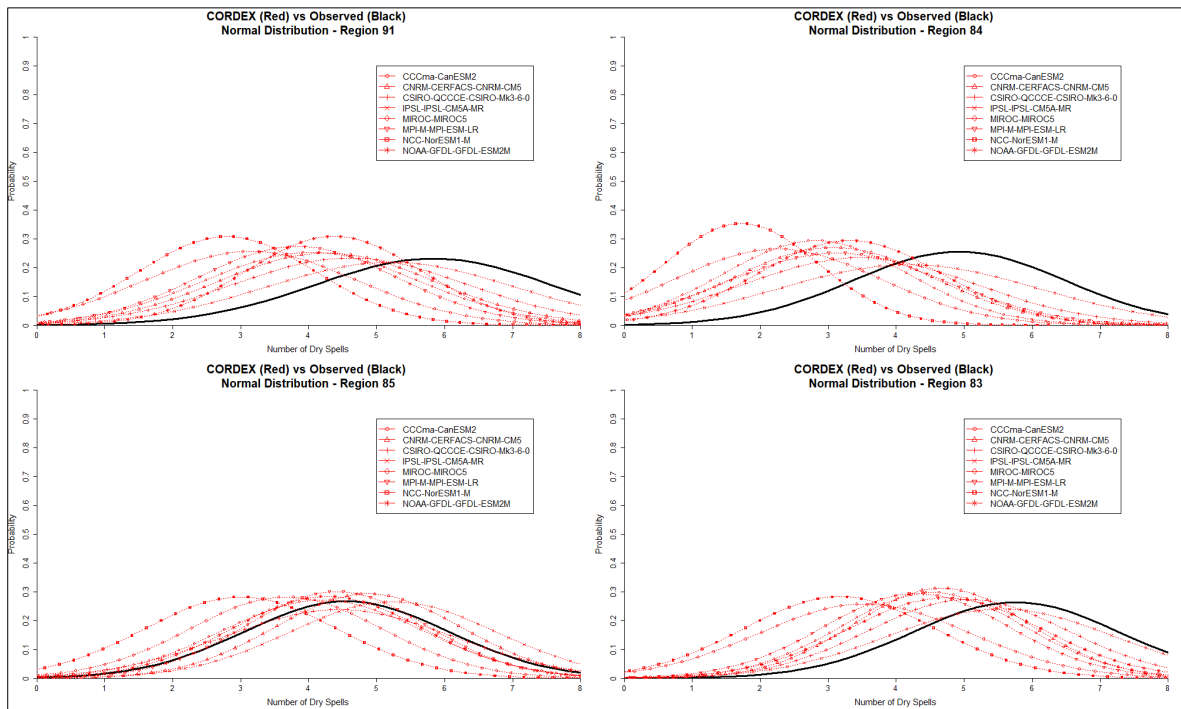


Figure 5.4: Probability density functions for the eight CORDEX models (red) and observed (black) dry spell occurrences during mid-summer for districts 83, 84, 85 and 91

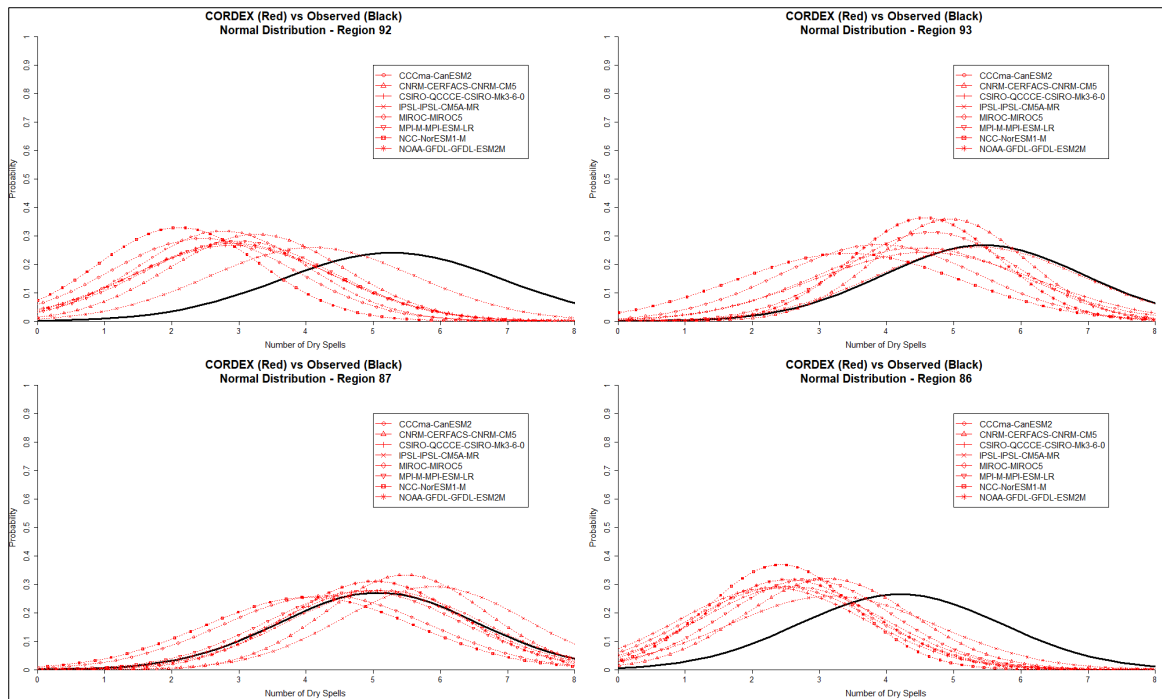


Figure 5.5: Probability density functions for the eight CORDEX models (red) and observed (black) dry spell occurrences during mid-summer for districts 86, 87, 92 and 93

Global studies that compare observed and modelled trends in climate extremes have shown reasonably good agreement with temperature trends, but poor agreement (or multi-model disagreement) with observed precipitation patterns or trends (e.g. Kharin et al., 2007; Kiktev et al., 2007). Other studies, again, show that the regional responses of observed trends in climate extremes are largely driven by large-scale processes, which might not be adequately simulated in global climate models (Meehl et al., 2004; 2005; Scaife et al., 2008). A number of regional studies show that the modelled trends capture observed trends reasonably accurately. However, the results were, to a certain degree, dependent on the climate extreme under consideration (Sillmann and Roeckner, 2008; Meehl and Tebaldi, 2004). Meque (2015) evaluated the capability of ten CORDEX RCMs in simulating southern African droughts. Only a few CORDEX RCMs succeeded in simulating southern African droughts, as observed. The ARPEGE model showed the best simulation performance. According to Meque (2015), this may be due to the stretching capability of the model, which helps eliminate boundary condition problems, which are present in other RCMs.

5.4.2 Upper-air tropical circulations diagnostics and ITCZ position

The climatology of the velocity potential (VP) field is presented for both the ERA5 data and the CORDEX model output (Figure 5.6). Note that the climatologies were calculated for all the months on all eight models, but only three models – CanESM2m (CCMA), CNRM-CM5 (CERFACS) and CSIRO-Mk3 (CSIRO) – were selected and presented here, since the results are mostly similar. The study also focuses more on the mid-summer period. Therefore, not all the monthly climatologies are presented. ERA5 observations (Figure 5.6, far left panel) shows a clear evolution of the VP field during different seasons.

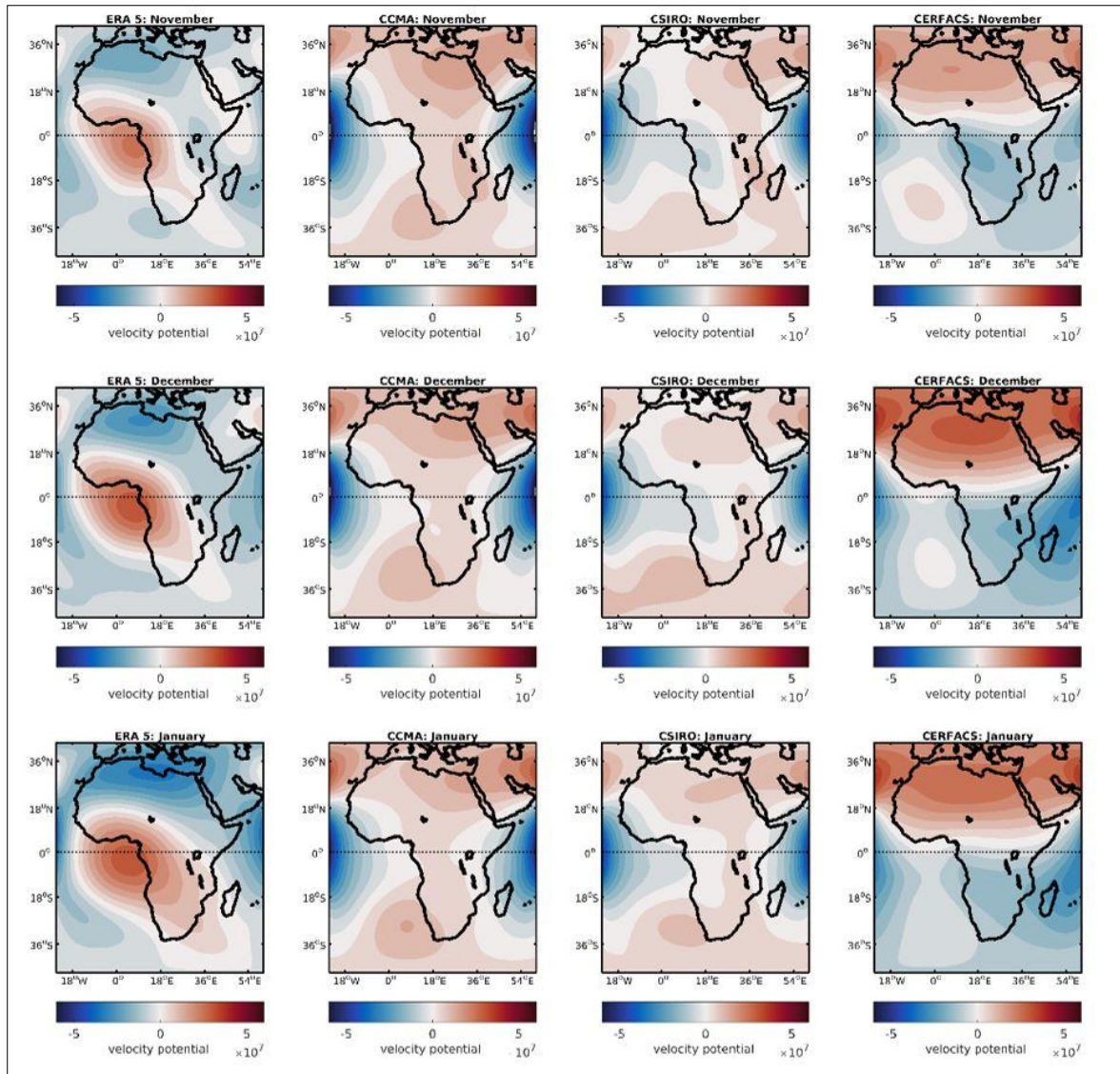


Figure 5.6: Early summer months' climatology of the velocity potential in ERA5 and the three models of CORDEX-Africa. Climatology-based period: 1979–2005. Contour intervals are $0.5 \times 10^7 \text{ m}^2 \text{ s}^{-1}$.

During the early summer months (November, December and January), the VP field maximum is mostly located to the south of the equator, as shown in Figure 5.6. However, it is located a bit further north of the equator during early spring, as the zone of moist air follows heating in the northern hemisphere (Figure 5.7). The zonal mean field of VP confirms this seasonality further (Figure 5.8). The VP maximum is generally located in the southern hemisphere during summer months, especially during the late summer months (December and January, indicated by the red stars). The correct seasonality of the VP is not observed in most of the CORDEX models due to the misrepresentation of their climatology, as seen in figures 5.6 and 5.7. The VP of most models seems to be distributed throughout the two hemispheres, with maximum values occurring in the opposite location as observed in the ERA5 data.

It also becomes evident, when looking at zonal mean fields, that the models' climatology is not simulating the VP as it is observed. The maximum VP is occurring in the opposite location contrary to the observed data. Even though this is the case, it is noted that some CORDEX models capture the zonal mean pattern for some months reasonably well, although they are still not able to maintain the proper evolution.

For, example, the ITCZ location, as simulated by the CSIRO model, seems to occur in the southern hemisphere in December, and is not seen in other months (Figure 5.8). It is also worth mentioning that this inconsistency has been noted in other months for some models, even though it is not presented here.

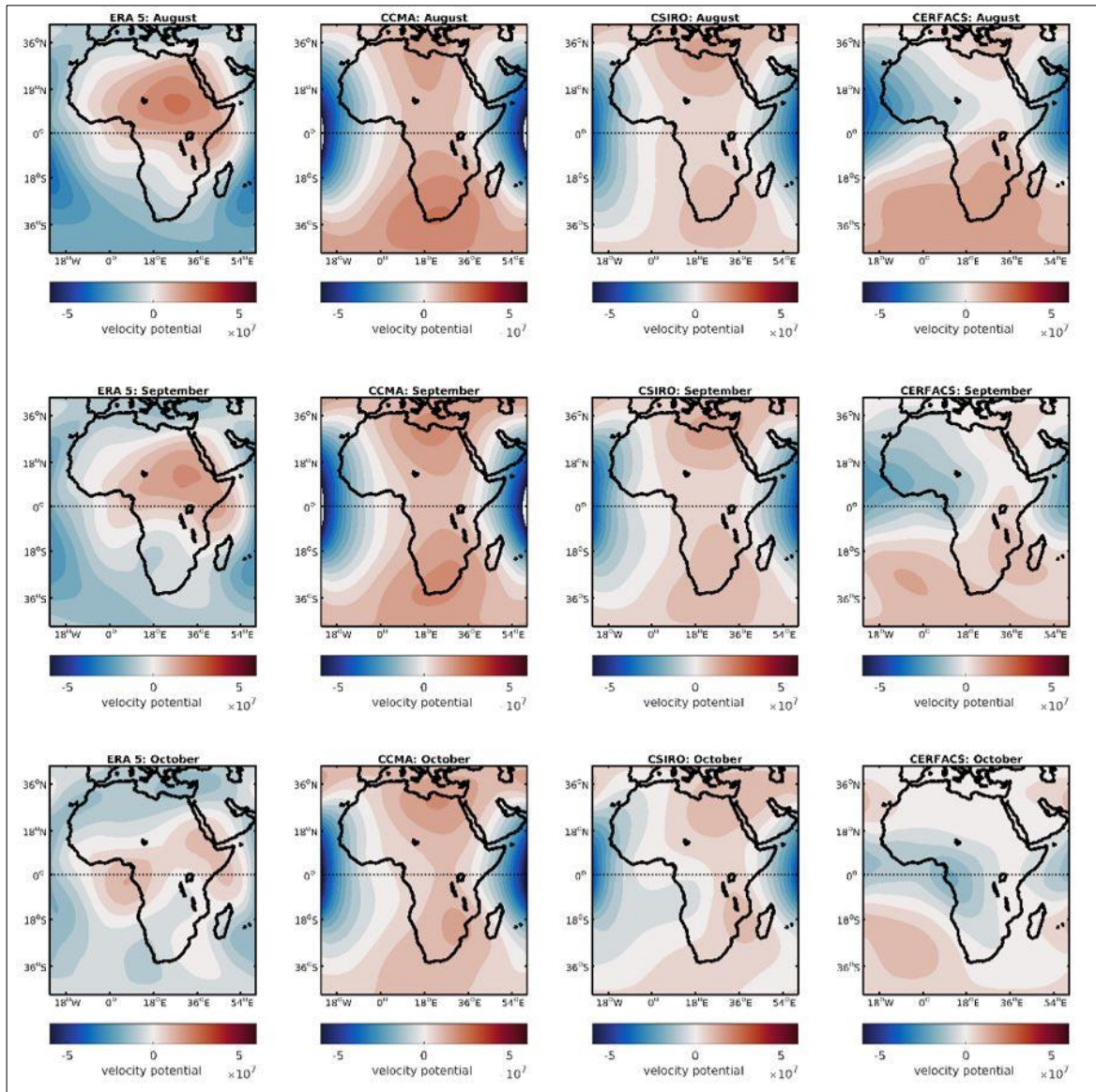


Figure 5.7: The late winter to spring months' climatology of the velocity potential in ERA5 and the three CORDEX-Africa models. Climatology-based period: 1979–2005. Contour intervals are $0.5 \times 10^7 \text{ m}^2 \text{ s}^{-1}$.

In an attempt to assess the potential relationship between rainfall and the location of the ITCZ, an observation study was conducted using the ERA5 dataset. The ITCZ location index was created for the months of October to March (Figure 5.9). A negative index indicates a more southward shift of the ITCZ's location, while a positive index indicates a more northward shift, compared to the climatological position. Different sets (months) of indices were then correlated with the rainfall for all 94 districts. The relationship was assessed for different lead times to capture potential predictability. Rainfall was also accumulated over a two-month period to cover the defined mid-summer period of the study (e.g. November–December, December–January, etc.). The relationship between the November ITCZ position and the November–December rainfall districts is presented in Figure 5.10. It is worth noting that this relationship is computed for a lead time of 0 (i.e. November ITCZ initial conditions predicting November–December rainfall).

There seems to be a relationship between the rainfall and ITCZ position for some of the districts, with correlation values ranging from 0.3 to 0.5 that are statistically significant at the 95% level of confidence (Figure 5.10, districts with red stars). The relationship is clearly negative, suggesting that a more southward ITCZ location could be related to above-normal rainfall. These results are consistent with an earlier study (Olivier, 2015), which looked at the relationship between rainfall and the ITCZ. However, using rainfall as a proxy for identifying location, most of the districts in the study area (Figure 5.1) also reflect this correlation. It is, however, worth mentioning that the low correlation values may suggest that the ITCZ controls the seasonality of rainfall, rather than its seasonal variability.

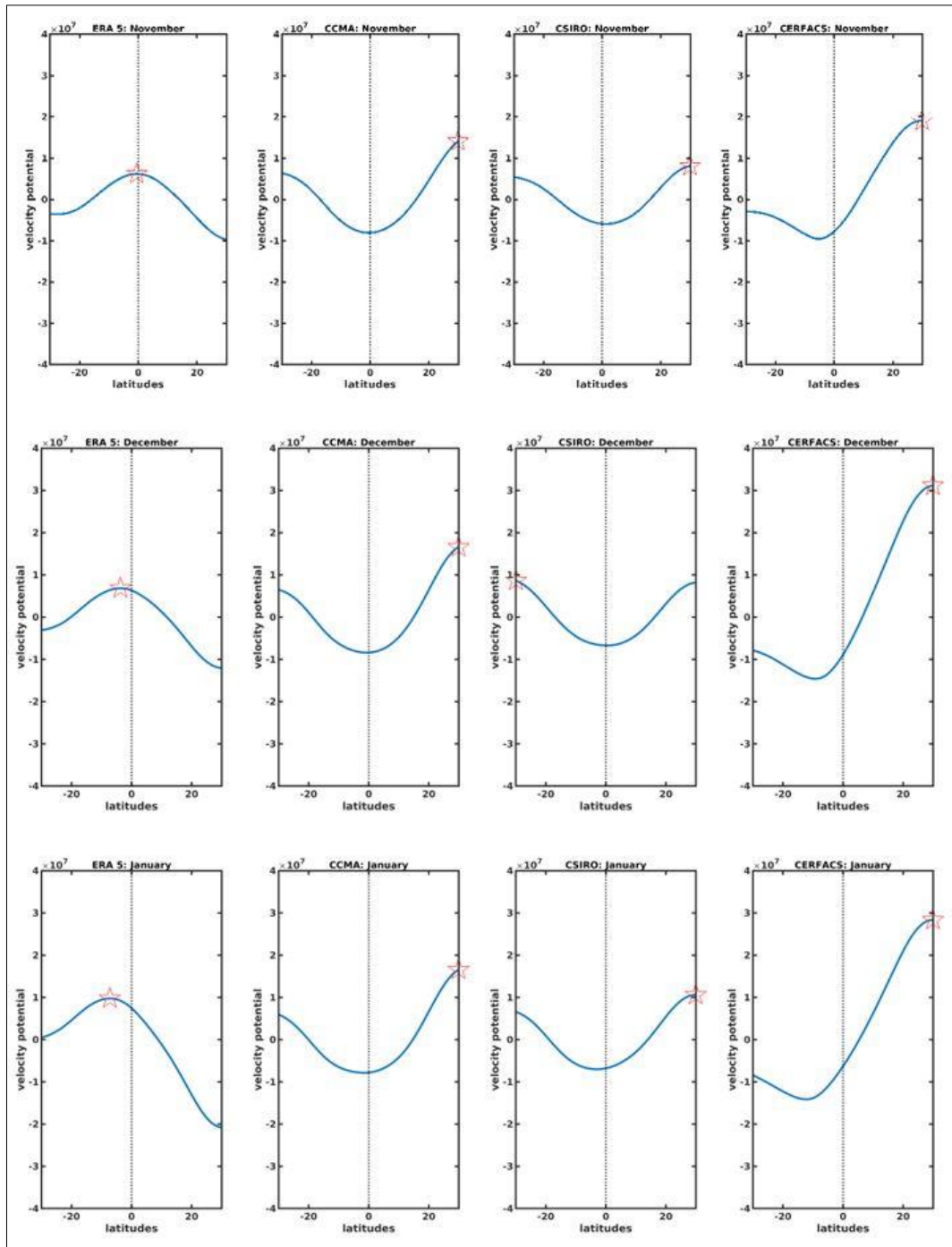


Figure 5.8: Zonal mean velocity potential field for the corresponding VP CORDEX region as shown in Figure 5.1. Red stars serve as the estimate for the location of the ITCZ. Latitudes have been limited from 30° N to 30° S for defining the region of the tropics.

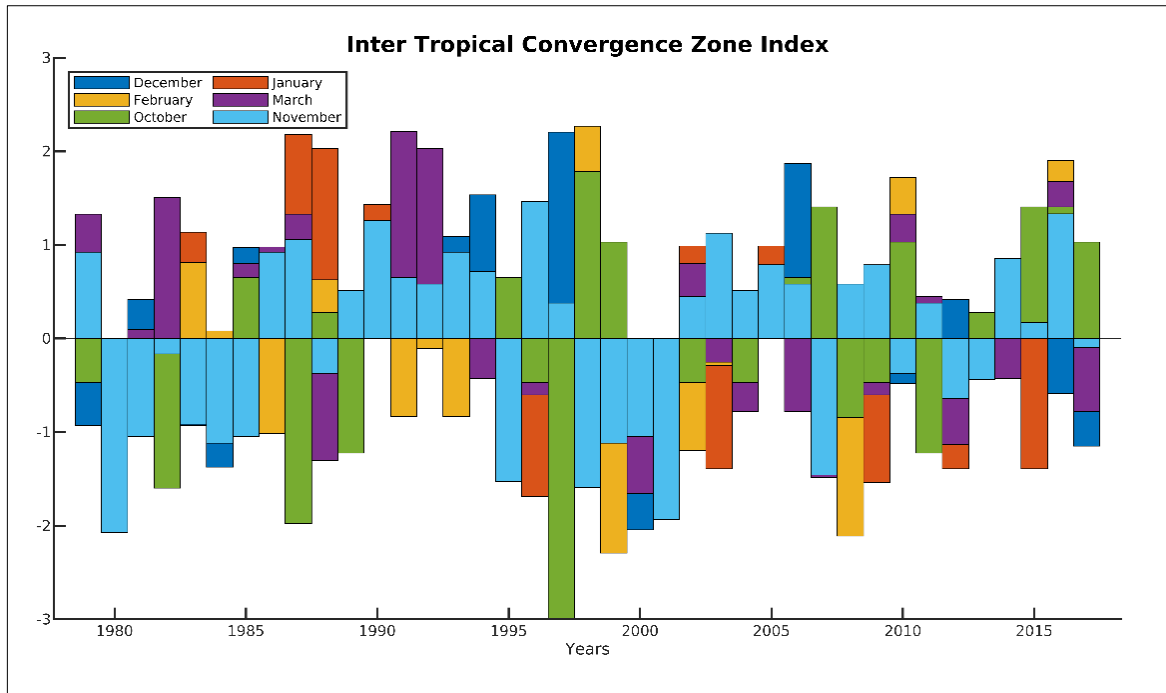


Figure 5.9: ITCZ location standardised index for different months (i.e. October to March)

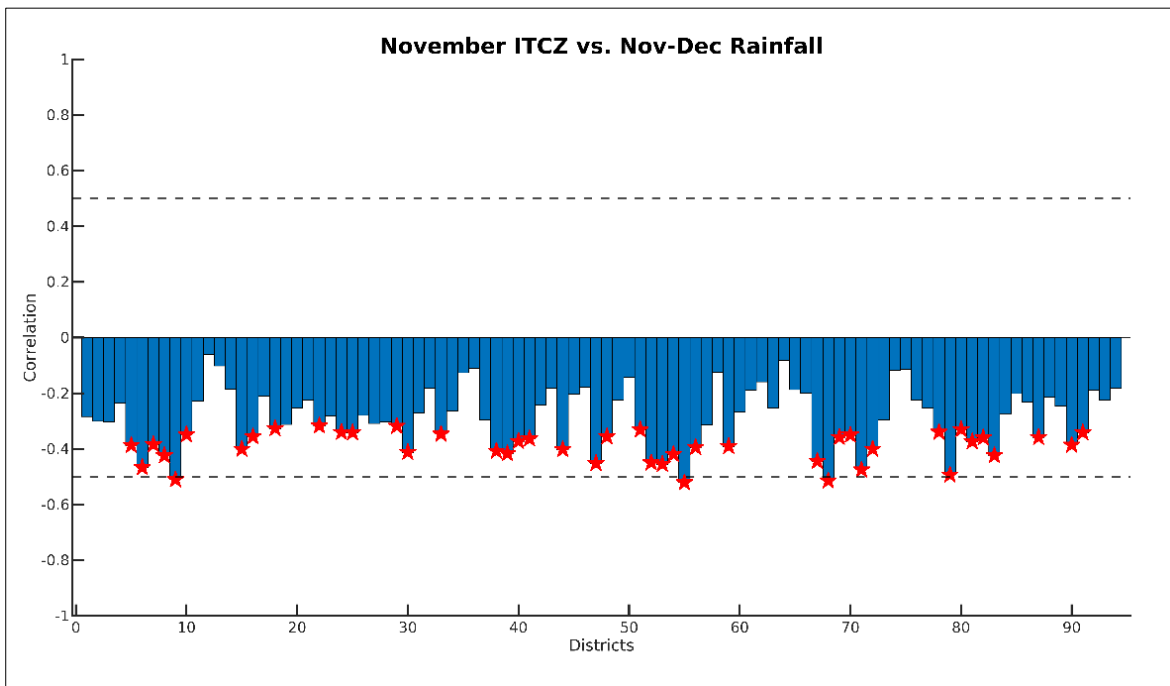


Figure 5.10: Correlation between the November ITCZ position and November–December rainfall for all 94 districts. Districts where correlation is significant at the 95% level of confidence are indicated with red stars.

5.5 CONCLUSIONS

Changes in extreme weather and climate events have significant impacts on agriculture and food security. Internationally, many studies have demonstrated that short- and long-term droughts have a negative impact on agricultural production. Information on the length and frequency of dry spells is critical for crop production and agricultural water management. Changes in rainfall amount and distribution caused by climate change can have a negative effect on crop growth and yield. Therefore, information on future projections of dry spells is equally important for sustainable crop production and food security. The mid-summer period is particularly important since a lack of rain during this period may have a negative impact on crop growth and yield.

The aim of this study is to investigate whether mid-summer dry spells are captured in historical climate model simulations over the summer rainfall region of South Africa. Daily rainfall data from eight individual CMIP5 GCMs downscaled using RCA4 (CORDEX-Africa) for the reference period 1951–2005 was used for the dry-spell analysis. The study also evaluated whether large-scale upper-air circulations are captured in the model simulations.

Generally, the underestimation of dry spells is detected between the modelled and observed climatological dry spell occurrences for the mid-summer period. Some regions within the study area, however, seem to capture the climatological occurrence of dry spells well, though, which suggests possible small-scale inadequacies in the models. This is an avenue for further investigation. The dry-spell simulation by the models is severely hampered by the general wet bias of the CORDEX simulations.

The study also evaluated whether the large-scale circulations are captured in the model simulations using upper-air tropical circulation diagnostics and the position of the ITCZ. It has been demonstrated, using ERA5 observations, that the dynamic field velocity potential may offer an opportunity to estimate the general location of the ITCZ. There is a negative relationship between the early summer rainfall (November–December) and the position of the ITCZ in November. These results lay a foundation for exploring the impact of the ITCZ on the intra-seasonal variability of rainfall over South Africa, as well as the associated mid-summer dry-spell frequencies. The study could not assess the relationship between district rainfall and the position of the ITCZ in the CORDEX models due to inconsistencies between observed scenarios and the model-simulated climatology of the velocity potential field. While there is no clear understanding of why the models' climatology is different to that of the observed scenarios, an earlier study indicated that boundary condition problems are present in most CORDEX RCMs.

The researchers recommend assessing other CORDEX RCMs, as well as comparing them to statistical downscaling methods. They also recommend the use of tropical rainfall distribution to calculate the position of the ITCZ rather than upper-air tropical circulations.

CHAPTER 6: CLIMATE CHANGE PROJECTIONS OF THE MID-SUMMER DRY SPELLS OVER THE MAIZE-PRODUCING REGION OF SOUTH AFRICA

6.1 ABSTRACT²

This study examines dry spells for the mid-summer period, using consecutive dry days (CDD) and pentads' total rainfall output from historical climate model simulations. Results from CORDEX RCA4 simulations for the major maize-producing regions of South Africa are used for this purpose. First, historical observations were compared with model simulations from 1979 to 2005. Second, projections were made for CDD and pentad totals for two slice periods of 30 years: 2036–2065 and 2066–2095, under conditions of the representative concentration pathways (RCP) 4.5 and 8.5. Three thresholds of 1 mm, 2 mm and 3 mm of daily total rainfall for CDD, and 5 mm, 10 mm and 15 mm total rainfall for a pentad were used to analyse dry spells. Low correlation and low skill scores were detected between the individual modelled and observed total pentad's rainfall across the districts for the mid-summer period, indicating that individual model ensemble members often failed to simulate the total pentad's rainfall for South Africa's summer rainfall region. However, ensemble means of the eight CORDEX RCA4 simulations showed an improved correlation of about 68% in simulating the CDD and the pentads' total rainfall. The results suggest an increase in CDD and dry pentads for the two future projection slice periods.

Keywords: Dry spells; mid-summer; climate change; CORDEX; rainfall; projections

² When making reference to this section, please cite as follows: Adeola, A.M., Mengistu, M.G., Makgoale, T.E. and Olivier, C., 2021. Climate change projections of the mid-summer dry spells over the maize-producing region of South Africa. In: Mengistu et al. (Eds). 2021. An investigation of the historical and projected occurrence of the South African mid-summer drought and its implications for the agro-water budget. Water Research Commission, Pretoria, RSA, WRC Report K5/2830, Chapter 6.

6.2 INTRODUCTION

One of the major anticipated impacts of climate change on rainfall is an increase in variation patterns, which might directly or indirectly affect regional water sources. Warmer temperatures might enhance evaporation from the soil, resulting in surface drying. This will make regions with a low precipitation even drier and potentially contribute to the intensity and duration of dry spells and droughts in general. Climate change might therefore have a significant effect on water resources, agriculture and other climate-sensitive sectors (Thomas et al., 2007). In addition, extreme weather events such as droughts are widely projected to become more frequent, intense and severe as the global climate continues to warm up due to anthropogenic greenhouse gas emissions (Hegerl et al., 2004). Changes in extreme weather and climate events might have significant impacts on agriculture and are among the most serious challenges for food security and human wellbeing. Consequently, many studies have been conducted on analysing or generating possible near- to far-term future projections of likely changes in climatic variables and indices (Giorgi and Bi, 2005).

Short and long-term drought is known to have a negative impact on plant growth, agricultural production and food security, and therefore on the broader economy (Loukas and Vasiliades, 2004). Short-term drought (a dry spell) is defined as a period of dry days with a precipitation deficit, resulting in water shortages and arid conditions. Information on the expected length of dry spells is important to decide on what crop or variety of crops to plant, and for irrigation planning (Mathugama and Peiris, 2011). Dry spells can be used as indicators of drought conditions and are critical for crop production. Furthermore, changes in rainfall amount and distribution caused by climate change may also have a negative effect on crop yield and might make crop production in a marginal area unviable. Therefore, information on the future projection of dry spells is crucial for sustainable crop production and food security.

In recent decades, there has been strong evidence of increasing trends in the frequency, intensity and duration of extreme weather events, along with climate change (Wuebbles et al., 2014). Nowadays, advances in modelling the earth system using super computers allows for the use of global general circulation models to generate projections of extreme temperature and precipitation trends and indicators (Tebaldi et al., 2006). Global coupled ocean-atmosphere general circulation model simulations, forced with projected greenhouse gas and aerosol emissions, are the primary tools for studying possible future changes in climate mean, variability and extremes (Kharin et al., 2007). Recently, numerous regional climate models were used to assess the impact of climate change on hydrology and the environment (Frei et al., 2017; Chung et al., 2018; Varikoden et al., 2018).

Alexander and Arblaster (2009) have used multiple GCMs to simulate observed trends in dry spells over Australia, and to assess projected changes in climate extremes. They highlighted the importance of validating climate simulations with respect to historical observations. However, the ability of a climate model to estimate the present climate and reproduce historical trends leads to a higher confidence in projecting future climate (Reifen and Toumi, 2009; Wuebbles et al., 2014).

The periods of dryness (dry spells) and wetness (wet spells) are usually associated with variations in the rainfall time series. The analysis of rainfall spells (dry and wet spells) is based on defining a threshold, because the frequency distribution of the length of these spells depends on such a selected threshold (Barring et al., 2006). In several studies, different thresholds have been considered, subject to the characteristic of the spells that have been investigated. For example, Moon et al. (1994) used a threshold of 0.1 mm precipitation per day in South Korea, while Martin-Vide and Gomez (1999) used this threshold in Spain. In other studies, Frei et al. (2003) used a threshold of 1.0 mm precipitation per day for analysing spells in the European Alps. Douguedroit (1987), and Usman and Reason (2004) used this same threshold in France and southern Africa, respectively. Additionally, Perzyna (1994) used a threshold of 2.0 mm per day for analysing spells over southern Norway, while Ceballos et al. (2004) used a threshold of 10 mm rainfall per day to analyse wet and dry spells over a basin in Spain.

A threshold of 3 mm daily rainfall is proposed as the minimum rainfall depth required to satisfy crop water needs during the growing season (Reddy 1990). Consequently, in this study, a dry spell is defined as a period of five days (a pentad) during which rainfall totals are less than the different predefined thresholds. Three thresholds, 1 mm, 2 mm and 3 mm of daily total rainfall for CDD, and 5 mm, 10 mm and 15 mm total rainfall for a pentad, were used to analyse dry spells.

Therefore, the aim of this study is to investigate various climate change projections with respect to expected changes in mid-summer dry spells using dynamically downscaled CORDEX projection data. Consequently, climate change projections for consecutive dry days for the summer rainfall months (October to March), consecutive dry days for the mid-summer rainfall months (December to January) and total pentad rainfall for December (pentads 68 to 73) and January (pentads 1 to 6) for 2036–2065 and 2066–2095 under the conditions of RCP 4.5 and 8.5 are investigated.

6.3 DATA AND METHODS

6.3.1 Study area

The study area considered is the main maize-producing region of South Africa, which receives rainfall during the summer months (Figure 6.1). This region includes areas in the Free State, Gauteng, KwaZulu-Natal, Limpopo, Mpumalanga and North West. Summer is defined as the six-month period extending from October to March. A map illustrating the South African average rainfall totals over the period of October to March is depicted in Figure 6.2. Climatological rainfall totals from October to March are calculated and related, as a percentage, to the annual rainfall totals (defined here as June to May to capture the full period from October to March). Most of the north-eastern parts of South Africa receive above 80% of their annual rainfall from October to March. Parts of the eastern coastal areas still receive significant rainfall during these months, although they also receive rainfall during winter and spring, lowering the overall percentage of annual rain for October to March (NCAR, 2017). Mid-summer dry spells occur approximately between mid-December and mid-January (Usman and Reason, 2004). From the daily district rainfall, pentad summations were calculated following the methodology used by Grobler (1993). Pentads were calculated using Julian days. For example, Pentad 1 refers to 1–5 January and Pentad 73 refers to 27–31 December. The extra leap year day, 29 February, was added to Pentad 10. Twelve pentads between 2 December (the start of Pentad 68) and 30 January (the end of Pentad 6) were selected for a detailed analysis of the mid-summer rainfall for the study area.

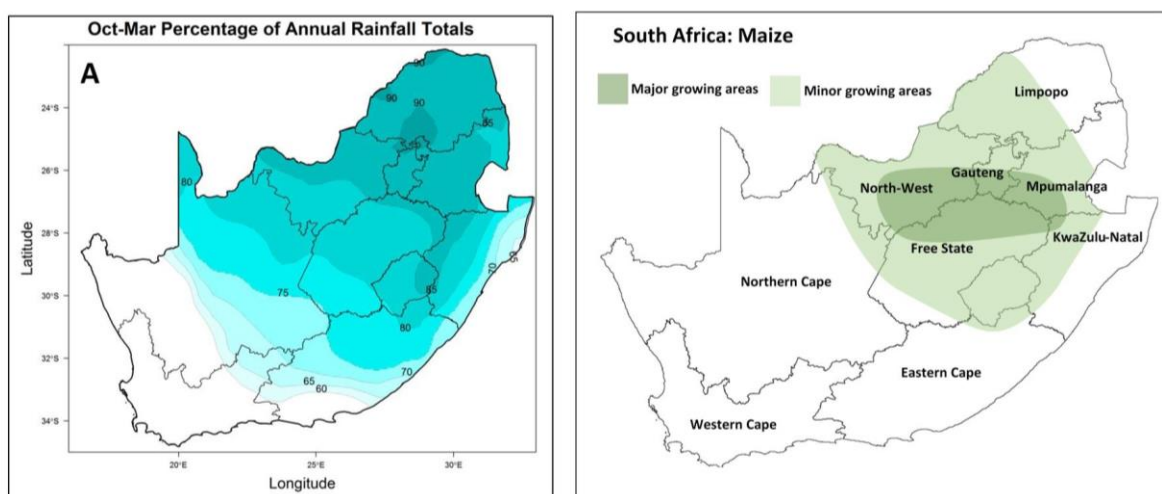


Figure 6.1: Map of South Africa showing (A) October to March rainfall totals compared with annual rainfall totals (1979 to 2019) using a CPC unified gauge-based analysis of global daily precipitation, and (B) the maize-growing areas (Maize Belt) of South Africa

6.3.2 Data and time periods

6.3.2.1 Observation

The recently released global reanalysis dataset (ERA5) of the European Centre for Medium-range Weather Forecasts was used in this study. ERA5 provides hourly estimates of a large number of atmospheric, land and oceanic climate variables. The data covers the earth over a 30 km x 30 km grid and resolves the atmosphere using 137 horizontally orientated levels from the surface up to a height of 80 km. ERA5 includes information about uncertainties for all variables at reduced spatial and temporal resolutions (ECMWF, 2019).

6.3.2.2 Models and model verification

Before climate model projections can be used, it is appropriate to first verify the historical model simulations against observations. Generally, if a model performs well in reflecting observed climate in its historical simulations, the model might normally also perform well in generating future climate projections. Historical (1979–2005) eight-member ensemble mean RCA4 RCM simulations of the mean number of consecutive dry days and pentads have been compared to the associated observed data. The global reanalysis dataset (ERA5) obtained from the ECMWF was used for observed rainfall (ECMWF, 2019).

Given the coarseness of the spatial resolution of global climate models and their applications at regional scales, the study used projections that were dynamically downscaled to a finer spatial resolution of $0.44^\circ \times 0.44^\circ$, specifically from simulations performed by the RRCA4 RCM during the CORDEX initiative. Eight ensemble members were used, meaning that the RCA4 RCM was forced by eight GCMs across its lateral boundaries. Therefore, eight ensemble member projections were available for calculating ensemble means (see Table 6.1). The RCA4 is a coupled ocean-atmosphere RCM based on the numerical weather prediction model HARLAM (Undén et al., 2002). Dry-spell signals from these historical simulations were applied in climate change projections of possible future changes in summer and mid-summer dry spells under the RCP conditions of “a medium-to-low” (RCP4.5) and “high” (RCP8.5) representative concentration pathway.

Table 6.1: Projections from eight global climate models used for downscaling to a finer spatial resolution ($0.4^\circ \times 0.4^\circ$) using the RCA4 regional climate model

Model name	Country	Resolution	Literature
CanESM2m	Canada	$2.8^\circ \times 2.8^\circ$	Arora et al. (2011)
CNRM-CM5	France	$1.4^\circ \times 1.4^\circ$	Voltaire et al. (2013)
CSIRO-Mk3	Australia	$1.9^\circ \times 1.9^\circ$	Rotstayn et al. (2013)
IPSL-CM5A-MR	France	$1.9^\circ \times 3.8^\circ$	Hourdin et al. (2013)
MIROC5	Japan	$1.4^\circ \times 1.4^\circ$	Watanabe et al. (2011)
MPI-ESM-LR	Germany	$1.9^\circ \times 1.9^\circ$	Ilyina et al. (2013)
NorESM1-M	Norway	$1.9^\circ \times 2.5^\circ$	Tjiputra et al. (2013)
GFDL-ESM2M	USA	$2.0^\circ \times 2.5^\circ$	Dunne et al. (2012)

6.3.2.3 Climate change projection scenarios

These regional climate models, with RCP2.6 and RCP6.0, were considered in the Fifth Assessment Report (AR5) (Taylor et al., 2012) of the International Panel on Climate Change (IPCC) (2018).

Modellers used these greenhouse gas (GHG) concentration (not emission) trajectories, which are all considered realistic, as atmospheric system forcing to generate climate response and change projections. The RCPs were defined according to their contribution to atmospheric radiative forcing in the year 2100, relative to pre-industrial values. For example, the additions to the earth's radiation budget as a result of an increase in GHGs are RCP2.6 = +2.6 W.m⁻²; RCP4.5 = +4.5 W.m⁻²; RCP6.0 = +6.0 W.m⁻²; and RCP8.5 = +8.5 W.m⁻². The RCP4.5 and RCP8.5 trajectories are associated with CO₂ concentrations of approximately 560 and 950 ppm, respectively, by the year 2100 (Riahi et al., 2011). The RCP8.5, also known as "business as usual", is projected to increase even further to a CO₂ concentration ceiling of approximately 1 200 ppm after the year 2100, while the RCP4.5 is based on active GHG emission reduction interventions that could lead to a ceiling of approximately 560 ppm (a doubling of concentrations since the start of the Industrial Revolution) by the year 2100, while concentrations could stabilise or even decrease after the year 2100.

The historical period used for both the observation and the model is 1979–2005 (27 years). The 27-year period was used against a 30-year period of projections due to the availability of ERA5 data not later than 1979. Future projections are presented for the two 30-year periods extending from 2036 to 2065 (near future) and 2066 to 2095 (far future). Projected changes are expressed relative to the historical 30-year period of 1979–2005. Daily model simulations of CDD and pentad values of rainfall totals were used to generate projections of the summer rainfall period (October to March) and mid-summer months (December to January). Projections are expressed in terms of a change in the mean values. Three thresholds of 1 mm, 2 mm and 3 mm total daily rainfall were used to analyse dry spells. In addition, pentad total rainfall is compared to the multi-model mean simulated pentad rainfall totals.

6.4 RESULTS AND DISCUSSIONS

6.4.1 Model evaluation

6.4.1.1 Model evaluation of consecutive dry days

The results of the comparison between the observed scenario and model ensemble number of consecutive dry days for October to March are presented in Figure 6.2 using three precipitation thresholds of 1 mm, 2 mm and 3 mm for the historical period 1979–2005. The results indicate that the ensemble model can depict the spatial distribution pattern of the observed CDD. A spatial correlation of 58% is computed between the observed scenario and model ensemble number of CDD for October to March. Particularly, the ensemble model underestimates CDD in October to March over North West, the southern part of the Free State, the western parts of Limpopo, Gauteng and the central interior parts of Mpumalanga and KwaZulu-Natal for all three thresholds. The overestimated CDD by the model are more dominant in the north-eastern parts of the Free State and the western parts of KwaZulu-Natal.

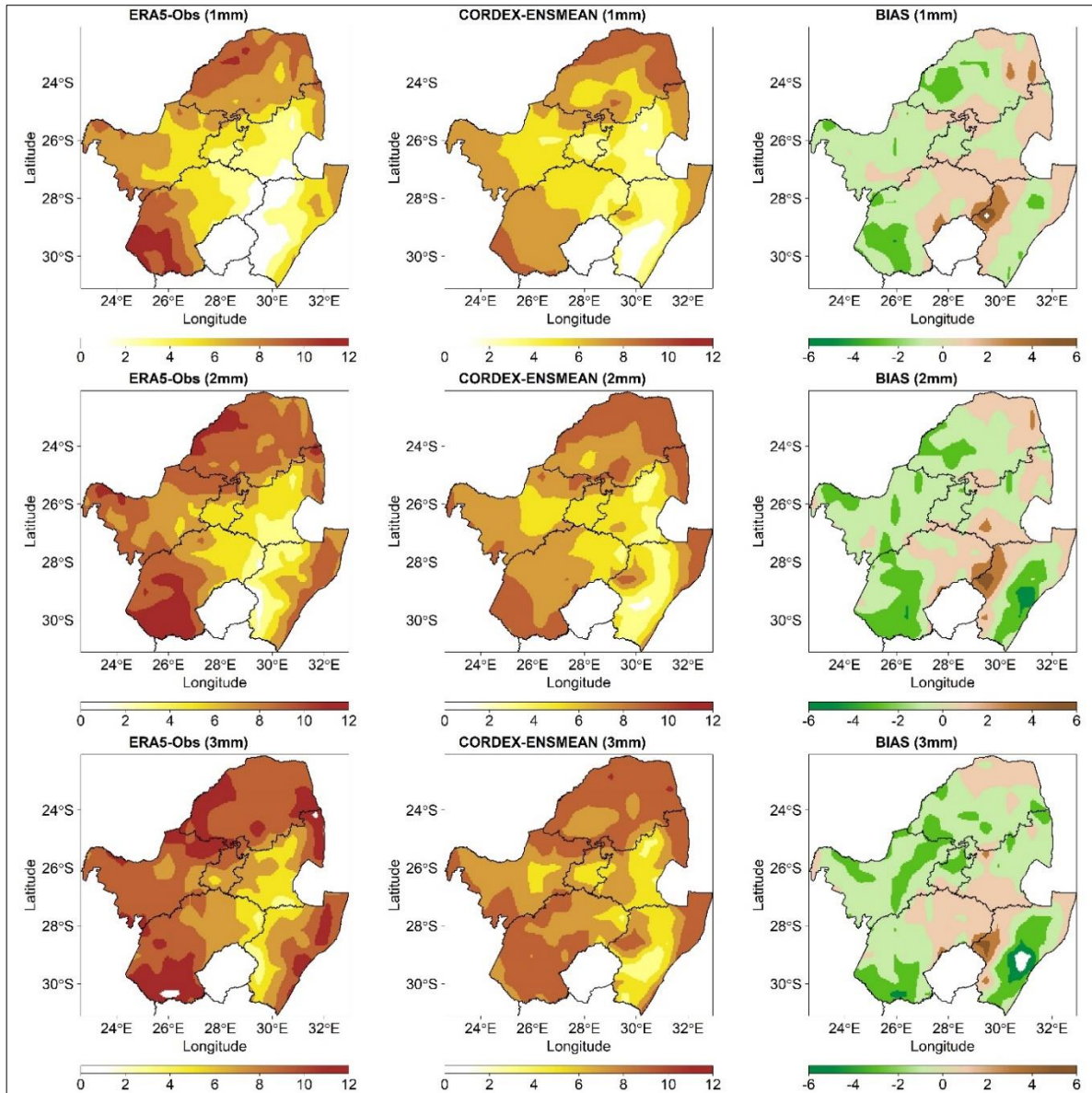


Figure 6.2: Comparison between the observed number of consecutive dry days for October to March from ERA5 (the first column) and the associated multi-model mean consecutive dry days simulated by the RCA4 RCM (the middle column) for the period 1979–2005. The mean bias between the observed scenario and the simulated number of consecutive dry days is indicated by the maps in the third column. A dry spell is computed for more than five consecutive days with rainfall less than 1 mm (first row), 2 mm (second row) and 3 mm (third row).

On the other hand, an average spatial correlation of 63% is indicated between the observed scenario and the model ensemble number of CDDs for December and January for the three precipitation thresholds of 1 mm, 2 mm and 3 mm (Figure 6.3). The ensemble model tends to underestimate December and January's figures over the southern Free State and North West, and overestimates CDD in December and January over northern Limpopo, the eastern Free State and western KwaZulu-Natal.

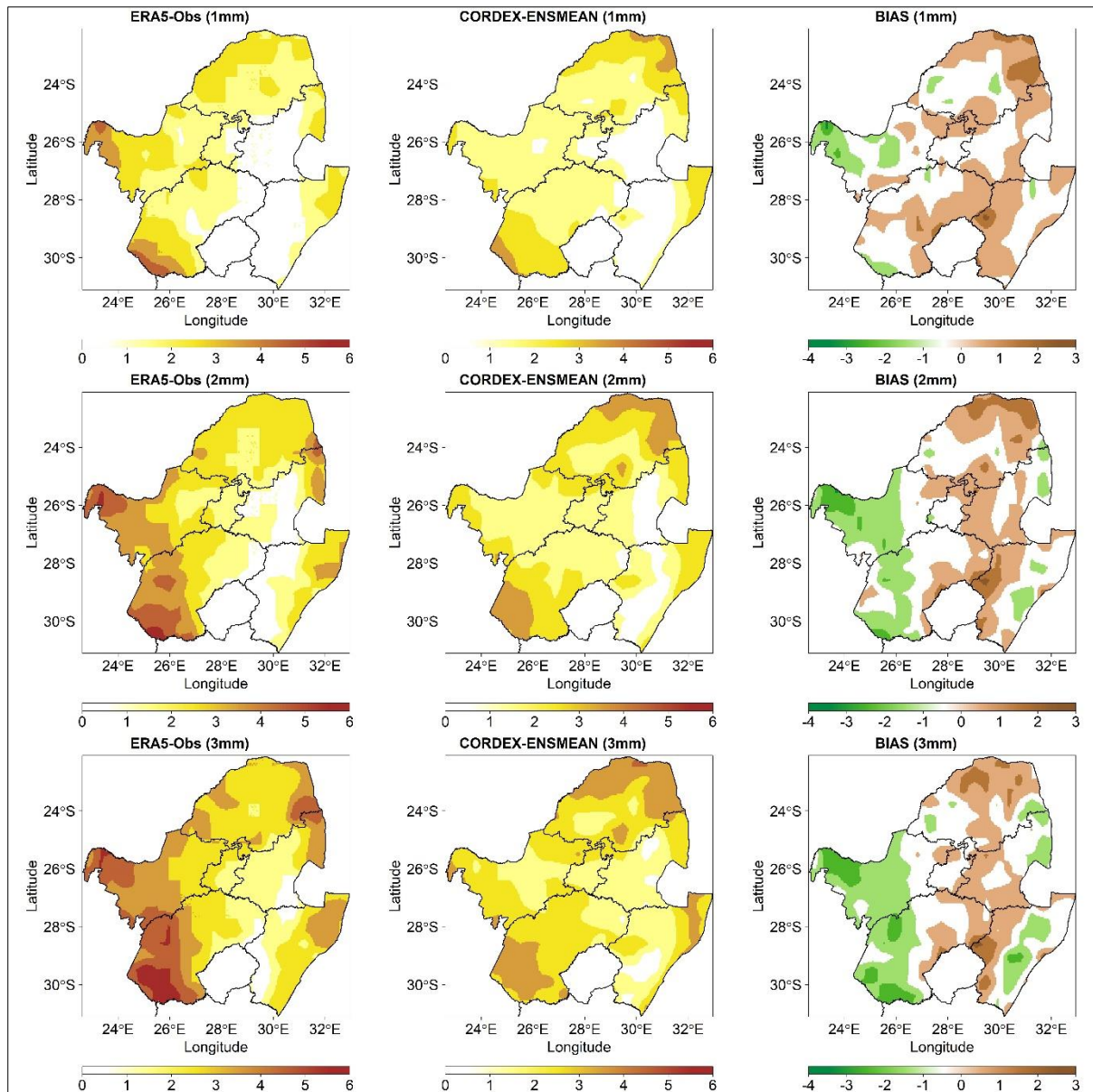


Figure 6.3: Comparison between the observed number of consecutive dry days for December to January from ERA5 (the first column) and associated multi-model mean consecutive dry days simulated by the RCA4 RCM (the middle column) for the period 1979–2005. The mean bias between the observed scenario and the simulated number of CDDs is indicated by the maps in the third column. A dry spell is computed for more than five consecutive days with rainfall less than 1 mm (first row), 2 mm (second row) and 3 mm (third row).

6.4.1.2 Model evaluation of pentads

The comparison between the observed scenario and model ensemble for total precipitation (mm) for pentads 68, 69, 70, 71, 72, 73, 1, 2, 3, 4, 5 and 6 for the mid-summer months (December and January) is computed and presented in figures 6.4 to 6.7 for the historical period 1979–2005. Generally, the results depict a similar spatial pattern in the observation and in the model simulation. An average spatial correlation of 68% is computed between the observed scenario and the model simulation pentads. The results further indicate that the multi-model simulations overestimate the pentads over central Gauteng (all pentads except pentads 2 and 3 during this period), KwaZulu-Natal and Mpumalanga, and including northern Limpopo for Pentad 71.

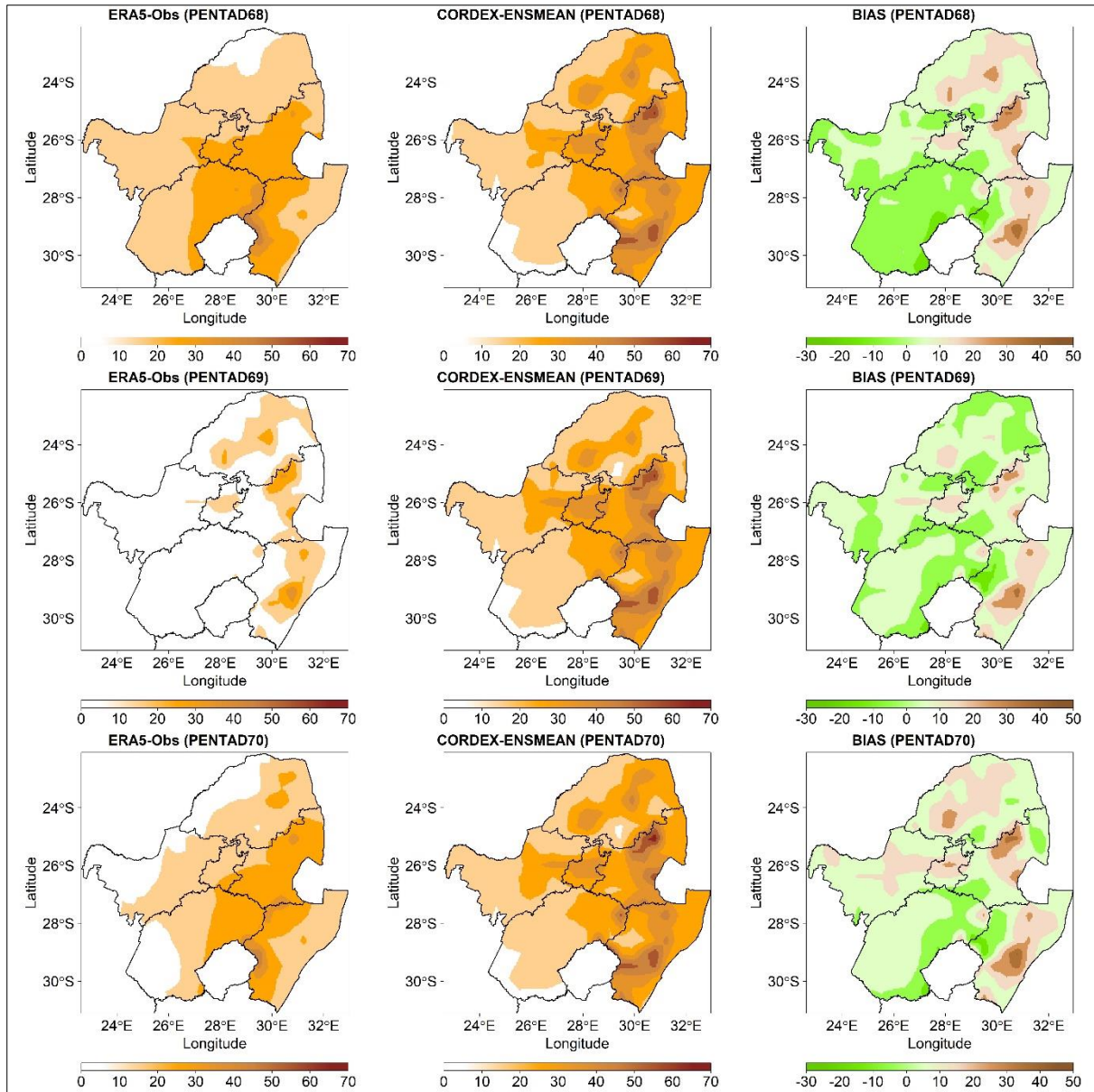


Figure 6.4: ERA 5 comparison between the observed pentads' total rainfall and multi-model mean simulated totals for pentads 68, 69 and 70 in terms of total precipitation (mm) for the period 1979–2005

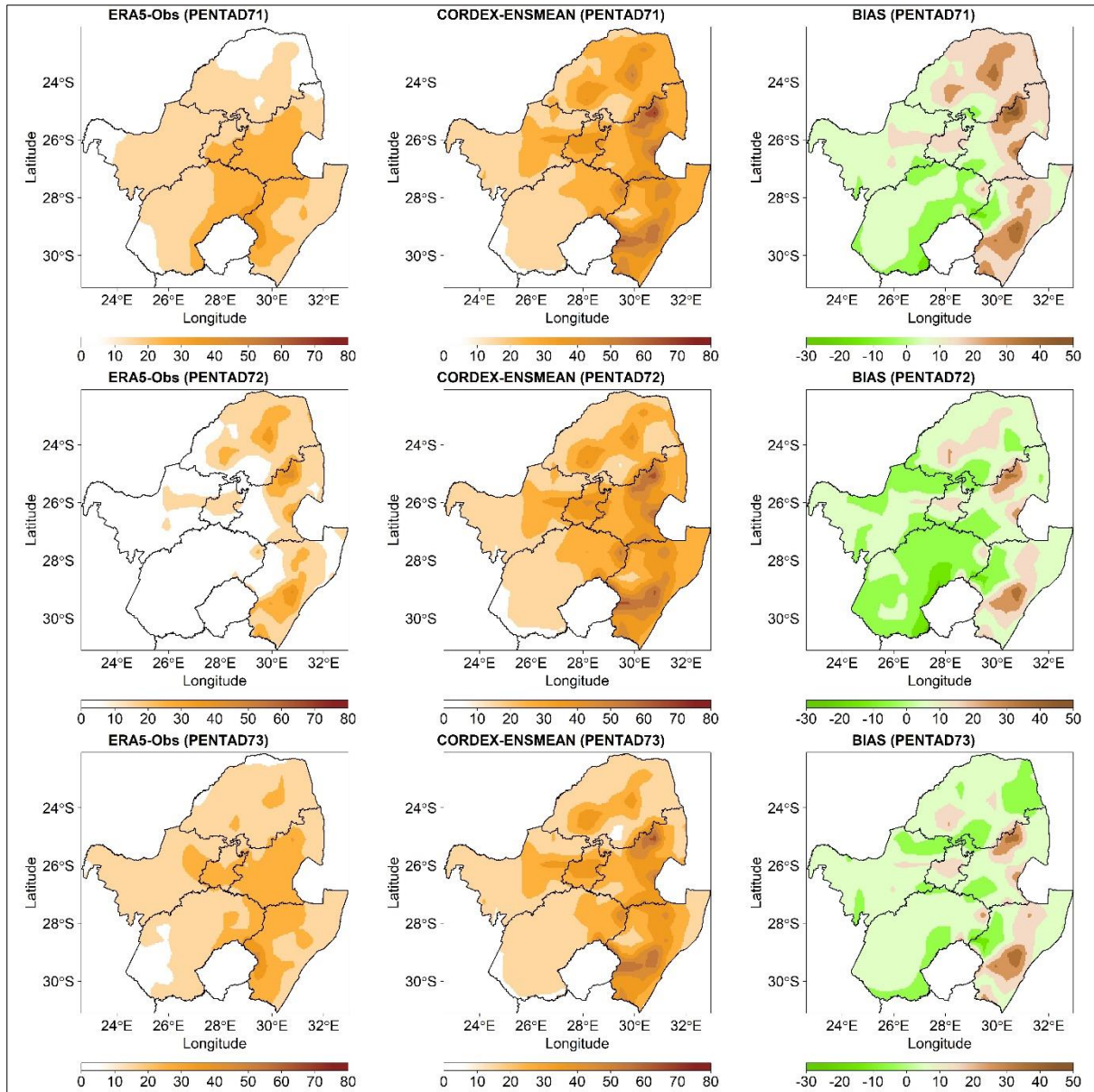


Figure 6.5: ERA 5 comparison between the observed pentads' total rainfall and multi-model mean simulated totals for pentads 71, 72 and 73 in terms of total precipitation (mm) for the period 1979–2005

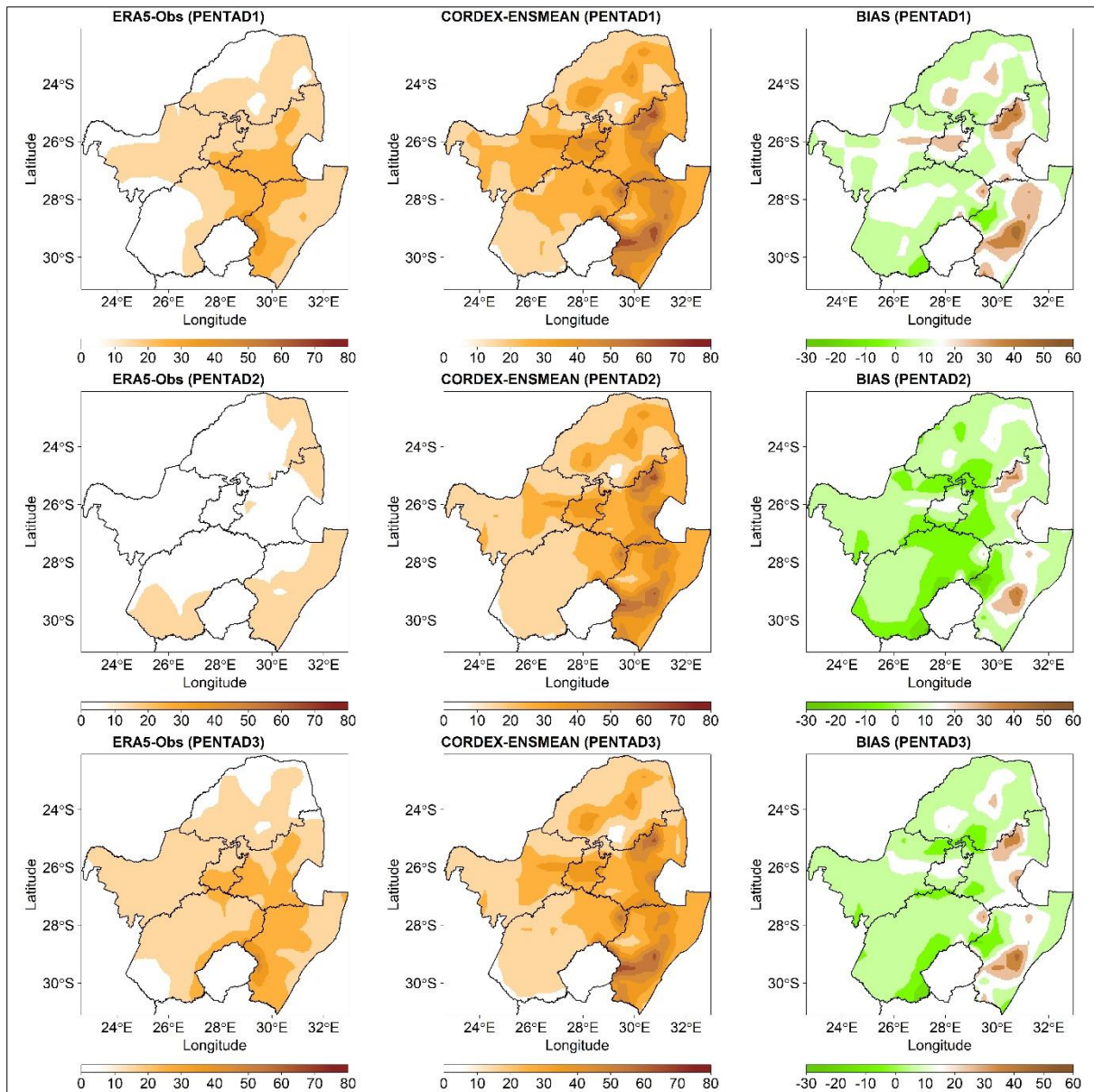


Figure 6.6: ERA 5 comparison between the observed pentads' total rainfall and multi-model mean simulated totals for pentads 1, 2 and 3 in terms of total precipitation (mm) for the period 1979–2005

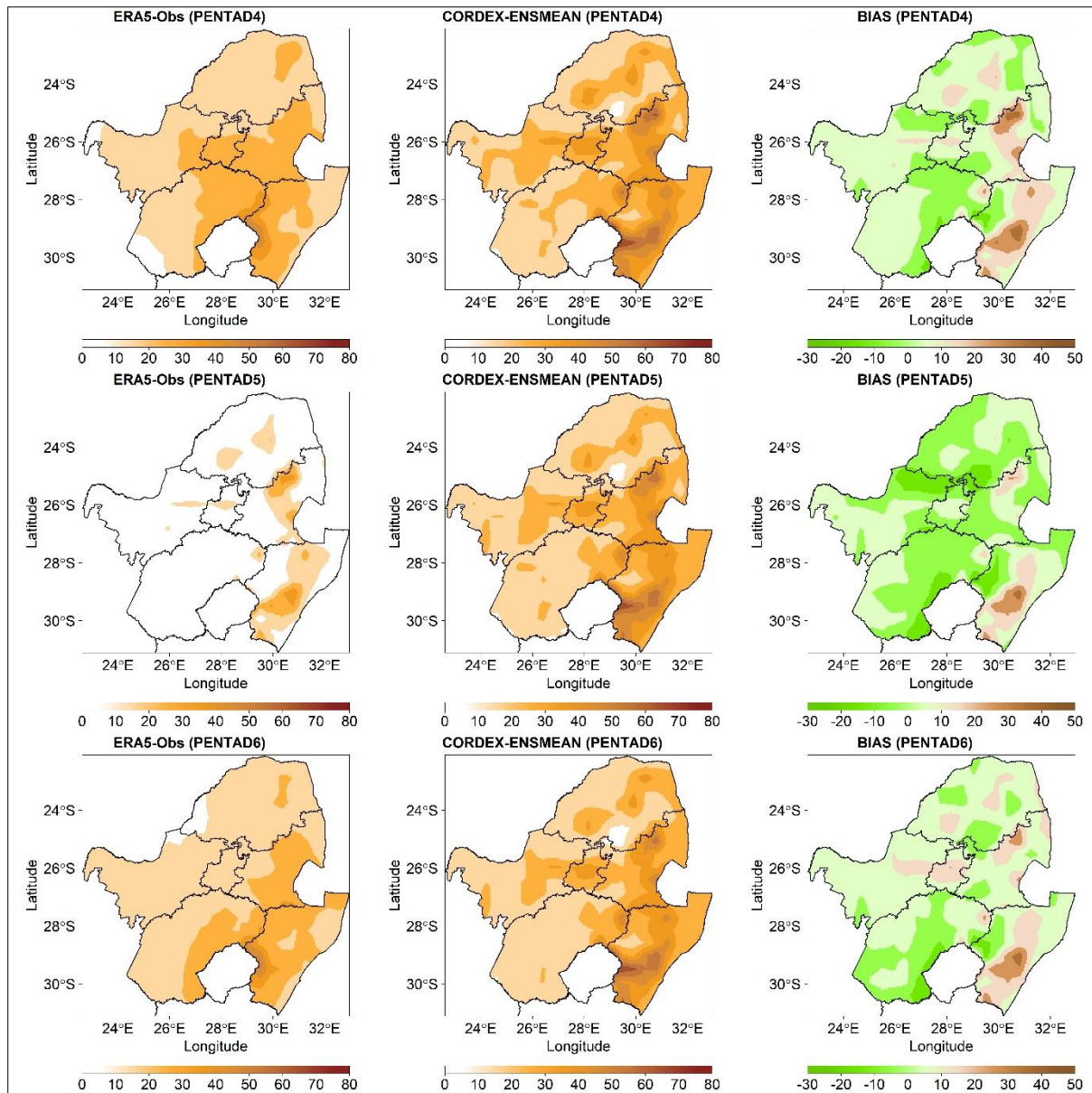


Figure 6.7: ERA 5 comparison between the observed pentads' total rainfall and multi-model mean simulated totals for pentads 4, 5 and 6 in terms of total precipitation (mm) for the period 1979–2005

6.4.2 Dry spell projections

6.4.2.1 Climate change projection of consecutive dry days

Figures 6.8 to 6.10 illustrate the projected climate mean of CDD at 1 mm, 2 mm and 3 mm thresholds for a two-time slice of the 30-year periods 2036–2065 and 2066–2095 under RCP4.5 and RCP8.5 for October to March, while figures 6.11 to 6.13 depict the data for December and January over the study area. For the thresholds 1 mm, 2 mm and 3 mm, the results show that average annual CDD are expected to increase in future under RCP4.5 with a further increase under RCP8.5 to the two-time slice of 2036–2065 and 2066–2095 as opposed to those in the baseline period (1976–2005). For instance, for October to March, five consecutive days with less than a 1 mm threshold are expected to increase by an average of 35 days under RCP4.5 and by 40 days under RCP8.5 in the northern part of Limpopo and the southern part of the Free State for the period 2036–2065.

Similarly, the projection indicated that the condition will further increase to an average of 40 days under RCP4.5 and 45 days under RCP8.5 in the northern part of Limpopo and the southern part of the Free State for the period 2066–2095. The projected CDD over Gauteng, central Mpumalanga and KwaZulu-Natal under RCP4.5 are averaged at 10 days. Under RCP8.5, the projected CDD are averaged at 15 days for the period 2036–2065, and are increased to 20 days under RCP4.5 and 25 days under RCP8.5 for the period 2066–2095.

The same pattern of increase is projected for CDD in the December to January period. The five consecutive days with less than 1 mm rainfall are expected to increase by an average of 12.5 days under RCP4.5 and by 15 days under RCP8.5 after 30 years of observed data and by 17.5 days under RCP4.5 and 17.5 days under RCP8.5 (with more magnitude) after 60 years of observed data over the northern part of Limpopo, the western and northern parts of North West, the north-eastern part of Mpumalanga and KwaZulu-Natal, and the southern part of the Free State. The 2 mm and 3 mm thresholds are expected to increase further.

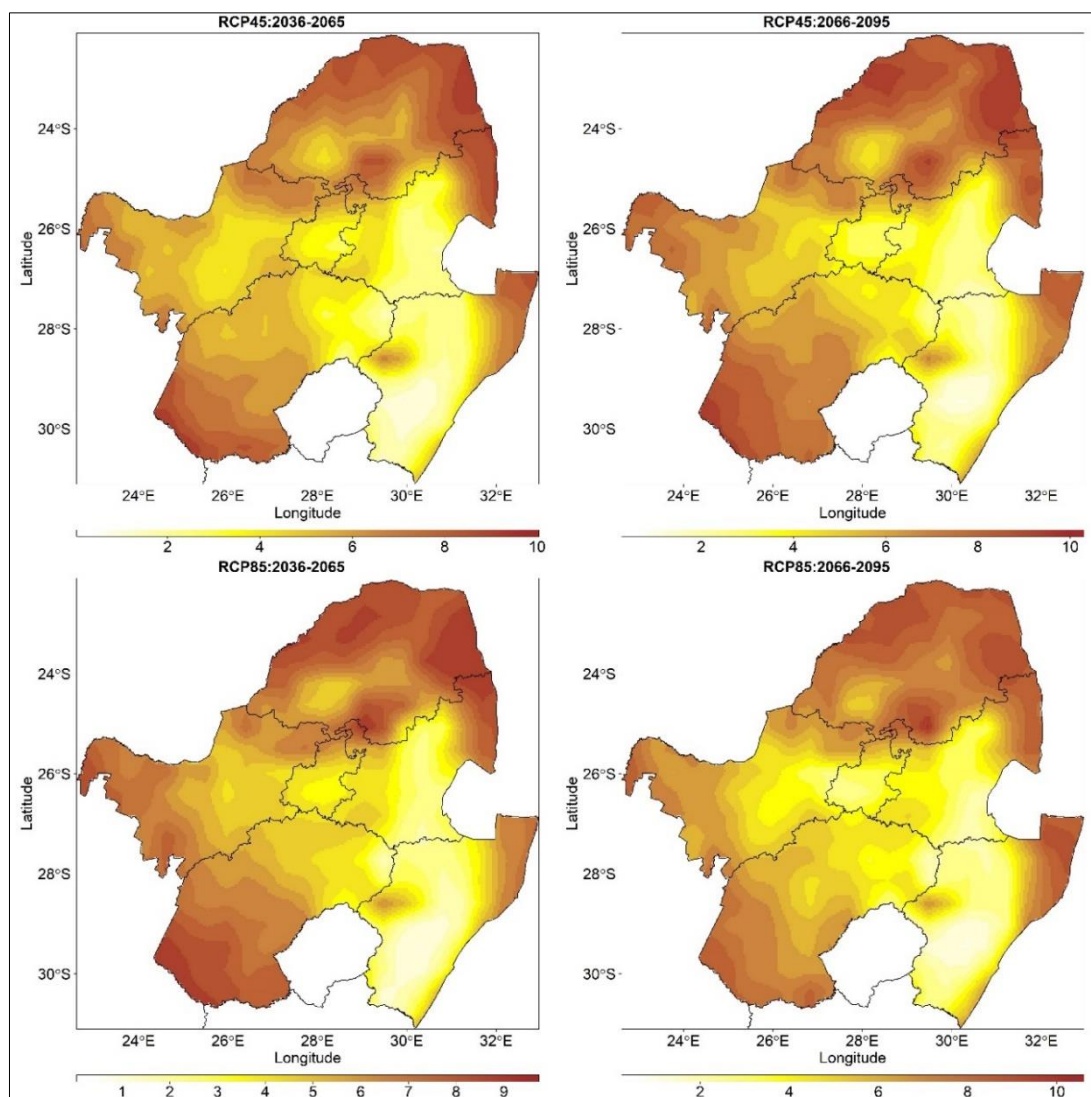


Figure 6.8: Projected number of consecutive dry days for summer (October to March) over the summer rainfall areas of South Africa using a precipitation threshold of 1 mm for the periods 2036–2065 (top left) and 2066–2095 (top right) under the conditions of RCP4.5, and 2036–2065 (bottom left) and 2066–2095 (bottom right) under the conditions of RCP8.5. A dry spell is defined as more than five consecutive days with less than 1 mm of rainfall.

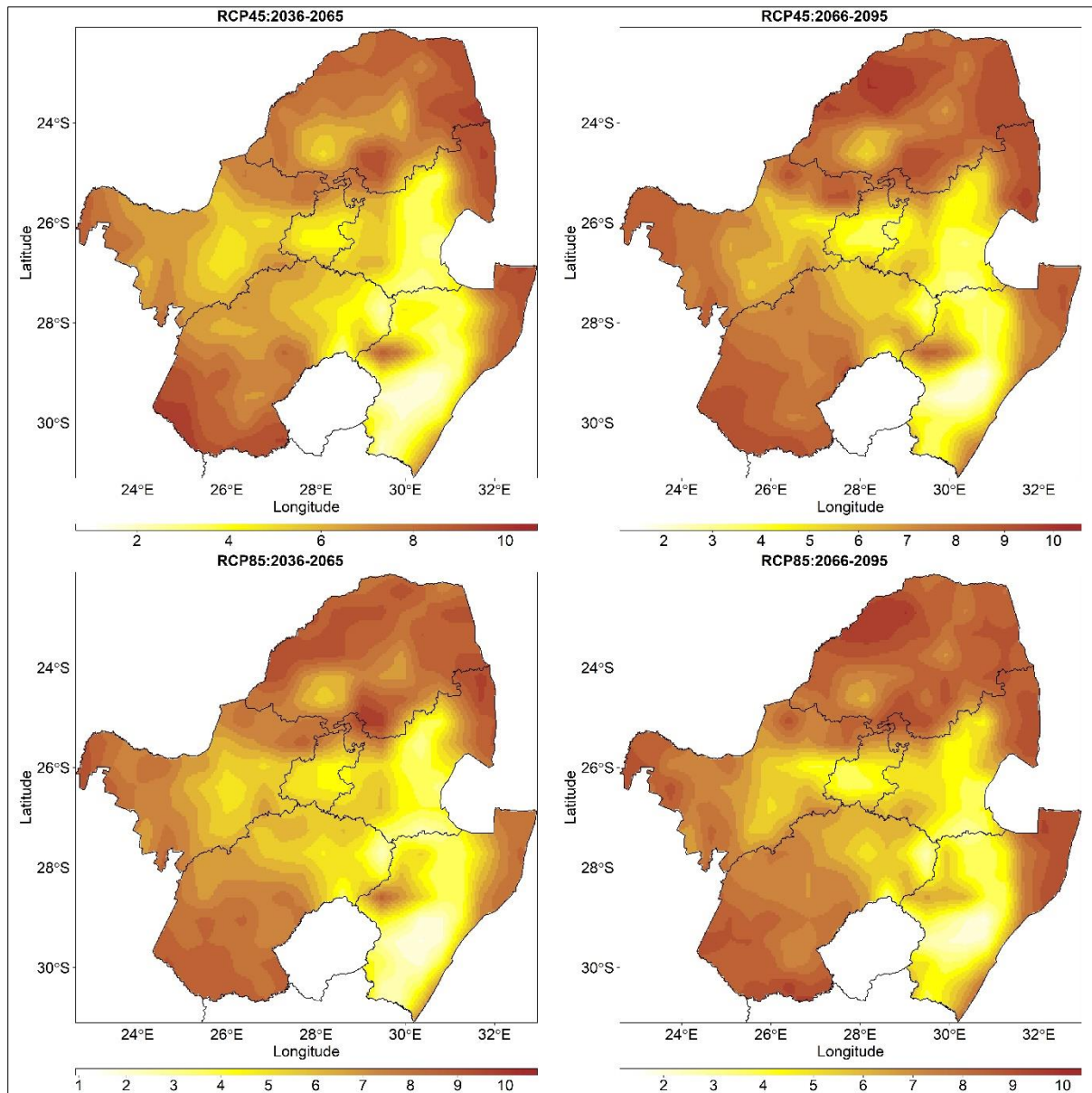


Figure 6.9: Projected number of consecutive dry days for summer (October to March) over the summer rainfall areas of South Africa using a precipitation threshold of 2 mm for the periods 2036–2065 (top left) and 2066–2095 (top right) under the conditions of RCP4.5, and 2036–2065 (bottom left) and 2066–2095 (bottom right) under the conditions of RCP8.5. A dry spell is defined as more than five consecutive days with less than 2 mm of rainfall.

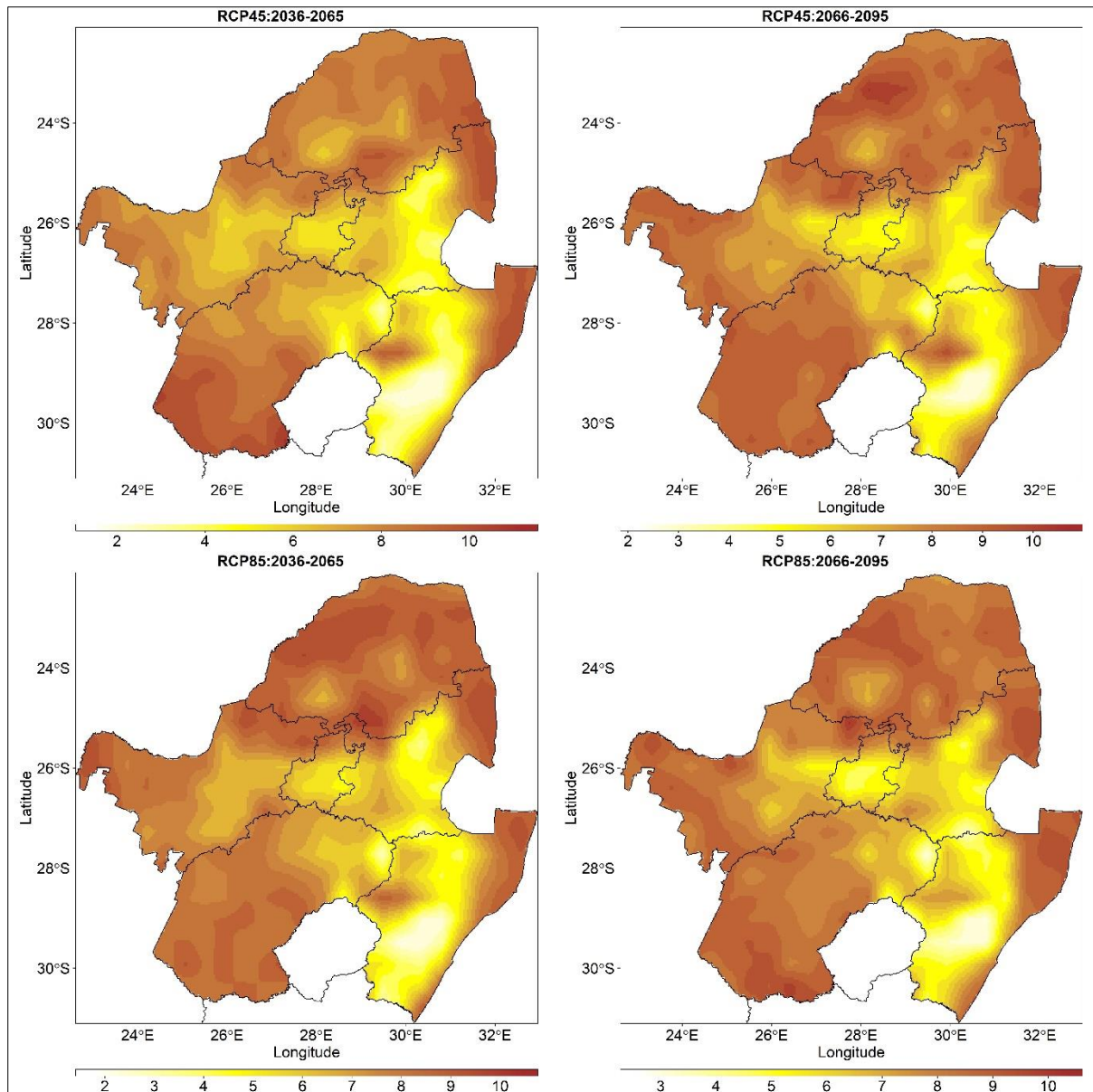


Figure 6.10: Projected number of consecutive dry days for summer (October to March) over the summer rainfall areas of South Africa using a precipitation threshold of 3 mm for the periods 2036–2065 (top left) and 2066–2095 (top right) under the conditions of RCP4.5, and 2036–2065 (bottom left) and 2066–2095 (bottom right) under the conditions of RCP8.5. A dry spell is defined as more than five consecutive days with less than 3 mm of rainfall.

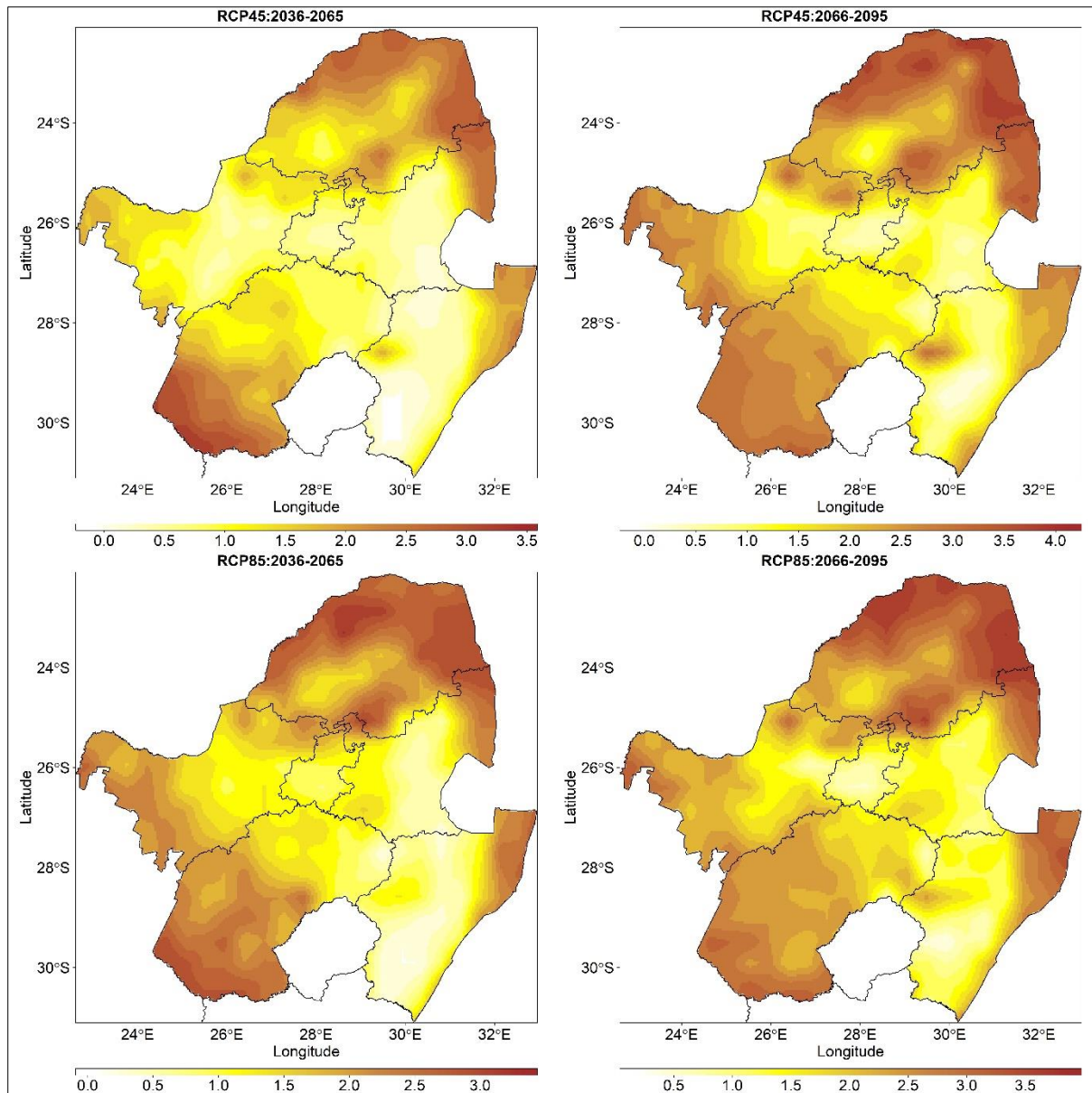


Figure 5.11: Projected number of consecutive dry days for mid-summer (December to January) over the summer rainfall areas of South Africa using a precipitation threshold of 1 mm for the periods 2036–2065 (top left) and 2066–2095 (top right) under the conditions of RCP4.5, and 2036–2065 (bottom left) and 2066–2095 (bottom right) under the conditions of RCP8.5. A dry spell is defined as more than five consecutive days with less than 1 mm of rainfall.

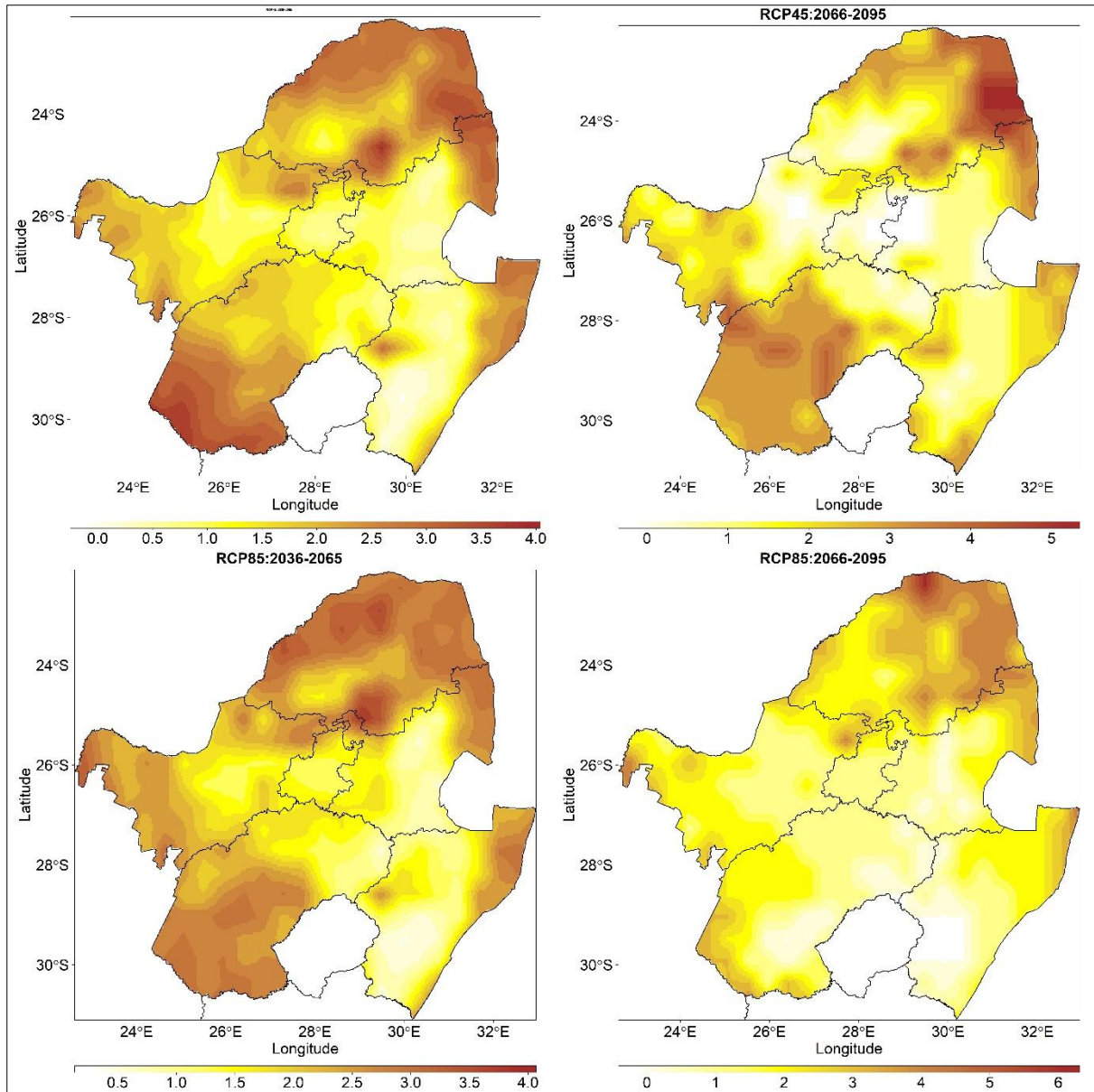


Figure 6.12: Projected number of consecutive dry days for mid-summer (December to January) over the summer rainfall areas of South Africa using a precipitation threshold of 2 mm for the periods 2036–2065 (top left) and 2066–2095 (top right) under the conditions of RCP4.5, and 2036–2065 (bottom left) and 2066–2095 (bottom right) the under conditions of RCP8.5. A dry spell is defined as more than five consecutive days with less than 2 mm of rainfall.

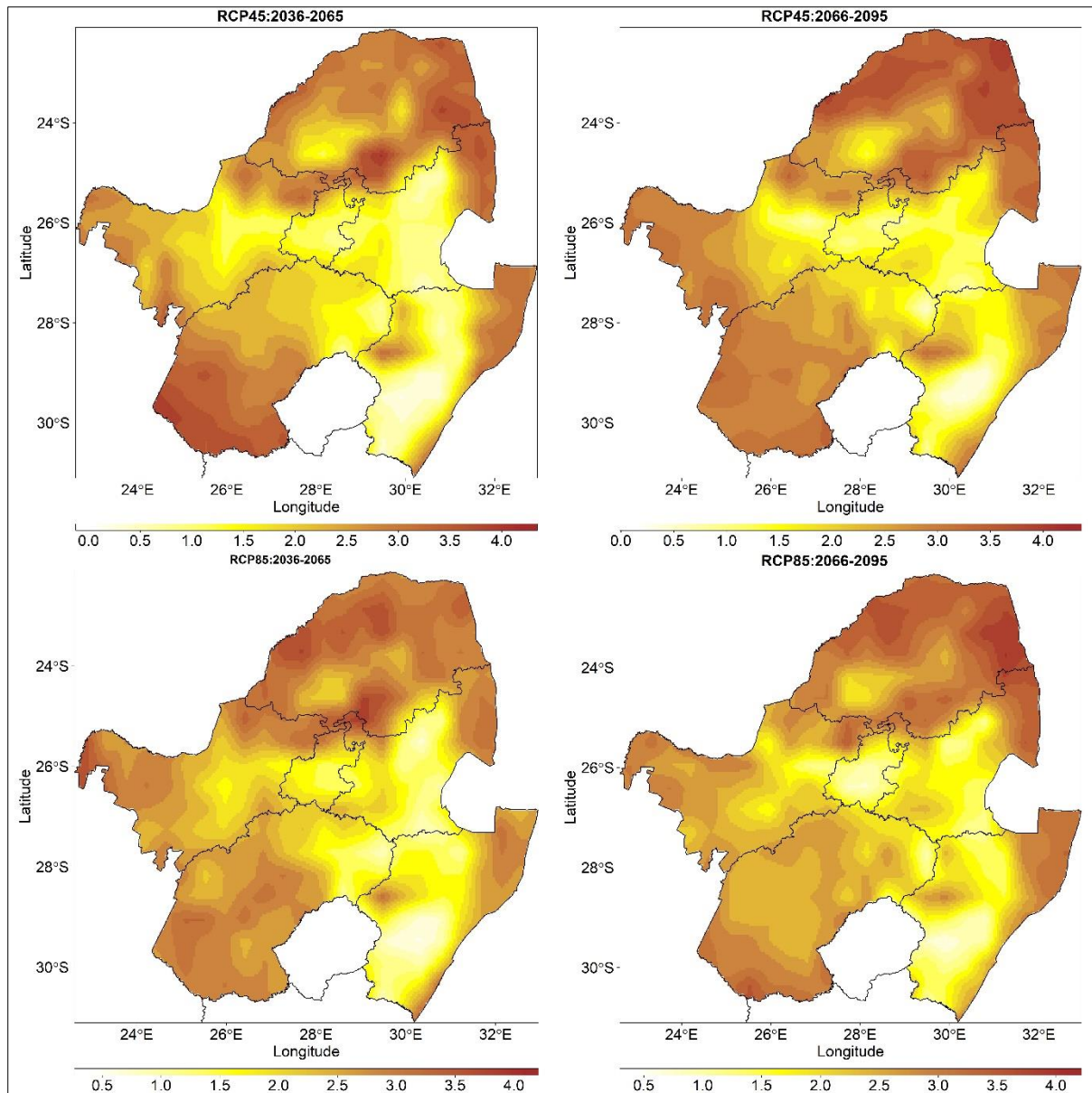


Figure 6.13: Projected number of consecutive dry days for mid-summer (December to January) over the summer rainfall areas of South Africa using a precipitation threshold of 3 mm for the periods 2036–2065 (top left) and 2066–2095 (top right) under the conditions of RCP4.5, and 2036–2065 (bottom left) and 2066–2095 (bottom right) under the conditions of RCP 8.5. A dry spell is defined as more than five consecutive days with less than 3 mm of rainfall

6.4.2.2 Climate change projection of pentads

The projected pentads' total precipitation (mm) for the periods 2036–2065 and 2066–2095 under RCP4.5 and RCP8.5 for the mid-summer pentads (December and January) are presented in figures 6.14 to 6.25, showing pentads 1 to 6 and 68 to 73. The total precipitation (mm) of Pentad 1 (1–5 January) is projected for 2036–2065 and 2066–2095.

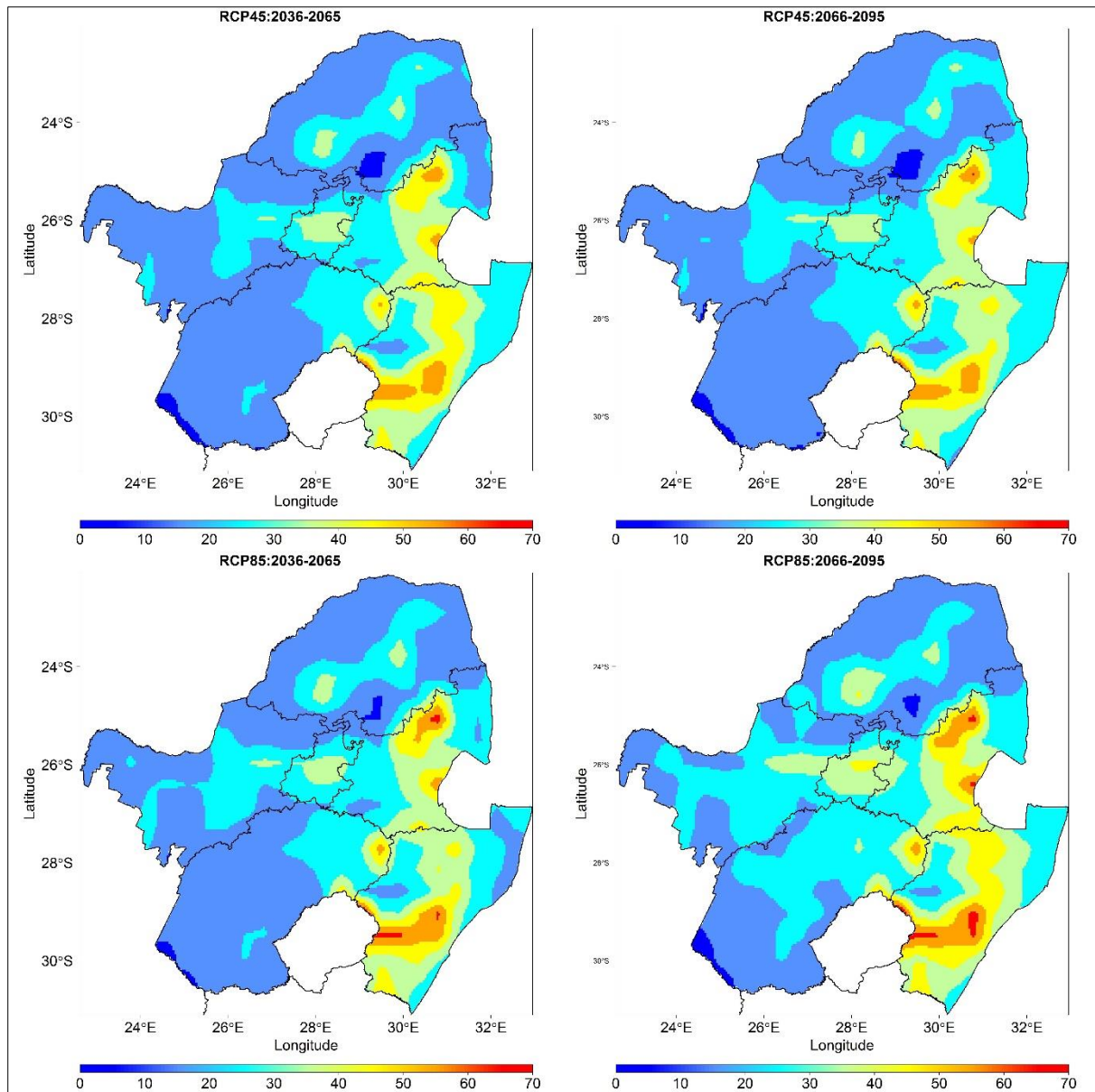


Figure 6.14: Projected total precipitation (mm) for Pentad 1 (1–5 January for the periods 2036–2065 (top left) and 2066–2095 (top right) under the conditions of RCP4.5, and 2036–2065 (bottom left) and 2066–2095 (bottom right) under the conditions of RCP8.5

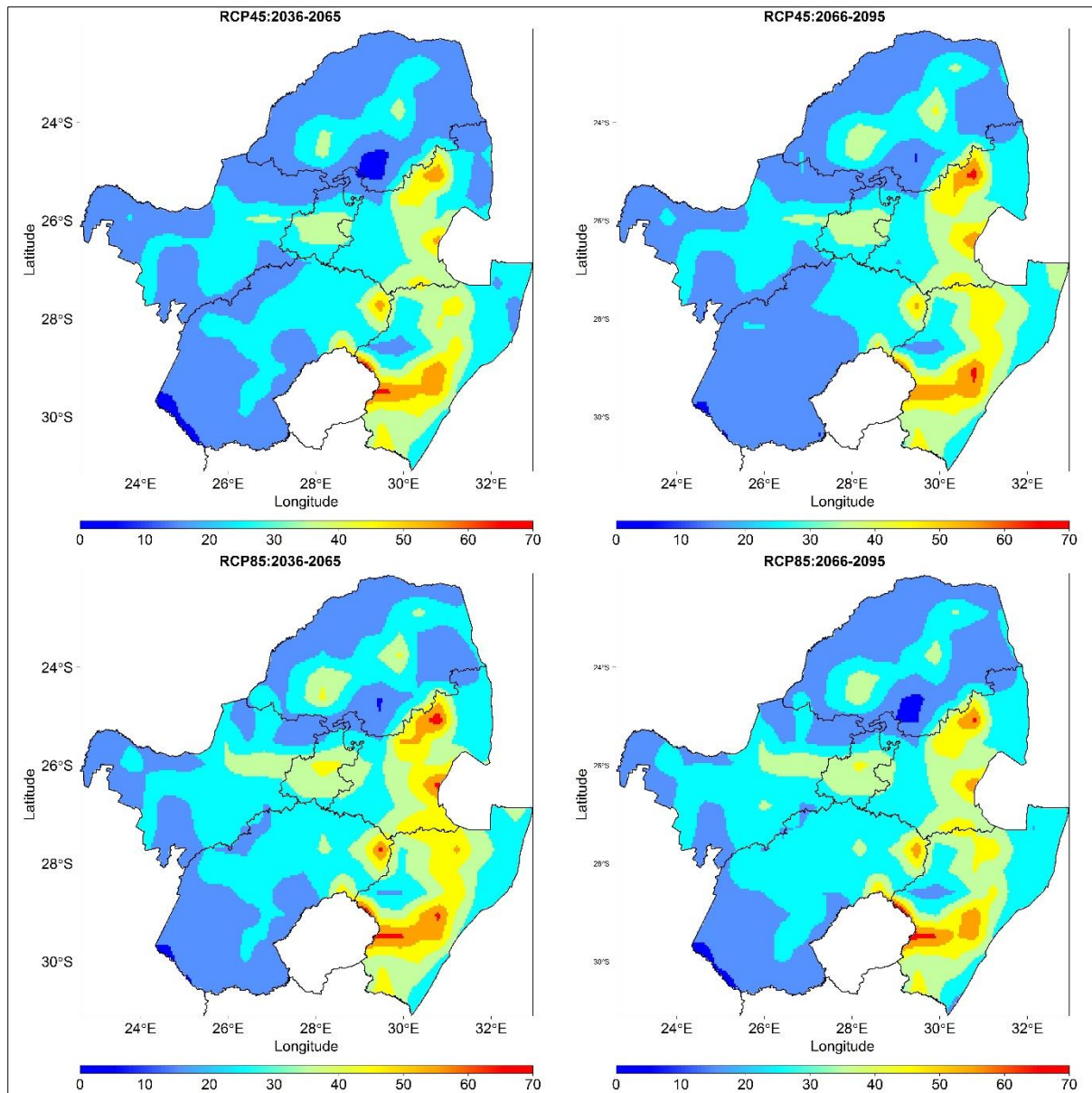


Figure 6.15: Projected total precipitation (mm) for Pentad 2 (6–10 January) for the periods 2036–2065 (top left) and 2066–2095 (top right) under the conditions of RCP4.5, and 2036–2065 (bottom left) and 2066–2095 (bottom right) under the conditions of RCP8.5

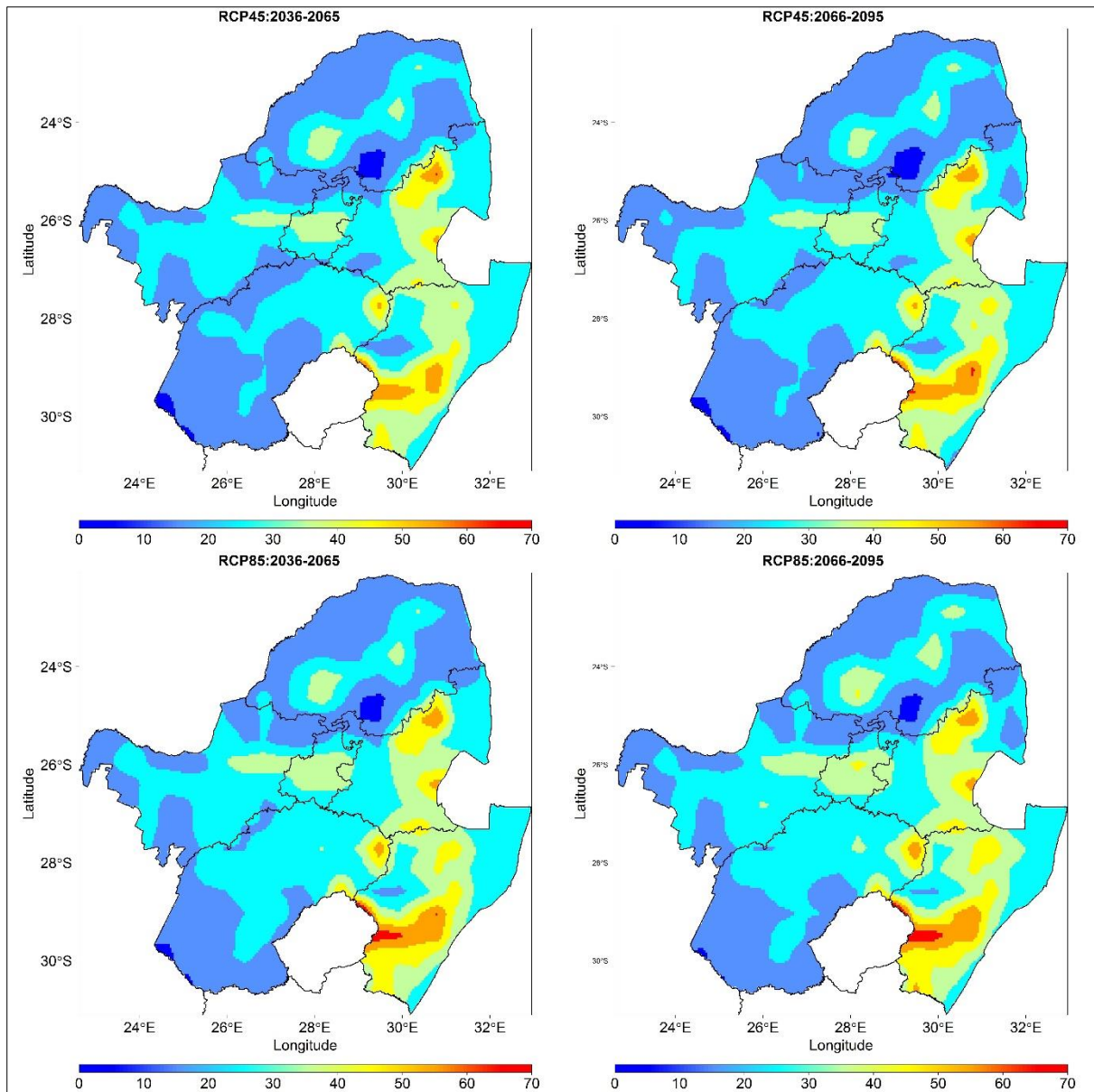


Figure 6.16: Projected total precipitation (mm) for Pentad 3 (11–15 January) for the periods 2036–2065 (top left) and 2066–2095 (top right) under the conditions of RCP4.5, and 2036–2065 (bottom left) and 2066–2095 (bottom right) under the conditions of RCP8.5

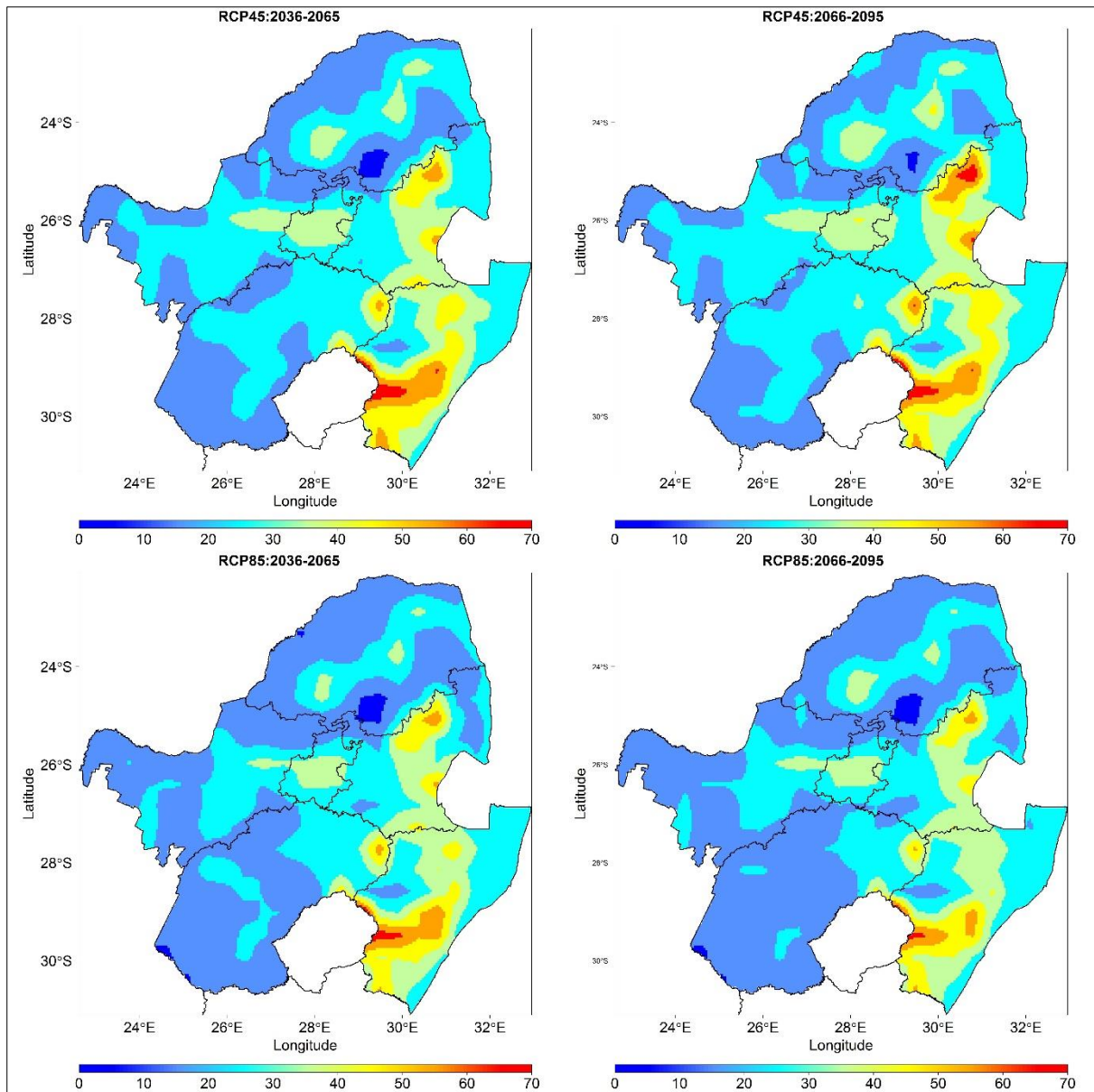


Figure 6.17: Projected total precipitation (mm) for Pentad 4 (16–20 January) for the periods 2036–2065 (top left) and 2066–2095 (top right) under the conditions of RCP4.5, and 2036–2065 (bottom left) and 2066–2095 (bottom right) under the conditions of RCP8.5

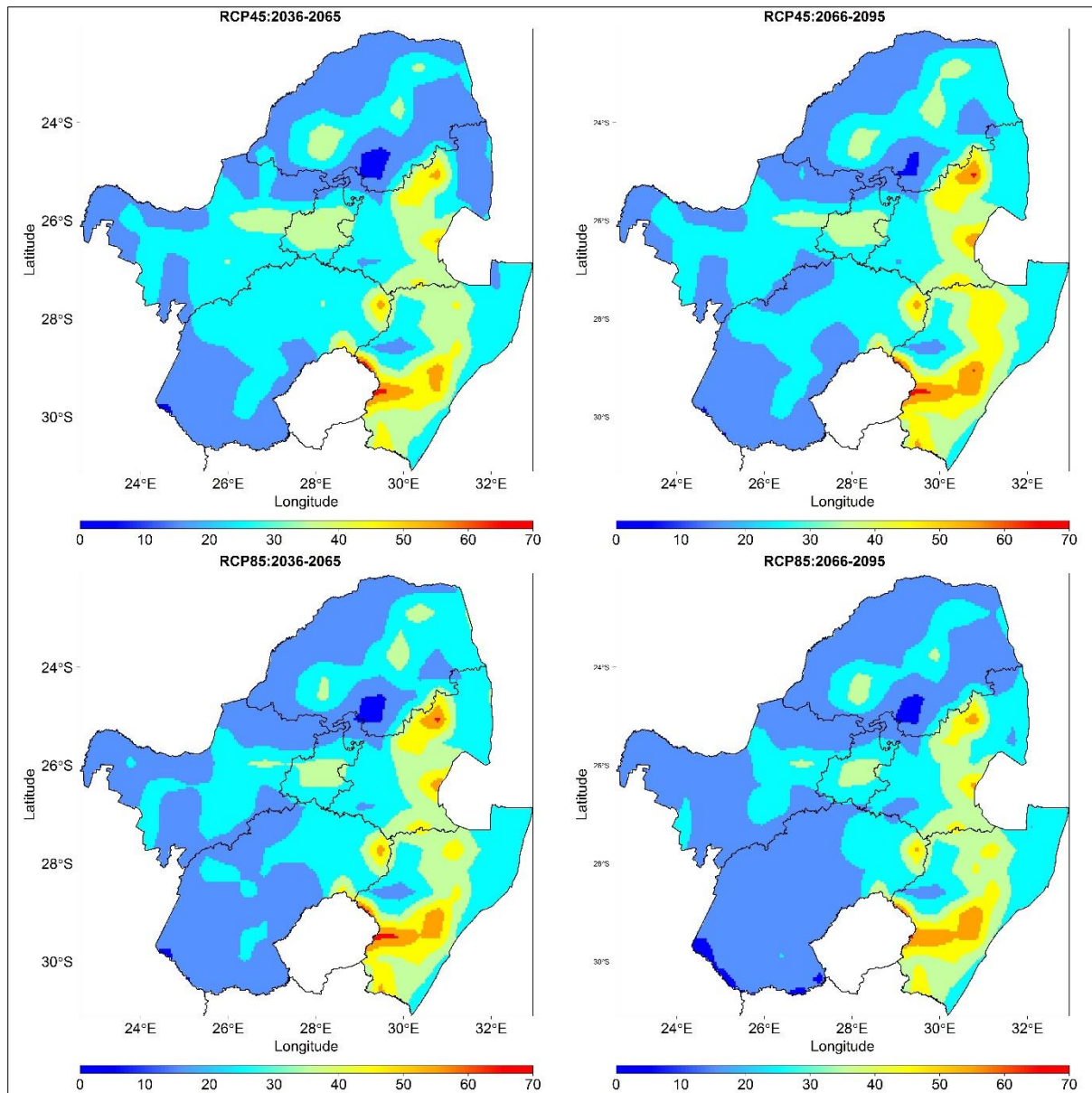


Figure 6.18: Projected total precipitation (mm) for Pentad 5 (21–25 January) for the periods 2036–2065 (top left) and 2066–2095 (top right) under the conditions of RCP4.5, and 2036–2065 (bottom left) and 2066–2095 (bottom right) under the conditions of RCP8.5

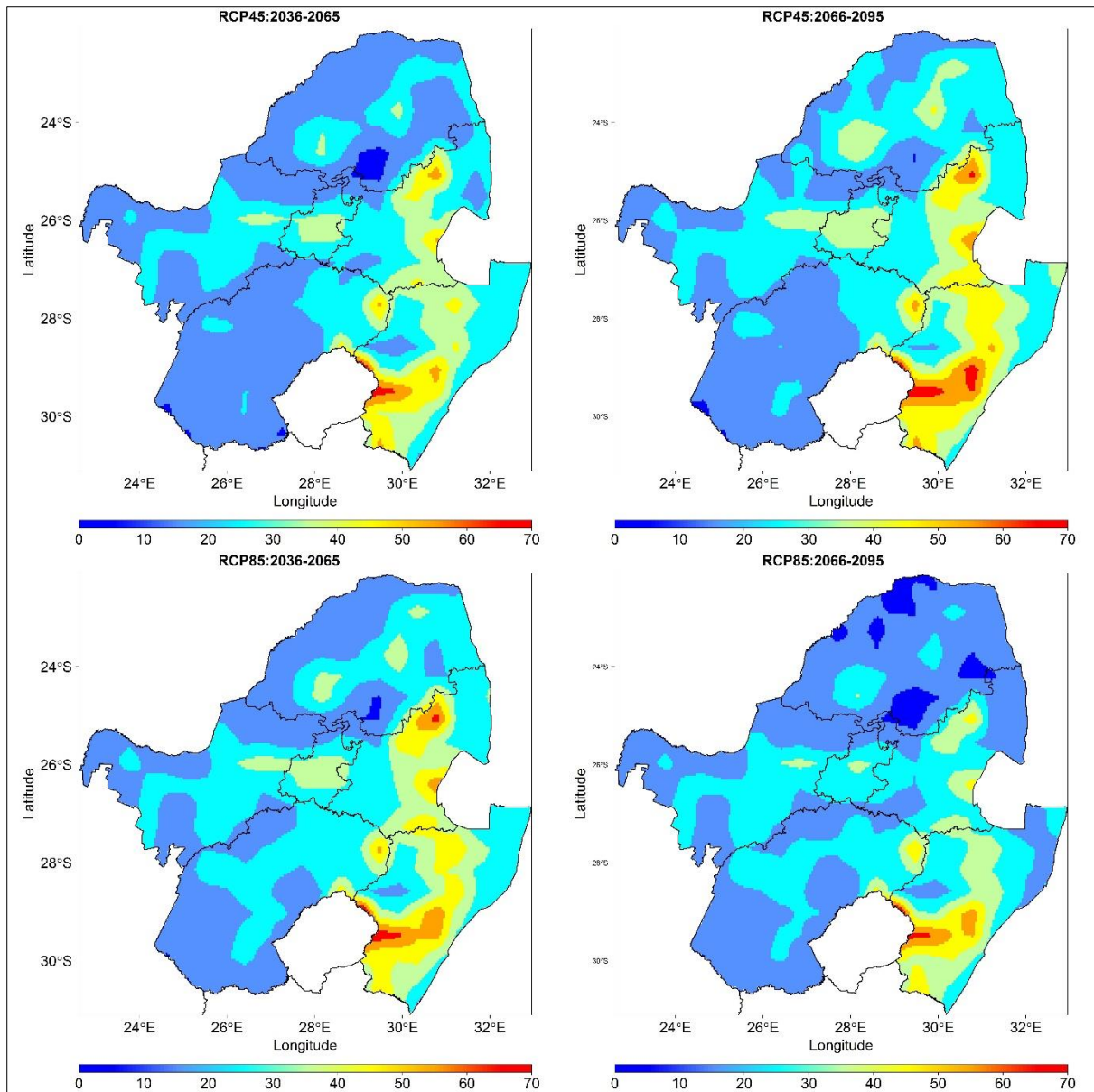


Figure 6.19: Projected total precipitation (mm) for Pentad 6 (26–30 January) for the periods 2036–2065 (top left) and 2066–2095 (top right) under the conditions of RCP4.5, and 2036–2065 (bottom left) and 2066–2095 (bottom right) under the conditions of RCP8.5

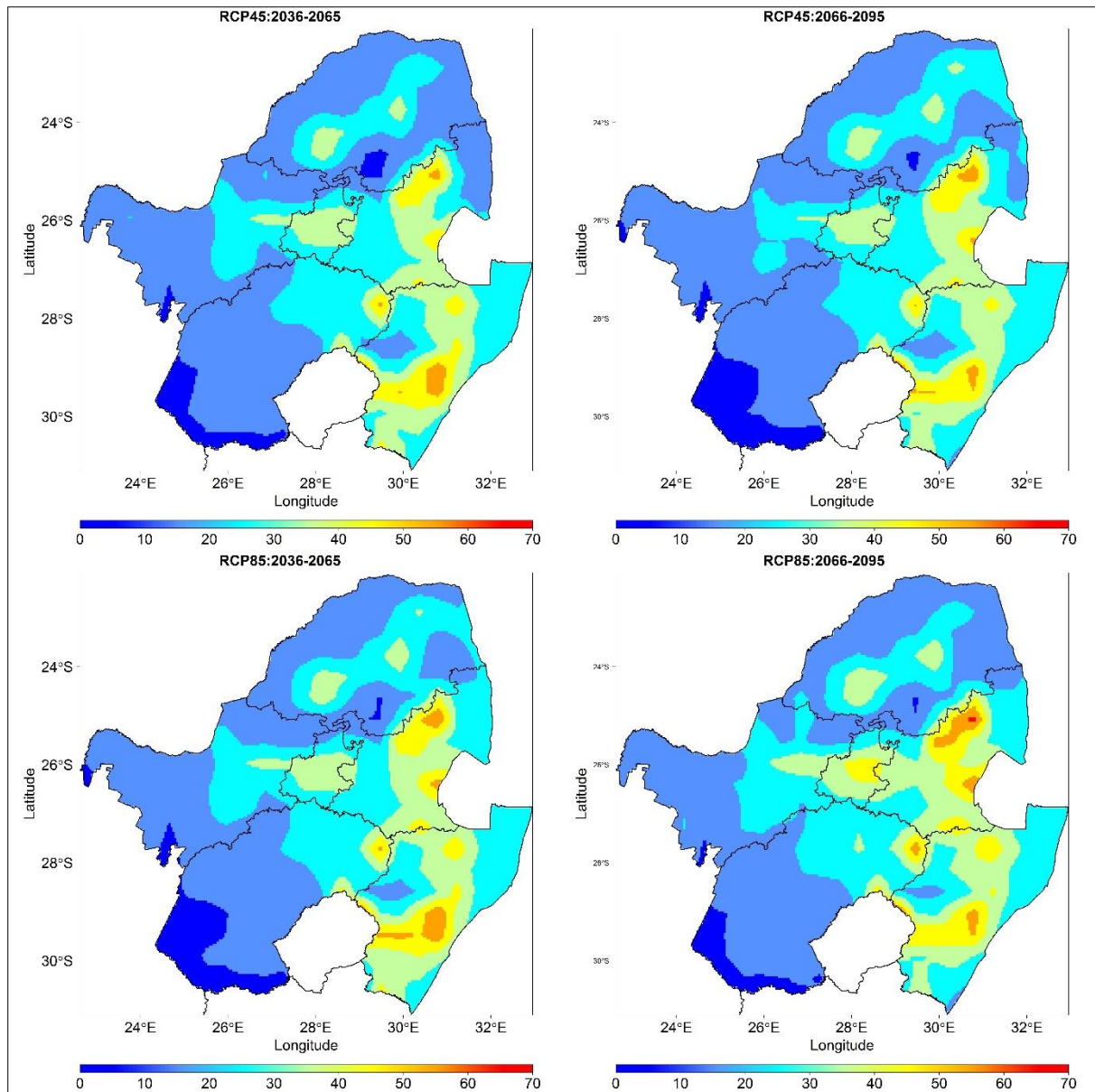


Figure 6.20: Projected total precipitation (mm) for Pentad 68 (2–6 December) for the periods 2036–2065 (top left) and 2066–2095 (top right) under the conditions of RCP4.5, and 2036–2065 (bottom left) and 2066–2095 (bottom right) under the conditions of RCP8.5

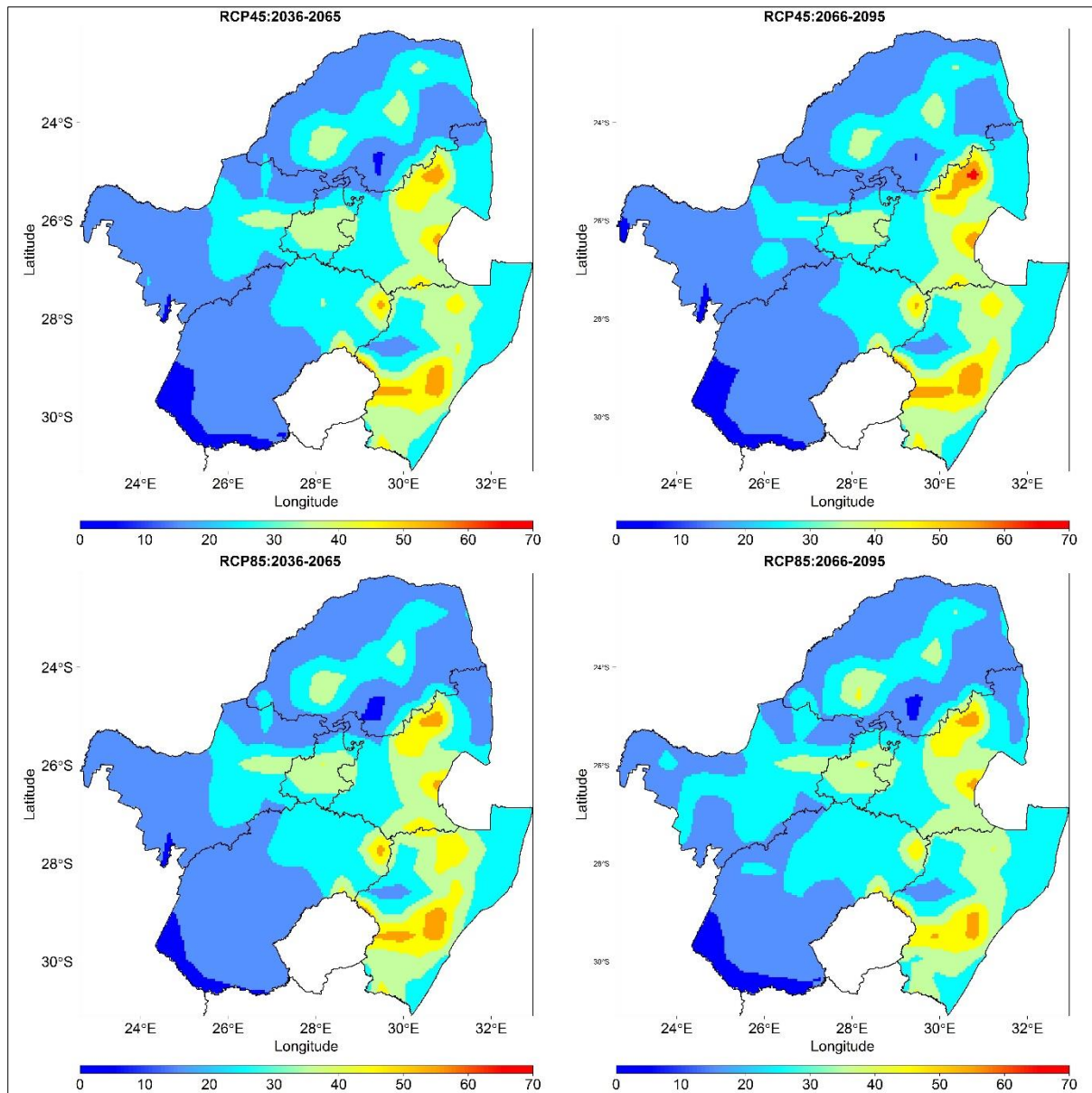


Figure 6.21: Projected total precipitation (mm) for Pentad 69 (7–11 December) for the periods 2036–2065 (top left) and 2066–2095 (top right) under the conditions of RCP4.5, and 2036–2065 (bottom left) and 2066–2095 (bottom right) under the conditions of RCP8.5

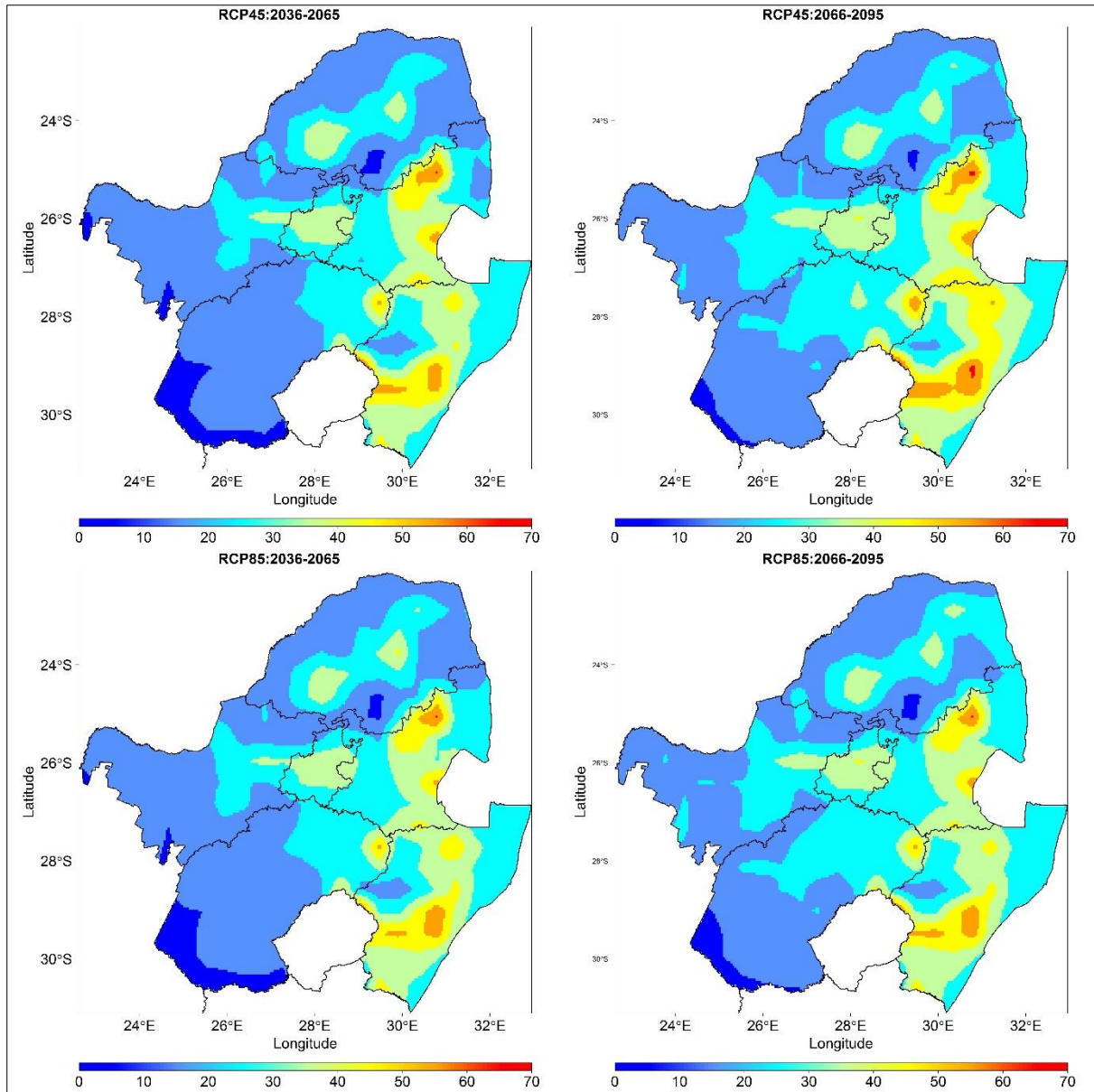


Figure 6.22: Projected total precipitation (mm) for Pentad 70 (12–16 December) for the periods 2036–2065 (top left) and 2066–2095 (top right) under the conditions of RCP4.5, and 2036–2065 (bottom left) and 2066–2095 (bottom right) under the conditions of RCP8.5

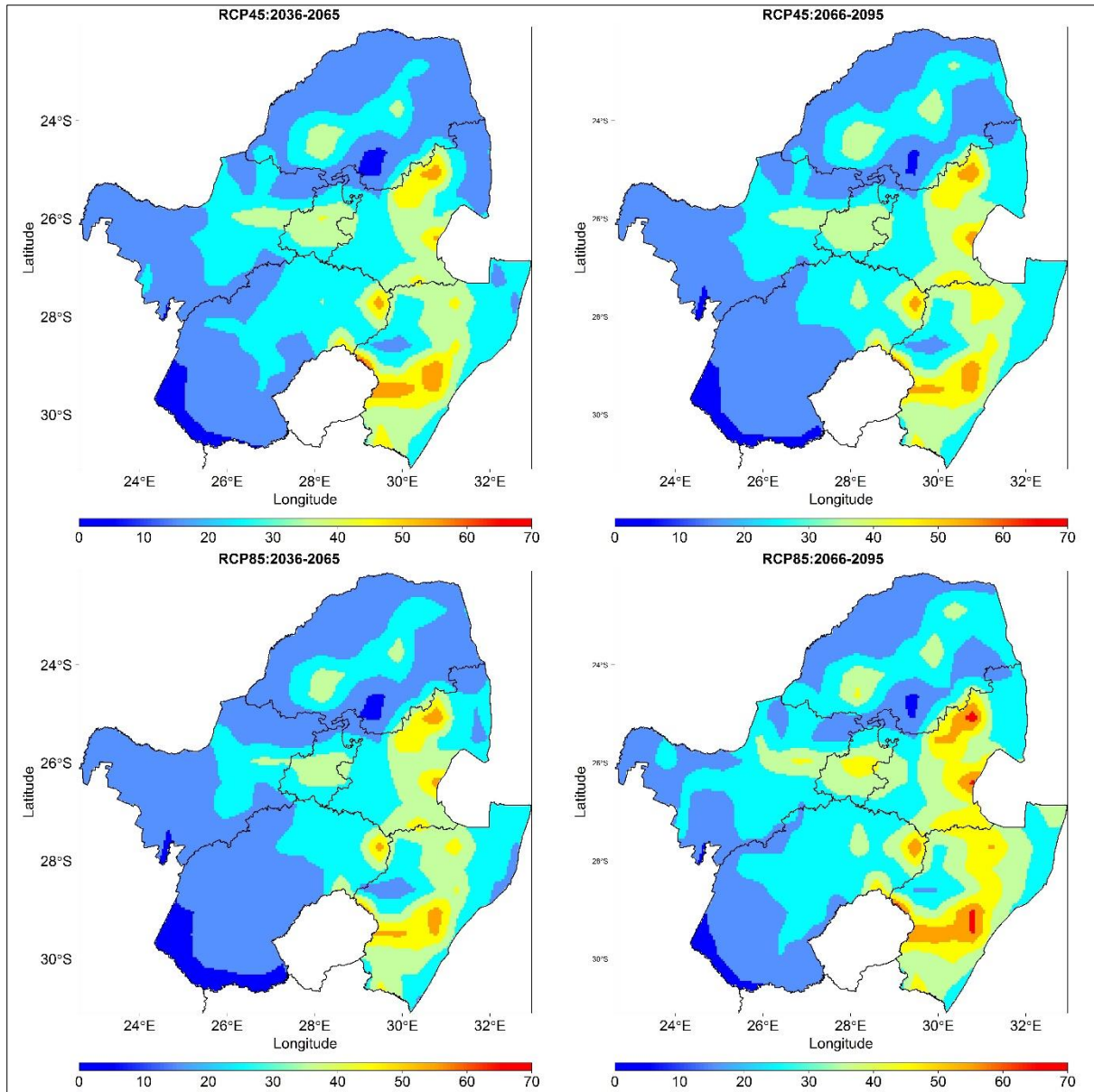


Figure 6.23: Projected total precipitation (mm) for Pentad 71 (17–21 December) for the periods 2036–2065 (top left) and 2066–2095 (top right) under the conditions of RCP4.5, and 2036–2065 (bottom left) and 2066–2095 (bottom right) under the conditions of RCP8.5

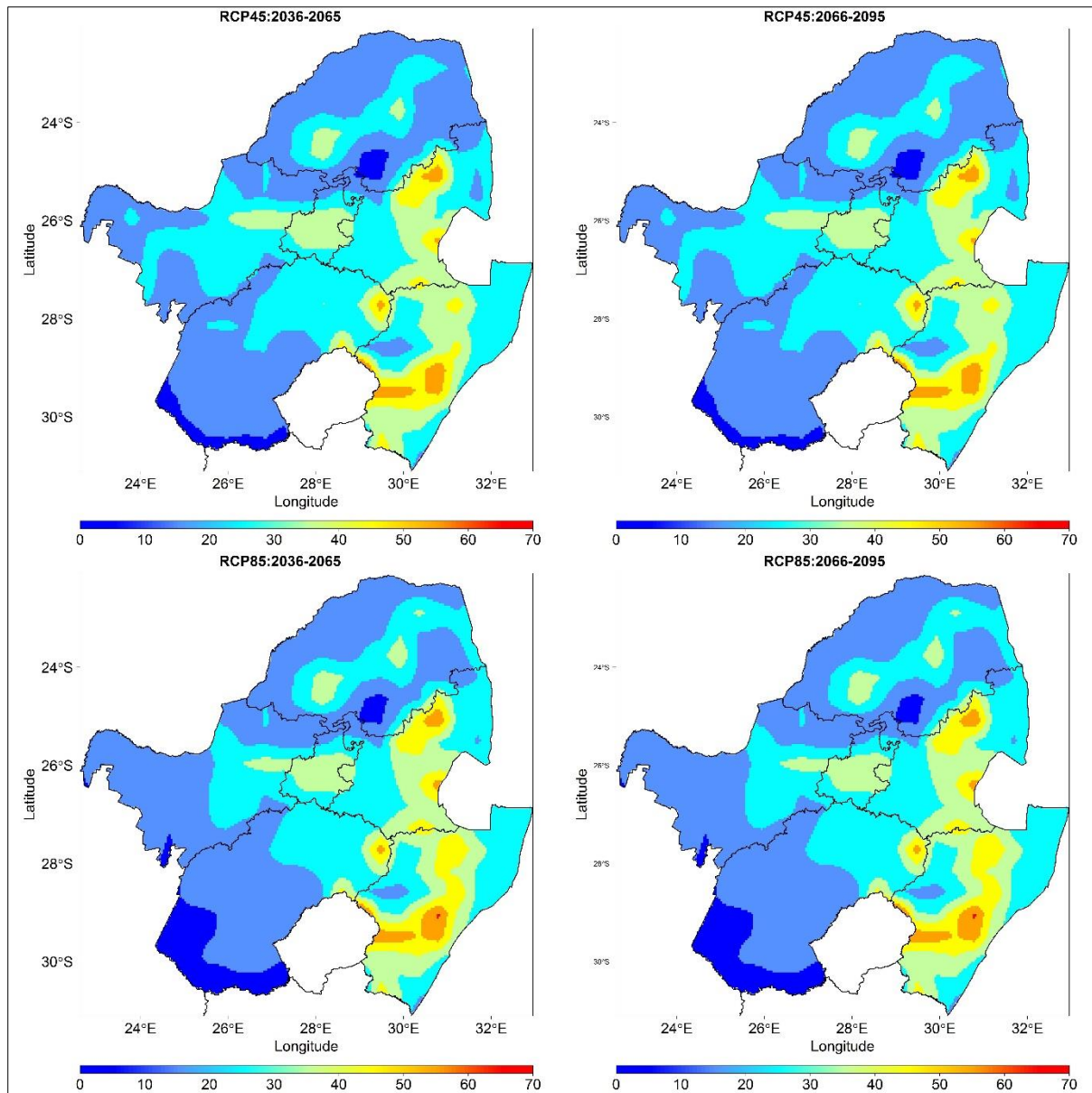


Figure 6.24: Projected total precipitation (mm) for Pentad 72 (22–26 December) for the periods 2036–2065 (top left) and 2066–2095 (top right) under the conditions of RCP4.5, and 2036–2065 (bottom left) and 2066–2095 (bottom right) under the conditions of RCP8.5

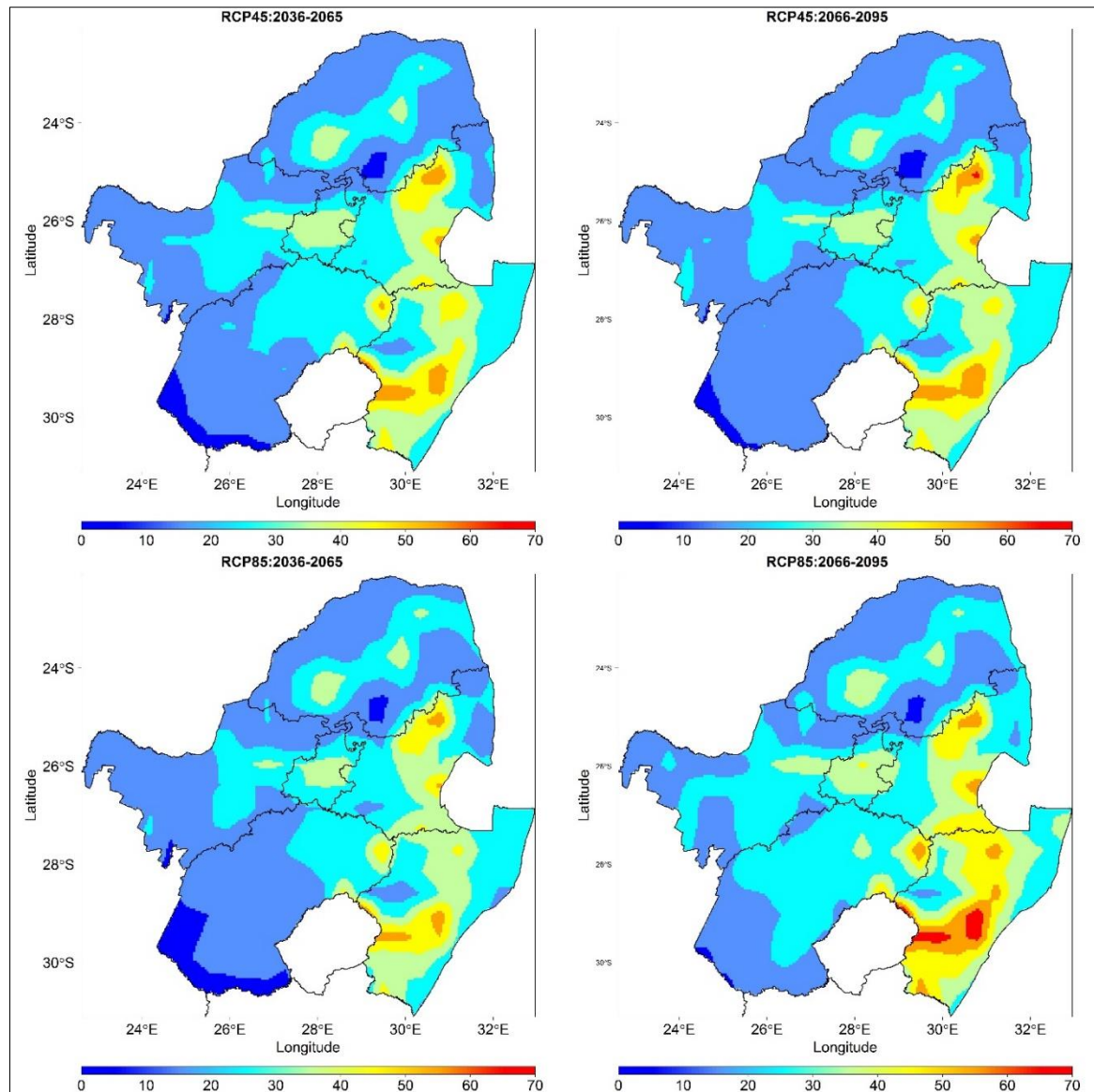


Figure 6.25: Projected total precipitation (mm) for Pentad 73 (27 –31 December) for the periods 2036–2065 (top left) and 2066–2095 (top right) under the conditions of RCP4.5, and 2036–2065 (bottom left) and 2066–2095 (bottom right) under the conditions of RCP8.5

6.5 CONCLUSIONS

Scenarios, according to the IPCC, are images of the future. They are neither forecasts nor predictions. They allow one to establish and assess the socio-economic and environmental vulnerability of pre-climate change references, determine the impacts of those changes, and assess vulnerability after adaptation. Consequently, understanding the vulnerability of a region due to climate change is imperative for adaptation and policy development. Future projections of climate extremes, and consecutive dry days for the summer season (October to March) and the mid-summer months (December and January) were computed using the ensemble mean of eight CMIP5 global climate models under two RCP scenarios. In general, there is a good spatial correlation between the dynamically downscaled GCMs (CORDEX) and the ERA5 output. The results showed that CDD for the three selected thresholds (1 mm, 2 mm and 3 mm) are projected to increase across the study area under both scenarios. Furthermore, the magnitudes of increase under RCP8.5 are projected to be higher than under RCP4.5.

Overall, the results of this study help to illustrate the future conditions of the major maize-producing regions of South Africa under the risk of climate extreme events. The outcomes will serve as a convenient resource to assess the impacts of climate change on agriculture, the environment and water resources to enhance local decision making, adaptation and strategic planning to ensure food security.

CHAPTER 7: THE IMPACT OF MID-SUMMER DRY SPELLS ON THE AGRO-WATER BUDGET AND MAIZE YIELD POTENTIAL IN THE MAJOR MAIZE-GROWING REGIONS OF SOUTH AFRICA

7.1 ABSTRACT³

Water stress is one of the major limiting factors in dryland maize production in South Africa. The maize-growing season experiences different rainfall characteristics, such as dry spells, which affect phenology and crop yields. The mid-summer period is particularly important for agriculture since a lack of rain during this period negatively affects crop growth and yield. This study investigated the impact of South African mid-summer dry spells on the annual water budget and on maize yield. A simple water balance model was used to assess the impact of mid-summer dry spells on the agricultural water budget. The AquaCrop model was used to investigate the impact of dry spells on maize yield in the primary maize-growing regions of South Africa. The climatic water budget results showed moisture deficits for all pentads during the mid-summer, with median deficits ranging from 5 to 25 mm per pentad. The highest deficit was experienced in Pentad 73 (27–31 December) and Pentad 1 (1–5 January). The warm and dry western maize-growing region had the highest total deficits (> 130 mm) during the mid-summer period, compared to the cool and temperate eastern maize-growing regions. The impact of mid-summer dry spells on maize yield was also assessed using the AquaCrop model for three years with high, medium and low frequencies of dry spells. The results indicated that the impact of mid-summer dry spells on maize yield was evident, showing higher yields for the 2004/05 growing season with a low frequency of dry spells. The 2000/01 growing season, with its high frequency of mid-summer dry spells, produced the lowest yield. The impact of mid-summer dry spells on maize yield is more pronounced on the dry, warm western maize-growing region of South Africa, which showed the lowest yield compared to the cool, temperate eastern maize-growing regions.

Keywords: Pentad; rainfall; mid-summer; dry spells; water budget; maize yield

³ When making reference to this section, please cite as follows: Mengistu, M.G., Daniel, S., Masithela, T. and Olivier, C. 2021. The impact of mid-summer dry spells on the agro-water budget and maize yield potential in the major maize-growing regions of South Africa. In: Mengistu et al. (Eds). 2021. An investigation of the historical and projected occurrence of the South African mid-summer drought and its implications for the agro-water budget. Water Research Commission, Pretoria, RSA, WRC Report K5/2830, Chapter 7.

7.2 INTRODUCTION

Southern Africa's summer rainfall experiences significant rainfall variability, with recurrent wet and dry spells and severe droughts (Richard et al., 2001). Several studies on rainfall variability in southern Africa have reported both intra-seasonal and inter-annual variability in summer, which is the main cropping season in the region (Landman and Tennant, 2000; Usman and Reason, 2004; Tadross et al., 2005; Mupangwa et al., 2011; Cr  tat et al., 2011). This observed variability in rainfall and its impact on crop yield makes the southern African region prone to food insecurities. Although the relationships between total rainfall and crop yield are clear, it is often the variability in seasonal rainfall characteristics, such as onset, cessation and dry spells, that are important and have the most adverse effect on agriculture (Tadross et al., 2009).

Drought occurs when there is a temporal imbalance of water availability due to a persistent lower-than-average precipitation over a certain period of time (Pereira et al., 2009). Several studies in the past have focused on the occurrence, intensity, impact and prediction of drought on an annual and seasonal basis. However, short-term droughts (dry spells) are equally vital to the agricultural sector, as the timing of the occurrence and intensity of the dry period is more important than seasonal shortfalls in rainfall. Usman and Reason (2004) highlighted that a season with above-average rainfall may not be better than a below-average season over an agricultural region if the rainfall during the season is not well distributed in space and time. Crops are more likely to do well with evenly distributed rains than with intermittent heavy showers interrupted by prolonged dry periods (Usman and Reason, 2004).

Water stress is one of the major limiting factors in dryland (rain-fed) agriculture. Its effects include stunted growth, delayed maturity and low crop productivity (Mzezewa et al., 2010). Various dryland crops, such as maize, are vulnerable to drought and are sensitive to water stress (Tadross et al., 2009; Mupangwa et al., 2011; Zinyengere et al., 2014). The maize-growing season experiences different rainfall characteristics, such as dry spells, which may impact on phenology and lead to reduced crop yield (Tadross et al., 2009; Moeletsi and Walker, 2012). Numerous studies have confirmed that the maize crop is more sensitive to water stress during its silking and pollination stages, compared to the vegetative stage (Grant et al., 1989; Du Plessis, 2003; Masupha et al., 2016). Generally, it was found that dryland maize production in South Africa is significantly affected by the amount and distribution of rainfall during the crop-growing season (Benhil, 2002). Furthermore, the occurrence of mid-summer dry spells, from approximately mid-December to mid-January, has a negative impact on yield if coincided with the flowering stage of maize (Du Plessis, 2003).

In crop production, water stress (soil water deficit), is a function of precipitation, evapotranspiration, as well as several soil properties (Nesmith and Ritchie, 1992). It is often useful to use water balance models to quantify components of a water budget. However, crop growth models represent the interactions between the plant and its environment (Jame and Cutforth, 1996) and are better suited to investigate the impact of water stress on crop yield. A number of models simulate the growth and development of maize, such as the CSM-CERES Maize model (Jones et al., 1986), Hybrid-Maize (Yang et al., 2004) and the Decision Support System for Agrotechnology Transfer (DSSAT) (Hoogenboom et al., 2010). However, these models require field calibration and a number of input parameters. The FAO's AquaCrop simulation model provides a sound theoretical framework to investigate the maize yield response to environmental stress (Farahani et al., 2009).

AquaCrop is a simple model that uses minimum data inputs during calibration to produce reliable estimates of crop growth and yield response to water availability (Raes et al., 2009; Steduto et al., 2009). AquaCrop is a crop water productivity model (Steduto et al., 2009; Raes et al., 2018) that has been broadly tested for simulating the maize yield response to water (Hsiao et al., 2009; Heng et al., 2009). AquaCrop simulates crop growth and yield based on the water-driven growth model that relies on the conservative behaviour of biomass per unit transpiration relationship (Steduto et al., 2009).

Raes et al. (2018) noted that these conservative parameters require no adjustment to the localised environments' favourable or limiting conditions as their modulation is triggered by stress response functions.

The aim of this study is to evaluate the impact of South African mid-summer dry spells on maize yield using the AquaCrop model. A simple water balance model is used to assess the impact of mid-summer dry spells on the agricultural water budget across the major maize-growing areas in South Africa.

7.3 DATA AND METHODOLOGY

7.3.1 Climatic water budget

Daily climate data from the South African Weather Service's data bank was used to investigate the impact of mid-summer dry spells on the water budget and maize yield for the summer rainfall region of South Africa. From the summer rainfall region, only 16 districts (Figure 7.1A) with homogeneous rainfall and seasonality (Kruger, 2011) from the maize-growing areas (Figure 7.1B) were used for further analysis. The number of stations used per district and the length of the dataset used for the analysis varied from district to district, as shown in Table 7.1. Rainfall was measured at either individual rainfall stations or automatic weather stations. As mentioned in Kruger and Nxumalo (2017), measurements at manual stations were done at 08:00 SAST and represent the accumulated rainfall over the preceding 24 hours, while AWS data represents the total rainfall accumulated over the period between 08:00 SAST the previous day and 08:00 SAST the current day. Only stations that were operational throughout the study period were selected, with at least 90% of daily values available. In cases where zero rainfall was recorded for relatively long periods, while surrounding stations recorded significant rainfall amounts, the data was flagged and removed (Kruger and Nxumalo, 2017).

Air temperature was averaged from the available stations in the district to create a district average of daily maximum and minimum air temperatures. Solar radiation (R_s) and reference evapotranspiration (ET_0) were estimated using the Hargreaves and Samani (1982) method:

$$R_s = (KT) \cdot (R_a) \cdot (TD)^{0.5} \quad (10)$$

where TD is the maximum daily temperature minus the minimum daily temperature ($^{\circ}\text{C}$); R_a is extra-terrestrial radiation (mm/day); KT is an empirical coefficient; and T_c is the average daily temperature ($^{\circ}\text{C}$).

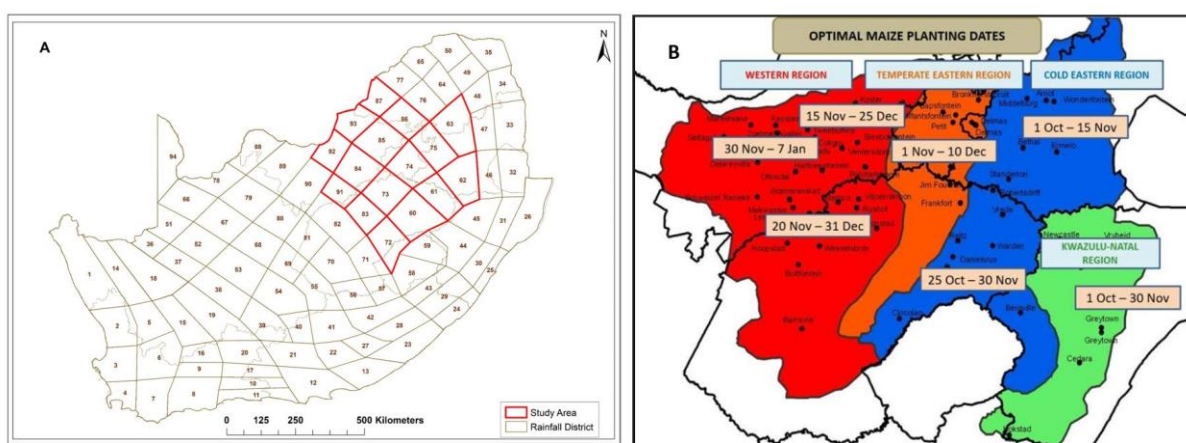


Figure 7.1: (A) Rainfall districts for South Africa with provincial borders (SAWB, 1972), showing the 16 selected districts with red polygons. (B) A map showing the major maize-growing regions with optimum planting dates (Source: Grain SA and Agbiz Research)

Table 7.1: The length of the district climate dataset used for the water budget and yield analysis

District	Start date	End date	Number of stations used for ET _o	Number of years
60	1985	2015	2	30
61	1988	2015	1	27
62	1993	2015	2	22
63	1994	2015	1	21
72	1990	2015	1	25
73	1990	2015	1	25
74	1992	2015	2	23
75	1994	2015	1	21
83	1991	2015	2	24
84	1992	2015	1	23
85	1994	2015	2	21
86	1994	2015	1	21
87	1994	2015	1	21
91	1994	2015	1	21
92	1985	2015	2	30
93	1985	2015	1	30

$$ET_o = 0.0135*(KT)*(Ra)*(TD)^{0.5}*(T_c+17.8) \quad (11)$$

where TD is the maximum daily temperature minus the minimum daily temperature (°C); R_a is the extra-terrestrial radiation (mm/day); KT is an empirical coefficient (0.162); and T_c is the average daily temperature (°C).

From the daily district data, pentad summations were calculated following the methodology used in Grobler (1993). Pentads were calculated using Julian days, for example, Pentad 1 refers to 1–5 January and Pentad 73 refers to 27–31 December. The extra leap year day, 29 February, was added to Pentad 10. Eight pentads between 12 December (the start of Pentad 70) and 20 January (the end of Pentad 4) were selected for a detailed analysis of the mid-summer rainfall for the study area.

A simple climatic water budget analysis was used following the methodology of Thornthwaite (1948) and Thornthwaite and Mather (1955), which uses precipitation (P) and potential or reference evapotranspiration (ET_o) to estimate moisture surplus or deficit. Surplus moisture is the water above what is lost naturally from the soil when P is greater than ET_o. Deficit moisture is water that would be lost above what is in the soil when P is less than ET_o.

7.3.2 Maize yield estimation

The FAO's AquaCrop simulation model was used to estimate maize yield and investigate the impact of mid-summer dry spells on maize yield. The FAO's AquaCrop model is a water-driven simulation model (generic crop water productivity model) (Raes et al., 2018; Steduto et al., 2009). It requires relatively few input parameters to simulate the yield response to water for most major field and vegetable crops. Its parameters are explicit and mostly intuitive, and the model maintains a sufficient balance between accuracy, simplicity and robustness (Raes et al., 2018; Steduto et al., 2009). The use of water productivity normalised for climate makes AquaCrop applicable to diverse locations and seasons (Karunaratne et al., 2010).

The AquaCrop model uses canopy ground cover (CC) instead of leaf area index (LAI) as the basis to calculate transpiration and separate soil evaporation from transpiration. Biomass is then calculated as the product of transpiration and a water productivity parameter:

$$B = WP \times \Sigma Tr \quad (12)$$

where B is above-ground biomass ($t \text{ ha}^{-1}$), WP is water productivity (biomass per unit of cumulative transpiration), and Tr is crop transpiration. Crop yield (Y) is then calculated as the product of the above-ground dry biomass and the Harvest Index (HI):

$$Y = B \times HI \quad (13)$$

AquaCrop requires soil, crop and atmosphere input data files and parameters. The climate component requires daily weather data on maximum and minimum air temperature, rainfall, ET_0 and CO_2 concentration. The soil profile file requires basic soil characteristics, such as volumetric water content at saturation, field capacity, permanent wilting point and saturated hydraulic conductivity of the different soil profile depths. The crop input data includes parameters such as phenology, development and water stress groups, plant density, emergence time, canopy senescence and maturity time, flowering period and the duration of yield formation, rooting depth and reference HI. Other input data includes information related to ground water, irrigation and field management.

Due to the variation in the soils on which maize is grown, a default sandy clay loam soil with moderate soil fertility was used for the simulations. For the crop input data, the following recommended optimum planting dates for maize are used: the beginning of October to the first week of November for the cooler eastern maize-producing areas; from the last week in October to mid-November for the temperate central regions; and from the last two weeks in November to mid-December for the drier western areas (ARC-GCI, 2002; Du Toit et al., 2002). Target yield plays an important role in determining the required plant density for each maize-producing area. To acquire a maize yield of four tons per hectare in each of the production regions of the study area, a plant density of 20 000 plants per hectare for the warm western region, 21 000 for the central temperate region, and 25 000 per hectare for the cool eastern region was used (Du Plessis, 2003). The maize cultivars grown in each region also differ, hence a cultivar with 120 growing season lengths was used for the simulations. Three planting dates for the different maize-production regions were used, as shown in Table 7.2 in the AquaCrop simulations. Since the objective of the study was to investigate the impact of mid-summer dry spells on the yield of maize, three different growing seasons with a high, medium and low frequency of dry spells during mid-summer were used in the analysis.

Table 7.2: The range of planting density and planting dates for the three major maize-growing areas of South Africa

Production region	Planting density (plants/ha)	First planting date	Second planting date	Third planting date
Cool eastern region (districts 60, 61, 62, 63)	25 000	15 October	20 October	25 October
Temperate eastern region (districts 72, 73, 74, 75)	21 000	30 October	5 November	10 November
Warm and dry western region (districts 83, 84, 85, 86, 87, 92, 93)	20 000	20 November	25 November	30 November

7.4 RESULTS AND DISCUSSION

7.4.1 Climatic water budget

Rainfall in the study area is highly variable from year to year with a high evapotranspiration that often exceeds the rainfall. Rainfall distribution for District 62 (in the cool eastern region), District 74 (in the temperate eastern region) and District 84 (in the warm, dry western region) is presented in figures 7.2A, 7.3A and 7.4A, respectively. Evapotranspiration (ET_o) distribution for District 62, 74 and 84 is also presented in Figure 7.2B, 7.3B and 7.4B, respectively. The black line is the median, the box covers the first and third quantiles (25th and 75th percentiles), the whiskers are 1.5 times the interquartile range, and the dots are outliers outside this range. The results show high variability in total pentad rainfall during the mid-summer pentads (figures 7.2A, 7.3A and 7.4A). Peak evapotranspiration is also experienced for all districts during the mid-summer pentads (pentads 70, 71, 72, 73, 1, 2, 3 and 4), as shown in figures 7.2B, 7.3B and 7.4B.

Generally, dry spells occur due to inadequate rainfall, although the evaporative demand of the atmosphere is another determining factor. A simple climatic water budget analysis (Thornthwaite, 1948) was used to assess the impact of mid-summer dry spells on the agricultural water budget of the major maize-growing areas. Precipitation (P) and reference evapotranspiration (ET_o) were used to estimate moisture surplus or deficit for the mid-summer pentads, as shown in figures 7.5, 7.6 and 7.7. Surplus moisture is the water above what is lost naturally from the soil when P is greater than ET_o . Deficit moisture is water that would be lost above what is in the soil when P is less than ET_o .

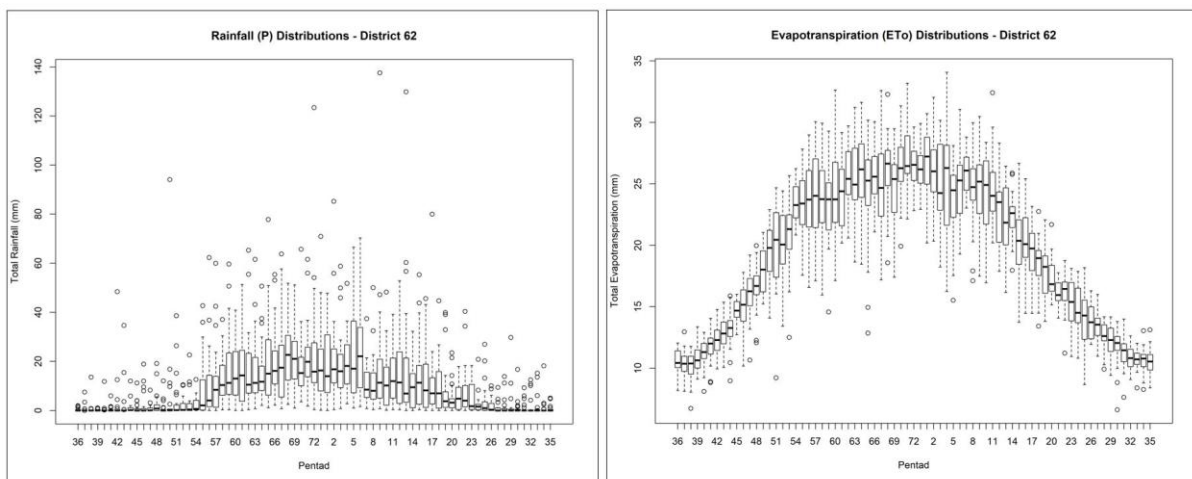


Figure 7.2: Mean climatic total pentad rainfall distribution (A) and evapotranspiration (ET_o) distribution (B) for District 62 within the cool eastern maize-growing region of South Africa

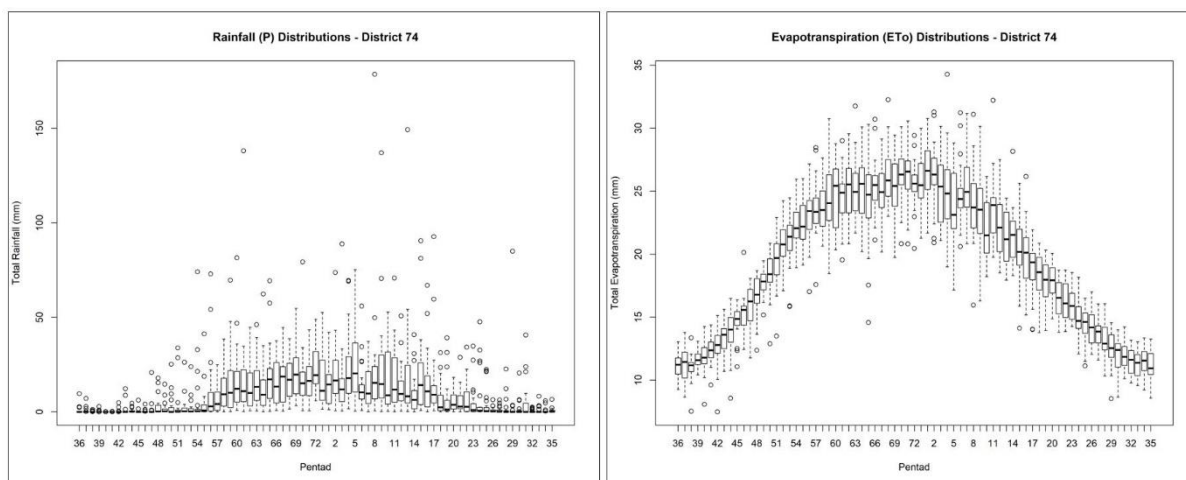


Figure 7.3: Mean climatic total pentad rainfall distribution (A) and evapotranspiration (ET_0) distribution (B) for District 74 within the temperate eastern maize-growing region of South Africa

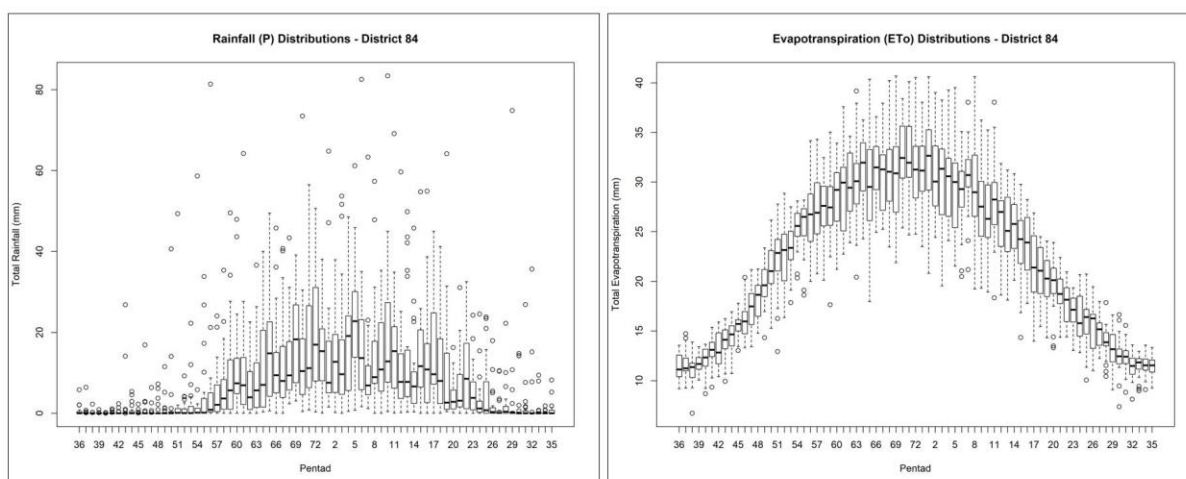


Figure 7.4: Mean climatic total pentad rainfall distribution (A) and evapotranspiration (ET_0) distribution (B) for District 84 within the warm and dry western maize-growing region of South Africa

The difference between the P and ET_0 results indicate a moisture deficit for all the districts and pentads during the mid-summer (figures 7.5 to 7.7), with median deficits ranging from 5 to 25 mm per pentad. The highest deficit is experienced in Pentad 1 for districts 62 and 84. Pentad 73 showed high deficits for District 74 (Figure 7.6). In general, District 84 (Figure 7.7) in the warm, dry maize-growing region had the highest deficit, with medians greater than 15 mm per pentad, compared to districts 62 and 74. The total climatic water budget for all the mid-summer pentads and districts in the study area are summarised in Table 7.3. Districts 91, 92 and 93 (in the warm, dry western maize-growing region) and District 72 (in the temperate eastern region) have the highest total deficits (> 130 mm) during the mid-summer period (Table 7.3).

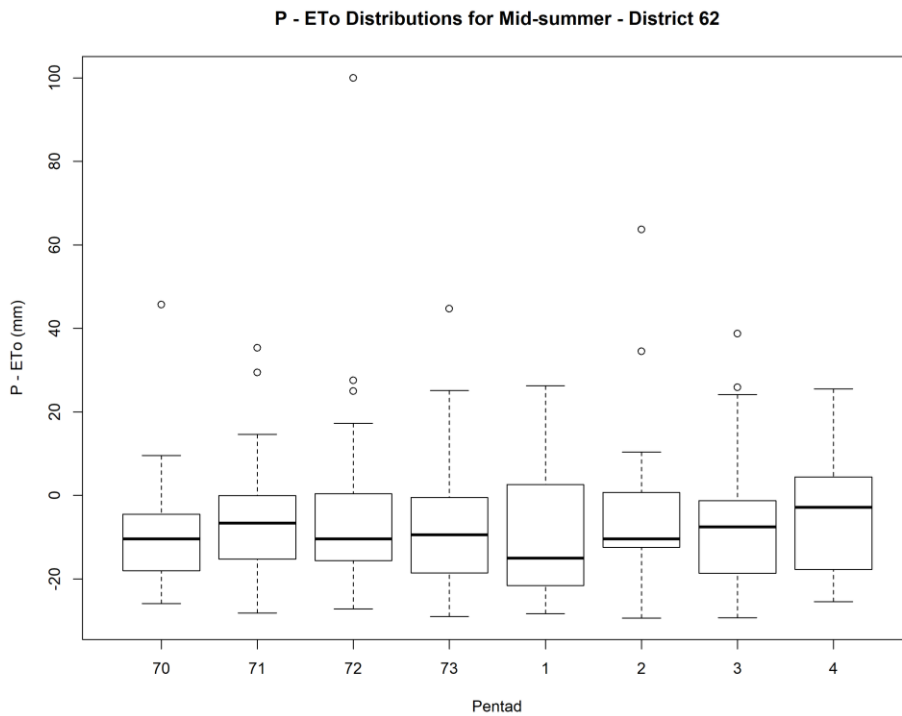


Figure 7.5: Mid-summer climatic water budget ($P - ET_o$) distribution for District 62 within the cool eastern maize-growing region of South Africa. The black line is the median, the box covers the first and third quartiles (25th and 75th percentiles), the whiskers are 1.5 times the interquartile range and the dots are outliers outside this range.

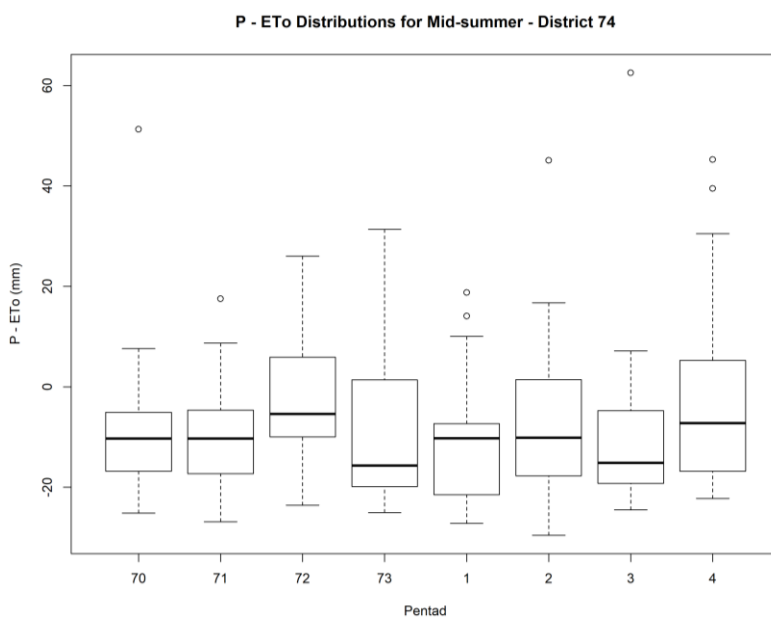


Figure 7.6: Mid-summer climatic water budget ($P - ET_o$) distribution for District 74 within the temperate eastern maize-growing region of South Africa. The black line is the median, the box covers the first and third quartiles (25th and 75th percentiles), the whiskers are 1.5 times the interquartile range and the dots are outliers outside this range.

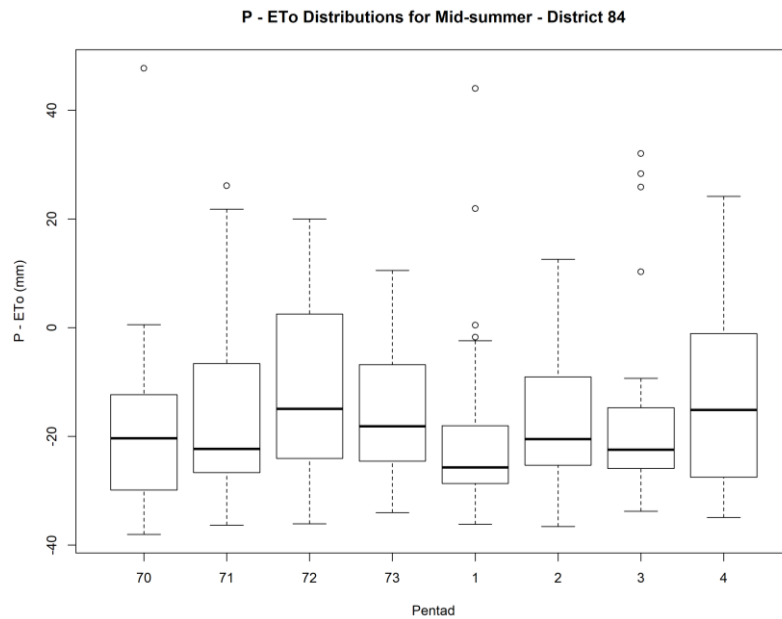


Figure 7.7: Mid-summer climatic water budget ($P - ET_o$) distribution for District 84 within the warm, dry western maize-growing region of South Africa. The black line is the median, the box covers the first and third quartiles (25th and 75th percentiles), the whiskers are 1.5 times the interquartile range and the dots are outliers outside this range.

Table 7.3: Summary of the climatic water budget ($P - ET_o$) for all the districts in the study area during mid-summer

District	P70	P71	P72	P73	P1	P2	P3	P4	Mid-summer total
60	-11.5	-12.5	-8.1	-16.0	-13.1	-12.0	-13.1	-8.8	-95.0
61	-6.3	-8.0	-5.2	-11.0	-8.4	-7.0	-10.5	-6.5	-62.8
62	-8.1	-5.6	-2.0	-6.6	-7.5	-3.7	-5.8	-4.8	-44.2
63	-5.9	-6.3	-3.5	-2.7	-7.0	-5.3	-9.6	-5.8	-46.0
72	-17.7	-19.3	-16.4	-16.8	-17.1	-16.3	-17.2	-12.6	-133.4
73	-16.0	-13.8	-10.3	-17.3	-17.1	-14.7	-15.5	-17.2	-121.9
74	-8.6	-9.3	-3.4	-9.7	-10.3	-5.8	-9.3	-1.8	-58.3
75	-6.1	-9.9	-7.9	-10.1	-4.8	-7.8	-8.2	-2.2	-57.1
83	-18.7	-20.3	-15.4	-18.9	-18.1	-21.5	-22.3	-19.2	-154.4
84	-17.9	-14.1	-10.9	-15.7	-18.1	-17.1	-15.4	-12.8	-122.1
85	-10.9	-14.8	-13.2	-14.1	-11.9	-12.8	-12.3	-2.0	-92.0
86	-5.2	-6.2	-1.2	-5.0	-6.8	-3.6	-9.5	0.3	-37.2
87	-15.4	-16.0	-13.3	-17.7	-16.5	-12.3	-16.4	-13.0	-120.5
91	-20.3	-15.4	-13.5	-16.7	-16.8	-15.7	-16.7	-17.3	-132.4
92	-20.6	-16.9	-17.2	-18.0	-19.9	-16.3	-16.5	-13.7	-139.0
93	-18.4	-19.3	-15.2	-19.4	-20.5	-16.6	-17.2	-14.4	-140.9

These results indicate that the evaporative demand of the atmosphere is high during the mid-summer season, and that water deficits are experienced in the maize-growing areas of the summer rainfall region of South Africa. The climatic water budget results presented in Table 7.3 showed water deficits for all mid-summer pentads and may have a negative impact on maize yield if compounded with soil water deficits.

7.4.2 Maize yield estimation using AquaCrop

The AquaCrop model is used to investigate the impact of mid-summer dry spells on maize yield in the major maize-growing regions of South Africa. The impact of mid-summer dry spells on maize yield was assessed over a period of three years with a high, medium and low frequency of dry spells (figures 7.8 to 7.10). An analysis of the total pentad rainfall for eight pentads in December and January was completed to investigate the deviation from the climatological average of the number of dry pentads during the mid-summer period. Anomalies of dry pentad frequency are presented in figures 7.8 to 7.10 using three thresholds for districts 62, 74 and 84. Negative values indicate fewer dry pentads, while positive values indicate more dry pentads during the mid-summer period. Three growing seasons, 1999/2000 (medium-frequency dry spells), 2000/01 (high-frequency dry spells) and 2004/05 (low-frequency dry spells) were selected from figures 7.8 to 7.10 for more detailed AquaCrop yield simulations.

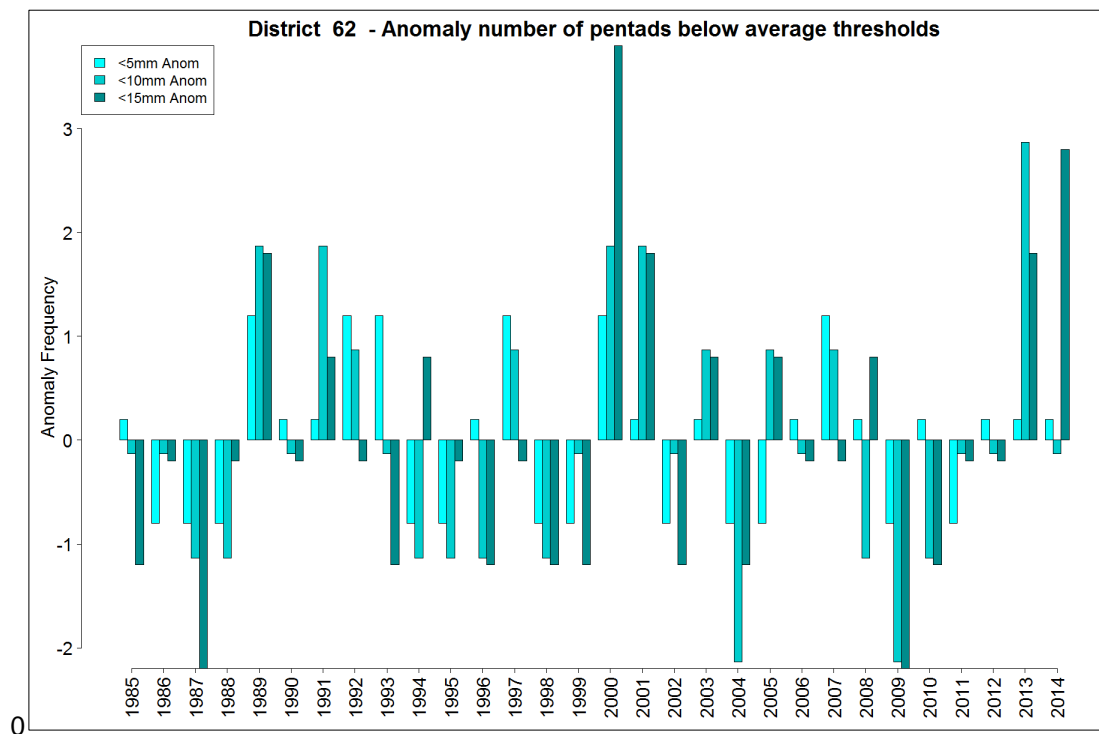


Figure 7.8: Pentad anomaly frequency below average thresholds of 5 mm, 10 mm and 15 mm for the eight mid-summer pentads in December and January for District 62 in the cool eastern maize-growing region of South Africa

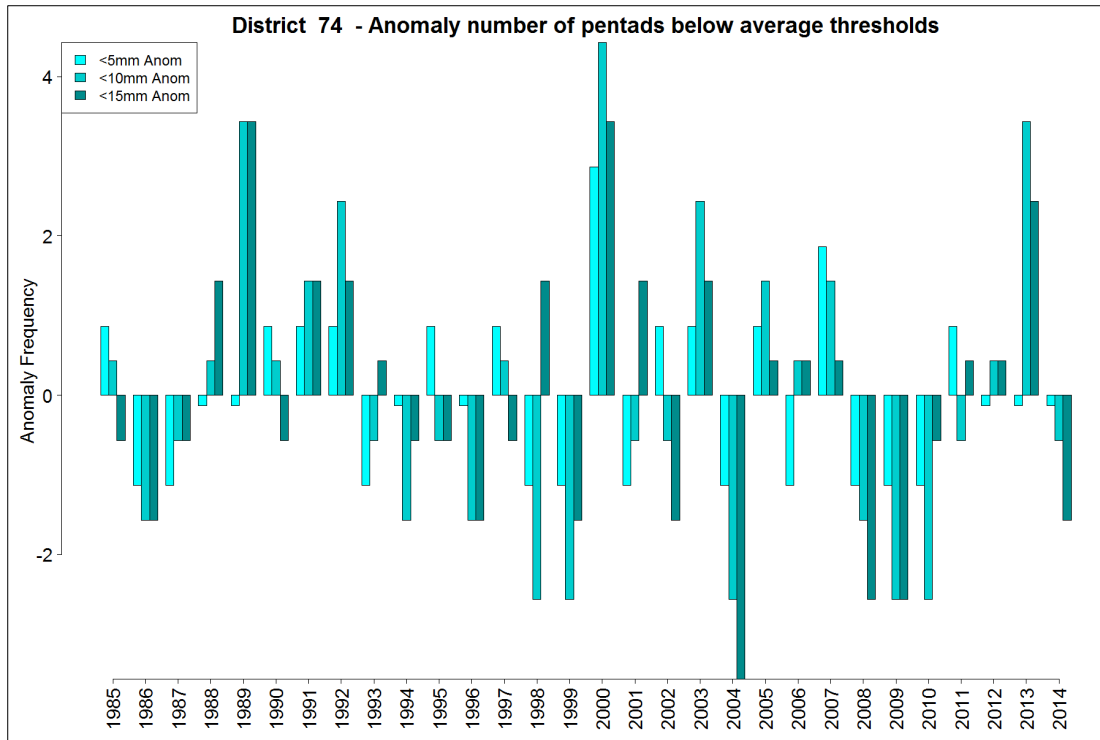


Figure 7.9: Pentad anomaly frequency below average thresholds of 5 mm, 10 mm and 15 mm for the eight mid-summer pentads in December and January for District 74 in the temperate eastern maize-growing region of South Africa

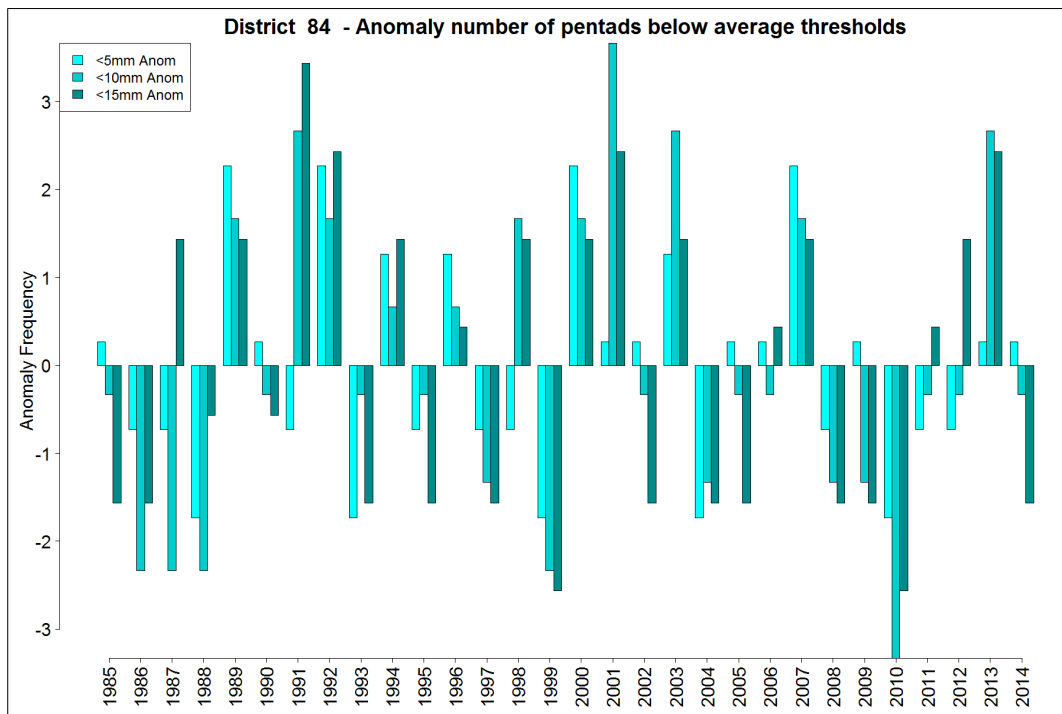


Figure 7.10: Pentad anomaly frequency below average thresholds of 5 mm, 10 mm and 15 mm for the eight mid-summer pentads in December and January for District 84 in the warm, dry western maize-growing region of South Africa

AquaCrop is used to simulate crop growth and yield response to water availability, and uses green canopy cover to describe crop development, where the yields are separated into biomass and Harvest Index (Raes et al., 2009). Biomass accumulation is calculated as a product of water productivity (WP) and transpiration (Tr). The AquaCrop default biomass water productivity value of 32.0 g m⁻² and its HI value of 48% were used for the maize yield simulations in this study. Water productivity values of 30–35 g m⁻² is generally accepted for C4 cereal crops in AquaCrop.

The effect of water stress on canopy expansion is simulated by multiplying the canopy growth coefficient with the water stress coefficient for canopy expansion. As root zone depletion (Dr) increases and drops below the upper threshold, the stress coefficient becomes smaller than 1 and the canopy expansion starts to be reduced (Raes et al., 2018). An example of an AquaCrop simulation showing the effect of water stress due to dry spells for the 2000/01 maize-growing season for District 62 is presented in Figure 7.11. The effect of water stress during the flowering stage of the maize crop is clearly visible on the actual canopy cover and root zone depletion.

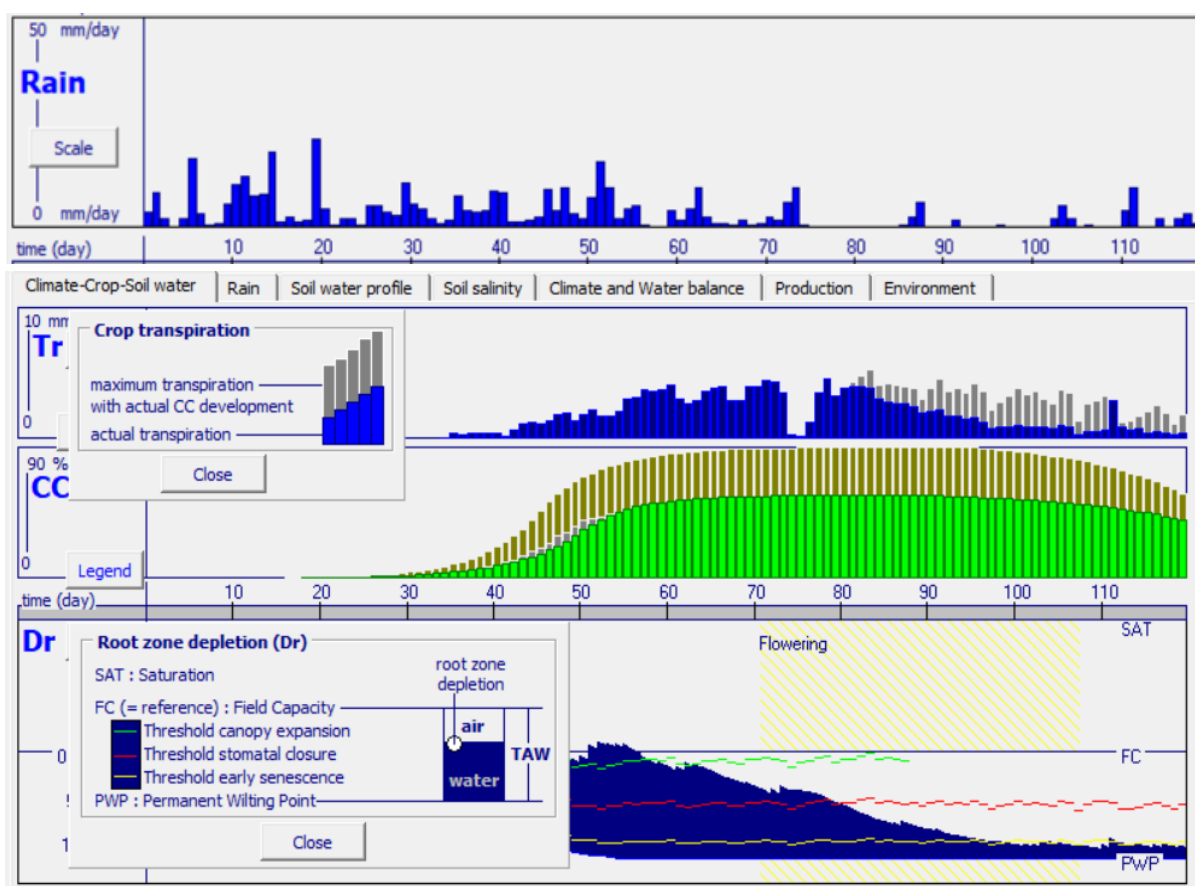


Figure 7.11: AquaCrop maize crop growth simulation for District 62 showing rainfall, canopy cover and transpiration, and root zone water depletion for the 2000/01 maize-growing season

Maize yield simulations using AquaCrop (t ha⁻¹) for three growing seasons, with varying frequency of dry spells and three recommended planting dates, are presented in tables 7.4 to 7.6 for districts 62, 74 and 84, respectively. For the wet and cool eastern maize-growing region (District 62), early planting on 15 October produced higher yields, followed by the 20 October planting for all three maize-growing seasons (Table 7.4). As shown in Table 7.4, the impact of mid-summer dry spells on maize yield is evident, showing yields that are higher in the 2004/05 growing season, associated with a lower frequency of dry spells, and vice versa. In the temperate eastern maize-growing region (District 74), yield is also lower for 2000/01 – a growing season with a high frequency of mid-summer dry spells (Table 7.5).

The first planting date (30 October) produced a higher yield for the three growing seasons, as shown in Table 7.5. With its low frequency of mid-summer dry spells, lower yields were simulated in the 2004/05 growing season, compared to the 1999/2000 growing season for District 74. These lower yields could likely be due to lower total rainfall and/or the distribution of rains during this growing season, compared to the 1999/2000 growing season.

For the dry, warm western maize-growing region (District 84), early planting on 20 November also produced higher yields (Table 7.6). The 2000/01 growing season, with a higher frequency of mid-summer dry spells, produced the lowest yield (as shown in Table 7.6), compared to the other two growing seasons, which had a lower number of dry pentads. The impact of mid-summer dry spells on maize yield is more pronounced in this region, showing the lowest yield compared to the cool, temperate eastern maize-growing regions.

Table 7.4: AquaCrop maize yield estimates ($t\ ha^{-1}$) using three recommended planting dates and three years of varying dry-spell frequencies for District 62 in the cool eastern maize-growing region of South Africa

Planting date	Maize yield ($t\ ha^{-1}$)		
	1999/2000 (medium-frequency dry spells)	2000/01 (high-frequency dry spells)	2004/05 (low-frequency dry spells)
15 October	4.99	4.56	5.94
20 October	4.96	4.34	5.73
25 October	4.87	4.23	5.70

Table 7.5: AquaCrop maize yield estimates ($t\ ha^{-1}$) using three recommended planting dates and three years of varying dry-spell frequencies for District 74 in the temperate eastern maize-growing region of South Africa

Planting date	Maize yield ($t\ ha^{-1}$)		
	1999/2000 (medium-frequency dry spells)	2000/01 (high-frequency dry spells)	2004/05 (low-frequency dry spells)
30 October	4.24	2.56	3.45
5 November	4.24	2.53	3.03
10 November	4.03	2.84	3.00

Table 7.6: AquaCrop maize yield estimates ($t\ ha^{-1}$) using three recommended planting dates and three years of varying dry-spell frequencies for District 84 in the warm, dry western maize-growing region of South Africa

Planting date	Maize yield ($t\ ha^{-1}$)		
	1999/2000 (medium-frequency dry spells)	2000/01 (high-frequency dry spells)	2004/05 (low-frequency dry spells)
20 November	4.23	1.71	4.39
25 November	4.16	1.81	4.27
30 November	4.19	2.24	4.08

Maize is mostly planted on drylands in most parts of South Africa, and is sensitive to water stress (Zinyengere et al., 2014). Several studies have shown that maize plants are more sensitive to water stress during silking and pollination, compared to the vegetative stage (Du Plessis, 2003; Masupha et al., 2016). Mid-summer dry spells often coincide with the flowering stage of the maize crop and can have damaging effects on maize yield (Sun et al., 2007). The AquaCrop maize yield simulation results presented in this study confirm the negative impact of mid-summer dry spells on maize yield. Mid-summer dry spells occur with different intensities, duration and frequency across the major maize-growing areas of South Africa (Mengistu et al., 2020). The duration and intensity of dry spells have shown an increasing trend in dry spells from east to west of the study area. This is also evident in the AquaCrop maize yield results (tables 7.4 to 7.6), showing that the warm western maize-growing region is impacted the most by mid-summer dry spells.

7.5 SUMMARY AND CONCLUSIONS

Southern Africa is subjected to annual and seasonal rainfall variability, which has a significant impact on crop yield and food security. Seasonal rainfall characteristics, such as dry spells during the crop-growing season, may have adverse effects on plant growth and crop yield. The maize-growing season experiences different rainfall characteristics, such as dry spells, which affect phenology and crop yield. Several studies have confirmed that the maize crop is more sensitive to water stress during its pollination stage. Moreover, the occurrence of mid-summer dry spells from mid-December to mid-January will have a negative impact on yield if it coincides with the flowering stage of maize. The aim of this study was to investigate the impact of South African mid-summer dry spells on the annual water budget and maize yield. A simple water balance model was used to assess the impact of mid-summer dry spells on the agricultural water budget. The AquaCrop model was used to investigate the impact of dry spells on maize yield in the primary maize-growing areas of South Africa.

The climatic water budget results showed that moisture deficits occur in all districts and pentads during mid-summer, with median deficits ranging from 5 to 25 mm per pentad. The highest deficit was experienced in pentads 73 and 1. The warm, dry western maize-growing regions experience the highest total deficits during the mid-summer period, compared to the cool, temperate eastern maize-growing regions. The impact of mid-summer dry spells on maize yield was also assessed using the AquaCrop model for three years with a high, medium and low frequency of dry spells. Three recommended planting dates were used for the maize yield simulations. The results indicate that the impact of mid-summer dry spells on maize yield is evident, showing higher yields for the 2004/05 growing season, which is associated with a lower frequency of dry spells. The 2000/01 growing season, which is associated with a higher frequency of mid-summer dry spells, produced the lowest yield. The impact of mid-summer dry spells on maize yield is more pronounced in the dry, warm western maize-growing region, which shows the lowest yield, compared to the cool, temperate eastern maize-growing regions.

The major maize-growing areas of South Africa experience water deficits and high evaporative demand during the mid-summer pentads. The climatic water budget and AquaCrop model results indicate that dry spells have a negative impact on maize yield. Optimum planting dates were also investigated from the recommended dates for the three major maize-growing regions of South Africa. Planting dates should be adjusted to ensure that the water-sensitive growth stages do not coincide with the mid-summer dry-spell periods. The findings from this study will assist farmers and decision makers to adjust their planting dates of summer crops to ensure favourable growing conditions during the water stress-sensitive growth stages. Information on the climatic water budget could also be used as a guide for planning supplementary irrigation during the mid-summer dry period.

CHAPTER 8: GUIDELINES AND EARLY WARNING SYSTEM

8.1 BACKGROUND⁴

Water stress is one of the major limiting factors in dryland agriculture. Its effects include stunted growth, delayed maturity and low crop productivity. Rainfall distribution and temperature are some of the limiting factors that affect crop productivity. Various crops, such as maize, are vulnerable to dry spells during specific phenological stages. The flowering stage of maize has been found to be the most sensitive to water stress (Figure 8.1), for example, leading to reductions in crop growth, biomass production and yield. Therefore, planting dates should be chosen to ensure that this stage coincides with normally favourable growing conditions and not with mid-summer dry spells (Du Plessis, 2003). Adjusting the planting date to within the optimum planting period is one of the management practices that can increase maize yield. However, optimum planting dates are location specific and depend on the onset and cessation of rainfall and soil temperature. The aim of this guideline chapter is to produce and implement an early warning system and recommended planting dates for maize production, which will assist farmers to avoid mid-summer dry spells during the critical flowering stage. Planting dates with high risk can be identified for the major maize-growing regions of South Africa based on the likely occurrence of mid-summer dry spells and the time between planting and flowering.

⁴ When making reference to this section, please cite as follows: Mengistu, M.G., Olivier, C., Daniel, S. and Masithela, T. 2021. Guidelines and early warning system. In: Mengistu et al. (Eds). 2021. An investigation of the historical and projected occurrence of the South African mid-summer drought and its implications for the agro-water budget. Water Research Commission, Pretoria, RSA, WRC Report K5/2830, Chapter 8.

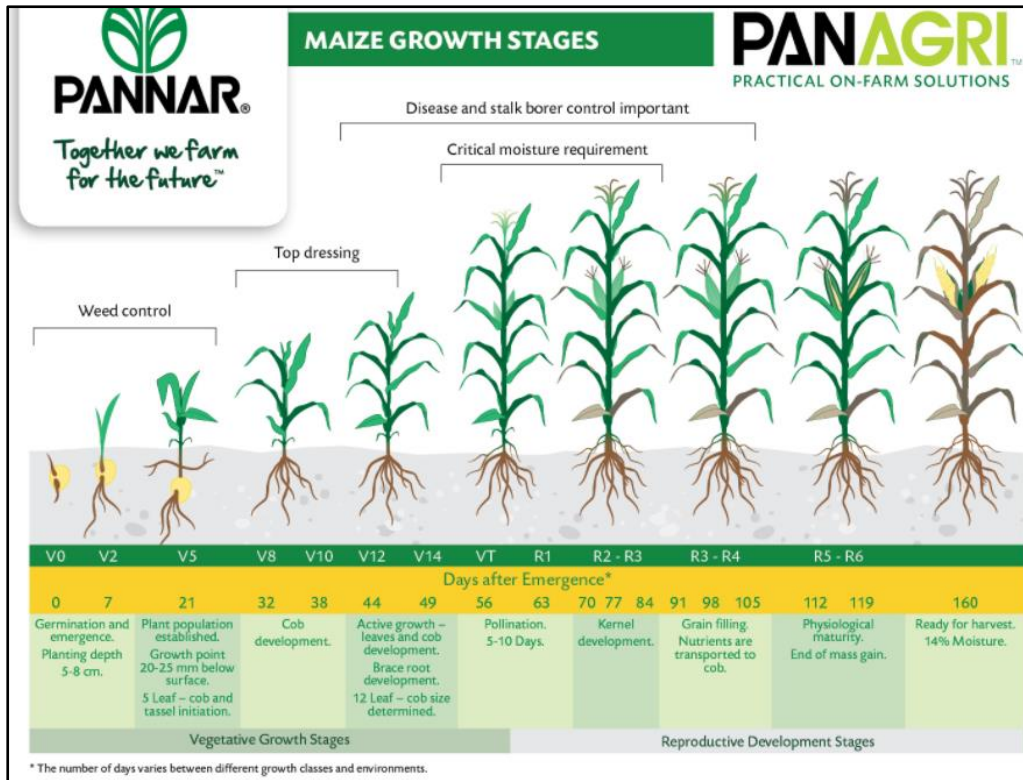


Figure 8.1: Maize growth stages (PANNAR, 2016)

8.2 DATA AND METHODOLOGY

Daily rainfall data from the South African Weather Service’s data bank from 1979 to 2014 was used to investigate mid-summer dry spells. From the summer rainfall region, which receives rain mostly from October to March, only 16 districts (Figure 8.2) with homogeneous rainfall and seasonality for the maize-growing areas (Figure 8.3) were used. The study area receives 80% or more of its total annual rainfall between October and March.

The Markov chain probability model was used for dry-spell analysis using a threshold value of 3 mm rainfall per day (15 mm per pentad). Reddy (1990) used a threshold of 3 mm per day, which is the minimum rainfall depth threshold value for crops to satisfy their crop water requirement during a growing season. A pentad with less than 15 mm rainfall was considered a dry pentad and a pentad with 15 mm or more rainfall a wet pentad. The Markov chain probability model calculates the initial probabilities of having a dry or a wet spell for a given pentad.

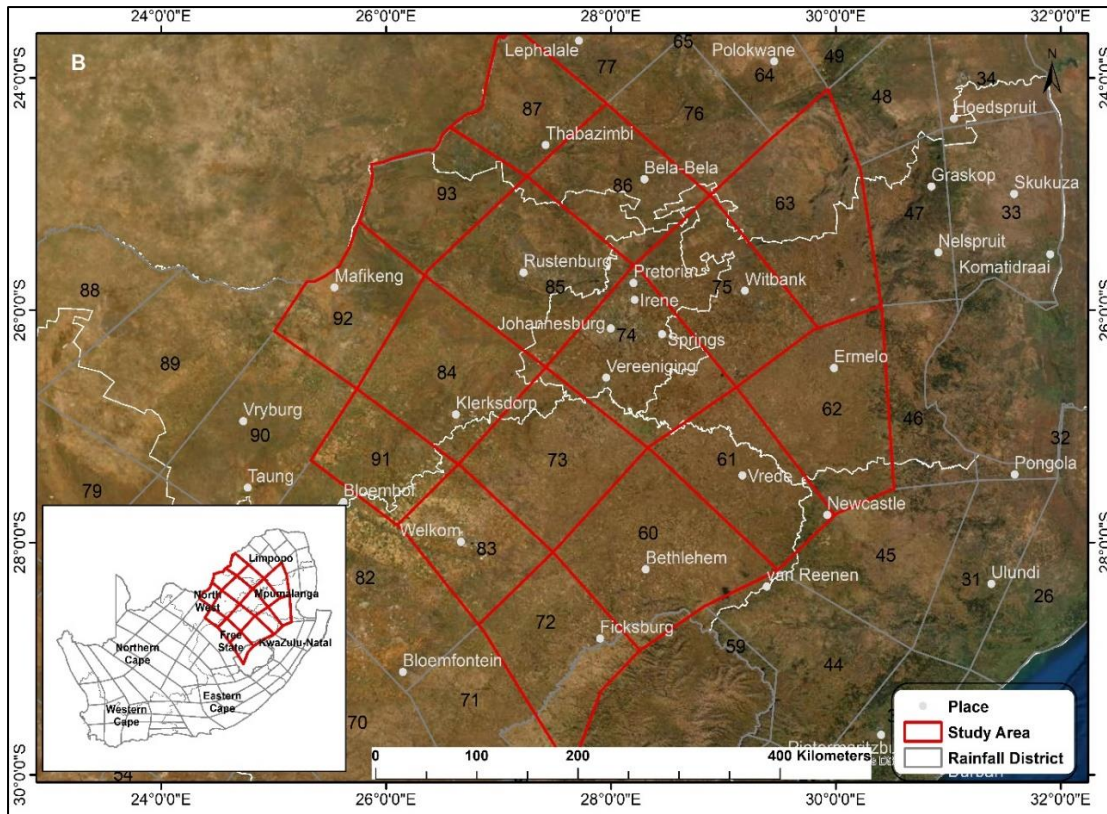


Figure 8.2: Rainfall districts for South Africa with provincial borders (SAWB, 1972), showing the 16 selected districts with red polygons

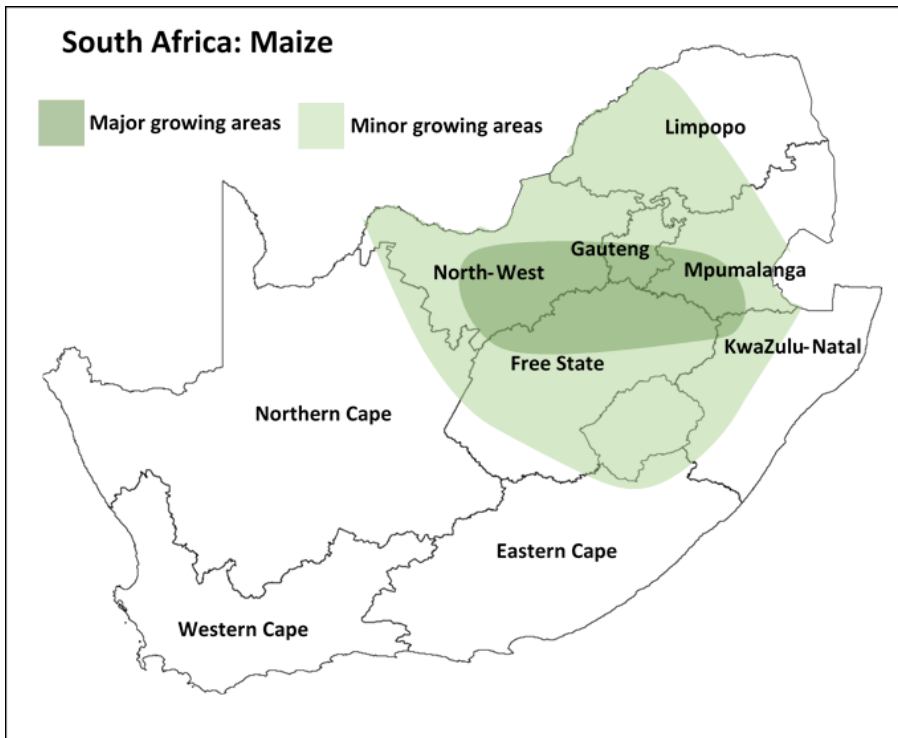


Figure 8.3: A map showing South Africa's maize-growing areas (AgWeb, 2015)

For the climate change predictions of rainfall, CORDEX model simulations, dynamically downscaled over the African domain at a spatial resolution of $0.44^\circ \times 0.44^\circ$, were utilised. Specifically, RCA4, forced across its lateral boundaries by the CMIP5 global circulation models (shown in Table 5.1) (Taylor et al., 2012), was used. The RCA4 model is a coupled ocean-atmosphere regional climate model based on the HARLAM numerical weather prediction model (Undén et al., 2002). In terms of climate projections, three projected time intervals were considered. These are the current climatology, spanning 2006–2035; the near-future, defined as the period starting from 2036–2065; and the distant future, spanning 2066–2095. The CORDEX-Africa model simulations under RCP4.5 and RCP8.5 scenarios across the selected time intervals were used in the analysis. The IPCC describes RCP4.5 as an intermediate scenario. Emissions peak around 2040 and start declining by approximately 2045. In RCP8.5, emissions continue to rise throughout the 21st century. This is generally taken as the basis for worst-case climate change scenarios.

Multi-model ensembles, i.e. models produced by combining multiple model ensemble members, were used for the climate change rainfall characteristic predictions. This involves the combination of information from all participating models, a process that is believed to increase the skill, reliability and consistency of ensemble models. In this study, multi-model ensembles refer to a set of model simulations from different CORDEX-Africa models (Table 5.1), which were created using the Simple Multi-model Averaging (SMA) technique (Georgakakos et al. 2004).

The onset of rain is defined as the last day on which rainfall of 25 mm or above has been accumulated over the previous 10 days, and at least 20 mm accumulated in the subsequent 20 days (Tadross et al., 2009). The additional 20 mm of cumulative rainfall over the next 20 days ensures that there is enough moisture for germination and the early development stage. The cessation of the rainy season is defined as three consecutive dekads (10-day periods) with less than 20 mm rainfall each, occurring after 1 February (Tadross et al., 2009).

Daily SAWS district rainfall data was used to calculate the onset and cessation for each season for the respective observed and simulated (historical and future) scenarios. Onset was calculated as days since 1 September (the earliest potential start to the summer season) and cessation as days since 1 February (the earliest expected cessation date) of the following year. This data was then fitted to a normal distribution curve, from which the cumulative probabilities were calculated at various confidence levels.

8.3 GUIDELINES AND EARLY WARNING SYSTEM

8.3.1 Observed and projected rainfall onset

The cumulative probability of rainfall onset for the study site using daily SAWS rainfall district data from 1979 to 2014 and climate change projections is presented in Figure 8.4 for regions 62 and 86, as well as in tables 8.1 to 8.7. The graphs showing the probability of rainfall onset for all regions in the study site are presented in Appendix B.

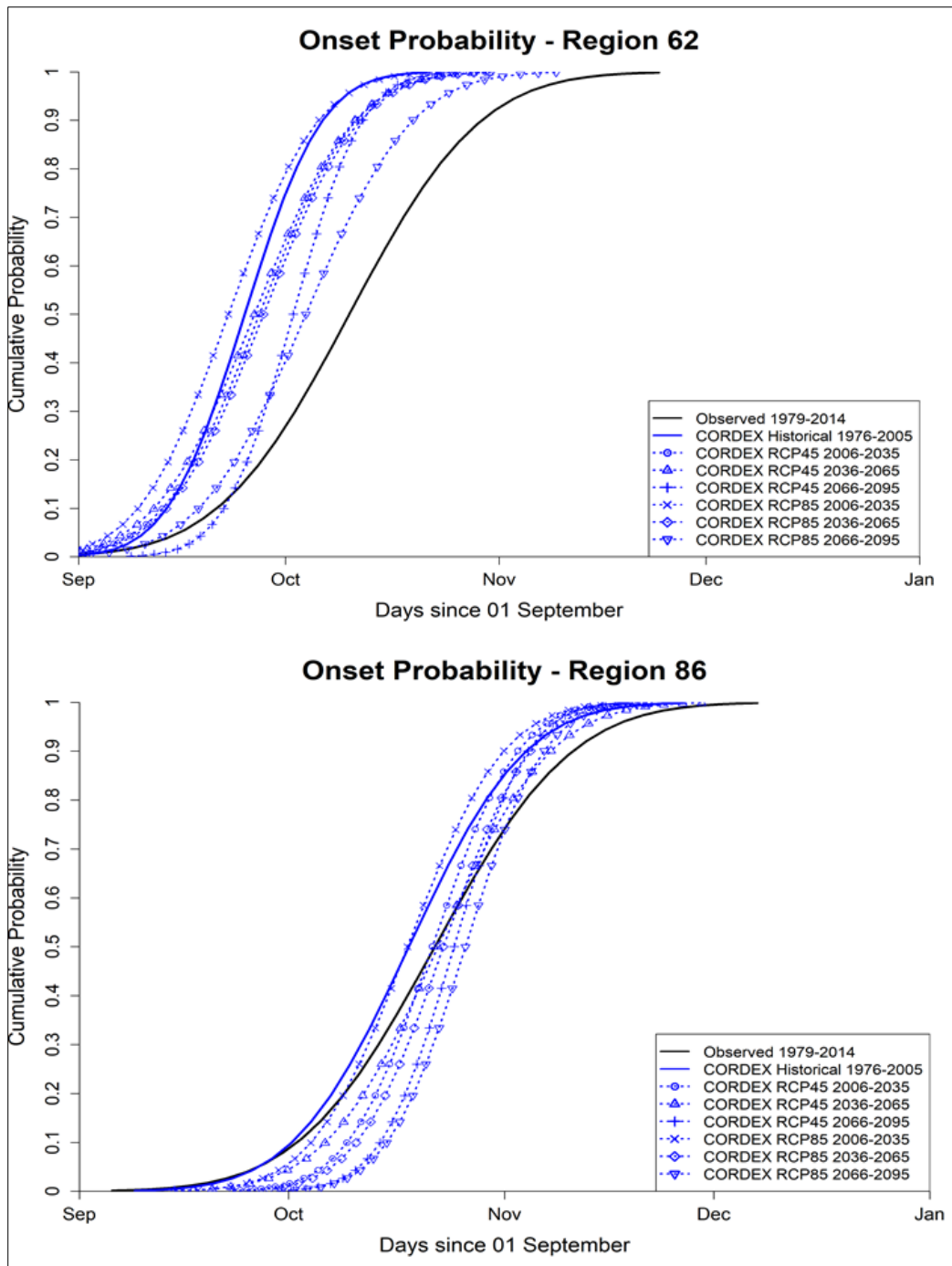


Figure 8.4: The cumulative probability of rainfall onset for regions 62 and 86 using the daily SAWS rainfall district data and climate change projections

Table 8.1: Probability of rainfall onset for the study site using daily SAWS rainfall district data from 1979 to 2014. Probability indicates onset to occur on or before the listed dates.

Region	Probability of onset of rainfall			
	95%	90%	85%	80%
60	27 November	19 November	13 November	8 November
61	14 November	8 November	3 November	30 October
62	4 November	29 October	26 October	23 October
63	11 November	5 November	2 November	30 October
72	25 November	16 November	11 November	7 November
73	3 December	25 November	19 November	14 November
74	13 November	06 November	2 November	30 October
75	5 November	31 October	28 October	26 October
83	13 December	3 December	27 November	21 November
84	9 December	29 November	23 November	18 November
85	29 November	22 November	16 November	12 November
86	16 November	11 November	7 November	4 November
87	15 December	6 December	30 November	26 November
91	10 December	1 December	25 November	20 November
92	23 December	14 December	7 December	2 December
93	28 December	16 December	9 December	3 December

Table 8.2: Probability of rainfall onset for the study site using daily CORDEX historical data from 1976 to 2005. Probability indicates onset to occur on or before the listed dates.

Region	Probability of onset of rainfall (historical 1976–2005)			
	95%	90%	85%	80%
60	21 October	18 October	16 October	14 October
61	7 October	4 October	2 October	30 September
62	10 October	6 October	4 October	2 October
63	26 October	23 October	21 October	19 October
72	24 November	18 November	14 November	11 November
73	31 October	27 October	24 October	22 October
74	14 October	10 October	8 October	6 October
75	22 October	19 October	16 October	14 October
83	7 November	3 November	30 October	28 October
84	3 November	31 October	28 October	26 October
85	13 November	8 November	5 November	2 November
86	9 November	4 November	1 November	29 October
87	3 December	28 November	25 November	22 November
91	4 November	31 October	29 October	27 October
92	8 November	5 November	2 November	31 October
93	3 December	28 November	24 November	22 November

Table 8.3: Probability of rainfall onset for the study site using daily CORDEX data for RCP4.5 from 2006 to 2035. Probability indicates onset to occur on or before the listed dates.

Region	Probability of onset of rainfall (RCP4.5 2006–2035)			
	95%	90%	85%	80%
60	22 October	18 October	15 October	13 October
61	8 October	5 October	2 October	30 September
62	15 October	11 October	9 October	6 October
63	24 October	21 October	19 October	17 October
72	15 November	10 November	7 November	4 November
73	5 November	1 November	29 October	27 October
74	16 October	12 October	9 October	7 October
75	20 October	16 October	13 October	11 October
83	4 November	31 October	28 October	26 October
84	7 November	3 November	1 November	30 October
85	14 November	10 November	7 November	4 November
86	6 November	3 November	1 November	30 October
87	29 November	25 November	22 November	20 November
91	4 November	1 November	30 October	28 October
92	9 November	6 November	4 November	2 November
93	22 November	19 November	16 November	14 November

Table 8.4: Probability of rainfall onset for the study site using daily CORDEX data for RCP4.5 from 2036 to 2065. Probability indicates onset to occur on or before the listed dates.

Region	Probability of onset of rainfall (RCP4.5 2036–2065)			
	95%	90%	85%	80%
60	27 October	22 October	19 October	17 October
61	11 October	7 October	4 October	2 October
62	15 October	11 October	8 October	6 October
63	3 November	30 October	27 October	24 October
72	15 November	10 November	6 November	4 November
73	2 November	30 October	27 October	25 October
74	17 October	13 October	10 October	7 October
75	26 October	21 October	18 October	16 October
83	31 October	28 October	25 October	23 October
84	2 November	31 October	29 October	28 October
85	12 November	8 November	5 November	3 November
86	12 November	8 November	4 November	2 November
87	30 November	26 November	23 November	21 November
91	5 November	2 November	30 October	28 October
92	8 November	5 November	3 November	1 November
93	6 December	1 December	27 November	24 November

Table 8.5: Probability of rainfall onset for the study site using daily CORDEX data for RCP4.5 from 2066 to 2095. Probability indicates onset to occur on or before the listed dates.

Region	Probability of onset of rainfall (RCP4.5 2066–2095)			
	95%	90%	85%	80%
60	27 October	23 October	20 October	18 October
61	11 October	8 October	6 October	4 October
62	15 October	12 October	10 October	9 October
63	3 November	30 October	28 October	26 October
72	20 November	14 November	11 November	8 November
73	9 November	5 November	2 November	31 October
74	20 October	16 October	14 October	12 October
75	25 October	21 October	19 October	17 October
83	12 November	7 November	3 November	31 October
84	8 November	5 November	2 November	31 October
85	12 November	9 November	6 November	4 November
86	7 November	4 November	2 November	1 November
87	27 November	24 November	21 November	19 November
91	10 November	6 November	3 November	1 November
92	13 November	8 November	6 November	3 November
93	2 December	27 November	24 November	22 November

Table 8.6: Probability of rainfall onset for the study site using daily CORDEX data for RCP8.5 from 2006 to 2035. Probability indicates onset to occur on or before the listed dates.

Region	Probability of onset of rainfall (RCP8.5 2006–2035)			
	95%	90%	85%	80%
60	27 October	22 October	18 October	16 October
61	7 October	4 October	1 October	29 September
62	9 October	6 October	3 October	1 October
63	31 October	26 October	23 October	21 October
72	12 November	8 November	5 November	2 November
73	3 November	30 October	28 October	25 October
74	15 October	11 October	8 October	5 October
75	24 October	19 October	16 October	14 October
83	2 November	28 October	26 October	23 October
84	5 November	1 November	30 October	28 October
85	13 November	8 November	4 November	1 November
86	5 November	1 November	29 October	27 October
87	30 November	26 November	23 November	20 November
91	6 November	2 November	31 October	29 October
92	9 November	5 November	3 November	31 October
93	28 November	24 November	21 November	18 November

Table 8.7: Probability of rainfall onset for the study site using daily CORDEX data for RCP8.5 from 2036 to 2065. Probability indicates onset to occur on or before the listed dates.

Region	Probability of onset of rainfall (RCP8.5 2036–2065)			
	95%	90%	85%	80%
60	24 October	20 November	17 October	15 October
61	11 October	07 November	5 October	3 October
62	16 October	12 November	9 October	7 October
63	3 November	30 November	28 October	26 October
72	20 November	15 November	11 November	8 November
73	4 November	1 November	29 October	28 October
74	14 October	11 October	9 October	7 October
75	25 October	21 October	18 October	16 October
83	4 November	30 October	27 October	24 October
84	5 November	2 November	31 October	30 October
85	12 November	9 November	6 November	4 November
86	8 November	5 November	2 November	31 October
87	28 November	24 November	21 November	19 November
91	5 November	2 November	31 October	30 October
92	14 November	10 November	7 November	5 November
93	29 November	24 November	21 November	19 November

Table 8.8: Probability of rainfall onset for the study site using daily CORDEX data for RCP8.5 from 2066 to 2095. Probability indicates onset to occur on or before the listed dates.

Region	Probability of onset of rainfall (RCP8.5 2066–2095)			
	95%	90%	85%	80%
60	29 October	25 October	22 October	20 October
61	15 October	12 October	9 October	7 October
62	24 October	19 October	16 October	14 October
63	13 November	8 November	5 November	2 November
72	26 November	20 November	16 November	13 November
73	6 November	3 November	1 November	30 October
74	21 October	17 October	15 October	13 October
75	31 October	27 October	24 October	22 October
83	1 November	30 October	28 October	26 October
84	8 November	5 November	2 November	1 November
85	12 November	9 November	7 November	5 November
86	10 November	7 November	4 November	3 November
87	01 December	27 November	24 November	22 November
91	10 November	6 November	3 November	1 November
92	13 November	9 November	7 November	5 November
93	1 December	26 November	23 November	21 November

8.3.2 Observed and projected rainfall cessation

The cumulative probability of rainfall cessation for the study site using the daily SAWS rainfall district data from 1979 to 2014 and climate change projections is presented in Figure 8.5 (regions 62 and 86), as well as in tables 8.9 to 8.16 and

to

. The graphs showing the probability of rainfall cessation for all regions in the study site are presented in Appendix C.

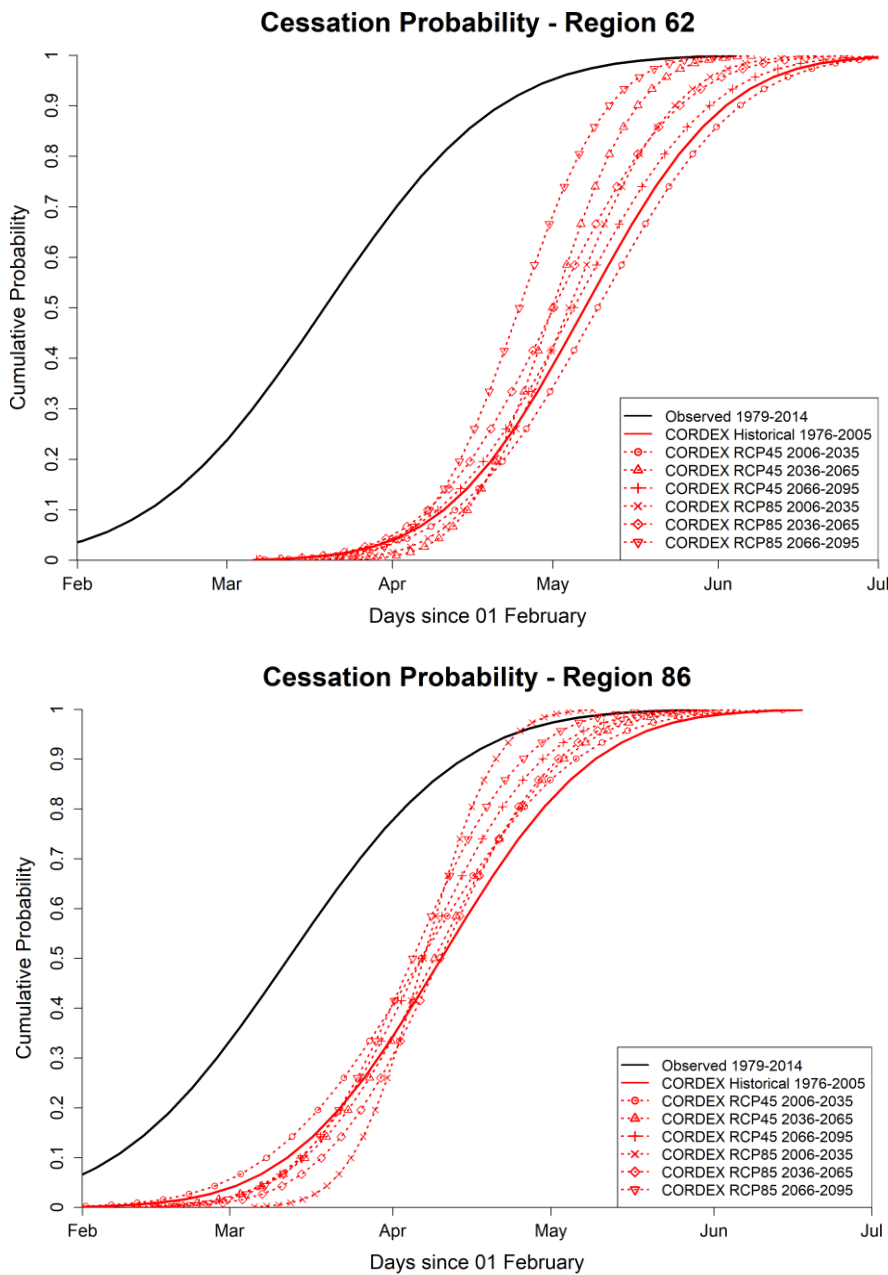


Figure 8.5: The cumulative probability of rainfall cessation for regions 62 and 86 using the daily SAWS rainfall district data and climate change projections

Table 8.9: Probability of rainfall cessation for the study site using daily SAWS rainfall district data from 1979 to 2014. Probability indicates cessation to occur on or before (after February) the listed dates.

Region	Probability of cessation of rainfall			
	95%	90%	85%	80%
60	9 May	28 April	21 April	15 April
61	5 May	25 April	19 April	14 April
62	5 May	25 April	18 April	13 April
63	8 May	28 April	22 April	17 April
72	23 May	11 May	3 May	27 April
73	12 May	1 May	24 April	19 April
74	7 May	28 April	22 April	17 April
75	6 May	25 April	18 April	13 April
83	7 May	26 April	18 April	12 April
84	15 May	5 May	28 April	22 April
85	7 May	27 April	20 April	14 April
86	24 April	14 April	8 April	3 April
87	21 April	11 April	4 April	29 March
91	12 May	1 May	23 April	17 April
92	12 May	30 April	22 April	16 April
93	26 April	15 April	8 April	3 April

Table 8.10: Probability of rainfall cessation for the study site using daily historical CORDEX data from 1976 to 2005. Probability indicates cessation to occur on or before (after February) the listed dates.

Region	Probability of cessation of rainfall (historical 1976–2005)			
	95%	90%	85%	80%
60	14 June	5 June	30 May	26 May
61	19 June	12 June	7 June	3 June
62	10 June	2 June	28 May	24 May
63	2 June	25 May	19 May	15 May
72	22 May	12 May	5 May	29 April
73	23 May	17 May	12 May	9 May
74	5 July	26 June	20 June	16 June
75	13 June	4 June	29 May	24 May
83	19 June	10 June	4 June	30 May
84	19 May	13 May	8 May	5 May
85	2 May	25 April	21 April	17 April
86	18 May	9 May	4 May	29 April
87	27 March	22 March	18 March	15 March
91	27 May	20 May	16 May	12 May
92	12 May	5 May	1 May	27 April
93	31 March	24 March	19 March	15 March

Table 8.11: Probability of rainfall cessation for the study site using daily CORDEX data from 2006 to 2035 for RCP4.5. Probability indicates cessation to occur on or before (after February) the listed dates.

Region	Probability of cessation of rainfall (RCP4.5 2006–2035)			
	95%	90%	85%	80%
60	19 June	11 June	6 June	2 June
61	30 June	22 June	16 June	12 June
62	13 June	5 June	31 May	27 May
63	20 May	14 May	9 May	6 May
72	5 June	24 May	17 May	11 May
73	20 May	13 May	9 May	5 May
74	26 June	17 June	12 June	7 June
75	8 June	31 May	26 May	22 May
83	14 June	5 June	30 May	26 May
84	20 May	14 May	10 May	6 May
85	26 April	20 April	17 April	14 April
86	14 May	6 May	30 April	26 April
87	27 March	22 March	18 March	15 March
91	22 May	16 May	12 May	9 May
92	6 May	1 May	27 April	23 April
93	30 March	24 March	19 March	16 March

Table 8.12: Probability of rainfall cessation for the study site using daily CORDEX data from 2036 to 2065 for RCP4.5. Probability indicates cessation to occur on or before (after February) the listed dates.

Region	Probability of cessation of rainfall (RCP4.5 2036–2065)			
	95%	90%	85%	80%
60	2 June	27 May	23 May	20 May
61	13 June	6 June	1 June	29 May
62	21 May	17 May	14 May	11 May
63	26 May	19 May	14 May	10 May
72	3 June	24 May	17 May	11 May
73	23 May	15 May	10 May	5 May
74	20 June	13 June	8 June	4 June
75	29 May	22 May	18 May	15 May
83	6 June	29 May	24 May	19 May
84	12 May	6 May	2 May	29 April
85	1 May	26 April	22 April	19 April
86	10 May	3 May	29 April	25 April
87	3 April	28 March	24 March	21 March
91	30 May	23 May	18 May	15 May
92	9 May	3 May	29 April	26 April
93	5 April	29 March	25 March	21 March

Table 8.13: Probability of rainfall cessation for the study site using daily CORDEX data from 2066 to 2095 for RCP4.5. Probability indicates cessation to occur on or before (after February) the listed dates.

Region	Probability of cessation of rainfall (RCP4.5 2066–2095)			
	95%	90%	85%	80%
60	30 May	24 May	19 May	16 May
61	20 Jun	11 Jun	6 June	1 June
62	7 June	30 May	25 May	22 May
63	24 May	17 May	12 May	8 May
72	29 May	18 May	11 May	5 May
73	14 May	8 May	4 May	1 May
74	1 July	22 June	16 June	11 June
75	18 June	9 June	2 June	28 May
83	24 May	18 May	14 May	11 May
84	10 May	4 May	1 May	28 April
85	1 May	24 April	20 April	16 April
86	6 May	29 April	25 April	22 April
87	24 March	19 Mar	16 March	14 March
91	13 May	8 May	5 May	2 May
92	29 April	25 April	21 April	19 April
93	27 March	21 March	17 March	13 March

Table 8.4: Probability of rainfall cessation for the study site using daily CORDEX data from 2006 to 2035 for RCP8.5. Probability indicates cessation to occur on or before (after February) the listed dates.

Region	Probability of cessation of rainfall (RCP8.5 2006–2035)			
	95%	90%	85%	80%
60	19 June	10 June	4 June	31 May
61	10 June	4 June	31 May	27 May
62	29 May	24 May	20 May	17 May
63	11 May	6 May	3 May	30 April
72	13 June	1 June	24 May	17 Maye
73	24 May	16 May	12 May	8 May
74	30 June	22 June	17 June	13 June
75	30 May	23 May	19 May	15 May
83	14 June	6 June	31 May	26 May
84	15 May	9 May	5 May	2 May
85	10 May	3 May	28 April	24 April
86	24 April	21 April	18 April	16 April
87	29 March	24 March	20 March	17 March
91	20 May	14 May	10 May	7 May
92	9 May	3 May	29 April	25 April
93	24 March	19 March	15 March	12 March

Table 8.15: Probability of rainfall cessation for the study site using daily CORDEX data from 2036 to 2065 for RCP8.5. Probability indicates cessation to occur on or before (after February) the listed dates.

Region	Probability of cessation of rainfall (RCP8.5 2036–2065)			
	95%	90%	85%	80%
60	8 June	31 May	26 May	21 May
61	11 June	4 June	30 May	26 May
62	31 May	25 May	20 May	17 May
63	11 May	5 May	1 May	28 April
72	12 June	31 May	23 May	16 May
73	25 May	17 May	12 May	7 May
74	17 June	10 June	5 June	1 June
75	20 May	14 May	10 May	7 May
83	12 June	03 Jun	28 May	24 May
84	26 May	18 May	13 May	9 May
85	27 April	21 April	17 April	13 April
86	9 May	2 May	28 April	25 April
87	5 April	29 March	25 March	21 March
91	21 May	15 May	11 May	8 May
92	23 May	14 May	8 May	3 May
93	23 March	17 March	14 March	11 March

Table 8.16: Probability of rainfall cessation for the study site using daily CORDEX data from 2066 to 2095 for RCP8.5. Probability indicates cessation to occur on or before (after February) the listed dates.

Region	Probability of cessation of rainfall (RCP8.5 2066–2095)			
	95%	90%	85%	80%
60	26 May	20 May	15 May	12 May
61	4 June	29 May	25 May	21 May
62	16 May	12 May	8 May	6 May
63	7 May	2 May	28 April	25 April
72	19 May	8 May	1 May	26 April
73	18 May	11 May	6 May	2 May
74	30 May	25 May	21 May	18 May
75	22 May	16 May	12 May	9 May
83	29 May	22 May	18 May	14 May
84	30 April	26 April	23 April	21 April
85	22 April	17 April	13 April	10 April
86	2 May	26 April	22 April	19 April
87	29 March	23 March	20 March	17 March
91	18 May	13 May	9 May	6 May
92	28 April	23 April	20 April	17 April
93	25 March	19 March	16 March	13 March

8.3.3 Optimum planting dates and occurrence of mid-summer dry spells

Planting during the recommended optimum period for an area will assist farmers to gain higher yields using favourable climatic conditions. Dry spells during the flowering stage of maize can cause yield losses. The flowering stage may vary between different cultivars of maize and the growing environment. For example, the flowering stage occurs about 65 days after emergence in medium-growing maize hybrids. Different varieties of maize are planted in the study area. The flowering stage varies from region to region depending on the maize cultivar used.

The optimum planting dates based on the rainfall onset, duration and occurrence of mid-summer dry spells are presented in Table 8.17. The information presented in Table 8.17 can be used as a general guideline and early warning system for optimum maize planting dates for the major maize-growing regions. The occurrence and duration of mid-summer dry spells will also assist in identifying high-risk dates and avoiding water stress during the maize-flowering period for the different maize-growing regions and locations.

Table 8.17: Optimum planting dates based on the cumulative probability (> 80%) of onset and high-risk dates with consecutive dry pentads during mid-summer. High-risk mid-summer dates are based on the Markov chain dry-spell probability analysis

Region	Optimum planting dates	High-risk mid-summer period	Duration of high-risk period (days)
60	8 November to 27 November	27 December to 15 January	20
61	30 October to 14 November	27 December to 15 January	20
62	23 October to 4 November	27 December to 5 January	10
63	30 October to 11 November	27 December to 15 January	20
72	7 November to 25 November	12 December to 5 January	25
73	14 November to 3 December	27 December to 15 January	20
74	30 November to 13 November	1 January to 15 January	15
75	26 October to 5 November	1 January to 10 January	10
83	21 November to 13 December	27 December to 20 January	25
84	18 November to 9 December	27 December to 15 January	20
85	12 November to 29 November	27 December to 5 January	10
86	4 November to 16 November	1 January to 15 January	15
87	26 November to 15 December	22 December to 5 January	15
91	20 November to 10 December	22 December to 15 January	25
92	2 December to 23 December	22 December to 5 January	15
93	3 December to 28 December	22 December to 5 January	15

CHAPTER 9: CONCLUSIONS AND RECOMMENDATIONS

9.1 CONCLUSIONS

Rainfall is one of the most important factors limiting dryland crop production in South Africa. It is often not only the occurrence of a dry spell, but also its intensity and when this dry period occurs that is of vital significance. Various crops, such as maize, are vulnerable to dry spells during specific phenological stages. The flowering stage has been found to be the stage in which maize is most sensitive to water stress, leading to reductions in crop growth, biomass production and crop yield. The mid-summer period is of particular significance, since a lack of rain for a few days during this period may affect crop yields considerably. It has been observed that, in the summer rainfall region of South Africa, there is a hiatus in rainfall during mid-summer and dry spells occur with different intensities and frequencies across the major maize-growing areas. The factors that control this switch in rainfall regimes need to be understood so that timely predictions can be made for the occurrence of short-term mid-summer dry spells. The aim of this project was to conduct an in-depth study of the mid-summer dry spells in the major maize-growing areas of South Africa.

The research required high-quality rainfall data, which was obtained from the South African Weather Service's data network. This facilitated the investigation of the frequency, intensity and duration of mid-summer dry spells in the summer rainfall areas of South Africa. The study included an investigation into the ability of climate models to capture these mid-summer dry spells, as well as a synoptic weather system analysis to identify the atmospheric forcing that drives such dry spells. The AquaCrop water productivity model was used to simulate the impact of mid-summer dry spells on maize yields. Lastly, guidelines and an early warning system were developed, which can be used to select optimum maize-planting dates for the major maize-growing regions in South Africa.

The results show that, climatologically, the mid-summer months do not necessarily experience lower rainfall than the early and late summer months. However, during mid-summer, dry pentads occur with different intensities, duration and frequencies across the maize-growing areas of the summer rainfall region of South Africa. The analysis of the duration and intensity of dry spells also showed a decrease from west to east in the study area. Two main weather patterns dominate the mid-summer season: the strong subtropical ridge influence, and the troughs and easterly weather. The results also show that ENSO has a strong influence on the mid-summer weather patterns. However, other climate drivers, such as SAM and SWIO, show no significant influences. Notably, even though ENSO has an impact on the weather patterns, it does not seem to be a driver of dry spells specifically.

Generally, comparison of the CORDEX RCA4 simulations with the historical observations for the mid-summer period show that RCA4 simulations underestimate dry spells compared to the climatologically observed values. Investigations of the upper-air tropical circulation diagnostics and position of the ITCZ also show that the RCA4 simulations differ from the observed scenarios, indicating that large-scale upper-air circulations are not well captured in the model simulations. Climate change predictions indicate that dry spells are projected to increase across the study area under both the RCP4.5 and RCP8.5 scenarios, with more pronounced increases under RCP8.5 than under RCP4.5.

The climatic water budget analysis showed moisture deficits for all pentads during mid-summer, with the highest deficit experienced in Pentad 73 (27–31 December) and Pentad 1 (1–5 January). The warm, dry western maize-growing region has the highest total deficits during mid-summer, compared to the cool, temperate eastern maize-growing regions.

The AquaCrop model simulations indicate that the impact of mid-summer dry spells on maize yield is evident, showing higher yields for the growing season with a low frequency of dry spells. The impact of mid-summer dry spells on maize yield is more pronounced in the dry, warm western maize-growing region of South Africa, showing the lowest yield compared to the cool, temperate eastern maize-growing regions.

The major maize-growing areas of South Africa experience water deficits and high evaporative demand during mid-summer. The results indicate that dry spells have a negative impact on maize yield. Planting dates should be adjusted to ensure that the water-sensitive growth stages do not coincide with the mid-summer dry spells. In addition, soil and water conservation techniques, such as in-field rainwater harvesting, are a viable option to alleviate water stress in rainfed maize production.

9.2 RECOMMENDATIONS

The results of the dry-spell analyses indicate that mid-summer dry spells occur at different intensities, duration and frequency across the maize-growing areas of the summer rainfall region of South Africa. The maize-growing season experiences different rainfall characteristics, such as dry spells, which affect phenology and crop yield. The research presented in this study will contribute significantly to research on short-term drought (dry spells) in South Africa and addresses some of the research gaps in dry-spell analysis studies, which are of utmost importance for rainfed crop production. The findings from this study will assist farmers and decision makers to strategically adjust the planting dates of their summer crops to ensure favourable growing conditions during the water stress-sensitive growth stages. Information about dry spells could also be used to select a crop variety for a given location and to plan supplementary irrigation practices.

Planting during the recommended optimum period for an area will assist farmers to gain higher yields using favourable climatic conditions. The optimum planting dates based on the information of rainfall onset, duration and occurrence of mid-summer dry spells presented in Table 8.17, coupled with seasonal rainfall forecasts, can be used as a general guideline and early warning system for optimum maize-planting dates for the major maize-growing regions. Information on the occurrence and duration of mid-summer dry spells will also assist farmers and decision makers to identify high-risk dates and avoid water stress during the maize-flowering period for the different maize-growing regions and locations.

The pattern of onset and cessation of rainfall is changing in the study area, specifically for the warm western maize-growing regions. The optimum planting dates for some areas in the warm western maize-growing region are already shifting towards late December and January. Future research should focus on the analysis and characteristics of dry spells in the warm western maize-growing region and their impacts on crop yield.

Climate change predictions using CORDEX RCA4 simulations indicate that dry spells are projected to increase across the study area. In general, an underestimation of dry spells is detected between the model simulated and observed climatological dry spell occurrences for the mid-summer season. However, some regions within the study area seem to capture the climatological occurrence of dry spells well, which suggests possible small-scale inadequacies in the models – an avenue for further investigation. Therefore, it is recommended that mid-summer dry-spell analysis should also be assessed using other CORDEX regional climate models, as well as comparing them to statistical downscaling methods.

CHAPTER 10: REFERENCES

- AGWEB (2015). South Africa major and minor corn growing areas. AgWeb/NOAA/USDA. <https://www.agweb.com/article/south-africa-corn-crop-seen-shrinking-further-as-drought-spreads-blmg>
- ALEXANDER LV and ARBLASTER JM (2009). Assessing trends in observed and modelled climate extremes over Australia in relation to future projections. *International Journal of Climatology: A Journal of the Royal Meteorological Society* **29** (3) 417–435.
- ARORA VK, SCINOCCHA JF, BOER GJ, CHRISTIAN JR, DENMAN KL, FLATO GM, KHARIN VV, LEE WG and MERRYFIELD WJ (2011). Carbon emission limits required to satisfy future representative concentration pathways of greenhouse gases. *Geophysical Research Letters* **38** (5) L05805. DOI: 10.1029/2010GL046270.
- BÄRRING L, HOLT T, LINDERSON ML, RADZIEJEWSKI M, MORIONDO M and PALUTIKOF JP (2006). Defining dry/wet spells for point observations, observed area averages, and regional climate model gridboxes in Europe. *Climate Research* **31** (1) 35–49.
- BECKER A, FINGER P, MEYER-CHRISTOFFER A, RUDOLF B, SCHAMM K, SCHNEIDER U and ZIESE M (2013). A description of the global land-surface precipitation data products of the Global Precipitation Climatology Centre with sample applications including centennial (trend) analysis from 1901–present. *Earth System Science Data* **5** (1) 71–99.
- BENHIL J (2002). *Climate, water and agriculture: Impacts on and adaptation of agroecological systems in South Africa. A case study of the Republic of South Africa.* University of Pretoria, South Africa.
- BHALOTRA YPR, DEPARTMENT OF METEOROLOGICAL SERVICES AND TRANSPORT and COMMUNICATIONS MINISTRY OF WORKS (1984). *Climate of Botswana, Part I: Climatic controls.* Ministry of Works and Communications, Botswana.
- CEBALLOS A, MARTÍNEZ-FERNÁNDEZ J and LUENGO-UGIDOS MÁ (2004). Analysis of rainfall trends and dry periods on a pluviometric gradient representative of Mediterranean climate in the Duero Basin, Spain. *Journal of Arid Environments* **58** (2) 215–233.
- CHUNG JX, JUNENG L, TANGANG F and JAMALUDDIN AF (2018). Performances of BATS and CLM land-surface schemes in RegCM4 in simulating precipitation over CORDEX Southeast Asia domain. *International Journal of Climatology* **38** (2) 794–810.
- COLLINS WJ, BELLOUIN N, DOUTRIAUX-BOUCHER M, GEDNEY N, HALLORAN P, HINTON T, HUGHES J, JONES CD, JOSHI M, LIDDICOAT S, MARTIN G, O'CONNOR F, RAE J, SENIOR C, SITCH S, TOTTERDELL I, WILTSHIRE A and WOODWARD S (2011). Development and evaluation of an Earth-system model – HadGEM2. *Geoscientific Model Development Discussions* **4** 997–1062. DOI: 10.5194/gmd-4-1051-2011.
- CRÉTAT J, MACRON C, POHL B and RICHARD Y (2011). Quantifying internal variability in a regional climate model: A case study for Southern Africa. *Climate Dynamics* **37** (7) 1335–1356.
- CRÉTAT J, RICHARD Y, POHL B, ROUAULT M, REASON C and FAUCHEREAU N (2012). Recurrent daily rainfall patterns over South Africa and associated dynamics during the core of the austral summer. *International Journal of Climatology* **32** 261–273.

- DOUGUEDROIT A (1987). The variations of dry spells in Marseilles from 1865 to 1984. *Journal of Climatology* **7 (6)** 541–551.
- DUFFY KJ and MASERE TP (2015). Effect of within-season daily rainfall distribution on maize crop yields. *Outlook on Agriculture* **44 (4)** 267–271.
- DU PLESSIS J (2003). Maize production, Directorate Agricultural Information Services, Department of Agriculture, in cooperation with ARC-Grain Crops Institute Publication.
- DU TOIT AS, PRINSLOO MA, WAFULA BM and THORNTON PK (2002). Incorporating a water-logging routine into CERES-Maize, and some preliminary evaluations. *Water SA* **28 (3)** 323–328.
- DUNNE JP, JOHN JG, ADCROFT AJ, GRIFFIES SM, HALLBERG RW, SHEVLIAKOVA E, STOUFFER RJ, COOKE W, DUNNE KA, HARRISON MJ, KRASTING JP, MALYSHEV SL, MILLY PCD, PHILLIPPS PJ, SENTMAN LT, SAMUELS BL, SPELMAN MJ, WINTON M, WITTENBARG AT and ZADEH N (2012). GFDL's ESM2 Global Coupled Climate-Carbon Earth System Models. Part I: Physical formulation and baseline simulation characteristics. *Journal of Climate* **25 (19)** 6646–6665.
- ECMWF (2019). Copernicus Climate Data Store. <https://cds.climate.copernicus.eu/>.
- ENGELBRECHT CJ, LANDMAN WA, ENGELBRECHT FA and MALHERBE J (2015). A synoptic decomposition of rainfall over the Cape south coast of South Africa. *Climate Dynamics* **44** 2589–2607.
- FARAHANI HJ, IZZI G and OWEIS TY (2009). Parameterization and evaluation of the AquaCrop model for full and deficit irrigated cotton. *Agronomy Journal* **101 (3)** 469–476.
- FREI C, CHRISTENSEN JH, DÉQUÉ M, JACOB D, JONES RG and VIDALE PL (2003). Daily precipitation statistics in regional climate models: Evaluation and intercomparison for the European Alps. *Journal of Geophysical Research: Atmospheres* **108 (D3)**.
- FREI P, KOTLARSKI S, LINIGER MA, SCHÄR C (2017). Snowfall in the Alps: Evaluation and projections based on the EURO-CORDEX regional climate models. *The Cryosphere Discussion*. <https://doi.org/10.5194/tc-2017-7>. [Article in review].
- GEORGAKAKOS KP, SEO DJ, GUPTA H, SCHAAKE J and BUTTS MB (2004). Towards the characterization of streamflow simulation uncertainty through multimodel ensembles. *Journal of Hydrology* **298 (1-4)** 222–241.
- GIORGI F and MEARNS LO (2002). Calculation of average, uncertainty range, and reliability of regional climate changes from AOGCM simulations via the “reliability ensemble averaging” (REA) method. *Journal of Climate* **15 (10)** 1141–1158.
- GIORGI F and BI X (2005). Regional changes in surface climate interannual variability for the 21st century from ensembles of global model simulations. *Geophysical Research Letters* **32** L13701. DOI: 10.1029/2005GL023002.
- GROBLER EJML (1993). *Die midsomerdroogte in die sentrale dele van die somerreenvaalse streke van Suid-Afrika*. Doctoral thesis, Stellenbosch University, Stellenbosch, South Africa.
- GUPTA AS, JOURDAIN NC, BROWN JN and MONSELESAN D (2013). Climate drift in the CMIP5 models. *Journal of Climate* **26 (21)** 8597–8615.

HARGREAVES GH and SAMANI ZA (1982). Estimating potential evapotranspiration. *Journal of the Irrigation and Drainage Division* **108 (3)** 225–230.

HARRISON MSJ (1984). A generalized classification of South African summer rain-bearing synoptic systems. *Journal of Climatology* **4 (5)** 547–560.

HART NCG, REASON CJC and FAUCHEREAU N (2010). Tropical–extratropical interactions over southern Africa: Three cases of heavy summer season rainfall. *Monthly Weather Review* **138 (7)** 2608–2623.

HART NCG, REASON CJC and FAUCHEREAU N (2012). Cloud bands over southern Africa: seasonality, contribution to rainfall variability and modulation by the MJO. *Climate Dynamics* **41** 1199–1212.

HEGERL GC, ZWIERS FW, STOTT PA and KHARIN VV (2004). Detectability of anthropogenic changes in annual temperature and precipitation extremes. *Journal of Climate* **17 (19)** 3683–3700.

HENG LK, EVETT SR, HOWELL TA and HSIAO TC (2009). Calibration and testing of FAO aquacrop model for rainfed and irrigated maize. *Agronomy Journal* **101** 488–498.

HEWITSON B and CRANE R (2002). Self-organizing maps: Applications to synoptic climatology. *Climate Research* **22** 13–26.

HIPEL KW and MCLEOD AI (1994). *Time series modelling of water resources and environmental systems*, Elsevier Academic Press, Burlington, MA.

HOLTON JR (2004). *An introduction to dynamic meteorology*, Elsevier Academic Press, Burlington, MA.

HOOGENBOOM G, JONES JW, WILKENS PW, PORTER CH, BOOTE KJ, HUNT LA, ... and KOO J (2010). Decision support system for agrotechnology transfer (DSSAT) Version 4.5. University of Hawaii, Honolulu, HI.

HOUDIN F, FOUJOLS MA, CODRON F, GUEMAS V, DUFRESNE JL, BONY S, DENVIL S, GUEZ L, LOTT F, GHATTAS J and BRACONNOT P (2013). Impact of the LMDZ atmospheric grid configuration on the climate and sensitivity of the IPSL-CM5A coupled model. *Climate Dynamics* **40 (9–10)** 2167–2192.

HSIAO TC, HENG L, STEDUTO P, ROJAS-LARA B, RAES D and FERERES E (2009). AquaCrop – the FAO crop model to simulate yield response to water: III. Parameterization and testing for maize. *Agronomy Journal* **101 (3)** 448–459.

ILYINA T, SIX KD, SEGSCHNEIDER J, MAIER-REIMER E, LI H and NÚÑEZ-RIBONI I (2013). Global ocean biogeochemistry model HAMOCC: Model architecture and performance as component of the MPI-Earth system model in different CMIP5 experimental realizations. *Journal of Advances in Modeling Earth Systems* **5 (2)** 287–315.

INTERGOVERNMENTAL PANEL ON CLIMATE CHANGE (IPCC) (2018). *Global warming of 1.5 °C: An IPCC special report on the impacts of global warming of 1.5 °C above pre-industrial levels and related global greenhouse gas emission pathways, in the context of strengthening the global response to the threat of climate change, sustainable development, and efforts to eradicate poverty*. Intergovernmental Panel on Climate Change.

- JAME YW and CUTFORTH HW (1996). Crop growth models for decision support systems. *Canadian Journal of Plant Science* **76 (1)** 9–19.
- JONES CA, KINIRY JR and DYKE PT (1986). *CERES-Maize: A simulation model of maize growth and development*, Texas A&M University Press, College Station.
- JONES C, GIORGI F and ASRAR G (2011). The coordinated regional downscaling experiment: CORDEX – an international downscaling link to CMIP5. *CLIVAR Exchanges* **16 (2)** 34–40.
- JURY MR and LEVEY K (1993). The climatology and characteristics of drought in the eastern Cape of South Africa. *International Journal of Climatology* **13** 629–641.
- JURY MR, PATHACK B, RAUTENBACH CJDW and VAN HEERDEN J (1996). Drought over South Africa and Indian Ocean SST: Statistical and GCM results. *The Global Atmosphere and Ocean System* **4** 47–63.
- KALOGNOMOU EA, LENNARD C, SHONGWE M, PINTO I, FAVRE A, KENT M, HEWITSON, B, DOSIO A, NIKULIN G, PANITZ H-J and BÜCHNER M (2013). A diagnostic evaluation of precipitation in CORDEX models over southern Africa. *Journal of Climate* **26 (23)** 9477–9506.
- KARNAUSKAS KB, SEAGER R, GIANNINI A and BUSALACCHI AJ (2013). A simple mechanism for the climatological midsummer drought along the Pacific coast of Central America. *Atmósfera* **26 (2)** 261–281.
- KARUNARATNE AS, AZAM-ALI SN, AL-SHAREEF I, SESAY A, JØRGENSEN ST and CROUT NMJ (2010). Modelling the canopy development of bambara groundnut. *Agricultural and Forest Meteorology* **150 (7–8)** 1007–1015.
- KHARIN VV, ZWIERS FW, ZHANG X and HEGERL GC (2007). Changes in precipitation and temperature extremes in the IPCC ensemble of global coupled model simulations. *Journal of Climate* **20 (8)** 1419–1444. DOI: 10.1175/JCLI4066.1.
- KIKTEV D, CAESAR J, ALEXANDER LV, SHIOGAMA H and COLLIER M (2007). Comparison of observed and multimodeled trends in annual extremes of temperature and precipitation. *Geophysical Research Letters* **34** L10702. DOI: 10.1029/2007GL029539.
- KOHONEN T (2001). *Self-organizing maps*, third edition, Springer, Berlin, Germany.
- KRUGER AC (2011). Identification and quality control procedures for rainfall stations: 1961–2010. South African Weather Service Report, CLS-RES-REP-2011-10.1.
- KRUGER AC and NXUMALO MP (2017). Historical rainfall trends in South Africa: 1921–2015. *Water SA* **43 (2)** 285–297.
- LANDMAN WA and MASON SJ (1999). Operational long-lead prediction of South African rainfall using canonical correlation analysis. *International Journal of Climatology* **19** 1073–1090.
- LANDMAN WA and TENNANT WJ (2000). Statistical downscaling of monthly forecasts. *International Journal of Climatology: A Journal of the Royal Meteorological Society* **20 (13)** 1521–1532.
- LANDMAN WA and BERAKI A (2010). Multi-model forecast skill for mid-summer rainfall over southern Africa. *International Journal of Climatology* **32** 303–314.

- LENNARD C and HEGERL G (2015). Relating changes in synoptic circulation to the surface rainfall response using self-organising maps. *Climate Dynamics* **44** 861–879.
- LIBISELLER C and GRIMVALL A (2002). Performance of partial Mann-Kendall tests for trend detection in the presence of covariates. *Environmetrics: The Official Journal of the International Environmetrics Society* **13** (1) 71–84.
- LINDESAY JA (1988). South African rainfall, the Southern Oscillation and a Southern Hemisphere semi-annual cycle. *Journal of Climatology* **8** (1) 17–30.
- LOUKAS A and VASILIADES L (2004). Probabilistic analysis of drought spatiotemporal characteristics in Thessaly region, Greece. *Natural Hazards and Earth System Sciences* **4** 719–731. DOI: 10.5194/nhess-4-719-2004.
- MALHERBE J, DIEPPOIS P, MALULEKE P, VAN STADEN M, PILLAY DL (2016). South African droughts and decadal variability. *Natural Hazards* **80** 657–681.
- MARTIN-VIDE J and GOMEZ L (1999). Regionalization of peninsular Spain based on the length of dry spells. *International Journal of Climatology: A Journal of the Royal Meteorological Society* **19** (5) 537–555.
- MASON SJ (1995). Sea-surface temperature – South African rainfall associations, 1910–1989. *International Journal of Climatology* **15** (2) 119–135.
- MASON SJ and JOUBERT AM (1997). Simulated changes in extremes rainfall over Southern Africa. *International Journal of Climatology* **17** 291–301.
- MASUPHA TE, MOELETSI ME and TSUBO M (2016). Dry spells assessment with reference to the maize crop in the Luvuvhu River catchment of South Africa. *Physics and Chemistry of the Earth, Parts A/B/C* **92** 99–111.
- MATHUGAMA SG and PEIRIS TSG (2011). Critical evaluation of dry spell research, *International Journal of Basic Applied Sciences* **11** (6) 1–8. <http://data.giss.nasa.gov/gistemp>.
- MEEHL GA and TEBALDI C (2004). More intense, more frequent and longer lasting heat waves in the 21st century. *Science* **305** 994–997.
- MEEHL GA, ARBLASTER JM and TEBALDI C (2005). Understanding future patterns of precipitation extremes in climate model simulations. *Geophysical Research Letters* **32** (18) L18719. DOI: 10.1029/2005GL023680.
- MEEHL GA, WASHINGTON WM, AMMAN C, ARBLASTER JM, WIGLEY TML and TEBALDI C (2004b). Combinations of natural and anthropogenic forcings and 20th century climate. *Journal of Climate* **17** 3721–3727.
- MEQUE A (2015). Investigating the link between southern African droughts and global atmospheric teleconnections using regional climate models. University of Cape Town, Cape Town, South Africa.
- MIRON O and TYSON PD (1984). Wet and dry conditions and pressure anomaly fields over South Africa and the adjacent oceans, 1963–79. *Monthly Weather Review* **112** 2127–2132.
- MOELETSI ME and WALKER S (2012). Rainy season characteristics of the Free State province of South Africa with reference to rain-fed maize production. *Water SA* **38** (5) 775–782.

MOON SE, RYOO SB and KWON JG (1994). A Markov chain model for daily precipitation occurrence in South Korea. *International Journal of Climatology* **14 (9)** 1009–1016.

MUPANGWA W, WALKER S and TWOMLOW S (2011). Start, end and dry spells of the growing season in semi-arid southern Zimbabwe. *Journal of Arid Environments* **75 (11)** 1097–1104.

MZEZEWA J, MISI T and VAN RENSBURG L (2010). Characterisation of rainfall at a semi-arid ecotope in the Limpopo Province (South Africa) and its implications for sustainable crop production. *Water SA* **36 (1)**.

NATIONAL CENTER FOR ATMOSPHERIC RESEARCH (NCAR) (2017). The climate data guide: CPC unified gauge-based analysis of global daily precipitation.

NESMITH DS and RITCHIE JT (1992). Short-and long-term responses of corn to a pre-anthesis soil water deficit. *Agronomy Journal* **84 (1)** 107–113.

NETICH KF, MUCHERU-MUNA M, MUGWE JN, SHISANYA CA, DIELS J and MUGENDI DN (2014). Length of growing season, rainfall temporal distribution, onset and cessation dates in the Kenyan highlands. *Agricultural and Forest Meteorology* **188** 24–32.

NATIONAL OCEANIC AND ATMOSPHERIC ADMINISTRATION (NOAA) (2019). OOPC: State of the ocean climate. <https://stateoftheocean.osmc.noaa.gov/>.

OLIVIER C (2015). The Intertropical Convergence Zone and its association with seasonal South African rainfall. SASAS conference poster.

OORT AH and YIENGER JJ (1996). Observed interannual variability in the Hadley circulation and its connection to ENSO. *Journal of Climate* 2751–2767.

PANNAR (2016). Manage the growth stages of the maize plant with PANNAR. https://www.pannar.com/blog/detail/manage_the_growth_stages_of_the_maize_plant.

PERDIGÓN-MORALES J, ROMERO-CENTENO R, PÉREZ PO and BARRETT BS (2018). The midsummer drought in Mexico: Perspectives on duration and intensity from the CHIRPS precipitation database. *International Journal of Climatology* **38 (5)** 2174–2186.

PEREIRA LS, CORDERY I and IACOVIDES I (2009). *Coping with water scarcity: Addressing the challenges*, Springer Science and Business Media.

PERZYNA G (1994). Spatial and temporal characteristics of maximum dry spells in southern Norway. *International Journal of Climatology* **14 (8)** 895–909.

POHL B, RICHARD Y and FAUCHEREAU N (2007). Influence of the Madden-Julian Oscillation on southern African summer rainfall. *Journal of Climate* **20** 4227–4242.

RAES D, STEDUTO P, HSIAO TC and FERERES E (2009). AquaCrop – the FAO crop model for predicting yield response to water: II. Main algorithms and software description. *Agriculture Journal*.

RAES D, STEDUTO P, HSIAO TC and FERERES E (2018). AquaCrop Reference Manual. <http://www.fao.org/3/a-br246e.pdf>.

RIAH K, RAO S, KREY V, CHO C, CHIRKOV V, FISCHER G and RAFAJ P (2011). RCP 8.5 – a scenario of comparatively high greenhouse gas emissions. *Climatic Change* **109 (1)** 33–57.

REASON CJC and MULENGA H (1999). Relationships between South African rainfall and SST anomalies in the south west Indian Ocean. *International Journal of Climatology* **19** 1651–1673.

REASON CJC, ALLAN RJ, LINDESAY JA and ANSELL TJ (2000). ENSO and climatic signals across the Indian Ocean Basin in the global context: Part I – interannual composite patterns. *International Journal of Climatology* **20** 1285–1327.

REASON CJC (2001). Subtropical Indian Ocean SST dipole events and southern African rainfall. *Geophysical Research Letters* **28 (11)** 2225–2227.

REASON CJC and ROUAULT M (2002). ENSO-like decadal variability and South African rainfall. *Geophysical Research Letters* **29 (13)**.

REASON CJC, ROUAULT M, MELICE JL and JAGADHEESHA D (2002). Interannual winter rainfall variability in SW South Africa and large-scale ocean – atmosphere interactions. *Meteorology and Atmospheric Physics* **80 (1)** 19–29.

REASON CJC, LANDMAN W and TENNANT W (2006). Seasonal to decadal prediction of southern African climate and its links with variability of the Atlantic Ocean. *Bulletin of the American Meteorological Society* **87 (7)** 941–955.

REDDY SJ (1990). *Methodology: Agro-climatic analogue technique and applications as relevant to dry land agriculture*. Agro Climatology Series Eth 86/21-WMO/UNDP, NMSA 60 pp.

REIFEN C and TOUMI R (2009). Climate projections: Past performance no guarantee of future skill? *Geophysical Research Letters* **36 (13)**.

RICHARD Y, TRZASKA S, ROUCOU P and ROUAULT M (2000). Modification of the southern African rainfall variability/ENSO relationship since the late 1960s. *Climate Dynamics* **16** 883–895.

RICHARD Y, FAUCHEREAU N, POCCARD I, ROUAULT M and TRZASKA S (2001). 20th century droughts in southern Africa: Spatial and temporal variability, teleconnections with oceanic and atmospheric conditions. *International Journal of Climatology: A Journal of the Royal Meteorological Society* **21 (7)** 873–885.

ROTSTAYN LD, COLLIER MA, JEFFREY SJ, KIDSTON J, SYKTUS JI and WONG KK (2013). Anthropogenic effects on the subtropical jet in the Southern Hemisphere: Aerosols versus long-lived greenhouse gases. *Environmental Research Letters* **8**. DOI: 10.1088/17489326/8/1/014030.

ROUAULT M and RICHARD Y (2003). Spatial extension and intensity of droughts since 1922 in South Africa. *Water SA* **29** 489–500.

SOUTH AFRICAN WEATHER BUREAU (SAWB) (1972). *WB35: Climate of South Africa. Part 10: District rainfall for South Africa and the annual March of rainfall over southern Africa*. South African Weather Bureau, Pretoria.

SCAIFE AA, FOLLAND CK, ALEXANDER LV, MOBERG A and KNIGHT JR (2008). European climate extremes and the North Atlantic Oscillation. *Journal of Climate* **21 (1)** 72–83.

SCHNEIDER U, ZIESE M, MEYER-CHRISTOFFER A, FINGER P, RUSTEMEIER E and BECKER A (2016). The new portfolio of global precipitation data products of the Global Precipitation Climatology Centre suitable to assess and quantify the global water cycle and resources. *Proceedings of the International Association of Hydrological Sciences* **374** 29–34.

- SILLMANN J and ROECKNER E (2008). Indices for extreme events in projections of anthropogenic climate change. *Climatic Change* **86 (1)** 83–104.
- STEDUTO P, HSIAO TC, RAES D and FERERES E (2009). AquaCrop – the FAO crop model to simulate yield response to water: I. Concepts and underlying principles. *Agronomy Journal* **101 (3)** 426–437.
- STERN R, RIJKS D, DALE I and KNOCK J (2006). *INSTAT climatic guide*, University of Reading, Reading, UK.
- STOCKER T (ed.) (2014). *Climate change 2013: The physical science basis: Working Group I contribution to the Fifth Assessment Report of the Intergovernmental Panel on Climate Change*. Cambridge University Press.
- SUN L, LI H, WARD MN and MONCUNILL DF (2007). Climate variability and corn yields in semiarid Ceará, Brazil. *Journal of Applied Meteorology and Climatology* **46 (2)** 226–240.
- TADROSS MA, HEWITSON BC and USMAN MT (2005). The interannual variability of the onset of the maize growing season over South Africa and Zimbabwe. *Journal of Climate* **18 (16)** 3356–3372.
- TADROSS M, SUAREZ P, LOTSCH A, HACHIGONTA S, MDOKA M, UNGANAI L, LUCIO F, KAMDONYO D and MUCHINDA M (2009). Growing-season rainfall and scenarios of future change in southeast Africa: Implications for cultivating maize. *Climate Research* **40 (2–3)** 147–161.
- TALJAARD JJ (1986). Change of rainfall distribution and circulation patterns over southern Africa in summer. *Journal of Climatology* **6 (6)** 579–592.
- TALJAARD JJ (1996). *Atmospheric circulation systems, synoptic climatology and weather phenomena of South Africa. Part 6: Rainfall in South Africa*. Department of Environmental Affairs and Tourism.
- TANAKA HL, ISHIZAKI N and KITO A (2004). Trend and interannual variability of Walker, monsoon and Hadley circulations defined by velocity potential in the upper troposphere. *Tellus A: Dynamic Meteorology and Oceanography* **56 (3)** 250–269.
- TAMBOURATZIS T and TAMBOURATZIS G (2008). Meteorological data analysis using self-organizing maps. *International Journal of Intelligent Systems* **23** 735–759.
- TAYLOR KE (2001). Summarizing multiple aspects of model performance in a single diagram. *Journal of Geophysical Research* **106** 7183–7192.
- TAYLOR KE, STOUFFER RJ and MEEHL GA (2012). An overview of CMIP5 and the experimental design. *Bulletin of the American Meteorological Society* **93** 485–498.
- TEBALDI C, HAYHOE K, ARBLASTER JM and MEEHL GA (2006). Going to the extremes. *Climatic Change* **79 (3)** 185–211.
- TENNANT WJ and HEWITSON BC (2002). Intra-seasonal rainfall characteristics and their importance to the seasonal prediction problem. *International Journal of Climatology* **22** 1033–1048.
- THOMAS DSG, TWYMAN C, OSBAHR H and HEWITSON B (2007). Adaptation to climate change and variability: Farmer responses to intra-seasonal precipitation trends in South Africa. *Climatic Change* **83** 301–322. <https://doi.org/10.1007/s10584-006-9205-4>.
- THORNTHWAITE CW (1948). An approach toward a rational classification of climate. *Geographical Review* **38 (1)** 55–94.

THORNTHWAITE CW and MATHER JR (1955). Publications in climatology. The Water Balance **8** 1–104.

TJIPUTRA JF, ROELANDT C, BENTSEN M, LAWRENCE DM, LORENTZEN T, SCHWINGER J, SELAND Ø and HEINZE C (2013). Evaluation of the carbon cycle components in the Norwegian Earth System Model (NorESM). Geoscientific Model Development **6** 301–325. DOI: 10.5194/gmd-6-301-2013.

TODD MC and WASHINGTON R (1999). Circulation anomalies with tropical-temperate troughs in southern Africa and the south west Indian Ocean. Climate Dynamics **15** 937–951.

TODD MC, WASHINGTON R and PALMER PI (2004). Water vapour transport associated with tropical-temperate trough systems over southern Africa and the southwest Indian Ocean. International Journal of Climatology: A Journal of the Royal Meteorological Society **24 (5)** 555–568.

TOZUKA T, ABIODUN BJ and ENGELBRECHT FA (2014). Impacts of convection schemes on simulating tropical-temperate troughs over southern Africa. Climate Dynamics **42** 433–451.

TRENBERTH KE, STEPANIAK DP and CARON JM (2000). The global monsoon as seen through the divergent atmospheric circulation. Journal of Climate **13 (22)** 3969–3993.

TSHILILO FP (2017). Rainy season characteristics with reference to maize production for the Luvuvhu river catchment, Limpopo province, South Africa. Doctoral thesis.

TYSON PD, DYER TG and MAMETSE MN (1975). Secular changes in South African rainfall: 1880 to 1972. Quarterly Journal of the Royal Meteorological Society **101 (430)** 817–833.

TYSON PD (1981). Atmospheric circulation variations and the occurrence of extended wet and dry spells over Southern Africa. Journal of Climatology **1** 115–130.

TYSON PD (1986). *Climatic change and variability in Southern Africa*. Oxford University Press, Cape Town, South Africa.

UNDÉN P, RONTU L, JARVINEN H, LYNCH P, CALVO J, CATS G, CUXART J, EEROLA K, FORTELIUS C, GARCIA-MOYA JA, JONES C, LENDERLINK G, MCDONALD A, MCGRATH R, NAVASCUES B, NIELSEN NW, ODEGAARD V, RODRIGUEZ E, RUMMUKAINEN M, ROOM R, SATTLER K, SASS BH, SAVIJARVI H, SCHREUR BW, SIGG R, THE H and TIJM A (2002). HIRLAM-5 Scienti_c documentation, HIRLAM-5 Project, c/o Per Unden SMHI, S-601 76 Norrköping, Sweden.

UNGANAI LS and MASON SJ (2002). Long-range predictability of Zimbabwe summer rainfall. International Journal of Climatology: A Journal of the Royal Meteorological Society **22 (9)** 1091–1103.

USMAN MT and REASON CJC (2004). Dry spell frequencies and their variability over southern Africa. Climate Research **26 (3)** 199–211.

VAN HEERDEN J, TERBLANCHE DE and SCHULZE GC (1988). The southern oscillation and South African summer rainfall. Journal of Climatology **8** 577–597.

VAN SCHALKWYK L and DYSON LL (2013). Climatological characteristics of fog at Cape Town International Airport. Weather and Forecasting **28** 631–646.

VARIKODEN H, MUJUMDAR M, REVADEKAR JV, SOORAJ KP, RAMARAO MVS, SANJAY J, KRISHNAN R (2018). Assessment of regional downscaling simulations for long term mean, excess and

deficit Indian summer monsoons. *Global and Planetary Change* **162** 28–38. DOI: <https://doi.org/10.1016/j.gloplacha.2017.12.002>.

VOLDOIRE A, SANCHEZ-GOMEZ E, SALAS Y MÉLIA D, DECHARME B, CASSOU C, SÉNÉSI S, VALCKE S, BEAU I, ALIAS A, CHEVALLIER M, DÉQUÉ M, DESHAYES J, DOUVILLE H, FERNANDEZ E, MADEC G, MAISONNAVE E, MOINE MP, PLANTON S, SAINT-MARTIN D, SZOPA S, TYTECA S, ALKAMA R, BELAMARI S, BRAUN A, COQUART L and CHAUVIN F (2013). The CNRM-CM5.1 global climate model: Description and basic evaluation. *Climate Dynamics* **40**. DOI: 10.1007/s00382-011-1259-y, 2091–2121.

WALKER ND (1990). Links between South African summer rainfall and temperature variability of the Agulhas and Benguela current systems. *Journal of Geophysical Research* **95 (C3)** 3297–3319.

WASHINGTON R and TODD M (1999). Tropical-temperate links in southern African and southwest Indian Ocean satellite-derived daily rainfall. *International Journal of Climatology* **19** 1601–1616.

WATANABE S, HAJIMA T, SUDO K, NAGASHIMA T, TAKEMURA T, OKAJIMA H, NOZAWA T, KAWASE H, ABE M, YOKOHATA T, ISE T, SATO H, KATO E, TAKATA K, EMORI S and KAWAMIYA M (2011). MIROC-ESM 2010: Model description and basic results of CMIP5-20c3m experiments. *Geoscientific Model Development* **4**. DOI: 10.5194/gmd-4-845-2011, 845–872.

WUEBBLES D, MEEHL G, HAYHOE K, KARL TR, KUNKEL K, SANTER B, WEHNER MF, COLLE B, FISCHER EM, FU R, GOODMAN A, JANSSEN E, KHARIN V, LEE H, LI W, LONG LN, OLSEN SC, PAN Z, SETH A, SHEFFIELD J and SUN L (2014). CMIP5 climate model analyses: Climate extremes in the United States. *Bulletin of the American Meteorological Society* **95 (4)** 571–583.

YANG HS, DOBERMANN A, LINDQUIST JL, WALTERS DT, ARKEBAUER TJ and CASSMAN KG (2004). Hybrid-maize – a maize simulation model that combines two crop modeling approaches. *Field Crops Research* **87 (2–3)** 131–154.

ZINYENGERE N, CRESPO O, HACHIGONTA S and TADROSS M (2014). Local impacts of climate change and agronomic practices on dry land crops in Southern Africa. *Agriculture, Ecosystems and Environment* **197** 1–10.

APPENDIX A: CAPACITY BUILDING

Capacity building and technology transfer

Capacity building and technology transfer activities included the scientific training of students for postgraduate qualifications, scientific papers published and delivered at international conference, and stakeholder engagement workshop. Research capacity was built by registering students at the University of Pretoria and the University of KwaZulu-Natal (Table A1). Capacity building was also achieved through the competency development of the SAWS project team members on different aspects of mid-summer dry spells.

Table A1: Students who have registered under the project for postgraduate qualifications.

Name	Degree	Status
Daniel Siphamandla	MSc Agrometeorology (University of KwaZulu-Natal)	Final year
Mathole Kelebogile	PhD Meteorology (University of Pretoria)	Final year

Scientific articles and conference papers

1. MENGISTU MG, OLIVIER C, BOTAI JO, ADEOLA AM and DANIEL S (2021). Spatial and temporal analysis of the mid-summer dry spells for the summer rainfall region of South Africa. *WaterSA*, DOI: 10.17159/wsa/2021.v47.i1.9447.
2. DANIEL S, MENGISTU MG, OLIVIER C and BOTA JOI (2020). Analysis of wet and dry spells in the summer rainfall region of South Africa. 14th KMS International Conference on Meteorological Research, Applications, and Services, 21–23 October 2020.
3. OLIVIER C, LANDMAN S, ENGELBRECHT C and MENGISTU MG. Synoptic analysis of the mid-summer dry spells for the summer rainfall region of South Africa. (Draft paper to be submitted to *International Journal of Climatology*).
4. MENGISTU MG, OLIVIER C, MATHOLE K, MAKGOALE T and ADEOLA A. Evaluation of CORDEX models in simulating historical dry spells over major maize producing regions of South Africa. (Draft paper).
5. ADEOLA AM, MENGISTU M, MAKGOALE TE and OLIVIER C. Climate change projections of the mid-summer dry spells over the maize producing region of South Africa. (Draft paper).
6. MENGISTU MG, DANIEL S, MASITHELA T and OLIVIER C. The impact of mid-summer dry spells on the agro-water budget and maize yield potential in the major growing regions of South Africa. (Draft paper).

Stakeholder engagement workshop

A virtual stakeholder engagement workshop was held on 26 February 2021. The objectives of the workshop were as follows:

- Disseminate research findings of the project
- Exchange and share information on mid-summer dry spells with stakeholders



An investigation of the historical and projected occurrence of the South African mid-summer dry spells and its implications for the agro-water budget (K5/2830)

Virtual Stakeholder Engagement Workshop

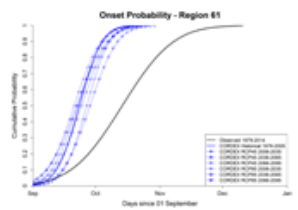
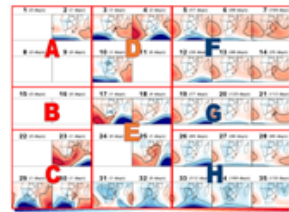
Date: 26 February 2021

Time: 10h00 - 13h00

The South African Weather Service (SAWS) is hosting an online stakeholder engagement workshop to share and exchange information on a recent Water Research Commission (WRC) funded project. The aim of the project is to:

- Perform a detailed temporal analysis on daily summer rainfall at different locations and identify singularities that are related to the South African mid-summer dry spells
- Perform synoptic diagnoses in order to identify the synoptic weather system and sea surface temperature drivers of the South African mid-summer dry spells
- Determine whether mid-summer drought anomalies are captured in historical climate model simulations
- Generate climate change projections of possible future changes in the time of occurrence, frequency and intensity of the South African mid-summer dry spells
- Use a crop model to estimate the impact of the South African mid-summer dry spells on the agrowater budget and maize yields
- Produce and implement a recommended planting date early warning system for application in the agricultural sector

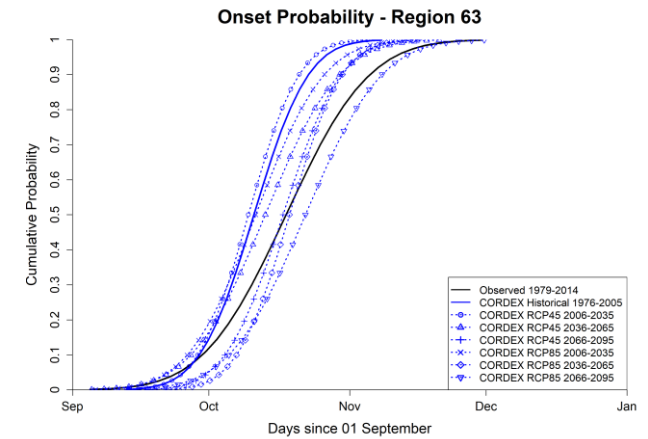
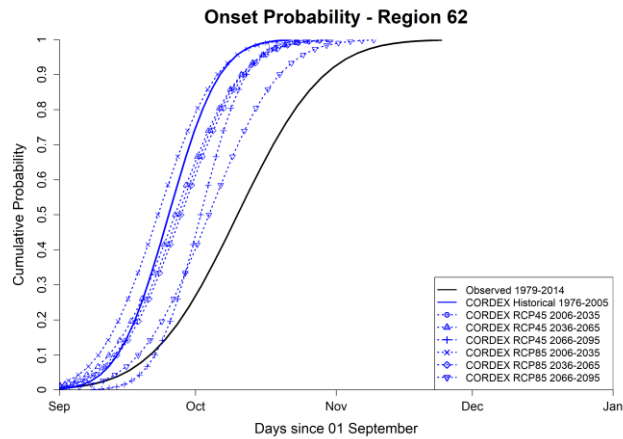
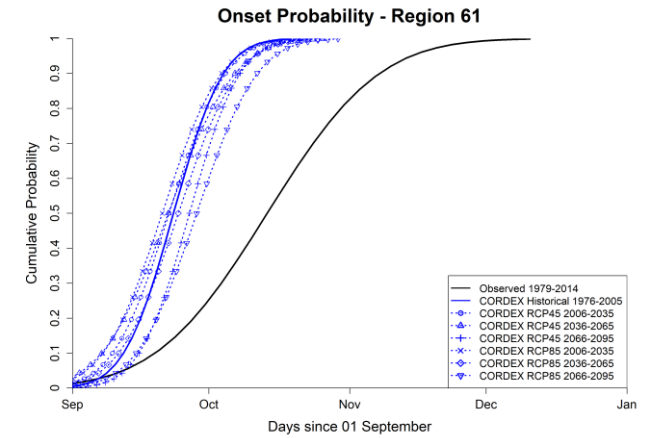
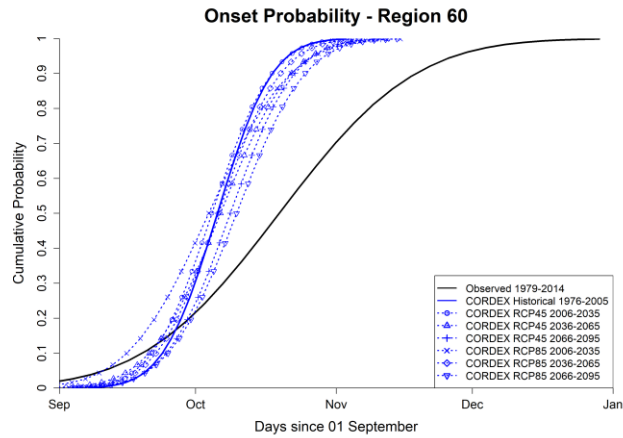
As an expert and key stakeholder in agriculture in South Africa you are invited to take part in the workshop in which we will present the research findings of the project. Figures attached here on the right are a preamble of some of the results and motivation for the project. These represent the study area and district rainfall data (top), circulation patterns in mid-summer that determine the occurrence of dry spells (middle) and change in the onset dates of summer rainfall from CORDEX climate change scenarios (bottom).



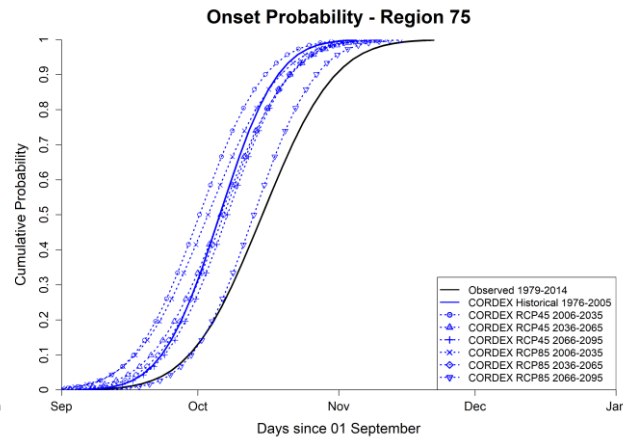
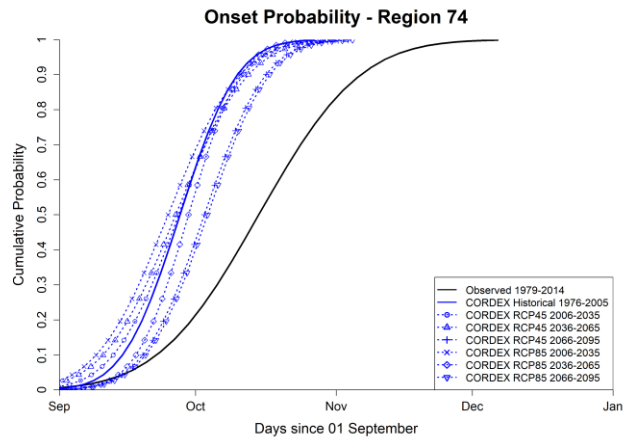
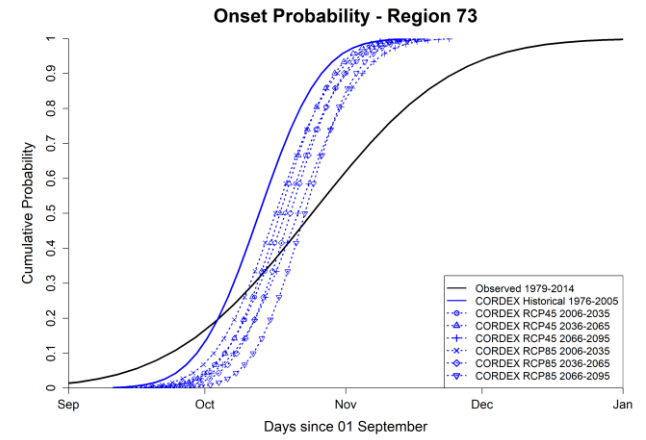
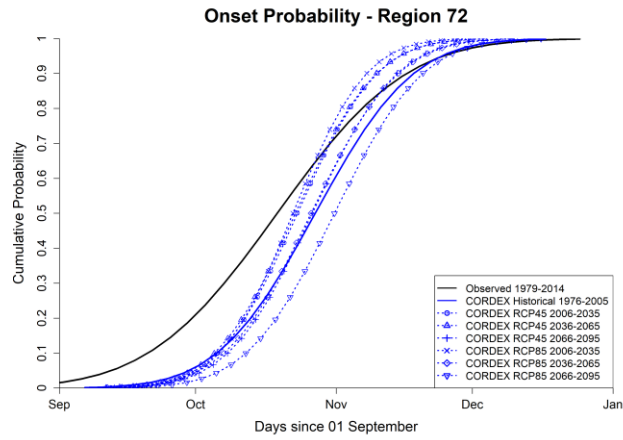
The workshop will be undertaken via MS Teams with the link attached at the bottom of the e-mail. For any additional information with regards to the project or the workshop please contact: Michael Mengistu (Michael.Mengistu@wethersa.co.za).

APPENDIX B: ONSET OF SUMMER RAINFALL

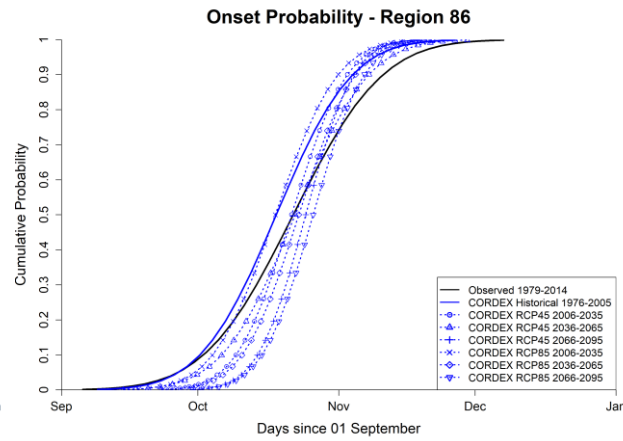
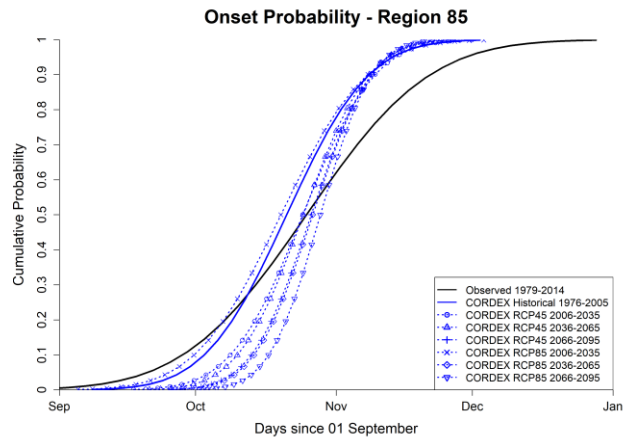
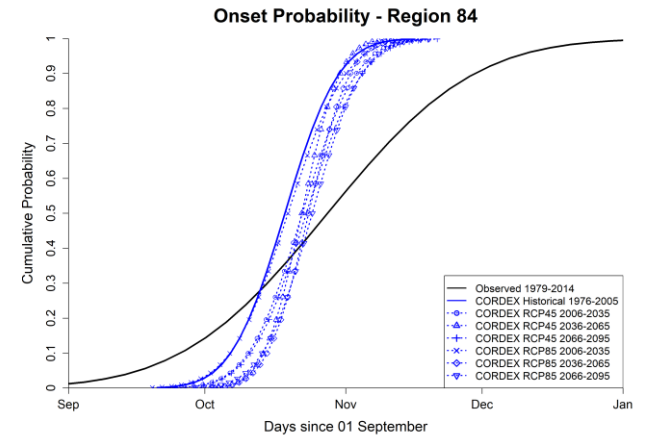
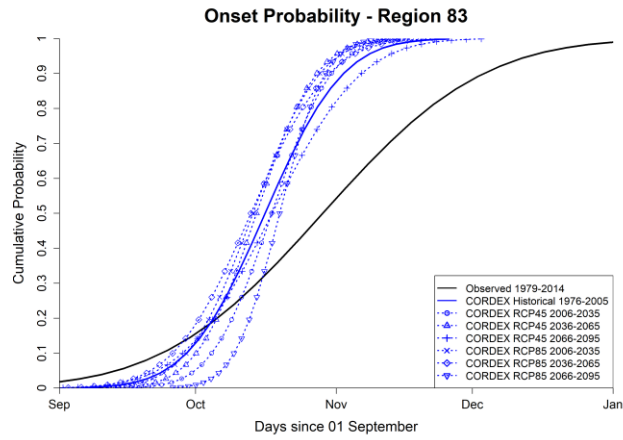
Cumulative probability graphs for onset to have occurred since 1 September of the same season are given below. The black line represents the observed climatological onset dates and the blue lines indicate the various simulated historical and future scenarios as indicated by the legend.



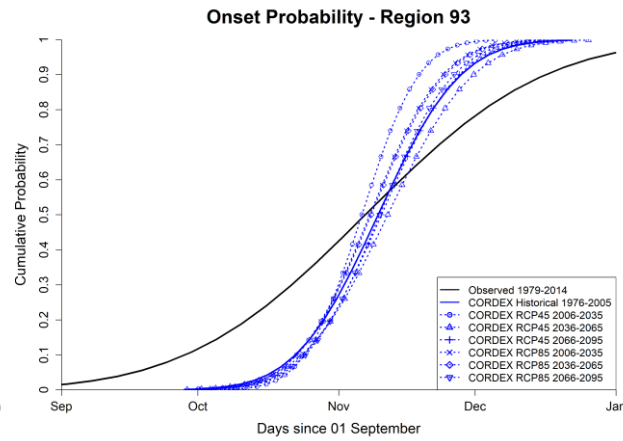
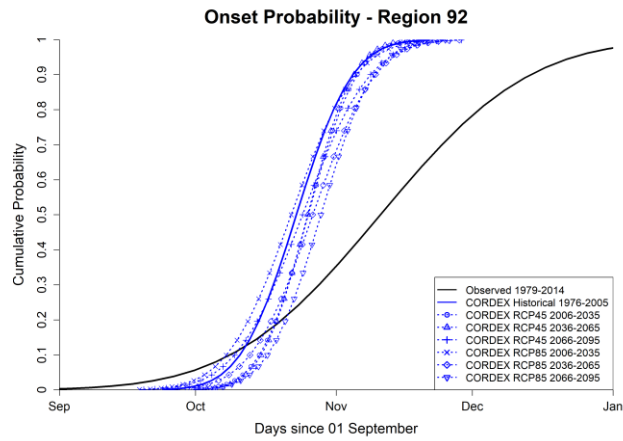
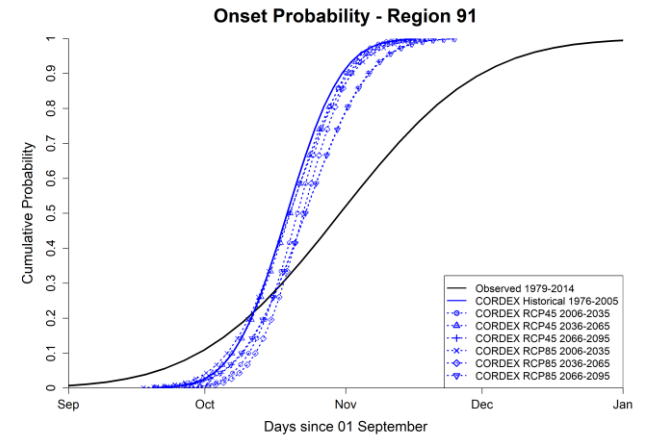
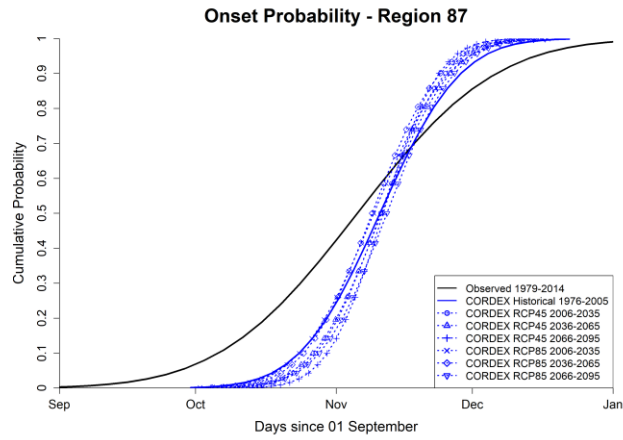
Investigation of the historical and projected occurrence of South African mid-summer drought



Investigation of the historical and projected occurrence of South African mid-summer drought

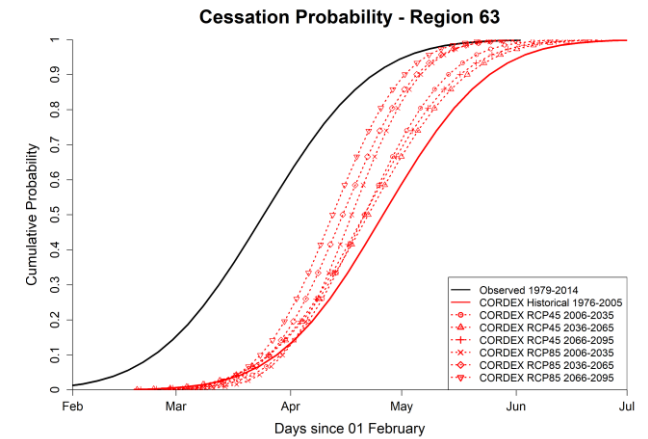
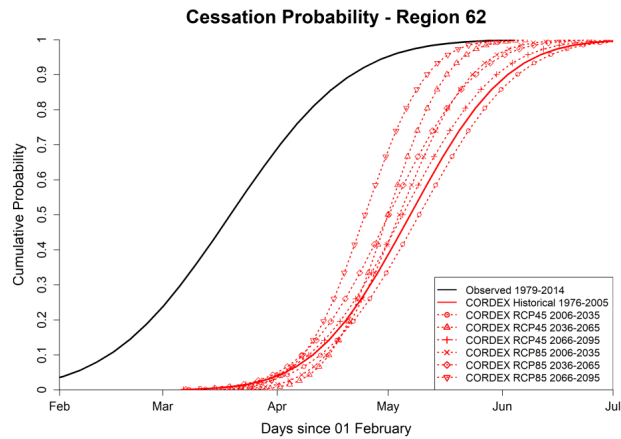
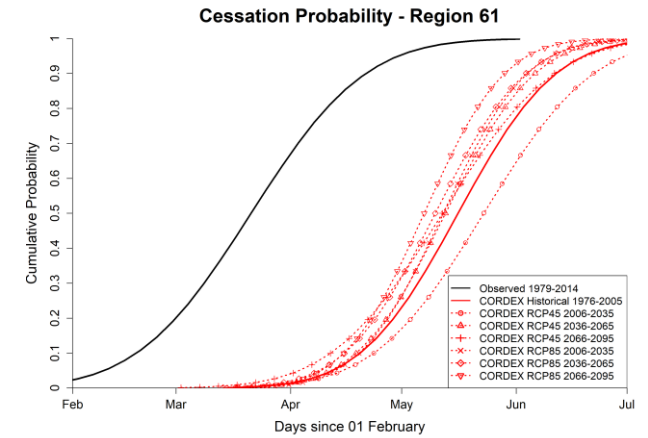
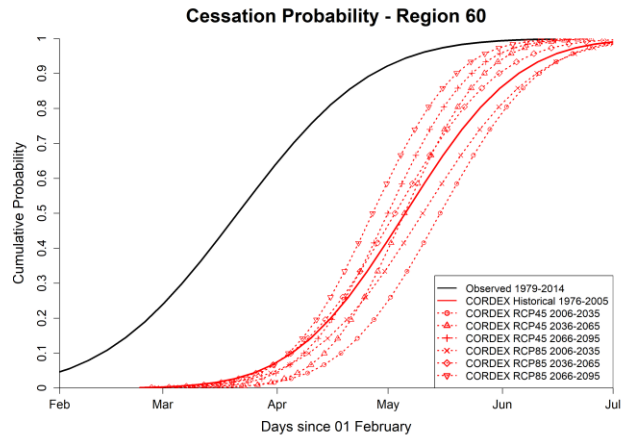


Investigation of the historical and projected occurrence of South African mid-summer drought

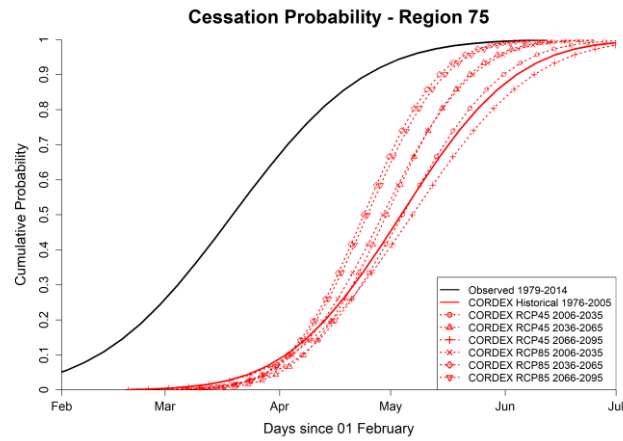
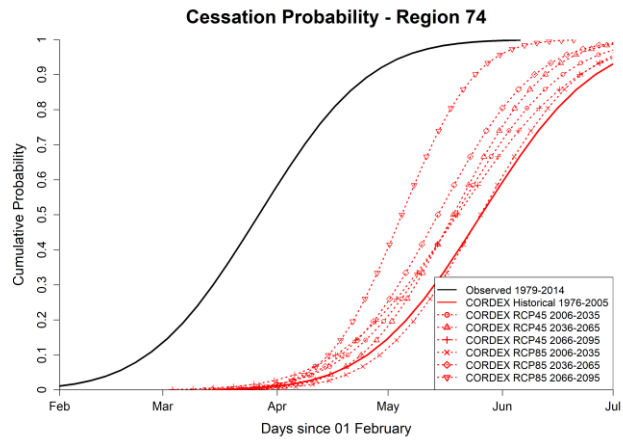
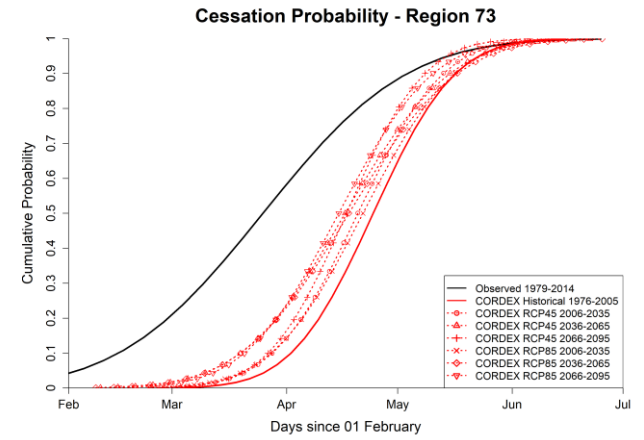
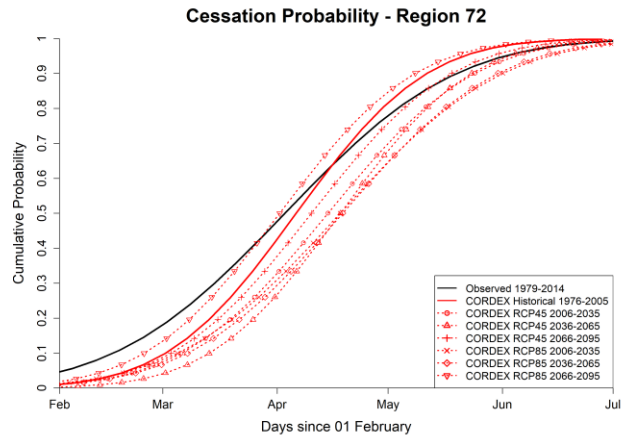


APPENDIX C: CESSATION OF SUMMER RAINFALL

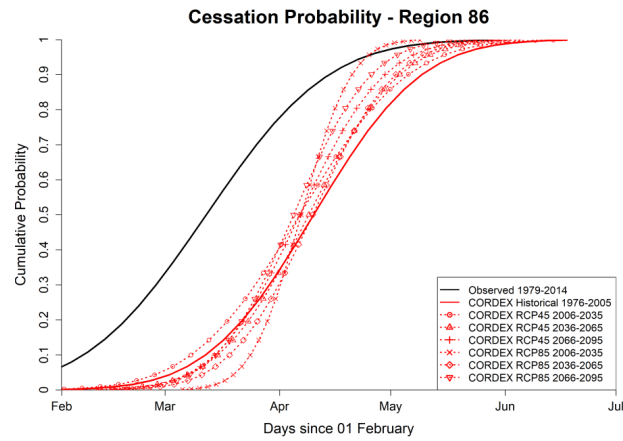
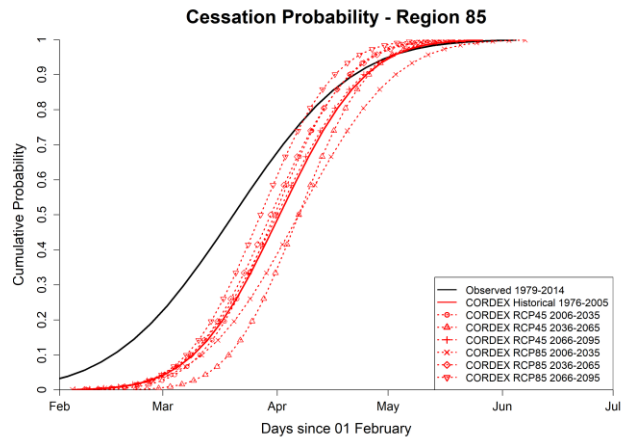
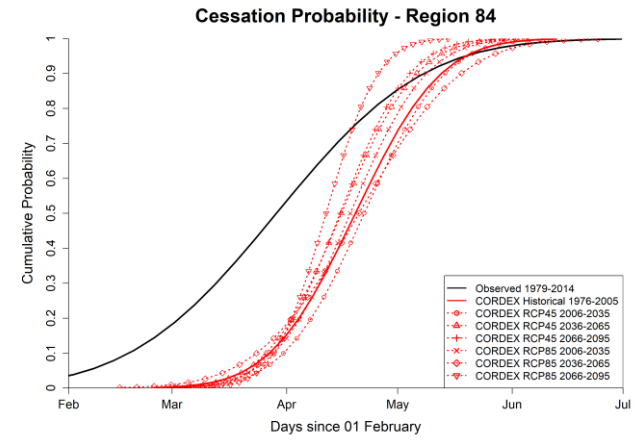
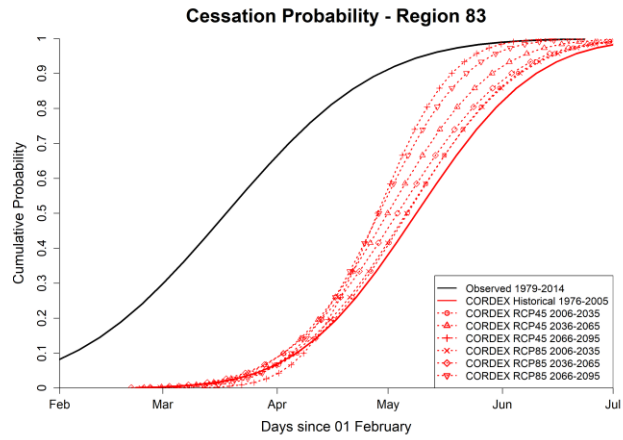
Cumulative probability graphs for cessation to have occurred since 1 February of the same season (in the following year) are given below. The black line represents the observed climatological cessation dates and the blue lines indicate the various simulated historical and future scenarios as indicated by the legend.



Investigation of the historical and projected occurrence of South African mid-summer drought



Investigation of the historical and projected occurrence of South African mid-summer drought



Investigation of the historical and projected occurrence of South African mid-summer drought

